



**HAL**  
open science

# Novel industrial applications for the separation and recovery of metals using aqueous biphasic systems

Eris Sinoimeri

► **To cite this version:**

Eris Sinoimeri. Novel industrial applications for the separation and recovery of metals using aqueous biphasic systems. *Polymers*. Université Grenoble Alpes [2020-..], 2021. English. NNT: 2021GRALI050 . tel-03934561

**HAL Id: tel-03934561**

**<https://theses.hal.science/tel-03934561>**

Submitted on 11 Jan 2023

**HAL** is a multi-disciplinary open access archive for the deposit and dissemination of scientific research documents, whether they are published or not. The documents may come from teaching and research institutions in France or abroad, or from public or private research centers.

L'archive ouverte pluridisciplinaire **HAL**, est destinée au dépôt et à la diffusion de documents scientifiques de niveau recherche, publiés ou non, émanant des établissements d'enseignement et de recherche français ou étrangers, des laboratoires publics ou privés.

## **THÈSE**

Pour obtenir le grade de

## **DOCTEUR DE L'UNIVERSITÉ GRENOBLE ALPES**

Spécialité : 2MGE : Matériaux, Mécanique, Génie civil, Electrochimie  
Arrêté ministériel : 25 mai 2016

Présentée par

**Eris SINOIMERI**

Thèse dirigée par **Isabelle BILLARD**, Directrice de recherches, Université Grenoble Alpes et codirigée par **Lenka SVECOVA**, Grenoble INP et **Ismaël GUILLOTTE**, Aperam Research centre.

Préparée au sein du **Laboratoire d'Electrochimie et de Physico-Chimie des Matériaux et des Interfaces** dans l'**École Doctorale I-MEP2 - Ingénierie - Matériaux, Mécanique, Environnement, Energétique, Procédés, Production**.

**Nouvelles applications industrielles pour la séparation et la récupération des métaux à partir de systèmes biphasiques aqueux**

**Novel industrial applications for the separation and recovery of metals using aqueous biphasic systems**

Thèse soutenue à huis clos le **28 mai 2021**, devant le jury composé de :

**Madame Isabelle BILLARD**

DR1, Université Grenoble Alpes, Directrice de thèse

**Madame Natalia PLECHKOVA**

INGENIEUR DOCTEUR, Queen's University Belfast Queen's University Ionic Liquid Laboratories (QUILL) Research Centre School of Chemistry and Chemical Engineering, Rapporteur

**Monsieur Laurent DUPONT**

PROFESSEUR, Université de Reims Champagne-Ardenne, Rapporteur

**Monsieur João Manuel da Costa Araújo Pereira COUTINHO**

PROFESSEUR, Departamento de Química – Universida de de Aveiro, Examineur

**Monsieur Marian CHATENET**

PROFESSEUR, Université Grenoble Alpes, Président du jury





# Acknowledgment

First of all, I would like to express my warmest gratitude to the Aperam company for having chosen me as part of this great project. This would not have been possible without the help and expertise of my two supervisors, Isabelle Billard for the academic aspect and Ismael Guillette for the industrial area.

I would like to express my infinite gratitude to Isabelle for teaching me how to do research. For teaching me what it means to work ethically and morally, taking responsibility for one's work, never losing the passion and love for what you are doing. Thank you for the endless scientific debates we have had, for the different points of view that have helped me to change my mind and come up with my own. I also thank you for all the non-scientific aspects that have been a very important part of my PhD journey. Thank you for welcoming me into your home to give me time to settle in France when I arrived. Thank you for taking me to the theatre with you, for the beautiful day spent picking mushrooms, doing randonnée in the mountains. Thank you for talking to me and showing me one of your greatest hobbies, chess and for your passion for Star Wars.

My gratitude equally goes to Ismael, for his extensive scientific knowledge on the subject and for his extraordinary organizational skills. I thank him because without him I would not have had that way of working with method and determination. I thank him for pushing me to do better and better and above all for teaching me how to defend my ideas.

I would also like to thank my two co-supervisors, Nadine for accompanying me through the first part of my PhD, thanks to the scientific discussions we had together, the chats and laughs we had, and Lenka for her impressive scientific writing skills, a key part of the thesis writing period, and for the enjoyable conference we spent together in Spain ((I still have to read that book you told me about while we were eating the squid ink risotto :)).

Now it's the turn of the best mates I have met in France. I couldn't have been luckier to have met the most fantastic colleagues in the world. Each one of you at Lepmi has taught me and left beautiful memories so it is impossible to make a list of importance. Thank you for the evenings of music, dance, tartiflette, raclette, ski, canyoning, acro-branch, Tuesday's cake (or was it Thursday?), for the bars, the endless chats, and laughs. Thank you for everything, for

taking me in, teaching me French, and being so patient with me. I want to devote two more words to Kitchen Party group. Thank you for every single moment we spent together. It was unforgettable! Without you, these three years would not have had the same importance. I would also like to thank the entire Lepmi team for helping and supporting me throughout my PhD.

My final thanks go to my family, who were able, even during this very difficult period of the pandemic, to always stand by me, even at a distance.



"Thousands of Volkswagen and Audi cars sit idle in the middle of California's Mojave Desert. Models manufactured from 2009 to 2015 were designed to cheat emissions tests mandated by the U.S. Environmental Protection Agency. Following the scandal, Volkswagen recalled millions of cars. By capturing scenes like this one, I hope we will all become more conscious of and more caring toward our beautiful planet."  
Photograph and caption by © Jassen Todorov, 2018 National Geographic Photo Contest



# Outline

List of publications and patent in the manuscript.....	10
List of abbreviations.....	10
Résumé de la thèse en français.....	11
Introduction .....	25
<b>A. State of the art .....</b>	<b>35</b>
1. Introduction.....	37
2. Pickling processes and treatment of spent pickling liquors at Aperam .....	37
4. Aqueous biphasic system.....	43
4.1. What is an ABS?.....	43
4.2. Metal repartition in polymer and IL-based ABS.....	63
4.3. Acid-based ABS.....	75
4.4. Can ABS based on PEG, PPG or [P <sub>44414</sub> ] Cl be a useful and green alternative to classical liquid-liquid extraction systems with organic solvents?.....	77
5. Conclusions.....	80
<b>B. Material and methods .....</b>	<b>81</b>
1. Introduction.....	83
2. Chemicals.....	83
3. Methods for obtaining binodal curves .....	85
❖ Turbidity method .....	85
❖ Battleship method.....	90
4. Analytical techniques for element characterization in liquid state .....	92
❖ TOC determination through CO <sub>2</sub> detection .....	92
❖ pH-meter for acidity determination and titration with NaOH or HCl (37%).....	93
❖ Polymer and water determination by TGA and Karl-Fischer.....	94
❖ Determination of metals concentration by AAS and ICP-MS .....	95
❖ Ion chromatography for chloride determination.....	96
❖ Sulfates determination by photometric kit.....	96
❖ PEG and IL concentration determination by NMR.....	97
❖ ESI-MS for metal speciation determination and distribution of molecular weight of PEG-400 .....	98
❖ Fe(II)/Fe(III) speciation through colorimetric technique .....	99
5. Composition of different sulfate and chlorinated baths .....	100
6. Stock solution single or multi-metal to mimic the UGCO bath and Na <sub>2</sub> SO <sub>4</sub> bath. ....	103

7. Extraction and repartition efficiency .....	106
Conclusions .....	107
<b>C. ABS formation and metal extraction in hydrochloric media .....</b>	<b>109</b>
1. Introduction .....	111
2. Preliminary tests on ABS formation and metal extraction on SPL from UGCO bath .....	112
3. Properties of ABS in HCl media .....	113
3.1. Systems without metals .....	113
3.2. System with single metal .....	115
4. ABS and metal extraction in UGCO bath .....	129
5. Conclusions .....	132
<b>D. ABS formation and metals extraction in Na<sub>2</sub>SO<sub>4</sub> media .....</b>	<b>135</b>
1. Introduction .....	137
2. Preliminary tests on ABS formation and metal extraction on SPL from Na <sub>2</sub> SO <sub>4</sub> bath .....	138
3. Properties of ABS in Na <sub>2</sub> SO <sub>4</sub> media .....	139
3.1. System without metals .....	139
3.2. System with single metal .....	140
3.3. System with double element .....	152
4. Binodal curve with Na <sub>2</sub> SO <sub>4</sub> bath .....	153
5. Conclusions .....	154
<b>E. Design of the industrial extraction of Cr (VI) from Na<sub>2</sub>SO<sub>4</sub> bath using PEG-400. ....</b>	<b>155</b>
1. Introduction .....	157
2. Step 1: extraction of chromium with a PEG-400 based-ABS .....	157
2.1. Optimization of the Cr(IV) extraction process .....	157
2.2. Test using laboratory pilot scale .....	160
2.3. Extraction column for Cr(VI) partition .....	164
2.4. Static mixer for Cr(VI) partition .....	165
2.5. What is the fate of Upper phase step 1 and the Lower phase step 1? .....	167
3. Step 2: separation of Cr(VI) from PEG-400 and Cr(III) recovery .....	167
3.1. UPS1 treatment with Na <sub>2</sub> CO <sub>3</sub> and NaOH .....	167
3.2. UPS1 treatment by light .....	173
3.3. Recovery and characterization of solid precipitation .....	179
3.4. The sort of solid precipitate and liquid phase step 2 .....	184
4. Step 3: PEG-400 recovery for further extraction cycles .....	184
4.1. Distillation process .....	185
4.2. Recycled polymer and pure water .....	187
5. Global view of the process loop .....	188

6. Conclusions.....	189
Conclusions and perspectives .....	191
Annex.....	197
1. HCl media and UGCO bath .....	197
1.1. Free chloride in the UGCO bath .....	197
1.2. PPG investigation on the UGCO bath – Victor Matia Fernandes Master’s project.....	197
1.3. DES investigation on the UGCO bath – Patricia Folio Master’s project.....	198
1.4. Binodal curves for systems composed of IL (or polymer) / synthetic solution single-metal that mimic the UGCO bath composition / water.....	203
2. Na <sub>2</sub> SO <sub>4</sub> media and sulfate bath.....	212
2.1. Binodal curves for the systems composed of IL (or polymer) / synthetic solution single-metal (or Na <sub>2</sub> SO <sub>4</sub> bath) / water. ....	212
List of tables .....	216
List of figures .....	217
Bibliography .....	224

## List of publications and patent in the manuscript

### Article

<https://doi.org/10.1039/D0CP03689G>

### Patent

CN102531139B 20131106 – *The method of chromium is removed to single stage method from acidic chromium containing wastewater.*

## List of abbreviations

SPL = Spent Pickling Liquor

ABS = Aqueous biphasic system

LLE = Liquid-liquid extraction

IL = Ionic liquid

AcABS = Acidic aqueous biphasic system

NMR = Nuclear Magnetic Resonance

ESI-MS = Electro spray ionization mass spectroscopy

ICP-MS = Inductively coupled plasma mass spectrometry

AAS = Atomic absorption spectroscopy

TOC = Total organic carbon

TGA = Thermal gravimetric analyses

IC = Ion chromatography

# Résumé de la thèse en français

## Introduction

Le 6e rapport sur l'état et les perspectives de l'environnement européen en 2020 (SOER 2020<sup>2</sup>) publié par l'Agence européenne pour l'environnement (AEE) prévoyait la nécessité d'agir de toute urgence pour relever le défi de la durabilité environnementale d'ici 2050. Dans ce contexte, Aperam, producteur d'acier inoxydable, s'est engagé à réduire son impact sur l'environnement en se fixant comme objectif d'être neutre en carbone d'ici 2050. Pour atteindre cet objectif, la société a lancé des projets sur des thèmes tels que la qualité de l'air, la réduction et la revalorisation des déchets, la réduction des émissions de CO<sub>2</sub> et le recyclage. C'est précisément dans le domaine du recyclage que ce projet de thèse a été développé.

Aperam a une capacité de production d'acier plat inoxydable et électrique de 2,5 millions de tonnes au Brésil et en Europe et est le leader des produits de spécialité de haute valeur. Avec une production d'acier inoxydable dans le monde d'environ 52,2 millions de tonnes seulement en 2019, il est clair que ce matériau est très demandé, surtout au cours de la dernière décennie. Mais qu'est-ce qui rend ce produit, découvert par Harry Brearley<sup>3</sup> il y a plus d'un siècle maintenant, si attrayant et si demandé ? Les aciers inoxydables, contrairement à l'acier simple qui ne contient que du fer et du carbone, sont des aciers contenant au moins 10,5% de chrome, moins de 1,2% de carbone et d'autres éléments d'alliage dans une matrice de fer (Figure 12). Ils sont divisés, selon leur structure cristallographique, en 4 grandes familles<sup>4</sup> : acier inoxydable ferritique (structure cubique centrée), acier inoxydable martensitique (structure cubique centrée métastable à température ambiante et structure cubique à face centrée à haute température), acier inoxydable duplex (mélange de grains avec structure cubique centrée et structure cubique à face centrée), et acier inoxydable austénitique (structure cubique à face centrée).

Dans une société où seule une petite partie des produits issus de l'industrie peut être recyclée, l'acier inoxydable fait partie des matériaux durables qui peuvent toujours être recyclés. Par contre, pour être classé comme un produit vert, le processus de fabrication de l'acier inoxydable, même à partir de la ferraille, doit encore être amélioré afin d'avoir un impact neutre sur l'environnement.

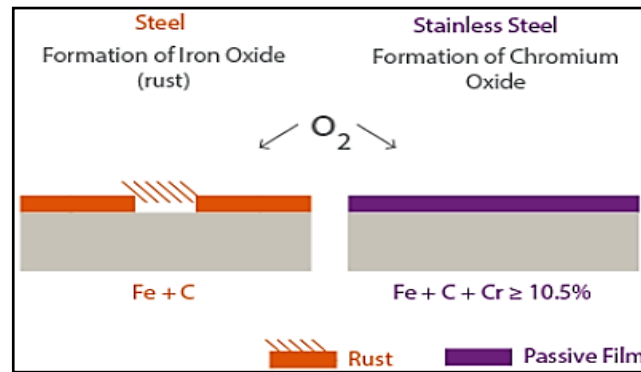


Figure 1. Principales différences entre l'acier et l'acier inoxydable. (site web Aperam).

Dans la branche européenne d'Aperam, en Belgique, le processus de fabrication de l'acier inoxydable comporte de nombreuses étapes, de la fusion à l'ajustement de la composition et à la coulée continue. Les brames formées par la coulée sont collectées et ensuite laminées à chaud pour former des bobines. Comme les étapes précédentes du processus se déroulent à haute température dans l'air, la surface des bobines est recouverte d'une épaisse couche d'oxyde noir. C'est pour cette raison que ces bobines sont appelées "bobines noires". Les bobines sont ensuite envoyées à l'une des trois usines de laminage à froid d'Aperam, en Europe, où elles sont traitées pour leur donner les propriétés finales requises par le client (épaisseur, largeur, finition de surface, etc.).

Une attention particulière a été accordée au processus de décapage, qui est un traitement qui permet d'éliminer les impuretés superficielles de la surface d'un produit. La procédure la plus courante implique l'utilisation d'une solution acide connue sous le nom de bain de décapage<sup>5</sup>. Aperam utilise différents types de bains de décapage pour mettre en œuvre ce processus, dont les bains UGCO et Na<sub>2</sub>SO<sub>4</sub> étudiés au cours du doctorat. Le bain UGCO est un bain de décapage breveté par Aperam, consistant en un mélange d'acide chlorhydrique (entre 100 et 180 g/L) et de fer(III) comme oxydant (entre 40 et 70g/L) travaillant à une température comprise entre 50 et 75°C. Le bain de Na<sub>2</sub>SO<sub>4</sub> contient du sel Na<sub>2</sub>SO<sub>4</sub> avec une petite quantité de H<sub>2</sub>SO<sub>4</sub>, pour un pH compris entre 2 et 5 et une température de travail comprise entre 70 et 90 °C.

À la fin du processus de décapage, et en fonction de la campagne de traitement qui a été effectuée sur les différents aciers inoxydables, les bains sont chargés de métaux dissous et lorsque leur concentration est trop élevée, ils précipitent pour former des boues. Les boues vont donc provoquer à la fois des défauts à la surface de l'acier et être responsables de la baisse d'efficacité du processus de décapage. Aperam collecte les bains de décapage usés (en anglais, Spent Pickling Liquor, SPL) des différents bains et les envoie vers la station de neutralisation. Le processus de neutralisation est à ce jour la

technique la plus utilisée pour traiter les SPLs. Il existe cependant d'autres techniques, telles que le traitement par pyro-métallurgie, l'extraction par solvant, l'utilisation de membranes, mais presque toutes sont très coûteuses, et certaines d'entre elles ne sont pas utiles en raison de la composition des bains d'Aperam ; par exemple, la teneur élevée en S et F, provenant des différents bains, empêche le traitement des SPLs par pyro-métallurgie. La neutralisation est donc la plus pratique, également d'un point de vue économique, mais elle présente certains inconvénients tels que les problèmes de mise en décharge de grandes quantités de déchets produits à la fin du processus. Pour les raisons économiques et environnementales ci-dessus, une alternative basée sur l'extraction des métaux et la régénération des bains par des systèmes biphasiques aqueux a été proposée au début du doctorat.

### **Système biphasique aqueux**

Le système biphasique aqueux (en anglais, Aqueous Biphasic System, ABS) est un système d'extraction liquide-liquide (LLE), constitué de mélanges de trois composants, le premier étant de l'eau, et les deux autres étant solubles dans l'eau. Ces trois composants, lorsqu'ils sont mélangés, permettent une séparation de phase dans les conditions expérimentales étudiées. Parmi ces conditions, la température et la concentration des composants jouent un rôle important dans la détermination de la séparation des phases. Dans ce manuscrit, les deux composants qui sont responsables et essentiels pour la formation de l'ABS, à l'exclusion de l'eau, seront appelés inducteurs biphasiques ; ils peuvent être des polymères, des liquides ioniques (IL), des sels ou des acides. Seules certaines combinaisons d'inducteurs sont capables de former un ABS : polymère A / polymère B, polymère / sel, polymère / IL, ILA / ILB, IL / sel et IL / acide. Dans certains cas, des additifs sont combinés avec les trois composants d'un ABS, et ceux-ci ont des rôles différents tels que favoriser la formation d'ABS, modifier le pH de travail, ou même faciliter la transition de certains composants d'une phase à l'autre et parfois le même additif peut jouer plus d'un rôle. Les résultats expérimentaux obtenus dans l'étude de ce type de système à trois composants sont représentés graphiquement au moyen de diagrammes de phase, où l'on trouve des courbes binodales et des conodales (en anglais, tie lines). Les données expérimentales portent notamment sur la détermination des compositions des phases supérieure et inférieure d'un système à trois composants une fois la séparation des phases obtenue. La quantification des composants a été réalisée en utilisant différentes techniques comme la spectroscopie d'absorption atomique, la résonance magnétique nucléaire ou la spectrométrie de masse à plasma inductif.

Les inducteurs biphasiques utilisés pendant la thèse sont les polymères polyéthylène glycol avec  $M_w=400$  Da (PEG-400) et polypropylène glycol avec  $M_w=425$  Da (PPG-425) et le liquide ionique chlorure de tributyl tétradécyl phosphonium [P<sub>44414</sub>] Cl (Figure 2).

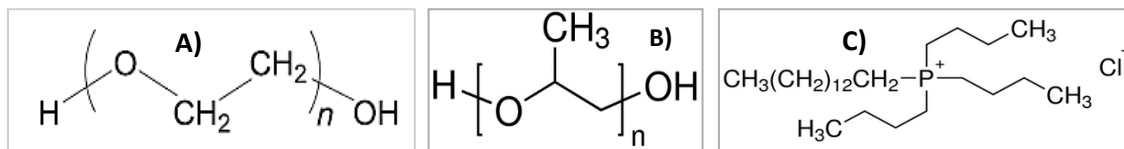


Figure 2. (A) PEG; (B) PPG, (C) [P 444 14] Cl.

La décision de travailler avec le PEG et le PPG était principalement basée sur le fait que ces polymères jouent un rôle de premier plan dans les procédés d'extraction des métaux utilisant l'ABS. L'un des premiers groupes de chercheurs à utiliser des polymères pour l'extraction des métaux par ABS était celui de Robin D. Rogers et de ses collègues<sup>6</sup>. Ils ont étudié<sup>6</sup> la séparation du Tc, du Cd et du Pb en utilisant un ABS composé de polymère / sel / H<sub>2</sub>O. Koch et al.<sup>7</sup> ont également utilisé le PEG pour la récupération du chrome à partir des solutions salines aqueuses. Bulgariu et al.<sup>8</sup> ont démontré l'extraction du Cd(II) avec des sels d'iodure (comme le NaI) en utilisant un ABS composé de PEG-1550/sulfate d'ammonium/H<sub>2</sub>O. Wang et al.<sup>9</sup> ont analysé le système PEG (1000/2000/4000) / Na<sub>2</sub>SO<sub>4</sub> / Na<sub>2</sub>MoO<sub>4</sub> / H<sub>2</sub>O sans ajout de produits extractant, montrant que le pourcentage d'extraction du molybdène varie en fonction de la quantité de polymère, de sulfate de sodium, de molybdène et de la température. Muruchi et al.<sup>10</sup> ont montré qu'il est possible de séparer sélectivement le Mo et le Re d'un effluent minier concentré en cuivre en utilisant du PEG-4000/PPG-400.

Un des points communs entre toutes ces études est la capacité de cette classe de polymères, quel que soit leur poids moléculaire, à fournir un système biphasique aqueux au contact d'un sel. La plupart de ces articles discutent du caractère hydrophobe/hydrophile des composants de l'ABS. Il semble notamment que le polymère perde son caractère hydrophile lorsqu'un composé ayant une plus grande affinité pour l'eau est ajouté au système, comme Na<sub>2</sub>SO<sub>4</sub>. C'est sur cette preuve que la formation d'ABS et l'extraction de métaux sont démontrées.

En ce qui concerne le liquide ionique [P 444 14] Cl, il a été choisi parce que des résultats prometteurs ont été obtenus par mon groupe de travail dans l'utilisation de ce liquide ionique pour l'extraction des métaux par l'ABS. Plus récemment, de nouveaux systèmes ont notamment été développés sur la base de l'utilisation de [P 444 14] Cl dans l'ABS acide (AcABS). Une recherche pionnière a été effectuée par le groupe de recherche PATH de Coutinho (Université d'Aveiro, Portugal) en collaboration avec notre équipe, sur la compréhension de l'ABS en présence de liquide ionique en milieu acide (HCl, HNO<sub>3</sub> ou H<sub>2</sub>SO<sub>4</sub>)<sup>11-12</sup>. Cette ligne de recherche s'est ensuite développée pour comprendre l'effet des ions métalliques sur les systèmes ABS à base de LI en milieu acide, et comprendre le mécanisme de répartition des ions métalliques<sup>13</sup>.

Ces dernières années, les liquides ioniques et les polymères se sont donc révélés être une bonne alternative aux solvants organiques courants utilisés dans les extractions par solvant. Cependant, pour

comprendre lequel des inducteurs biphasiques est le plus avantageux, il faut considérer leur efficacité dans le processus d'extraction en fonction de leurs caractéristiques physico-chimiques et enfin de leur caractère éco-durable.

### **ABS et extraction des métaux dans le bain d'UGCO**

Le bain UGCO utilisé est caractérisé par une concentration élevée de Fe (environ 90 g/L), Cr (environ 20 g/L) et Ni (environ 8 g/L), et une quantité moindre d'autres métaux tels que Mn, Mo et Cu (< 1 g/L). La demande d'Aperam concernant ce bain est d'en extraire le Cr et le Ni (avec une faible quantité de fer seulement) si possible, avec déshydratation du bain et élimination du cuivre (qui est un inhibiteur de la réaction de décapage). Comme alternative au procédé de neutralisation de ce bain, deux ABS sont proposés et étudiés, le [P<sub>44414</sub>] Cl / bain UGCO et le PEG-400 / bain UGCO.

Bien que ces systèmes ne se soient pas avérés efficaces pour répondre aux exigences de l'entreprise, en raison de la faible efficacité d'extraction des inducteurs biphasiques, la représentation graphique des données expérimentales obtenues était particulièrement intéressante. Ainsi, il a été décidé de travailler avec des solutions synthétiques monométalliques, pour mieux comprendre les phénomènes observés avec le bain UGCO. Les métaux considérés étaient le Ni(II), le Cr(III), le Fe(II) et le Fe(III).

En ce qui concerne les systèmes liquides ioniques, les courbes binodales obtenues en traçant les données expérimentales pour Ni(II) et Cr(III) sont celles que l'on trouve le plus fréquemment dans la littérature. Ces courbes sont présentées sur la Figure 3, et montrent comment, en augmentant la concentration de l'un des deux composants, la courbe se développe le long de l'axe du composant. Il s'est avéré que le Cr(III) favorise davantage la séparation de phase que Ni(II) et cela peut être constaté par la position de la courbe binodale qui est décalée plus à gauche dans le diagramme de phase de la Figure 3. Il en va de même lorsque les concentrations des métaux augmentent.

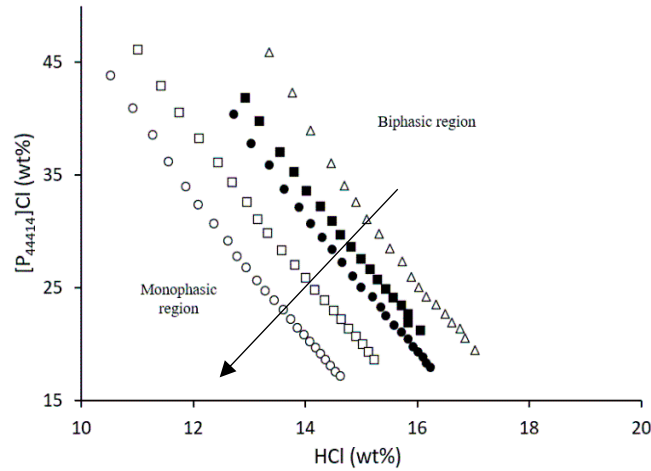


Figure 3. Courbes binodales des systèmes :  $[P_{44414}]Cl/[HCl\ 37\ \% \text{ en poids}]/H_2O$ ,  $[Me]=0\ \text{g/L}$  ( $\Delta$ ) ;  $[P_{44414}]Cl/[Ni(II)+HCl\ 37\ \% \text{ en poids}]/H_2O$  à  $5\ \text{g/L}$  ( $\blacksquare$ ) ou  $15\ \text{g/L}$  ( $\square$ ) de  $Ni(II)$  ;  $[P_{44414}]Cl/[Cr(III)+HCl\ 37\ \% \text{ en poids}]/H_2O$  à  $5\ \text{g/L}$  ( $\bullet$ ) ou  $15\ \text{g/L}$  ( $\circ$ ) de  $Cr(III)$  à  $25^\circ\text{C}$ . La flèche indique une augmentation de la concentration en métal.

Par contre, la représentation graphique des résultats obtenus pour des systèmes composés de  $Fe(II)$  ou de  $Fe(III)$  dévie de la forme classique. La Figure 4 montre, en particulier, le système avec  $Fe(III)$ . Comme on peut le voir, lorsque la concentration de  $Fe(III)$  augmente, la courbe prend une forme qui a été appelée dans cet ouvrage "forme d'oignon". Certaines courbes binodales de forme peu commune ont déjà été présentées dans la bibliographie, comme celle de Neves et al. <sup>14</sup> avec une forme d'épaule particulière ou celle proposée par Tome et al. <sup>15</sup> appelée courbe binodale de type "0".

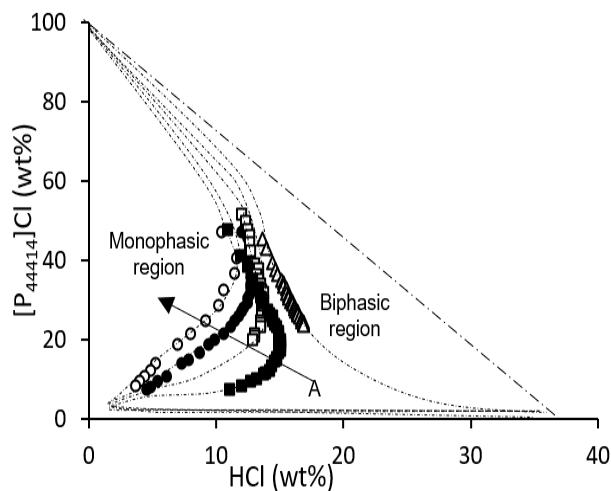


Figure 4. Courbes binodales des systèmes:  $[P_{44414}]Cl/[Fe(III)+HCl\ 37\ \text{wt}\%]/H_2O$  à  $[Fe(III)] = 0\ \text{g/L}$  ( $\Delta$ ),  $[Fe(III)] = 2.5\ \text{g/L}$  ( $\blacksquare$ ),  $[Fe(III)] = 5\ \text{g/L}$  ( $\square$ ),  $[Fe(III)] = 10\ \text{g/L}$  ( $\bullet$ ) et  $[Fe(III)] = 15\ \text{g/L}$  ( $\circ$ ) à  $25^\circ\text{C}$ .

Après avoir obtenu l'ABS en mélangeant le bain d'UGCO avec du PEG-600, une étude du système a été réalisée en considérant la contribution de chacun des métaux. Après une bibliographie minutieuse, il a été constaté qu'à ce jour, aucun ABS n'a été obtenu à partir de systèmes polymère/acide/H<sub>2</sub>O. Cela a été confirmé par l'investigation suivante, mais un résultat surprenant est apparu lorsque la contribution du FeCl<sub>3</sub> a été étudiée dans le système ci-dessus. Il s'avère que c'est précisément en raison de la présence de la forme anionique du FeCl<sub>3</sub> que des ABS sont obtenus lors de l'utilisation de PEG en milieu acide. La Figure 5 montre la courbe binodale pour le système PEG-600 / [Fe(III) – HCl] / H<sub>2</sub>O, et dans ce cas également, comme pour le système avec liquide ionique, la courbe présente une forme peu commune, qui a été appelée "forme d'oignon". De plus, les données expérimentales pour tracer le diagramme de phase de la Figure 5 ont été obtenues par deux méthodes d'analyse, la méthode du point de trouble et la méthode de la bataille navale. La première est l'une des méthodes les plus courantes utilisées pour déterminer les points expérimentaux d'une courbe binodale ; la seconde est une nouvelle méthode expérimentale qui a été élaborée au cours du doctorat pour accélérer le temps d'investigation. Il a été démontré que les deux méthodes donnent les mêmes résultats.

Les systèmes proposés dans cette section ont montré une efficacité d'extraction élevée pour le Fe, et une efficacité d'extraction faible pour le Cr et le Ni. De plus, il a été constaté que le liquide ionique peut extraire 50 % en poids de Cu dans le bain UGCO. C'est sur cette dernière ligne de recherche que des études plus approfondies sont encore nécessaires sur ce bain.

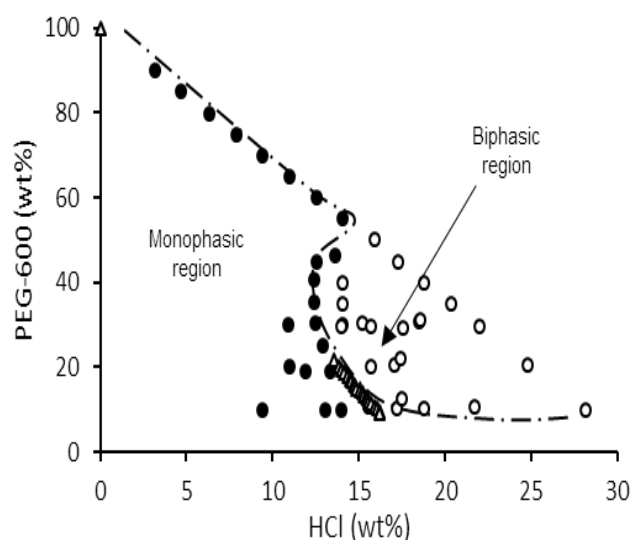


Figure 5. Diagramme de phase obtenu par la méthode de la bataille navale et de la turbidité pour le système PEG-600/[Fe(III)+HCl 37wt%]/H<sub>2</sub>O - [Fe(III)] = 40 g/L à 50°C. Région monophasique (●), région biphasique (○), courbe binodale obtenue par la méthode de turbidité (Δ). La ligne pointillée (- -) n'est qu'un guide pour l'œil.

### ABS et extraction de métaux dans le bain de Na<sub>2</sub>SO<sub>4</sub>

Le bain de Na<sub>2</sub>SO<sub>4</sub> contient le sel Na<sub>2</sub>SO<sub>4</sub> avec une petite quantité de H<sub>2</sub>SO<sub>4</sub>, pour un pH compris entre 2 et 5. De plus, il est riche en Cr (principalement Cr(VI) entre 5 et 20g/L), mais contient également du Fe, Ni, Mo et Cu. La demande d'Aperam sur ce bain est d'éliminer tous les métaux qui y sont dissous, de les récupérer sous forme métallique ou dans des boues ne contenant pas de S, afin de régénérer le bain de sulfate et de le réutiliser dans le processus de décapage. De la même manière que pour le bain UGCO usé, le bain Na<sub>2</sub>SO<sub>4</sub> usé a été traité avec différents inducteurs biphasiques pour obtenir un ABS. Dans ce cas, cependant, le liquide ionique [P<sub>44414</sub>] Cl n'a pas été pris en compte car l'ajout de chlorures dans le bain entraîne une réduction de l'efficacité du processus de décapage. Les inducteurs biphasiques utilisés à cette fin étaient le PEG-400 et le PPG-425. Contrairement au PPG-425, le PEG-400 a permis de répondre immédiatement aux besoins de l'entreprise. Des essais préliminaires ont été effectués en mélangeant 50 % en poids de PEG-400 et 50 % en poids de bain Na<sub>2</sub>SO<sub>4</sub> et, après avoir analysé les phases haute et basse de l'ABS, il se trouve que 99 % en poids de Cr est extrait dans la phase polymère, ce qui permet de nettoyer le bain de la plus grande quantité de métaux, en l'occurrence du chrome.

L'étude s'est poursuivie dans le même sens que pour le bain UGCO. Des solutions synthétiques monométalliques ont été préparées, et les métaux considérés cette fois-ci étaient : Ni(II), Mn(II), Cu(II), Mo(II), Fe(III), Cr(III), Cr(VI) et Mo(VI). La Figure 7 montre la représentation graphique des données expérimentales pour certains des systèmes susmentionnés. Comme il est possible de le voir, les courbes binodales des différents métaux se trouvent toutes dans la même partie du diagramme de phase, et cela se produit également lorsqu'il y a un changement de température ou de concentration de métal. La courbe binodale a également été obtenue directement à partir du bain de Na<sub>2</sub>SO<sub>4</sub> et s'est avérée être exactement dans la même position que les courbes obtenues pour les systèmes synthétiques. Ces résultats sont donc complètement opposés à ceux obtenus pour le système à base de HCl, qui était extrêmement sensible à toute variation.

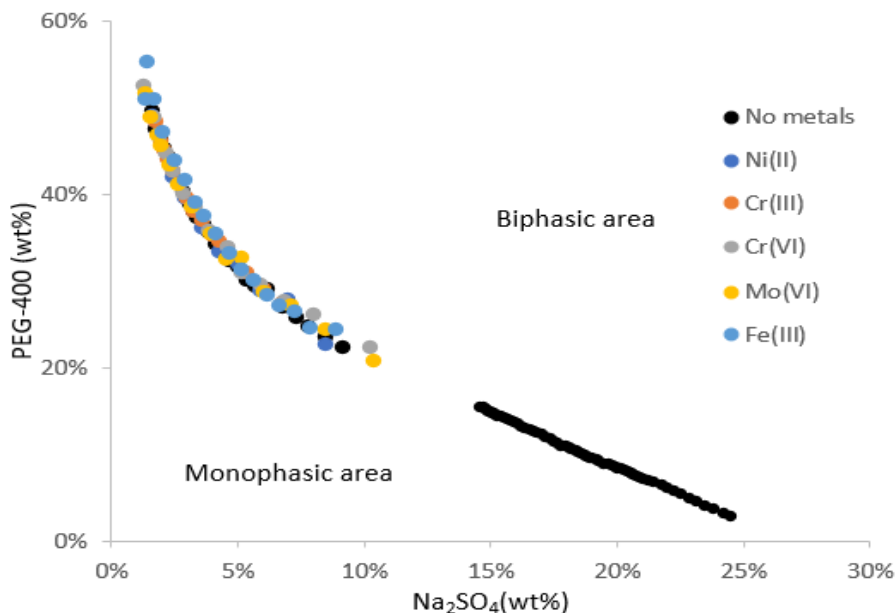


Figure 7. Courbe binodale pour l'ABS composé de PEG-400 /  $\text{Na}_2\text{SO}_4$  /  $\text{H}_2\text{O}$  et de métaux.

Lorsque la répartition des différents métaux en systèmes individuels a été envisagée, le PEG-400 s'est révélé très efficace pour l'extraction du Cr(VI) et du Mo(VI), alors que cette efficacité a diminué pour les autres métaux considérés (Figure 6).

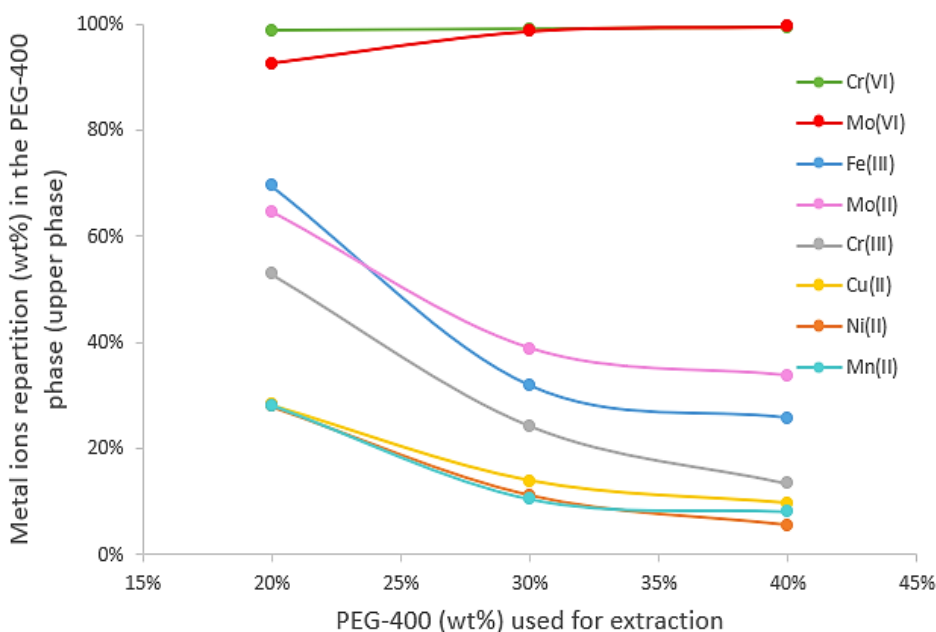


Figure 6. Ions métalliques extraits dans la phase supérieure du PEG-400 en milieu  $\text{Na}_2\text{SO}_4$  à partir de solutions synthétiques mono-métal.

Cette tendance de l'extraction semble être due à la spéciation différente des métaux en solution. Après une recherche bibliographique minutieuse, il a été constaté que le Cr(VI) et le Mo(VI) se présentent principalement sous forme d'oxoanions, tandis que le reste des métaux se trouve surtout sous

forme cationique ( $\text{Me}^+$ ) (diagramme de Pourbaix). Le mécanisme proposé ici diffère de celui du milieu HCl, où le  $[\text{FeCl}_4]^-$  est extrait par des oxygènes partiellement chargés positivement (en raison de la délocalisation des charges) présents dans la chaîne polymère. Dans ce cas, en raison de l'interaction avec  $\text{Na}^+$ , les différentes espèces oxoanioniques sont extraites dans la phase polymère. Cette tendance du PEG à extraire des espèces oxoanioniques a également été décrite par Sun et al<sup>16</sup> en 2018.

Les résultats prometteurs obtenus lors des essais préliminaires suivis de l'explication du mécanisme d'extraction du PEG ont permis de poursuivre l'étude de ce système. L'ABS obtenu pour le système de bain PEG-400 /  $\text{Na}_2\text{SO}_4$  a ainsi été inclus dans le processus total de d'extraction et de séparation du Cr(VI) du bain de sulfate.

La recherche s'est poursuivie en optimisant les paramètres expérimentaux du procédé de l'extraction du Cr(VI). Il en est ressorti que la quantité optimale de PEG à utiliser était de 40 % en poids, alors que la température de travail choisie se situait entre 70 et 80 °C. En adoptant ces paramètres, il a été possible de répondre à la plupart des exigences de l'entreprise, par exemple:

- récupérer plus de 90 % en poids de chrome dans le bain de sulfate,
- régénérer autant de bain de sulfate que possible,
- réduire au minimum la quantité de sulfates dans la phase polymère,
- et réduire la quantité de PEG à un minimum dans le bain régénéré.

Les expériences réalisées jusqu'à présent portaient sur de petits volumes. Ces expériences ont ensuite été répétées dans des volumes plus importants. En particulier, en ce qui concerne l'ABS obtenu pour le système PEG-400 /  $\text{Na}_2\text{SO}_4$  bain, un micro-pilote de 10 kg a été développé (Figure 8). Dans le micro-pilote, un mélangeur et un décanteur ont été utilisés pour réaliser ce processus. Le procédé a finalement montré les mêmes performances qu'auparavant, le Cr(VI) passe en phase polymère pour plus de 90 % en poids.

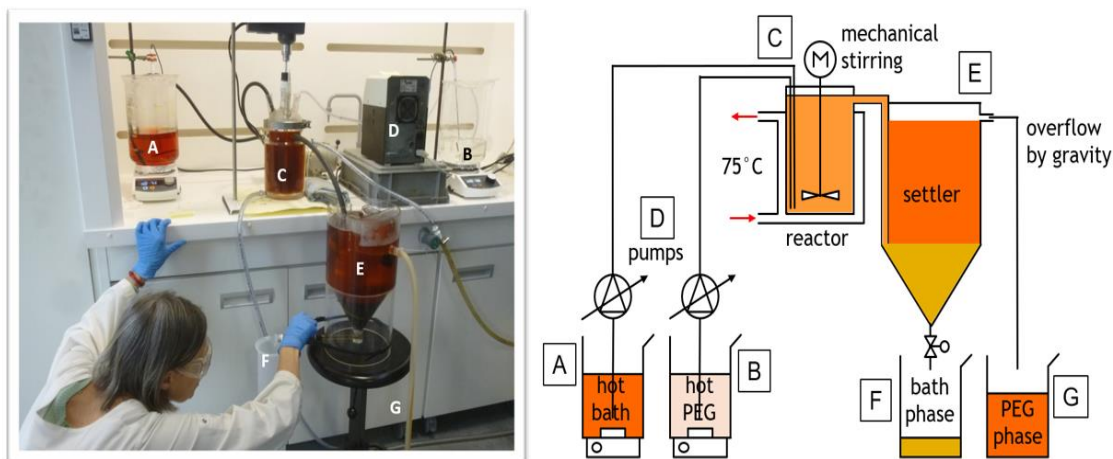


Figure 8. Instantané du processus (à droite) et schéma de l'étape 1 grand volume (10 kg) (à gauche).

Le cas où une colonne d'extraction est utilisée à la place d'un mélangeur et d'un décanteur a également été étudié, mais les résultats obtenus avec celle-ci n'étaient pas satisfaisants en raison des valeurs de densité du polymère et du bain de sulfate trop proches l'une de l'autre. Enfin, un mélangeur statique a été utilisé à la place du mélangeur classique, ce qui a permis de réduire considérablement l'encombrement de l'installation et d'obtenir de bons rendements dans la distribution de Cr(VI).

À ce stade du processus, la phase inférieure de l'ABS a été réintégrée comme source de bain frais dans le processus de décapage, tandis que la phase supérieure contenant du PEG et du Cr(VI) a poursuivi le processus. L'action de différents agents tels que  $\text{Na}_2\text{CO}_3$  ou  $\text{NaOH}$ , qui ont donné lieu à un deuxième ABS pour récupérer le Cr de la phase polymère, n'a donné de bons résultats que pour de petits volumes. Lorsque l'étape a été effectuée en grands volumes, le système a montré la formation d'une troisième phase solide indésirable. En revanche, le système PEG-Cr(VI) s'est comporté de manière particulière lors de son exposition à la lumière. Après une étude approfondie de la littérature, il a été constaté que la lumière peut favoriser la réduction du Cr(VI) en Cr(III) et que ce dernier précipite et se sépare ainsi du polymère. Après avoir choisi la source de lumière nécessaire pour accélérer la réduction du chrome, celui-ci a été séparé du polymère avec un rendement élevé. Le chrome en phase solide a ensuite été caractérisé par diverses techniques et s'est révélé être présent sous la forme de  $\text{Cr}(\text{OH})_3$ , de  $\text{CrO}_3$  et de  $\text{Cr}_2\text{O}_3$ . Enfin, le polymère a été régénéré par distillation et testé pour un second cycle d'extraction. Le PEG régénéré et le PEG frais se sont avérés aussi efficaces l'un que l'autre. L'eau obtenue à la fin du processus de distillation est très pure et peut être réintroduite dans le processus de décapage.

Le cycle global du processus est présenté à la Figure 9 et a été déposé (numéro de brevet CN102531139B 20131106) en septembre 2019.

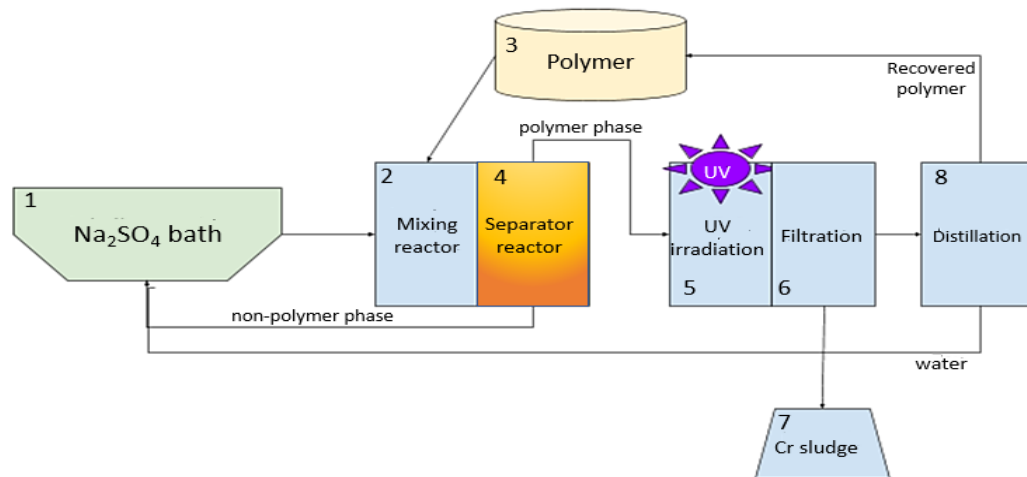


Figure 9. Schéma du brevet pour la récupération du Cr(VI) dans le bain de  $\text{Na}_2\text{SO}_4$ .

## Conclusions

L'objectif de la thèse était de régénérer deux bains différents, les bains UGCO et  $\text{Na}_2\text{SO}_4$  utilisés par Aperam dans le processus de décapage. Les procédés actuellement utilisés par Aperam sont basés sur la neutralisation de ces bains à l'aide de différents agents. Cependant, bien que la neutralisation soit très avantageuse d'un point de vue économique, elle pose des problèmes d'élimination des déchets. L'alternative qui a été proposée est d'utiliser des systèmes biphasiques aqueux pour régénérer les bains. Les exigences de l'entreprise concernant les deux bains avaient la même priorité et consistaient essentiellement à nettoyer les bains de la plupart des métaux dissous, à l'exception des métaux jouant un rôle dans le processus de décapage. Des systèmes d'extraction liquide-liquide appelés ABS ont été proposés comme alternative au processus de neutralisation.

Dans le premier cas, deux systèmes ABS ont été étudiés, l'un consistant en un liquide ionique [P<sub>44414</sub>] Cl et bain UGCO et l'autre composé de polymère PEG-600 et bain UGCO. Du point de vue de la sélectivité de l'extraction, les deux systèmes ne répondaient pas à la demande de l'entreprise, car tous deux extraient le Fe du bain, qui est essentiel dans le processus de décapage du bain d'UGCO et doit donc rester dans celui-ci. Ce qui était intéressant dans ces systèmes, c'était plutôt la représentation graphique des données expérimentales obtenues. Les ABS sont représentés dans la littérature au moyen de courbes binodales. Pour les systèmes avec le liquide ionique et Ni (ou Cr), les courbes binodales obtenues étaient similaires à la plupart de celles trouvées dans la littérature, c'est-à-dire que le développement de la courbe suivait l'augmentation de la composante utilisée le long de l'axe dans lequel la composante était située. Cependant, la courbe binodale avait une forme peu commune, appelée dans le manuscrit "forme d'oignon", lorsque l'on considère le système avec liquide ionique et Fe. Le

mécanisme d'extraction proposé est celui de l'échange d'ions, entre les composants constituant le liquide ionique et les espèces présentes en solution. En ce qui concerne le système polymère, aucun ABS n'a été démontré à ce jour lorsque PEG / HCl / H<sub>2</sub>O sont mélangés ensemble sous certaines conditions. Ce qui a été démontré dans ces travaux et qui s'est avéré être la découverte fondamentale la plus innovante est qu'en ajoutant du FeCl<sub>3</sub> au système, on obtient un ABS. Le mécanisme d'extraction proposé dans ce cas implique l'extraction de l'anion FeCl<sub>4</sub><sup>-</sup>, qui se lie avec les oxygènes partiellement chargés positivement (en raison de la délocalisation des charges) dans la chaîne polymère. L'étude de ce bain nécessite toutefois des recherches plus approfondies, car au cours des différents tests effectués, l'attention de la société s'est également portée sur d'autres métaux tels que le Cu(II) présent dans le bain UGCO, et l'un des résultats obtenus lors des tests préliminaires pour ce métal était la capacité du liquide ionique à extraire environ 50 % en poids du métal.

Pour le second bain, le bain de Na<sub>2</sub>SO<sub>4</sub>, l'ABS principalement étudié était celui constitué de PEG-600/bain Na<sub>2</sub>SO<sub>4</sub>. Cet ABS a immédiatement satisfait aux exigences de l'entreprise et l'enquête s'est poursuivie en intégrant l'ABS dans le processus général d'extraction du Cr(VI) du bain de sulfate. Ce processus comporte trois étapes clés :

- formation d'un ABS avec un mélange de PEG et de bain sulfate ;
- la séparation du chrome de la phase polymère accélérée par la présence d'une source de lumière ;
- la régénération du polymère par distillation.

Le procédé présenté pour le traitement des bains de sulfate est mis en œuvre de manière continue, notamment en termes de conception industrielle. En particulier, il est nécessaire de développer la boucle du procédé dans un pilote industriel pour vérifier la stabilité de l'ensemble du procédé sur une longue durée et également pour vérifier le rendement et la consommation des réactifs.



# Introduction

*Iceland, the lagoon of the Jokulsarlon glacier, icebergs floating due to rising temperatures.*



The 6th SOER 2020<sup>2</sup> (European environment - state and outlook 2020) published by the European Environment Agency (EEA) foresaw an urgent need for action in the challenge of environmental sustainability by 2050. The environmental situation is worsening considerably in Europe, as many known pollution problems persist, and new ones are emerging. Fundamental changes in lifestyles, production and consumption, knowledge and education are needed for Europe to move towards sustainability. For example, European waters are affected by external pressures from pollution and physical changes. Only 40% of Europe's surface water bodies have good ecological status and 38% have good chemical status. The situation is even worse for seawater, as 8 million tonnes of plastic waste ends up in the ocean every year, putting pressure on the marine environment and its ecosystems.

Regarding the air quality, it turns out that air pollution is the biggest environmental and health risk for Europeans. Today, 80% of all EU greenhouse gas emissions come from fossil fuels<sup>2</sup>. According to the latest numbers from 2017, only 17.5% of the EU's energy comes from renewable sources. The new policy is based not only on improving, but also on doing things differently. Recognizing the persistent environmental and climate challenges on a European and global scale, European environmental and climate policy is increasingly driven by long-term sustainability objectives, as envisaged in the vision of the EU's Seventh Environmental Action Program (7th EAP) 2050, the 2030 Agenda for Sustainable Development and the Paris Agreement on Climate Change. The decade from 2020 to 2030 will be crucial in determining Europe's opportunities in the 21st century. But it appears that the current rate of progress will not be sufficient to meet the climate and energy targets for the period 2030-2050. Among these goals we can include early climate action, improving water and soil conditions, increasing responsibility for consumption and production, clean energy production, etc. (Figure 10).

## SUSTAINABLE DEVELOPMENT GOALS



Source: EEA

Figure 10. Long-term Sustainable Development goals of 6th SOER 2020<sup>2</sup>

In fact, only in recent years, important policy developments have taken place around the frameworks of the low-carbon economy, the circular economy and the bioeconomy. Environmental and climate action is also pursued through broader institutional arrangements, such as climate-related expenditure representing at least 20% of the EU budget for 2014-2020 and the Sustainable Finance Initiative. All these agreements are coming from a global awareness of the need to improve our environmental impact in all fields.

In this context Aperam, a stainless steel manufacturer, committed itself to decrease its environmental impact with the target to be neutral in 2050. To achieve this goal, the company launched projects on thematic such as air quality, waste reduction and revalorization, CO<sub>2</sub> emission reduction and recycling. The process of stainless steels manufacturing is a source of several types of waste (dust, sludges, liquors etc.). Among them, the chemical surface treatments of the product use large quantities of acids which induce the formation of a large quantity of sludge containing metallic ions. These sludge are generally landfilled as hazardous waste.

Aperam has a flat Stainless and Electrical steel capacity of 2.5 million tonnes in Brazil and Europe and is the leader in high value specialty products. In addition to its industrial network, spread over six production facilities in Brazil, Belgium and France, Aperam has a highly integrated distribution, processing, and services network. Its products are sold to customers in more than 40 countries, for application in a large variability of fields among which aerospace, automotive, catering, construction, household appliances and electrical engineering, industrial processes, medical and oil & gas industries.

Commenting, Aperam CEO Tim di Maulo said:

*'Aperam is the world's greenest stainless-steel producer thanks to its European production route based on fully recyclable stainless-steel scrap, and the use of charcoal from our sustainably cultivated forests in Brazil.'*

In the 2019 Sustainability Report<sup>17</sup>, Aperam announces its 2030 environmental objectives and ambition to be carbon neutral in its European operations by 2050, contributing to the European Commission's Green Deal. The 2030 objectives against the 2015 baseline proposed by Aperam are: -15% CO<sub>2</sub> emissions, -11% energy usage (electricity and natural gas), -40% water intake, -70% in dust emissions, and target waste recycling rate >97%.

Therefore, a great emphasis has been placed by the company on the question of recycling (Figure 11). In addition to the standard actions that all companies take for the separate collection of normal waste, Aperam embraces metallurgy as a recycling channel and by-product recycling - the two key aspects of its responsibility in this area. In 2019, 24% of all Aperam's materials (consumables etc., for a total of 5.5 million tonnes) came from recycled sources. Moreover, the company also produces metals that are reusable several times and uses a large amount of recycled materials in its stainless steel production process. Moreover, Aperam already revalorizes a part of its industrial wastes in one of its subsidiaries named Recyco. This company treats dust and oxides coming from the melting shops.

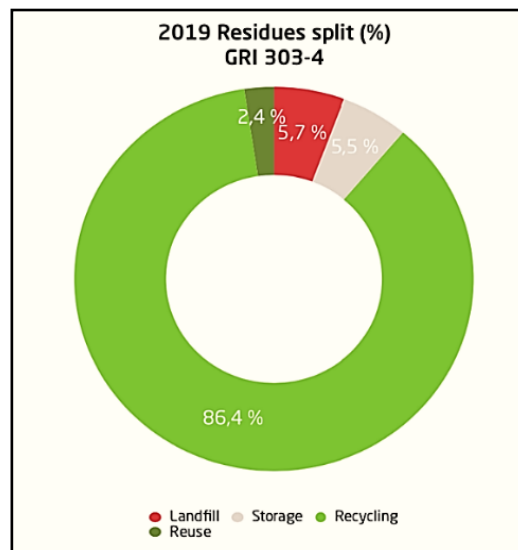


Figure 11. Aperam residues split in 2019 (from Aperam website).

With a stainless-steel production in the world of around 52.2 million tonnes only in 2019, it is clear that this material is of high demand, especially in the last decade. But, what makes this product, discovered by Harry Brearley<sup>3</sup> over a century ago now, so attractive and in demand?

Stainless steels, unlike simple steel which contains only iron and carbon, are steels containing at least 10.5% chromium, less than 1.2% carbon and other alloying elements in a matrix of iron (Figure 12). They are divided, according to their crystallographic structure into 4 large families<sup>4</sup>: ferritic stainless steel (body-centered cubic structure), martensitic stainless steel (metastable body-centered cubic at room temperature and face-centered cubic structure at high temperature), duplex stainless steel (mix of grains with body-centered cubic structure and face-centered cubic structure), and austenitic stainless steel (face-centered cubic structure). Considering the contribution that comes from each metal that makes up stainless steel, we can see that chromium is one of the most important elements. The corrosion resistance is directly proportional to the increase in concentration of this element. As regards nickel, it influences the ductility and toughness of a stainless steel and reduces the corrosion rate in the active state and its presence is therefore advantageous in acidic environments. There are

also many other elements such as molybdenum, manganese, aluminum, cobalt, titanium, nitrogen, sulfur, vanadium, tungsten etc. that are used to improve the characteristics of stainless steel (weldability, deep drawing, corrosion resistance, mechanical resistance etc.).

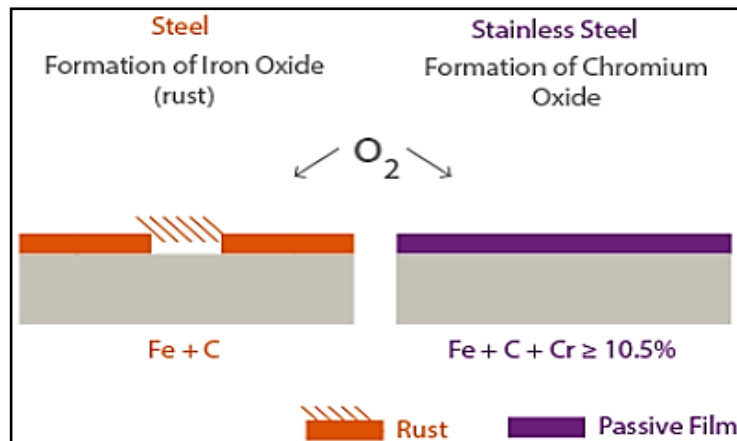


Figure 12. Main differences between steel and stainless-steel steel. (Aperam website)

In a society where only a small part of the products coming from the industry can be recycled, stainless steel results to be one of the sustainable materials which can be always recycled. However, to be classified as a green product, the process of manufacturing stainless steel, even from scrap, has still to be improved toward an environmental neutral impact.

In the European branch of Aperam, the melting, the composition adjustment and the continuous casting of stainless steels are carried out in the two plants in Belgium (Châtelet and Genk). The slabs formed by the casting are collected at Châtelet where they are hot rolled to form coils with an average weight of 25 tonnes and a thickness of between 2 and 12 mm (Figure 13). As the previous stages of the process are at high temperature in air, the surface of the coils is



Figure 13. Rolls of stainless steel produced by Aperam. Site of Isbergues (Fr).

covered by a thick layer of black oxide. Therefore, these coils are called "black coils". The coils are then sent to one of three cold rolling plants in Europe (Genk, Gueugnon and Isbergues) where they are processed to give them the properties required by the customer (thickness, width, surface finish, etc.). Among the first process steps the coils undergo the first pickling, which purpose is to remove the oxide from the surface, to erase the surface defects coming from the previous steps of the process and to remove a thin layer of metal depleted in chromium during the formation of the thick oxide. Various acid solutions are used to remove oxide layers from the surface of the metal, in whole or in part, which will then accumulate in the waste stream<sup>18</sup>. Depending on the surface finishing requested by the

customer, the coil can, after cold rolling, undergo another annealing and pickling steps. Indeed, the cold rolling performed to reach the target thickness for the coil induces a hardening of the metal. The metallurgical properties of the metal have to be regenerated *via* a final annealing. If this annealing is performed in oxidant atmosphere, it has to be followed by the final pickling treatment which has just to remove the thin oxide formed during the last annealing stage. The pickling baths used for this treatment are less aggressive than those used for the first pickling in order to maintain the surface properties as close as possible to those provided by the cold rolling (to avoid or minimize metal consumption).

For each pickling, the baths work continuously, as shown in Figure 14.

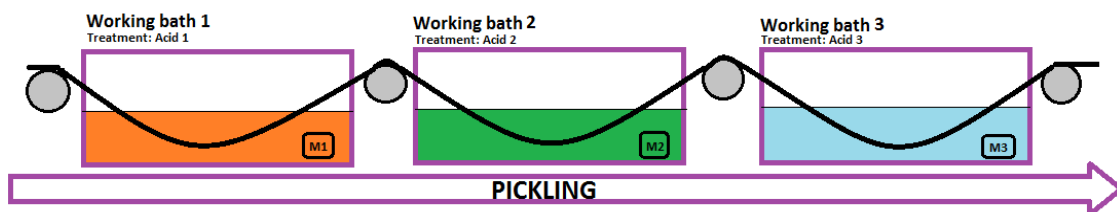


Figure 14. Schematic representation of 3 baths for pickling process. Each of the baths having a different composition in acids and salts.

As the objectives of the two types of pickling are different, the baths used differ by their compositions and/or by their concentrations. The first pickling uses a hydrochloric acid-based bath named UGCO (UGine Chlorhydric Oxidant) by Aperam (an extremely aggressive bath) and a hydrofluoric acid-based bath called UG3P (UGine Peroxide Pickling Process) by Aperam (a finishing bath used to remove the last oxide spots and also silicon oxide). The final pickling uses in a first part the electro-sulfate bath which uses indirect polarization to selectively oxidize the chromium (III) of the oxide into chromium (VI) which dissolves in the bath. In a second part electro-sulfuric, electro-nitric and lighter UG3P baths are used. A more detailed description of the pickling will be made in the following chapter.

The selectivity and the effect of each type of bath on the oxide layers and on the metal can be observed looking at the repartition of dissolved metal in the different baths (Figure 15).

UGCO bath		Na <sub>2</sub> SO <sub>4</sub> bath	
Type of Metal	Concentration (g/L)	Type of metal	Concentration (g/L)
Fe	88.86	Cr	13.51
Cr	18.87	Fe	0.62
Ni	7.88	Ni	0.38
Mn	1.08	Mn	0.097
Mo	0.36	Cu	0.048
Cu	0.35		

Figure 15. Concentration of metals in the UGCO (left) and Na<sub>2</sub>SO<sub>4</sub> (right) Aperam baths.

Thus, the metal dissolved in the sulfate bath is mainly chromium as the main reaction in this bath is the overoxidation of chromium while the partition of the metal ions dissolved in UGCO bath is close to the mean composition of the metal (about 80% of iron, 15% of Cr and 5% of other elements) as this bath mainly induces dissolution of the metallic surface.

The coming lines describe the composition of the baths that have been studied during this PhD and the corresponding requests formulated by Aperam.

- **Na<sub>2</sub>SO<sub>4</sub> bath.** The working temperature is between 70 and 90 °C. It contains Na<sub>2</sub>SO<sub>4</sub> with a small amount of H<sub>2</sub>SO<sub>4</sub>, for pH in the range 2 - 5. As visible in Figure 8, the bath is rich in Cr (mainly Cr(VI), but contains also Fe, Ni, Mo and Cu). This bath contains between 5 and 20 g/L of Cr(VI). The minimum content of 5g/L of Cr(VI) is necessary to inhibit the dissolution of the metal surface. The bath naturally enriches into Cr(VI) in time. When the concentration of Cr(VI) becomes close to 20 g/L, the pickling efficiency of the bath drops and so the bath is refreshed by dumping a part of it and replacing it by a metal free sodium sulfate solution. Due to the presence of sulfate ions, the sludge formed by the neutralization of this bath contain a lot of sulfur which prevents their valorization by conventional pyrometallurgical treatment. As the neutralization of the used bath is made by mixing of all the flows and not separately on each type of flow, the contamination of the neutralization sludge by the sulfur prevents the use of pyrometallurgical treatment for the entire stream. For this reason, the request of Aperam concerning this bath is to remove all the dissolved metals from it in such way that the metal ions could be recovered, under metallic form or in sludge not contaminated by sulfur, and that the bath cleaned from its metal could be reused for the surface treatment.

- **UGCO bath.** This bath is a patented pickling bath consisting in a mixture of hydrochloric acid (between 100 and 180 g/L) and iron(III) as an oxidizer (between 40 and 70 g/L) working at temperature between 50 and 75°C. This bath dissolves the oxide layer thank to the properties of the HCl and also dissolves a part of the metallic surface by both acid dissolution and oxidation of the metal by the iron(III). The pickling reactions consume the iron(III) and form iron(II). To maintain the oxidizing ability of the bath, the iron(II) is oxidized back into iron(III) by hydrogen peroxide. The high aggressiveness of this bath induces its fast loading in dissolved metals and a frequent need for fresh acid and hydrogen peroxide. However, the relatively low concentration of the commercial HCl acid (about 33 w%) induces some difficulties in the management of this bath. Indeed, if the bath evolves too far from its optimum settings, the return to the settings in terms of acid will request dumping of the bath to enable the addition of enough acid and will induce a loss of iron(III). To prevent such cases, this bath is in continuous management (addition and dumping) compared to all the others which are managed with additions on an hour basis. Although the presence of dissolved chromium and nickel is not detrimental for

the pickling efficiency, they are valuable metals, and they are currently difficult to recover in such acidic condition and in presence of large amount of iron<sup>19</sup>. The request of Aperam concerning this bath will be to extract Cr and Ni from it (with only a low amount of co-extracted iron) if possible, with dehydration of the bath (preventing its detrimental dilution) and removal of copper (which is an inhibitor of the pickling reaction).

The UGCO and Na<sub>2</sub>SO<sub>4</sub> bath treatments are of identical priority to Aperam. These two baths contain sludge, involving quality issues. If metals are extracted, sludge will not occur, thus increasing the quality of the bath. There are no requirements about the working temperature of the recovery processes. However, care should be taken to avoid Na<sub>2</sub>SO<sub>4</sub> precipitation at low temperature.

Therefore, due to economic problems and the regulation related to waste treatment, this project was proposed, focusing mainly on the following benefits:

- the increase of the efficiency of the pickling process (that decreases when the amount of the metal ions increases in the bath).
- the removal of metal ions allowing them to be reused (to produce further stainless steel) and increasing the lifetime of the pickling bath.
- the price of recovered metal ion in alloy form.
- the reduction of the quantity of polluting waste for which, if treated and upgraded, the company will not have to pay to landfill it.

The goal was to develop a process that could meet both the economic and environmental demands fixed by Aperam at the beginning of the PhD. We responded to Aperam's requests through the use of aqueous biphasic systems (ABS); those systems consist of a minimum of three components, one of which is always water while the other two are water soluble. ABS can be composed of polymers, ionic liquids, neutral salts, or acids. When these components are mixed at certain concentrations and temperature, they provide a biphasic system. A more detailed description of these systems will be presented in the "State of the art" chapter of this manuscript. For the moment it is important to remind that ABS have been widely used for the extraction of biological molecules, but to date no industrial-scale process using ABS has been proposed for the extraction of metals, with the exception of this manuscript. So, by using different types of ABS, it was possible to meet many of the challenging demands made by the company.

This manuscript is divided into 5 main chapters, excluding the introduction and conclusion:

A. State of the art

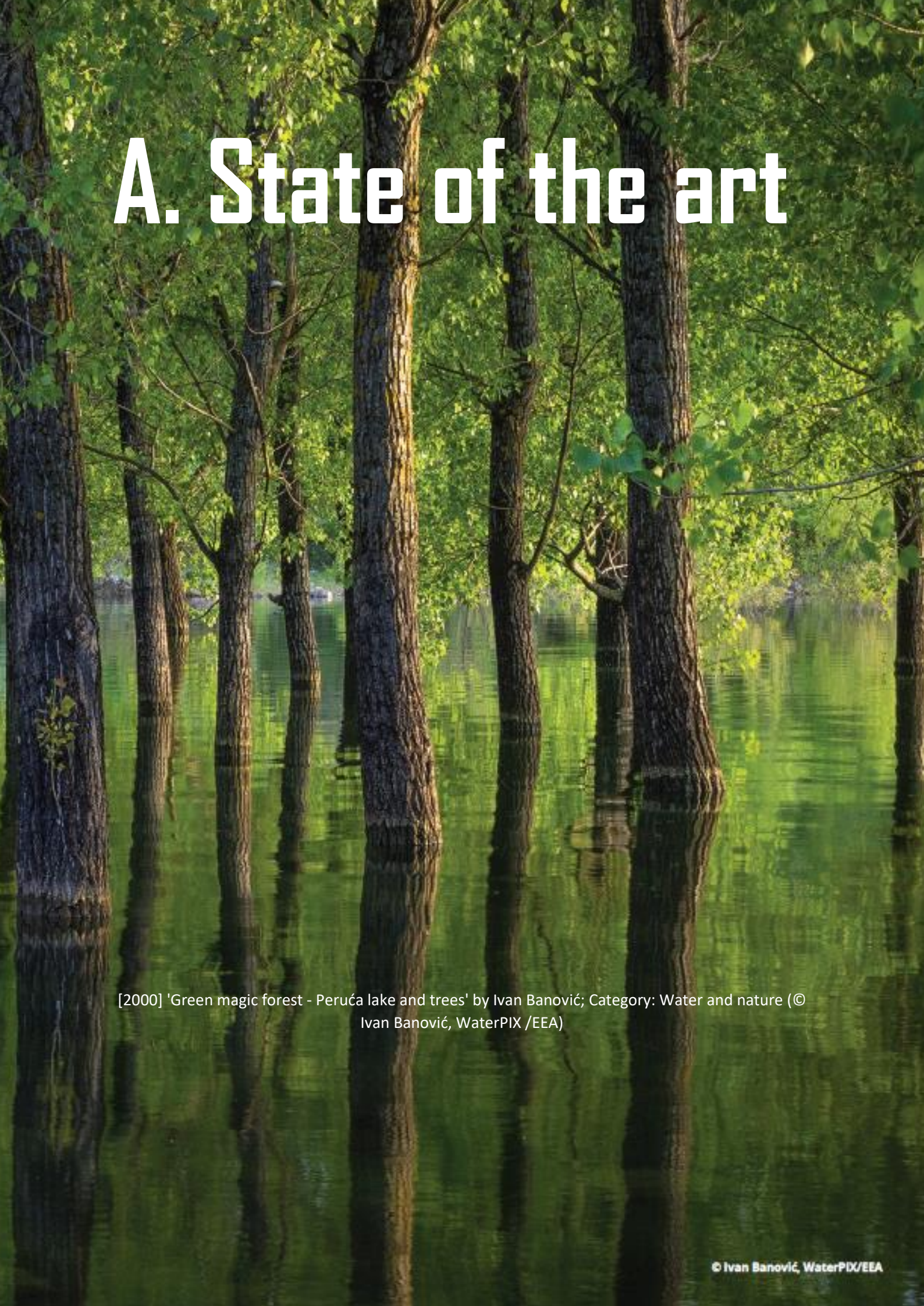
B. Materials and methods

C. HCl bath - results and discussion

D. Na<sub>2</sub>SO<sub>4</sub> bath - results and discussion

E. Design of the industrialization of the extraction of Cr(VI) from Na<sub>2</sub>SO<sub>4</sub> bath using PEG-400

# A. State of the art



[2000] 'Green magic forest - Peruća lake and trees' by Ivan Banović; Category: Water and nature (© Ivan Banović, WaterPIX /EEA)



## 1. Introduction

The first part of this chapter focuses on the description of the pickling processes, and how they are implemented in Aperam plants. As a waste product obtained from the pickling processes, spent pickling liquor (SPL) results to be one of the main pollution issues for metallurgical companies. Nowadays, several methods are used to treat SPL, but they are still very expensive and there are several problems in disposing of their products in landfills. This is where the thesis project originated, from the need to find an alternative to the existing processes used by Aperam to regenerate SPLs. The alternatives that have been proposed are the aqueous biphasic systems (ABSs). A brief historical exposition will be made starting with the first ABS up to the most recent one. The main components used in this manuscript that make up an ABS will be described. Moreover, in the chapter, it will be shown how the experimental data are displayed graphically. ABSs have been widely used over the years for biological systems, but more recently they have also found their way into the recovery of metals from industrial waste. The last part of the chapter is devoted to the new acid ABS (AcABS) for metals extraction.

## 2. Pickling processes and treatment of spent pickling liquors at Aperam

Pickling is a treatment that removes superficial impurities from the surface of a product. The most common procedure involves the use of an acidic solution known as pickling liquor, this is why it is called “pickling”<sup>5</sup>. In metallurgy, there are six major types of pickling: cryogenic, thermal (pyrolysis), energetic (plasma), electrochemical, chemical and mechanical. In particular, Aperam uses the last three. When the black coils arrive at the cold rolling plant, depending on the type of surface required by the customer, the coils undergo several annealing, pickling and cold rolling steps as displayed in the Figure 16.

## Surface finishes

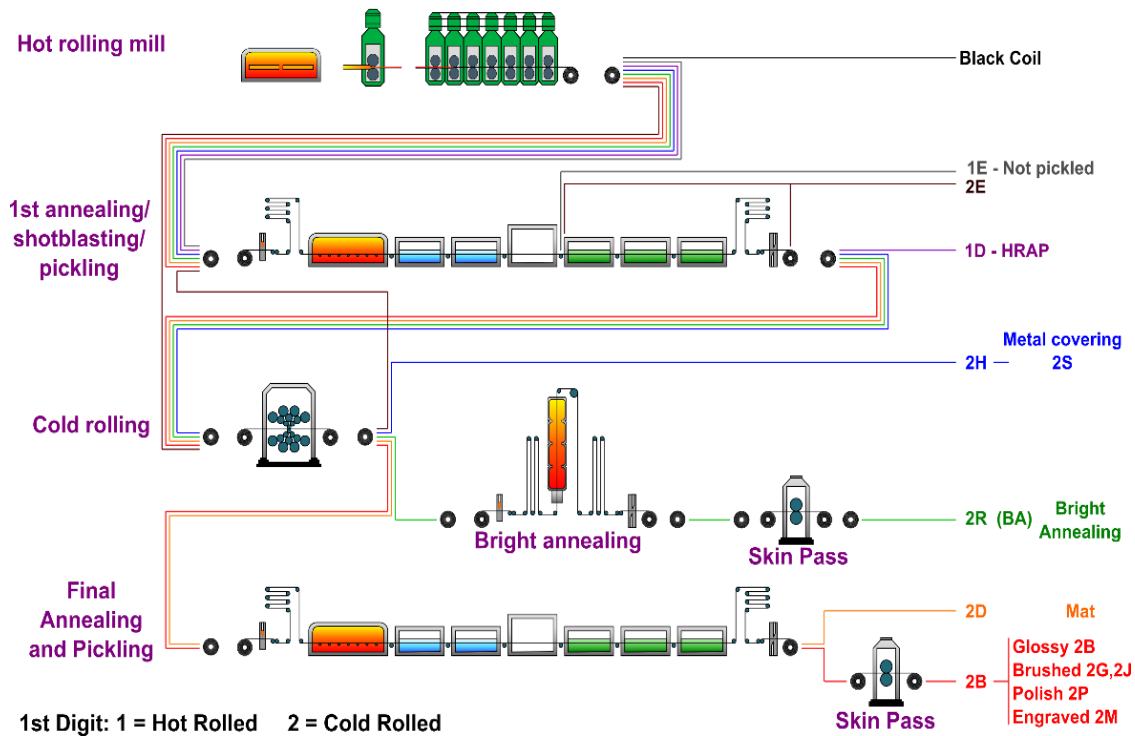


Figure 16. Surface finishing steps for stainless steel in Aperam lines.

Whatever the requested finishing is, the black coils will almost all be treated by a first annealing and a pickling step which aims to soften the work-hardened structure by hot rolling and to clean the surface in order to facilitate the cold rolling step. Indeed, the hot-rolling and the first annealing phases induce the formation of a thick oxide layer on the surface of the coils. Depending on the type of steel produced, the oxides present on the surface may vary in composition. For example, in AISI 304 stainless steel case, oxide scale is composed of iron, chromium and nickel, with silica, manganese and molybdenum oxide traces. In general, a thick oxide layer (10-30 $\mu\text{m}$ ) consisting of a compact inner layer of chromium-rich oxide and a brittle outer layer rich in iron and manganese oxides is found at black coils' surface. The purpose of the first pickling is to remove this thick oxide layer and also a few micrometers of the underlying metal layer (which is depleted in Cr due to the strong oxidation and which can present defects like scratches). The first pickling involves two steps, the mechanical pickling by a scale breaker (device which forces the strip to make several deflections on a short radius of curvature in order to induce cracks in the brittle part of the oxide layer) and shot blasting (blasting of small ball of steel on the surface to remove a part of the brittle oxide layer) which aims to facilitate the action of the chemical pickling section focused on the metal dissolution. For the latter, Aperam uses aggressive baths (hydrochloric and hydrofluoric boosted with an oxidizing reagent). Then there is a cold rolling stage, which enables the coil to reach the final thickness required by the customer. Since cold

rolling induces hardening of the surface, it is necessary to anneal the metal again to restore its metallurgical properties. If this annealing is carried out in a conventional gas furnace, it induces oxidation of the surface. "Final pickling" is used to remove the oxide layer formed by this annealing without affecting too much the surface quality of the metal. For this purpose, Aperam uses more selective and soft baths (e.g., sulfates). After pickling, the surface must be thoroughly rinsed, otherwise stains and defects may appear.

The ions can precipitate if they reach their solubility limits forming thus a sludge in the bath. This sludge can induce defects in the products by creating stains and discoloration but can also induce difficulties in the management of the bath by clogging the pipes. Therefore, when the amount of metals is too high, a refreshment (partial or total) is necessary. However, the presence of some metals is essential for the efficiency of the bath as for instance iron(III) as a reactant for UGCO bath and Cr(VI) as an inhibitor of metal dissolution in  $\text{Na}_2\text{SO}_4$  bath. If the problems of sludge formation is put aside, increasing the concentration of the dissolved metals which are not used as reactants for the pickling reaction will shift the equilibrium of the pickling reaction and thus reduce its efficiency to zero. At this point the bath of acids and metal oxides must be withdrawn and replaced with a fresh bath.

Therefore, exhausted bath is one of the most important environmental concerns in steel mills. It is estimated that for a production of 7,570,000 tonnes/year of steel a volume of 380,000  $\text{m}^3$ /year of SPL is produced in Europe (2017)<sup>20</sup>. The sludge produced after neutralization is estimated to be 190,000 tonnes/year. The environmental impact of liquid waste from spent pickling solutions is significant and their treatment is currently expensive. Their highly corrosive properties are harmful to the environment and they could present the following effects on the receiving environment<sup>20</sup>:

- Hydrolysis of ferrous salts into ferrous-ferric hydroxides, insoluble in water, results in an ochre sediment.
- The reduction of oxygen dissolved in water produced by the above reaction decreases the regenerative power of rivers.
- The proliferation of ferruginous bacteria and ferritic deposits affects flora and fauna.
- High Fe concentration in the solution discards waters to be used for food supply, household, or industrial purposes.

The toxic nature of certain additives used in metal surface treatment solutions such as corrosion inhibitors and surfactants have harmful effects to the environment due to:

- Contents of non-ferrous metals such as Zn, Cu ... in pickling/galvanizing baths.
- Gaseous emissions (nitrous and HCl gas) during the process.

- Liquid emissions due to subsequent washing.
- High salinity and organic load of effluents derived from the physio-chemical treatment of exhausted baths.

The current technique used by Aperam to dispose of SPLs from the baths is to collect them all together and send them to the neutralization and landfill line (Figure 17).

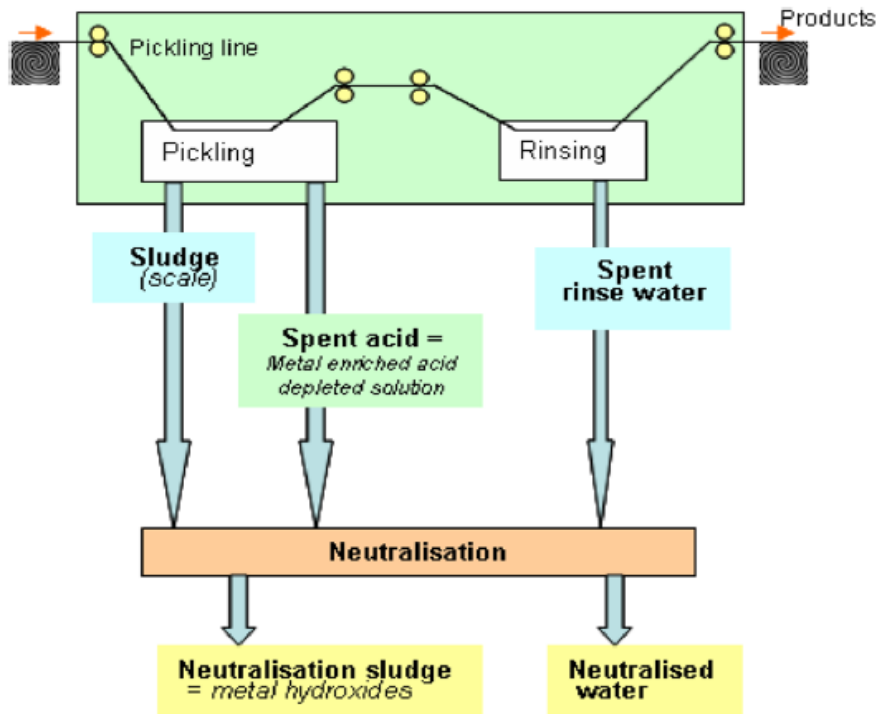


Figure 17. Pickling waste generated in the steel streamline<sup>19</sup>.

Neutralization is the most economical method used to date and consists of treating the SPL with bases or alkaline agent in order to neutralize the acidity and to transform metal ions into hydroxides which will then precipitate. The most used reagent is the quicklime which, in contact with water, provides slaked lime ( $\text{Ca}(\text{OH})_2$ )<sup>21</sup>, and the latter reacts with HCl. The reactions are as follows:



The products obtained are calcium chloride and water. Another advantage of the neutralization process of the mix of all the SPLs is the possibility of using a low quantity of reagents, as one part of the flux neutralizes part of the others.

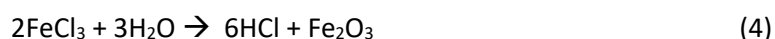
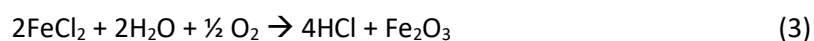
The main drawbacks of this method include:

- a) High sludge production after neutralization. Ozdemir *et al.*<sup>22</sup> showed that for 2 k-tonnes of SPL it was necessary to use about 1.3 k-tonnes of NaOH for the neutralization process; and in addition about 250 tonnes of iron hydroxide are produced as sludge.
- b) The sludge contains the anions of almost all the baths and so S and F which are detrimental for the use in pyrometallurgical treatment.
- c) The process is characterized by slow metal precipitation kinetics. Flocculation should be used to prevent this.
- d) Problem of landfill disposal, such as contamination of groundwater due to the leaching properties of heavy metals.

In the specific case of Na<sub>2</sub>SO<sub>4</sub> and UGCO baths, there are dedicated regeneration treatment for these baths, and they are based on the recovery of metals and reclamation of acids<sup>23</sup>. The two parts are often treated in the same process. Acid regeneration requires separating the dissolved metals from the acids and then re-concentrating the acids that can be used for further surface treatments.

For the Na<sub>2</sub>SO<sub>4</sub> bath, regeneration involves neutralizing the bath separately using bisulfite and soda ash to approximately pH 5 so that most of the metal precipitates. The precipitated metal is then filtered out and the bath is readjusted to pH 2 with sulfuric acid. The main advantages are that the bath is regenerated, Cr(VI) is kept in a smaller process cycle, while the main disadvantage is that a lot of acid and soda ash are consumed and the sludge obtained as products is not treatable due to its S content.

As for UGCO or hydrochloric baths the best way to regenerate them is with spray roasting. The spray roasting is based on a pyro-hydrolysis reaction. The pyrolysis of FeCl<sub>2</sub> producing hydrochloric acid from carbon steel pickling lines takes place according to the following chemical reactions:



The water and free acid components included in the initial solution rapidly evaporate at the temperature of reaction. The roasting gas thus contains the entire free and bonded acid in a form that can be absorbed. The spray roasting process works at a temperature below the sintering temperature of iron oxide. So, the iron oxide is obtained as a red powder. The quality of iron oxide mainly depends on the temperature and flow rate.

The drawbacks of this process are:

- The pyro-hydrolysis process is very energy intensive and expensive.

- The regeneration plant is very maintenance intensive due to the highly corrosive nature of the liquor at elevated operating temperatures.
- If the plant does not have much used bath to treat, it is not very easy and convenient to operate the process.
- These processes produce a significant amount of stack emissions containing HCl, particles and chlorine that led to exceeding emission limits.

Alternative methods for treating acid solution with dissolved metals are the evaporation and crystallization methods, the solvent extraction and membrane separation technology.

Considering the evaporation and crystallization method for SPL treatment, there are three ways of getting free acid from them: copper recovery<sup>24, 25</sup>, ferrous sulfate monohydrate<sup>26</sup> recovery, ferric chloride<sup>27</sup> recovery. With regard to, for example, ferric chloride<sup>27</sup>, the pickling liquor containing ferrous chloride and fortified with sufficient HCl quantity is converted to ferric chloride in the presence of oxygen in a tower at a temperature above 50 °C. The oxygen is introduced at the bottom of the tower and ferrous chloride at the top of the tower. The ferric chloride solution from the tower is subjected to evaporation so as to increase the concentration of the ferric chloride. The resultant concentrate is recycled back into the tower until a concentration of about 40 % by weight of ferric chloride is obtained.

The problems with evaporation and crystallization process are listed below:

- The Fe(II) sulfate recovery offer little promise as a general solution of the problem because of a limited market for the compound.
- The evaporation and condensation processes are very energy intensive and are not amenable to small-scale plant.

The solvent extraction (SX) is a process that consists of transferring a soluble metal from an aqueous to an organic phase. SX can be grouped into three classes, depending on the type of extractant used, basic extractant (quaternary and tertiary amine), neutral extractant [tri-n-octyl phosphine oxide (TOPO) and tri-n-butyl phosphate (TBP)] and acid extractant (CYANEX 272, DEHPA and LIX-84)<sup>28,29,30</sup>. Solvent extraction appears to have great advantages over other methods, especially in terms of process flexibility, and because it allows effluents to be treated over a wide range of metal ion concentrations. On the other hand, the disadvantages of using the SX are the following:

- when using basic extractants such as ALAMINE 336, emulsification occurs.
- among neutral extractants, the use of TBP leads to the formation of the third phase,
- and a high concentration of acidic extractant DEHPA is required to remove iron(III).

As regards to the membrane separation technology<sup>31,32</sup>, it is a physical barrier that allows certain compounds to pass through, depending on their physical and/or chemical properties. The advantages of this method are that it does not use any additional chemical compounds during the process, it is a very compact system easy to automate and control. The main problem with using membranes is their fouling, which limits their application.

Finally, for both SX and the use of membranes, the common problem is that both methods are used to separate metals. The recovery of metals must then take place through secondary processes such as back-extraction, electrodeposition, crystallization, or precipitation.

So far, some of the most common methods for treating SPL have been presented. The treatments listed vary according to the type of SPL to be treated, the quantity, quality, and composition. Some of these methods are no longer used, such as SX, and some others such as crystallization or membrane separation technology, which, although very flexible to various requirements, they are not very suitable for cost and safety reasons. Similarly, evaporation and pyro-hydrolysis are too expensive for the recovery of economically unattractive metals. Others require extensive maintenance, such as those that use membranes. And finally, the neutralization method, which is the most economical, causes large quantities of sludge and problems in its storage. For the above economic and environmental reasons, an alternative based on metal extraction and SPL regeneration through aqueous biphasic systems (ABS) will be proposed.

## 4. Aqueous biphasic system

### 4.1. What is an ABS?

Aqueous biphasic system (ABS) is a liquid-liquid extraction system (LLE), consisting of mixtures of three components, first one being water, and the other two being soluble in water. These components when mixed together provide a phase separation under some particular experimental conditions. After a careful literature investigation, it can be stated that there is no official acronym convention to define an aqueous biphasic system. In this manuscript the abbreviation ABS will be used instead of ATPS (aqueous two-phase system), also widely used in the literature.

Working parameters such as temperature and components' concentration play an important role in the occurrence of phase demixing. Indeed, the variation of these parameters can shift an aqueous

monophasic system (AMS), (where all the components are in the same homogeneous phase), to a aqueous biphasic system (ABS), (where the two phases result to be immiscible in each other and the components will be distributed between an upper and lower phase), and *vice versa* and these changes are perfectly reversible.

In this manuscript, the two components that are responsible and essential for ABS formation, excluding water, will be named biphasic inducers. They can be polymers, ionic liquids (IL), salts or acids, but not all of them provide ABS when mixed together. The biphasic inducers that provide ABS when coupled are polymer A / polymer B, polymer / salt, polymer / IL, IL<sub>A</sub> / IL<sub>B</sub>, IL / salt and IL / acid. Section 4.1.2. of this chapter will be devoted to the definition and description of the polymers and ionic liquid used during the PhD.

In some cases, some additives are added to the three components of an ABS, and these additives have different roles such as promoting ABS formation, changing the working pH, or even facilitating the transition of certain components from one phase to another and sometimes the same additive may play more than one role. In other cases, however, a compound may switch its role during the experiment, i.e. if at the beginning of the experiment this is used as a biphasic inducer, at the end of the experiment the same component may become an additive, depending on its concentration in the system. In fact, in this manuscript, we will refer to additives as those compounds present always in lower concentration in the system than the others. Moreover, in this manuscript, when the additive is used to change the pH, this will be referred to as a pH adjuster, while when the additive is used to promote the repartition of a component from one phase to another, this will be referred to as extracting agent.

As regards the order to present the components in an ABS, the following format will be adopted in this manuscript:

- ❖ Polymer A / polymer B / H<sub>2</sub>O
- ❖ Polymer / salt / H<sub>2</sub>O
- ❖ Polymer / IL / H<sub>2</sub>O
- ❖ IL<sub>A</sub> / IL<sub>B</sub> / H<sub>2</sub>O
- ❖ IL / acid / H<sub>2</sub>O
- ❖ IL / salt / H<sub>2</sub>O

For systems where there will be an additive, for example, an acid, the latter will be inserted in the second place:

- ❖ Polymer / [acid + salt] / water
- ❖ IL / [acid + salt] / water

The square bracket will be used in this manuscript to indicate that the biphasic inducer and additives were prepared in the same synthetic solution or are present in the same industrial solution. In the case where the additional contribution comes from a metal, it will be placed before the salt (or acid) and displayed in this way:

- ❖ Polymer / [Me (n.ox.) + acid (or salt)] / water
- ❖ IL / [Me (n.ox.) + acid (or salt)] / water

where Me (n.ox.) is the metal ion and the corresponding oxidation number.

To simplify the terminology, throughout the manuscript, only the term “ABS” will be used to indicate “three-components ABS” that will provide a phase repartition. In the bibliography, it has also been shown that by increasing the number of components used (e.g. in four-components systems), it is possible to obtain aqueous 3-phase systems (A3PS). A four-component system can consist of polymer / IL / salt / H<sub>2</sub>O. However, the A3PS are out of the scope of this thesis.

In the next section, a historical overview will be presented to show in which sectors ABS have been most widely used, from the oldest to the most recent systems.

#### 4.1.1. A short history of ABS existence and usages

The first ABS dates back to 1896 when Martinus Willem Beijerinck<sup>33</sup> accidentally obtained a biphasic system when mixing starch with gelatine. The ABS, however, found more concrete applications only with the discovery made by Per-Åke Albertsson in 1956, where ABS was used to purify chloroplasts<sup>34</sup>. Since then ABSs has been used mostly for the extraction of different biological compounds such as proteins<sup>35</sup>, DNA<sup>36</sup>, enzymes<sup>37</sup> etc. Therefore, ABS found direct use in the purification and separation of biomolecules for more than 50 years now and in particular the most used systems were those based either on polymer-polymer (PEG-dextran) or polymer-salt (PEG- phosphate, sulfate or citrate salts)<sup>38,39</sup>. In Table 1 are given some examples of ABS studied for extraction and purification of biological molecules.

Type of ABS	Representative examples			
	ABS Composition of	Product	Results	Ref.
Polymer-polymer	PEG-dextran	Chitinase	Successful partitioning of chitinase towards bottom phase	<sup>40</sup>

	PEG-dextran	Metal nanospheres and nanowires and DNA derivatized nanowires	Successful in situ binding Au nanospheres with Au nanowires	<sup>41</sup>
Polymer-salt	PEG-K <sub>2</sub> HPO <sub>4</sub>	B-phycoerythrin	Recovery yield = 90% Purification factor = 4	<sup>42</sup>
	PEG4000 – different sulfate salts + 8.8% NaCl	A-amylase	Purification = 53-fold Purity = 86%	<sup>43</sup>

Table 1. Types of ABS with representative example<sup>39</sup>.

In addition, the scientific community finds interest in ABS not only for the purification and extraction of biological molecules, but also for dealing with solutions coming from the metallurgical industry. Before the arrival of ABS for metal extraction, the most widely used systems were those based on liquid-liquid extraction using organic solvents. The introduction of polymer-based ABS systems for metal extraction represented a big step forward mainly for environmental reasons, as organic solvents have always been a major cause of pollution and health problems. In 1984, Zvarova et al.<sup>44</sup> published the first article on the use of polymer-based ABS for extraction of metals. They obtained a low metal extraction efficiency when the ABS additive-free composed of PEG / (NH<sub>4</sub>)<sub>2</sub>SO<sub>4</sub> / H<sub>2</sub>O was considered, while including additives that vary the pH or increase the extraction efficiency of metals (SCN<sup>-</sup>), they were able to achieve the aim of their investigation. From that moment on, ABS found increasing use in the extraction of metals, not only of the corresponding stable elements but also for their radioactive isotopes<sup>45,46</sup>.

With the arrival of the first ionic liquids in the 1970 (synthesis of pyridinium<sup>47</sup> and imidazolium salts<sup>48</sup>), they quickly started to replace the more polluting organic compounds in liquid-liquid extractions. In particular, it was with the synthesis of protic ionic liquids (PILs) that they found an extensive use in ABS due to their solubility in water<sup>49,50</sup>. However, what was the reason why ionic liquids quickly attracted the interest of the scientific community? To answer this question, it is necessary to go back to the early 2000s. Researchers from all over the world gathered in a round table at a crucial meeting in Crete, based on a NATO-sponsored advanced research seminar entitled 'Green Industrial Applications of ionic liquids'. It was from that moment onwards that ionic liquids were considered 'green' solvents.

As they started to be recognized as more environmentally friendly than organic solvents, ILs became an excellent alternative for obtaining ABS, both for biological processes and for metal extraction. To date there are many studies concerning ionic liquids as necessary constituents of ABS aimed at understanding the behaviour of these new biphasic inducers. Many of these systems are simple ones, with no intention of understanding how these compounds could purify molecules or extract metals<sup>51-52-53-</sup>

<sup>54</sup>. Gutowski et al.<sup>55</sup> demonstrated that the 1-butyl 3-methylimidazolium chloride, [C<sub>4</sub>mim]Cl, a hydrophilic IL, can induce aqueous biphasic systems when contacted with concentrated solutions of the water-structuring salt, K<sub>3</sub>PO<sub>4</sub>, forming an upper IL-rich phase and a lower K<sub>3</sub>PO<sub>4</sub>-rich phase, both of them containing water. It was not until 2007, however, that ionic liquids dominated in ABS for biological molecules. In fact, in 2007, Du *et al.*<sup>56</sup>, for the first time, reported the extraction of protein from human urine by using an IL-based ABS. Meanwhile, systems based on IL / salts / H<sub>2</sub>O have also found use in metal extraction processes<sup>57-49-50-58</sup>. Billard in the “Extraction of Metals with ABS”<sup>59</sup>, in 2016, presented a detailed list of metal ions extracted using IL-based ABS. Table 2 shows a part of the list from the one proposed by Billard where some common transition metals are involved. Billard also mentions systems where additive-free ABS are sufficient to achieve good extraction efficiency for metals, in contrast to the early ABS where additives were required.<sup>44</sup>

Metal, oxidation number	IL-ABS
Ag(I)	[C <sub>1</sub> C <sub>6</sub> im]BF <sub>4</sub> / HNO <sub>3</sub> / NaPF <sub>6</sub> / H <sub>2</sub> O
	[C <sub>1</sub> C <sub>4</sub> im]Cl / HNO <sub>3</sub> / K <sub>2</sub> HPO <sub>4</sub> / H <sub>2</sub> O
Au(III)	[C <sub>1</sub> C <sub>8</sub> im]Cl / HCl / H <sub>2</sub> O
	[C <sub>1</sub> C <sub>8</sub> im]Br / HBr / H <sub>2</sub> O
	[C <sub>8</sub> pyr]Br / HBr / H <sub>2</sub> O
Cd(II)	[TBA]Br / (NH <sub>4</sub> ) <sub>2</sub> SO <sub>4</sub> / H <sub>2</sub> O
Co(II)	Girard-IL / H <sub>2</sub> O
	[P <sub>444</sub> E <sub>i</sub> ][DEHP] / H <sub>2</sub> O (i=1,2,3)
Cr(III)	Girard-IL / H <sub>2</sub> O
Cu(II)	[Hbet][Tf <sub>2</sub> N] / bet / H <sub>2</sub> O
	Girard-IL / H <sub>2</sub> O
	[P <sub>444</sub> E <sub>i</sub> ][DEHP] / H <sub>2</sub> O (i=1,2,3)
Fe(III)	[C <sub>1</sub> C <sub>4</sub> im]FeCl <sub>4</sub> / H <sub>2</sub> O
Ni(II)	[Hbet][Tf <sub>2</sub> N] / bet / H <sub>2</sub> O
	Girard-IL / H <sub>2</sub> O
	[P <sub>444</sub> 14]Cl / NaCl / H <sub>2</sub> O
	[P <sub>444</sub> E <sub>i</sub> ][DEHP] / H <sub>2</sub> O (i=1,2,3)

Table 2. Transition metals with corresponding oxidation number extracted by IL-ABS processes<sup>59</sup>.

Over the years, the environment in which ABS developed has also changed. Since metals are often dissolved in acidic media in the metallurgical industry, various ABS were tested where the salt was replaced by acid. The new acid-based ABS (AcABS) for metal extraction was composed by IL / acid / H<sub>2</sub>O. A pioneering research has been carried out by Coutinho's research group PATH (University of Aveiro) in collaboration with our team, on the understanding of ABS in the presence of ionic liquid in acidic media (HCl, HNO<sub>3</sub> or H<sub>2</sub>SO<sub>4</sub>)<sup>11-12</sup>. This line of research then has developed further into understanding the effect of metal ions on IL-based ABS systems in acidic media, and understanding the mechanism of repartition of these metal ions<sup>13</sup>. Over the past 30 years, ABS systems based on ionic liquids have proven to be an alternative to the more outdated methods based on liquid-liquid extraction using organic solvents, and today it seems that this trend is in continuous development.

#### 4.1.2. Traditional and novel biphasic inducers: polymers and ILs

##### Polymers: PEG and PPG

In chemistry, a polymer is defined as a natural or artificial substance resulting from the spontaneous or induced union (polymerization) of several identical or different molecules (monomers). Depending on the greater or lesser number of structural units that form their molecule, polymers are distinguished into oligomers (dimers, trimers, etc. characterized by Mw < 10 kDa) and high polymers, the latter consisting of molecules (macromolecules) with a molecular weight that can exceed 10<sup>3</sup> kDa. The molecular weight of a polymer<sup>60</sup> is the sum of the atomic weights of the individual atoms that make up a molecule. It indicates the average length of the polymer chains in the bulk resin. All polymer molecules of a particular grade do not have the same molecular weight, and each polymer is characterized by a range or distribution of molecular weights. Depending on the type of polymerization, it is possible to obtain polymers by polyaddition or by polycondensation. Moreover, there are different classes of polymers and they vary according to their use; these include organic polymers such as plastics, inorganic polymers such as silicones, or even conductive polymers that have the electrical properties typical for conductive materials (*Treccani Encyclopedia Italy*)<sup>61</sup>. Among the polymers known to date, the polyether family has been chosen for investigation, in particular polyethylene glycol (PEG) and polypropylene glycol (PPG), since they seem to play a leading role in the metals' repartition.

Polyethylene glycol (PEG) (Figure 18) is part of the poly-ether family. It is synthesized using a ring-opening polymerization of ethylene oxide to produce a broad range of molecular weights (polydispersity). The most common name is polyethylene glycol and is always accompanied by the corresponding molecular weight.

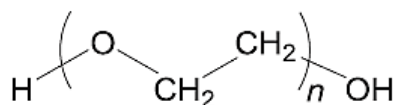


Figure 18. Polyethylene glycol (PEG).

As for polypropylene glycol (PPG) (Figure 2), it is obtained through polymerization processes starting from the monomer of propylene glycol. The main difference between PEG and PPG lies in the presence of an additional tertiary alkyl group (-CH<sub>3</sub>) in the latter. The presence of the alkyl group in the PPG makes the secondary hydroxyl groups of the PPG less reactive than the primary hydroxyl groups of the PEG.

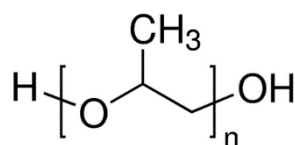


Figure 19. Polypropylene glycol (PPG)

In this manuscript, the polyethylene glycol will always be indicated with the abbreviation PEG followed by the molecular weight (e.g. PEG-400), and the polypropylene glycol will be mentioned with the abbreviation of PPG followed by its molecular weight value (e.g. PPG-425). In this manuscript, PEG and PPG are referred to as polyglycols when they are considered part of the same polymer family.

The solubility of these polymers in water is one of the most attractive parameters. Indeed, PPG and PEG are highly soluble in water, making them very suitable for the use in ABS. In order to understand the solubility of these two compounds in water, it is first necessary to refer to their carbon-oxygen ratio (C/O)<sup>62</sup>, where C represents the alkyl groups, responsible for the hydrophobic character, and O represents the hydroxyl groups and ether groups which favor the creation of hydrogen bonds with water and thus its hydrophilic character. From the repetitive unit of the two polymers, it turns that the C/O ratio of PEG is lower than C/O ratio of PPG. However, this remark only applies to low and equal molecular weights between PEG and PPG. In fact, when the molecular weight of the two compounds increases, despite the fact that the concept of polarity of the hydroxyl groups is always applicable, some secondary effects such as chain interactions or the formation of helical systems, decrease the solubility of these compounds in water<sup>63</sup>.

## 🚦 Ionic liquid: [P<sub>44414</sub>Cl]

Ionic liquids (IL) are salts which melt at 100°C or below. If their melting point is below 25°C, these compounds are called room temperature ionic liquids (RTILs)<sup>64</sup>. The most common cations and some possible anions are given in Figure 20<sup>65</sup>. ILs can be classified in different ways. Apart from the categories RTILs/non-RTILs, they can be divided into two large classes, protic ILs (PILs) and aprotic ones (AILs), based respectively on the presence or absence of an acid proton in the cation. The acid proton gives them good solubility in polar solvents (i.e. water), and thus the polar character<sup>66</sup>. A third classification of ionic liquids is obtained considering the way they are synthesized. Chloroaluminate ILs are part of the first-generation, the more air-stable ILs are part of the second generation, the halogen-free ILs of the third generation and, in the last few years, a biocompatible family of ionic liquids based on choline as a cation and an amino acid as an anion is being developed considerably; this fourth generation seems to be great alternative to the treatment of the biomasses and cellulose extraction<sup>67</sup>.

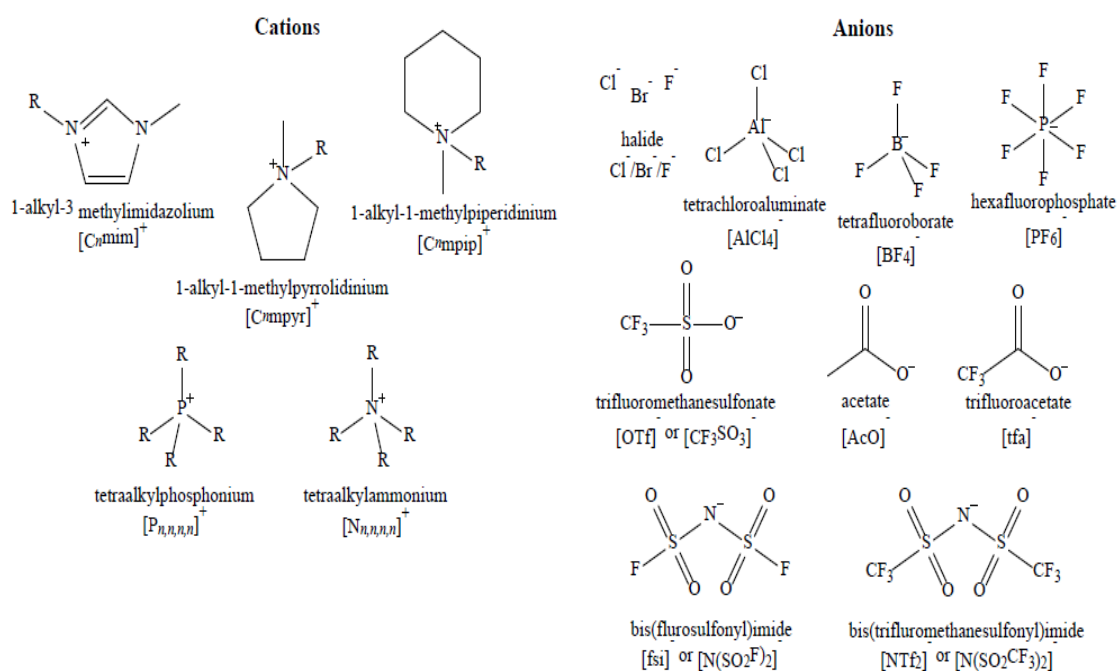


Figure 20. Most common cations and some possible anions in IL<sup>65</sup>.

Ionic liquids are used in different sectors such as: cosmetic, food, petrochemical, renewable energies, and pharmaceutical industries. Several branches of chemistry deal with the use of ionic liquids, from engineering to the use of ionic liquids as solvents and catalysts, from electrochemistry to biological systems<sup>64</sup>. Natalia Plechkova and Kenneth Seddon<sup>64</sup> proposed in 2008 a list of some well-known companies that are using the ionic liquids in their processes; among them, it is possible to find:

- **BASF.** In the BASIL process<sup>68</sup> (Biphasic Acid Scavenging utilizing Ionic Liquids), developed by BASF (Badische Anilin und Soda Fabrik), triethylamine is replaced by 1-methylimidazole, which acts as an acid scavenger. Methylimidazolium chloride is then formed, an ionic liquid with a melting point below the working temperature of the process (80°C).
- **Difasol and DIMERSOL**<sup>69</sup>. The Dimersol process, from which the DIFASOL process is derived, is the conventional technology for the dimerization and oligomerization of light olefins.
- **Degussa**<sup>70</sup>, now part of Evonik Industries, focused on trying to recover spent catalysts to improve purity by using a biphasic reaction mixture where the catalyst was dissolved in an IL. A range of imidazolium- and pyridinium-based ILs with [BF<sub>4</sub>]<sup>-</sup>/[RSO<sub>4</sub>]<sup>-</sup>/[NTf<sub>2</sub>]<sup>-</sup> anions were investigated by Degussa for the process.

The ionic liquid used in the PhD project is the tributyl tetradecyl phosphonium chloride (Figure 21). The choice to work with this IL was based on the promising results my team has achieved in the past few years. In this manuscript, the alpha-numeric form of abbreviation [P<sub>4.4.4.14</sub>] Cl will be adopted to mention the ionic liquid.

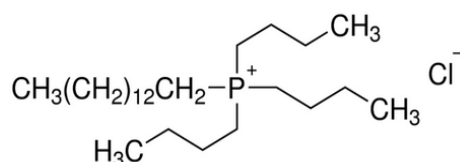


Figure 21. Tributyl-tetradecyl phosphonium chloride, [P<sub>4.4.4.14</sub>] Cl.

It is synthesized using a nucleophilic or electrophilic approach, as shown in Figure 22<sup>71</sup>. This ionic liquid is part of the alkyl tributyl phosphonium halides family, and it was applied for the first time in 1980 for the hydroformylation reaction of olefins in the presence of a ruthenium catalyst<sup>72</sup>.

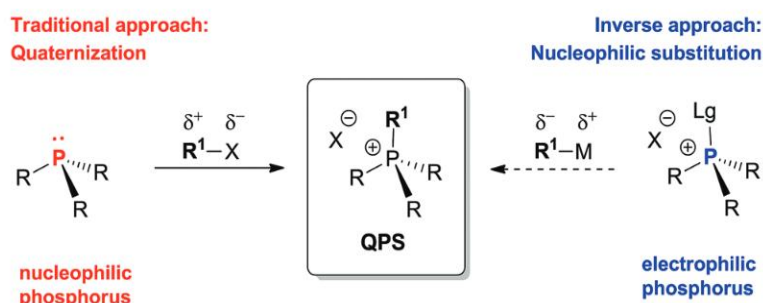


Figure 22. Nucleophilic (red) and electrophilic (blue) approaches to quaternary phosphonium salts (Lg: leaving group)<sup>71</sup>.

### 4.1.3. Graphic representations of ABS

In the literature, ABS are displayed by using phase diagrams<sup>73</sup>, and these are plotted for a given set of parameters. In Figure 23<sup>74</sup> are represented two different graphical displays of ABS composed of polymer / salt / H<sub>2</sub>O ( T = 20 °C). The polymer used is PEG-600 and the salt is Na<sub>2</sub>CO<sub>3</sub>. It will be referred to the representation in Figure 23<sup>74</sup>(a) as a triangular representation and in Figure 23<sup>74</sup>(b) as an orthogonal representation. The phase diagrams provide the same information, it is just a different way of representing data. In particular, the type of graph (b) simplifies the phase diagram of three-components system by only plotting two of three components on orthogonal representation. In both the representation the percentages of the components are expressed through the equation:

(a)  $\text{Component 1 (wt\%)} + \text{Component 2 (wt\%)} + \text{Component 3 (wt\%)} = 100\%$

Where in reference to Figure 23, component 1 is polymer, component 2 is salt, component 3 is water, and weight percentage (wt%) corresponds to 100 w.

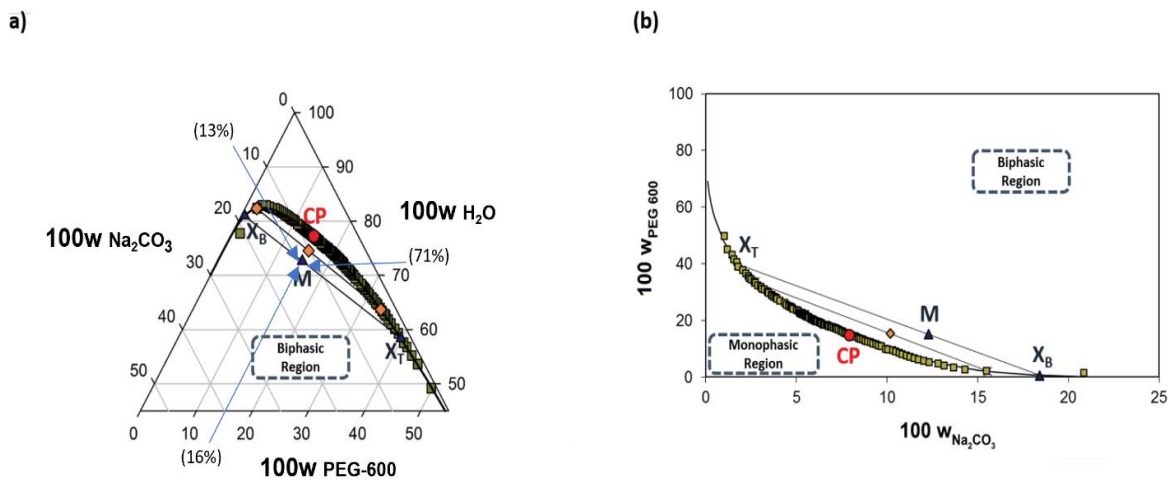


Figure 23. Phase diagram for the ternary system composed of PEG-600/Na<sub>2</sub>CO<sub>3</sub>/H<sub>2</sub>O at 20°C: (a) ternary representation and (b) orthogonal representation. CP=critical point of the diagram. M=random mixture in the biphasic region of the system. X<sub>T</sub>=composition of top phase and X<sub>B</sub>= composition of bottom phase. The labels 100W H<sub>2</sub>O, 100w Na<sub>2</sub>CO<sub>3</sub> and 100w PEG-600 represent the weight fraction percentages of H<sub>2</sub>O, Na<sub>2</sub>CO<sub>3</sub> and PEG-600 respectively<sup>74</sup>.

In this manuscript, the orthogonal representation of the phase diagram will be used instead of the triangular one. The phase diagram is characterized by the biphasic and monophasic areas, the binodal curve and the tie lines. The last two will be described in detail in the following part of this chapter. All these elements represent a graphical display of the experimental results obtained during the investigation on the behavior of a 3-component system (which can be, for example: Polymer / salt / water).

From an experimental point of view, the biphasic and monophasic areas represent, in the orthogonal display, the set of all those experimental points obtained by varying the working temperature and/or

the concentration of a three-components system. If these samples are characterized by one homogeneous phase where all components are dissolved, they will be located in the monophasic area, whereas if the experimental samples exhibit a two phases repartition, they will be located in the biphasic area. Each sample is represented as a point in the phase diagram for which the coordinates correspond to the proportion in the constituting elements of the mix. Furthermore, each point in the biphasic area is to be considered as a single and unique ABS obtained by controlling the working conditions such as the concentration.

When the experimental samples are neither in a homogeneous nor in a solution composed by two liquid phases, but present turbid appearance, these will be presented graphically by the points forming the binodal curve in the phase diagram. Thus, the binodal curve can be referred to as the border that delimits the monophasic and biphasic areas. These points can be collected experimentally through the cloud point titration method, which is the most common method used to date. A large section will be devoted in the next chapter (Materials and Methods) to the description of this method, applied more specifically for the systems investigated in the thesis.

Figure 24 shows a phase diagram according to the orthogonal representation, where on the x-axis is found component 1 and on the y-axis component 2, both expressed in wt%. Component 3 wt% is calculated through equation (a). The phase diagram has been drawn for illustrative purposes only and does not refer to any real experimental data. In the figure it is possible to see in red the binodal curve, which, in this case, has a common shape (where common means the structure that characterize most of the binodal curves presented in the bibliography). To the right of the binodal curve is the biphasic area and to the left the monophasic area. Only two points in Figure 24 were chosen for explanation:

- the point A, in the monophasic area, representing a hypothetical sample where the components are all dissolved, under certain concentration, to give a homogeneous solution (sample A characterized by the green solution in the Figure 24).

- the point B, in the biphasic area, which also represents a hypothetical sample where, under different concentrations from those of point A, two different aqueous solutions (homogeneous) of compound 1 and 2 (soluble) are mixed and a homogeneous solution is not obtained and a phase demixing is observed (sample B characterized by the blue and yellow phases in the Figure 24).

The orthogonal projections of points A and B on the x- and y-axis indicate how these compounds were prepared, i.e. the amount in wt% of component 1 and 2 required to obtain these samples. The missing difference to reach 100% is always in water.

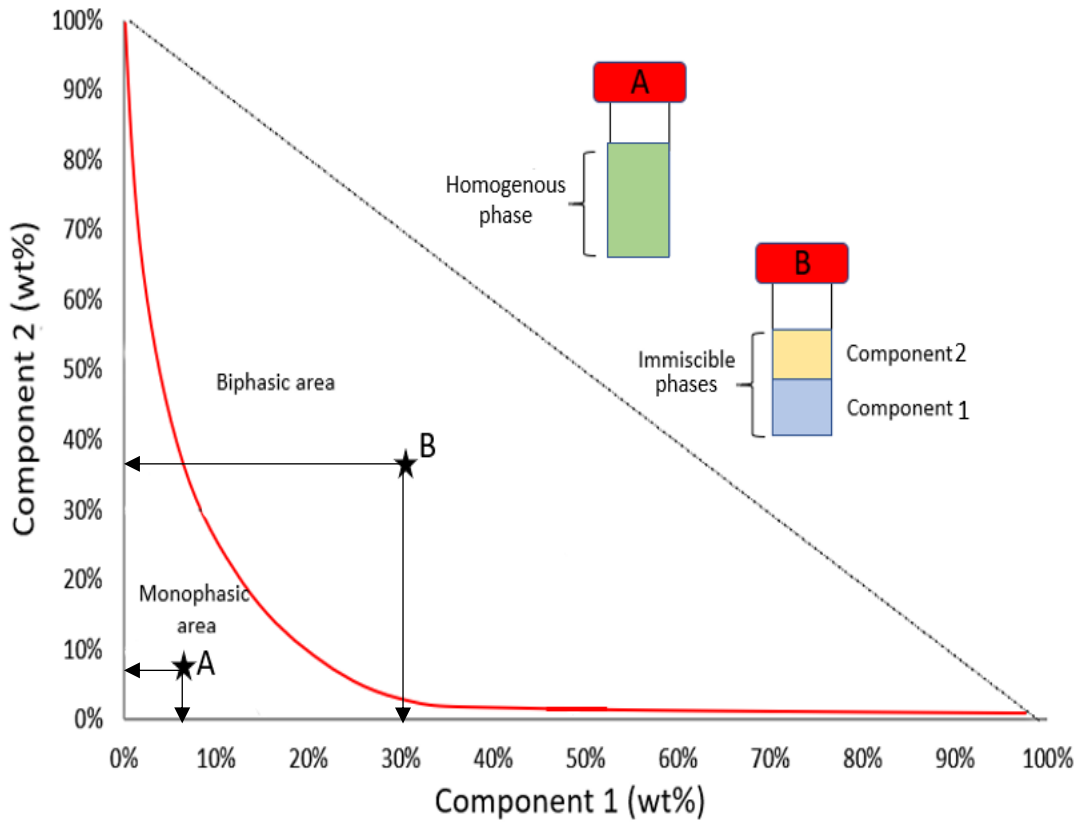


Figure 24. Non-experimental phase diagram, for representative purposes only. The binodal curve is shown in red. Point A located in the monophasic area characterized by a system, point B located in the biphasic area characterized by a two-phase immiscible system. The arrows indicate the initial composition values used to prepare samples A and B. The dotted line indicates the maximum limit of the phase diagram and corresponds to 100 (wt%) of the two components.

One of the best-known equation used to fit a binodal curve via the three-parameter equation is that of Merchuk et al.<sup>75</sup>, initially proposed to describe polymer / salt systems. It was then also applied for polymer / polymer and salt / salt systems.

(b) 
$$Y = A \exp(BX^{0.5} - CX^3)$$

X = Component 1 in wt%

Y = Component 2 in wt%

A, B, C = are constants obtained by the least-squares regression of the experimental binodal data.

In some cases, for example, when the binodal curve is sensitive to the working temperature, the constants are given as a function of the working temperature variation.<sup>76</sup>

Furthermore, for most of systems presented in literature, in the biphasic area it is possible to find the tie lines(TLs)<sup>73,77</sup>. In Figure 25 the tie lines are shown in grey, and each of these represents a group of *n* samples which have in common the same composition in the upper and lower phase but different volume distribution between the two phases. For example, considering the tie line in Figure 25, where

only 3 of the  $n$  experimental samples located on this line have been highlighted, and represented in Figure 25 by the 3 stars, these samples will have the same composition in the two phases and a different volume distribution as showed by the sketches of samples 1, 2, and 3, drawn to the right of the phase diagram. In all the 3 samples the component 2 will be found predominantly in the upper phase while component 1 is predominant in the lower phase.

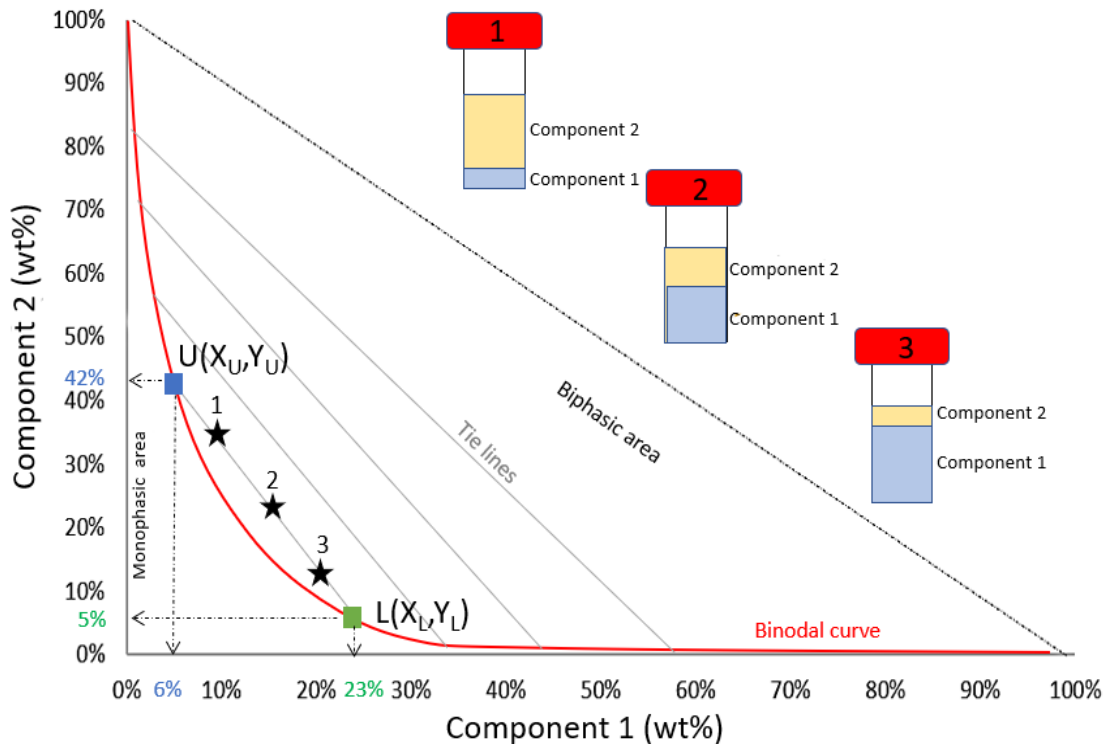


Figure 25. Scheme of an orthogonal ternary phase diagram composed of component 1, component 2, and water (in weight fraction, wt%) and the respective binodal curve (red), tie-lines (grey). Upper phase (component 1-rich phase) is plotted on the y-axis, and lower phase (component 2 rich-phase) is plotted on the x-axis. 1, 2, and 3 (\*) represent total compositions of three mixtures. The final composition of the top and bottom phase is represented by the nodes (▪, ▫) U and L, respectively.

In general, the compositions expressed in wt% of the upper and lower phase of the  $n$  biphasic experimental samples located in the same tie line, are displayed as in Figure 25, by the coordinates of points U and L.

The coordinates of point U:

- on the x-axis ( $X_U$ ), represents the wt% of component 1 in the upper phase,
- on the y-axis ( $Y_U$ ), represents the wt% of component 2 in the upper phase,

and the coordinates of point L:

- on the x-axis ( $X_L$ ) represents the wt% of component 1 in the lower phase,
- on the y-axis ( $Y_L$ ) represents the wt% of component 2 in the lower phase,

of each experimental sample (e.g. 1-2-3 sample in Figure 25) located on the same tie-line.

The most common method for the experimental determination of TLs is the gravimetric one<sup>75</sup> where a point is selected in the phase diagram, through which the TL will pass. The necessary components are then weighed and mixed thoroughly. The mixture is left at controlled temperature in a decanter overnight, and then the two fractions are weighed. Calling M, U and L the points representing the initial mixture, the upper phase and the lower phase, respectively, X the weight fraction of component 1 and Y the weight fraction of component 2, according to the Merchuk's empirical equation theory<sup>75</sup> the following mass balance equations can be written:

$$(c) \quad Y_U = \frac{Y_M}{a} - \frac{1-a}{a} Y_L$$

$$(d) \quad X_U = \frac{X_M}{a} - \frac{1-a}{a} X_L$$

$$(e) \quad Y_U = A \exp(BX_U^{0.5} - CX_U^3) = f(X_U)$$

$$(f) \quad Y_L = A \exp(BX_L^{0.5} - CX_L^3) = f(X_L)$$

where  $f(X)$  is a function of the binodal curve (presented in (b)), and  $a$  is the ratio between the weight of the upper phase on the weight of the mixture.

From the system of equations (c)-(f), is possible to derive the equation of TLs, as follows:

$$(g) \quad Y = Y_0 - (STL)X$$

Where STL is the absolute value of the slope of the tie line and is given by eq. (h) and  $Y_0$  is the point corresponding to  $X = 0$ .

$$(h) \quad STL = \frac{(Y_U - Y_L)}{(X_U - X_L)}$$

The STL can be expressed as a function of other variables, such as the tie line length (TLL). The TLL can be calculated using the following equation:

$$(i) \quad TLL = \sqrt{(X_U - X_L)^2 + (Y_U - Y_L)^2}$$

Furthermore, considering the tie line of point 1 (star 1 in the graph in Figure 25), this corresponds to segment UL and the ratio of the lengths of segments 1L and 1U corresponds to the upper and lower phase ratio (in wt%) as shown in the following equation:

$$(l) \quad \frac{m_U}{m_L} = \frac{V_U \rho_U}{V_L \rho_L} = \frac{1L}{1U}$$

where  $m$ ,  $V$ , and  $\rho$  are the masses, volumes, and densities of the upper (U) and lower (L) phases. If the phase densities are known, the volume ratio of the phases can be determined.

Another equation that has been used in the literature<sup>78</sup> to fit experimental data and obtain a binodal curve is the Setschenow's equation. It relates the solubility of the non-electrolyte in the presence ( $S$ ) and absence ( $S_0$ ) of salt to the salt concentration ( $C_S$ ) as:

$$(m) \quad \log \frac{S}{S_0} = K_S C_S$$

$K_S$  is the constant of Setschenow<sup>78</sup>.

In fact, according to Ananthapadmanabhan and Goddard<sup>79</sup> phase separation in aqueous polymer-salt systems may be viewed as the phenomenon related to the effect of an electrolyte on the solubility of a nonelectrolyte, i.e., known as the "salting-out" phenomenon.

This has been shown to be valid for several polymer/salt systems. However, Zaslavsky *et al.*<sup>80</sup> have shown that in some cases the equation does not fit perfectly with the experimental values and the binodal curve obtained. In particular, for the system analyzed by Zaslavsky and co-workers<sup>80</sup>, consisting of PEG-  $(\text{NH}_4)_2\text{SO}_4$ -  $\text{H}_2\text{O}$ , the binodal curve considered divided into three parts: a branch corresponding to the PEG-rich phase, a branch corresponding to the salt-rich phase, and a central part. They<sup>80</sup> thus showed that the Setschenow's equation reflected the curve obtained in the two extreme branches but not in the central part.

Both Merchuk's and Setschenow's equations are accepted when the experimental error is negligible or null. In addition, nowadays many mathematical models result to be good alternatives to these equations and, above all, both Merchuk's and Setschenow's equations have not been tested for binodal curves with different structure from the common ones. Some of these uncommon binodal curves will be presented in the section 4.1.5 of this chapter.

#### 4.1.4. *Coexisting solid and liquid phases in the biphasic area of the phase diagram*

As mentioned in the previous paragraph, a phase diagram is composed of a binodal curve where on the left there is the monophasic area and to the right the biphasic one. The biphasic area considered so far consists of samples characterized by a two liquids phase partition. In some cases, however, there are also areas on the phase diagram that do not exhibit a two liquid phase repartition where the formation of an additional phase can take place, e.g., a sample composed by liquid 1 + liquid 2 + a solid

(1L + 2L + S). Since the interest of the scientific community is to investigate the repartition of the components of an ABS into two liquid phases, the formation of a solid phase has not particularly attracted their interest. It is mainly for this reason that the systems such as (1L + 2L + S), although they have been known for a long time, have not been much investigated. In the following lines, two articles dealing with the investigation of these areas will be presented.

Back in 1994, Cheluget *et al.*<sup>81</sup> presented the coexistence of the liquid and solid phases in the biphasic area of system composed of PPG-425 / NaCl / H<sub>2</sub>O (T=25°C). As can be seen in the orthogonal representation in Figure 26, to the left of the binodal curve, it is possible to see one liquid phase (A) and therefore the monophasic part of the phase diagram. To the right of the binodal curve two liquid phases (B) are presented, and this corresponds to the biphasic area of the system. When the mass percentages (mass%) of the salt begin to increase more than about 26%, Cheluget and co-workers noticed the coexistence of a solid phase and a liquid phase (C).

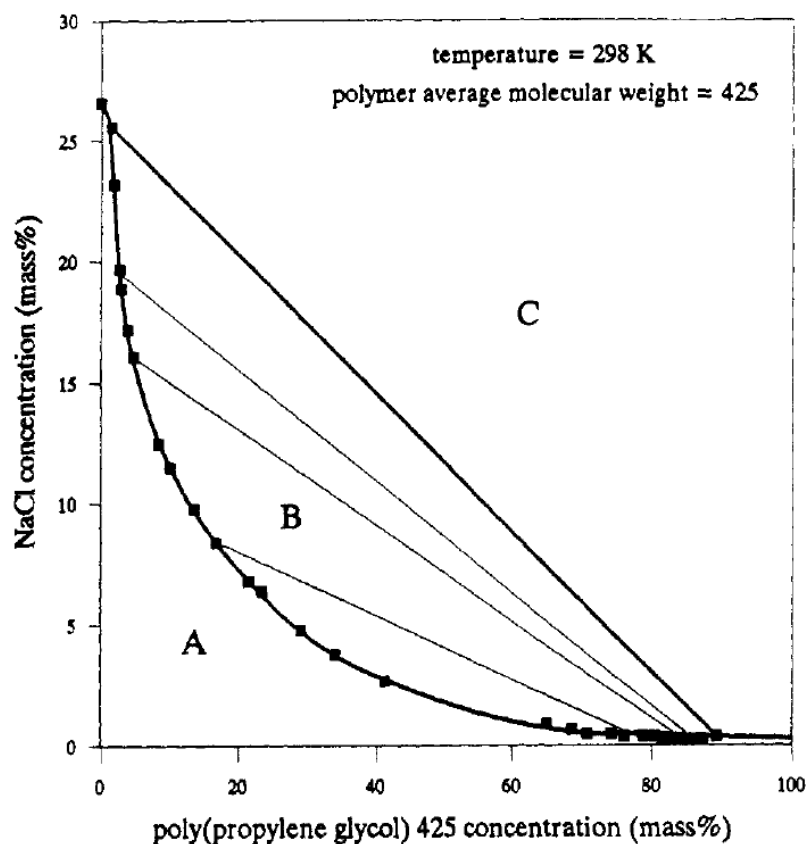


Figure 26. Phase diagram of PPG 425 + NaCl + water at 25 °C. A) one liquid phase, B) two liquid phases and C) one liquid phase and one solid phase<sup>81</sup>.

More recently in 2001, Toboada *et al.*<sup>82</sup> published a phase diagram and the corresponding binodal curve for the system PEG-4000/Na<sub>2</sub>SO<sub>4</sub>/H<sub>2</sub>O showing that on the right of the binodal curve, the phase diagram is characterized by areas with more than 2 liquids. In the phase diagram presented in Figure

27<sup>82</sup> the x-axis corresponds to PEG-4000 ( $W_3$ ) and the y-axis to  $\text{Na}_2\text{SO}_4$  salt ( $W_1$ ). Between 0 and 10  $W_1$  of  $\text{Na}_2\text{SO}_4$  and 0 and 60  $W_3$  of PEG-4000 the system is monophasic (L). In the same polymer range but increasing the salt concentration (between 10-35  $W_1$ ) the system turns biphasic (L+L). Keeping the polymer range constant (between 0-60  $W_3$ ) and by increasing the salt concentration to a  $W_1$  between 35 and 100 results in a solid phase, which Taboada et al. identify as  $\text{Na}_2\text{SO}_4$  salt, and two liquid phases (S+L+L). The system becomes more complex when the concentration of PEG-4000 exceeds  $W_3$  values greater than 60. In this case, the formation of the solid (or crystalline) phase may be due to competition in attracting water between the polymer and the salt. Water is the main component in each phase and the dissolved components have high affinity for it. Although PEG-4000, used by Taboada and co-workers, is more hydrophobic than the PEG-400 used in my investigation, the former has affinity for the aqueous medium too. If the inorganic phase is depleted in water, the salt concentration will increase causing direct precipitation of the salt.

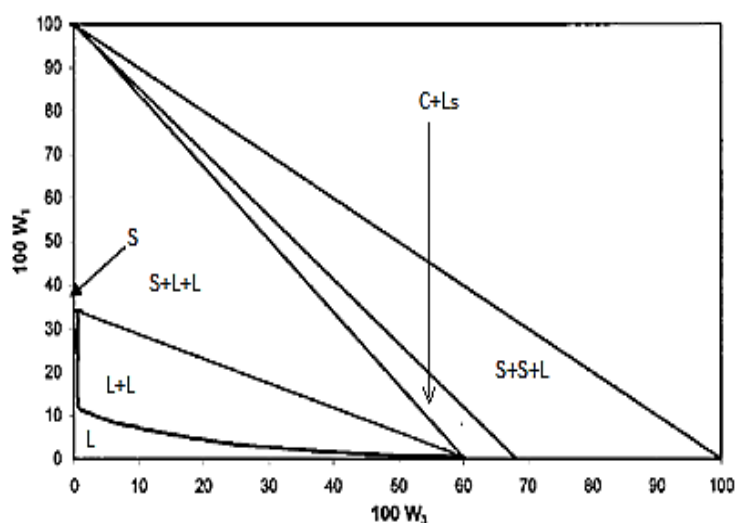


Figure 27. Phase diagram for  $\text{Na}_2\text{SO}_4$  (1) +  $\text{H}_2\text{O}$  (2) + PEG-4000 (3) at 25°C. S= solid, L=liquid, C=crystal, Ls=liquid saturated<sup>82</sup>.

#### 4.1.5. Parameters influencing the formation and component repartition in ABS

The researcher's interest in working with ABS lies mainly in the investigation on the biphasic area rather than the monophasic one, because as soon as a biphasic sample is formed, the components that constitute the sample will distribute between the upper and lower phase, as may also be the case when solutions containing several metals are considered. Therefore, the aim of the researcher is to obtain, by varying the working conditions of the system, the largest possible number of biphasic experimental samples. Graphically speaking this means increasing the number of experimental points in the biphasic area, thus enlarging the biphasic area, and moving the binodal curve closer to the axes.

Experimentally speaking, increasing the biphasic area means turning some of the monophasic samples into biphasic ones, as in many cases these systems are reversible. Finally, the larger the biphasic area is, the smaller the quantity of the components needed to obtain the ABS will be. The range of concentration where the phase demixing appears can be enlarged by varying certain parameters, such as those illustrated by the Figure 28.

Figure 28 (a) shows the binodal curves obtained by Schaeffer *et al.*<sup>83</sup> for the [P<sub>4.4.4.14</sub>]Cl / salts / H<sub>2</sub>O systems at 25°C. In the phase diagram, it is shown how by varying the cation of the chloride salt used, the binodal curve changes the position at fixed temperature. The researchers showed that considering the dotted line in Figure 28 (a) which corresponds to [P<sub>4.4.4.14</sub>]Cl = 15 wt%, the ability of the selected salts to induce phase separation at 25°C follows this trend: CaCl<sub>2</sub> > NaCl > KCl > MgCl<sub>2</sub> > CsCl > LiCl, according to the Hofmeister series for cations. The Hofmeister series or lyotropic series is a classification of ions in order of their ability to salt out or salt in proteins.<sup>84</sup> The salting-out and salting-in effect is related to the solubility of the components (i.e. proteins).

Figure 28 (b) shows the impact of temperature on ABS consisting of PEG-PPG / Na<sub>2</sub>SO<sub>4</sub> / H<sub>2</sub>O. The article published by Das *et al.*<sup>85</sup> shows how the binodal curve moves to the left of the phase diagram when the working temperature is increased (from 20 to 37 °C). This observation is explained by the researchers on the basis of the fact that, by increasing the temperature, the copolymer becomes more hydrophobic, and the salting-out effect of the salt becomes more pronounced.

Figure 28 (c) shows the impact of pH on ABS consisting of [N<sub>4,4,4,4</sub>]Br / C<sub>6</sub>H<sub>5</sub>K<sub>3</sub>O<sub>7</sub>/C<sub>6</sub>H<sub>8</sub>O<sub>7</sub> / H<sub>2</sub>O at T=25 °C, (C<sub>6</sub>H<sub>5</sub>K<sub>3</sub>O<sub>7</sub> is potassium citrate and C<sub>6</sub>H<sub>8</sub>O<sub>7</sub> is citric acid). The aim of the investigation proposed by Sintra *et al.*<sup>51</sup> is to understand the influence of parameters such as pH on the above system in order to be able to use it in purification processes of biological molecules. The researchers demonstrated that by passing from pH 5 to 8, the number of biphasic samples increases and therefore the biphasic area in the phase diagram.

Finally, Figure 28 (d) shows the research carried out by Ventura *et al.*<sup>86</sup>, where the impact of the length of the alkyl chain in the ionic liquid cation on the phase separation is investigated. The ABS analyzed by Ventura *et al.* consists of [1-C<sub>n</sub>-3-C<sub>1</sub>im] Cl / K<sub>2</sub>HPO<sub>4</sub> / H<sub>2</sub>O at T=25°C. Figure 28 (d) then shows ABS composed of three different imidazolium-based ILs and the inorganic salt K<sub>2</sub>HPO<sub>4</sub>. The system proposed by Ventura *et al.* shows that the increase in the aliphatic chain of the cation from C2 to C6 leads to an increase in the apparition of phase demixing due to the increase in hydrophobicity of the IL.

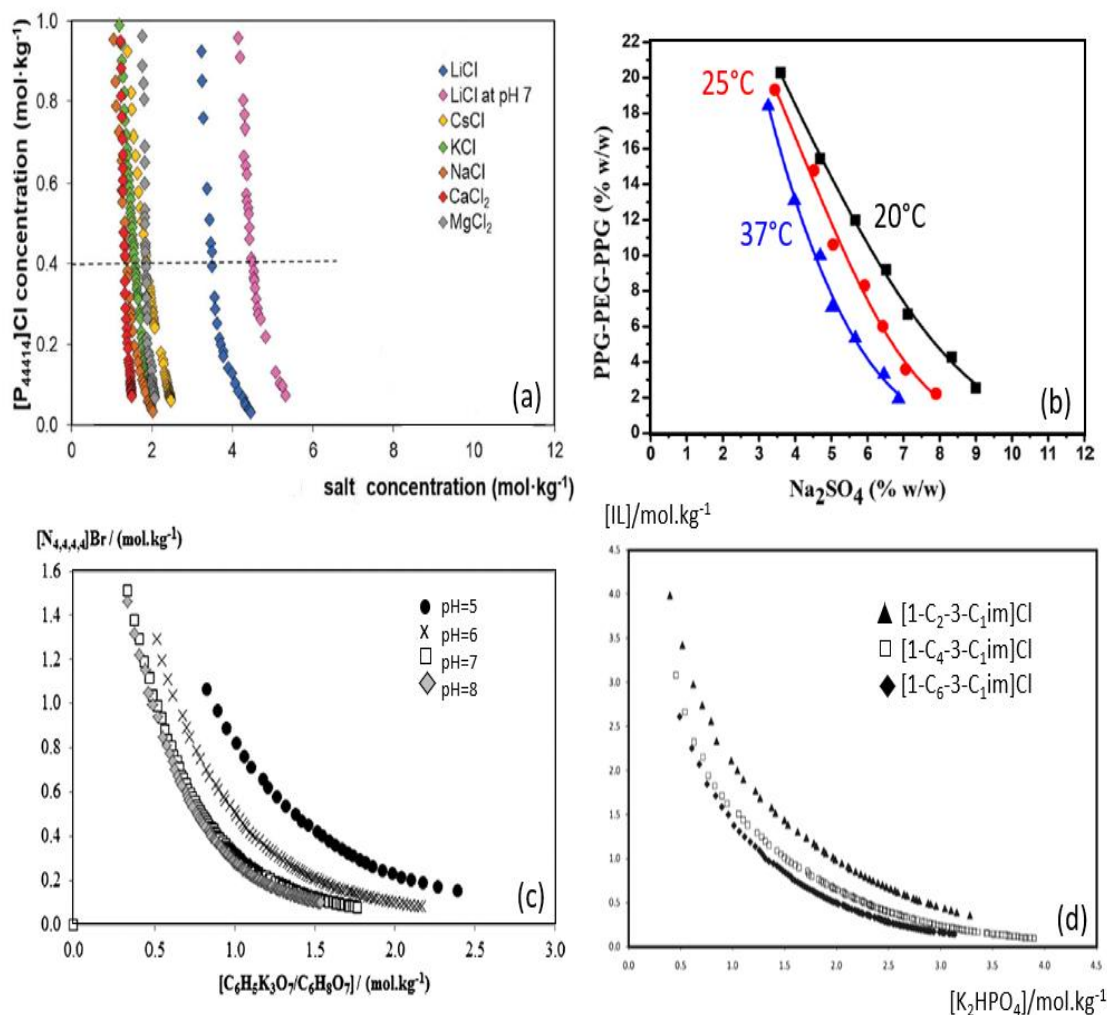


Figure 28. Different binodal curves that illustrated the effect of various parameters on the ability of phase demixing 83,85, 51, 86.

Not only the position, but the shape of the binodal curves can also be affected by the variation of working conditions such as pH, salt concentration and temperature. In the phase diagrams presented in Figure 29, some binodal curves with uncommon shape are compared to a binodal curve with common shape, where common shape means the shape most frequently found in the literature.

Figure 29 (a) and (b) belong to the investigation carried out by Neves *et al.*<sup>14</sup> from CICECO group (Portugal). They showed that the binodal curve of an IL /  $K_3PO_4$  /  $H_2O$  system at 25 °C, can change its shape when different chain lengths of the ionic liquid are considered. In particular, in Figure 29 (a) Neves *et al.*<sup>14</sup> obtained the binodal curve considering a system composed of  $[C_4mim]Cl$  /  $K_3PO_4$  /  $H_2O$  at 25 °C, while the curve displays an unusual shoulder shape when the considered systems are  $[im]Cl$  /  $K_3PO_4$  /  $H_2O$  ( $\diamond$ ),  $[C_1im]Cl$  /  $K_3PO_4$  /  $H_2O$  ( $\square$ ),  $[C_2im]Cl$  /  $K_3PO_4$  /  $H_2O$  (x) at 25 °C. They<sup>14</sup> thus demonstrated that changing the type of cation in the ionic liquid not only changes the position of the binodal curve but also its shape.

Figure 29(c), Tome *et al.*<sup>15</sup> proposed the phase diagram for ABS consisting of PEG 1500 / [C<sub>4</sub>mim]Cl / H<sub>2</sub>O at 50 (red) and 60 °C (black). The particular shape of this binodal curve was named "0" type. They showed that the two-phase regime of PEG-IL-based ABS decreases with increasing temperature, i.e. lower temperatures are favorable for biphasic formation. They finally stated that the formation of PEG-IL-based ABS is controlled by the solvation of the IL anion by water, which leads to the destruction of the hydrogen bonds established between the IL anion and the hydroxyl groups of the polymer.

Figure 29(d) shows the binodal curves for ABS composed of PPG400 / salt / H<sub>2</sub>O obtained from the research work of Sedeghi *et al.*<sup>87</sup> They showed that for these systems the binodal curve is different from the most common one displayed in Figure 29 (a) and the biphasic area outlined by the curves increases depending on the salt chosen according to this trend:

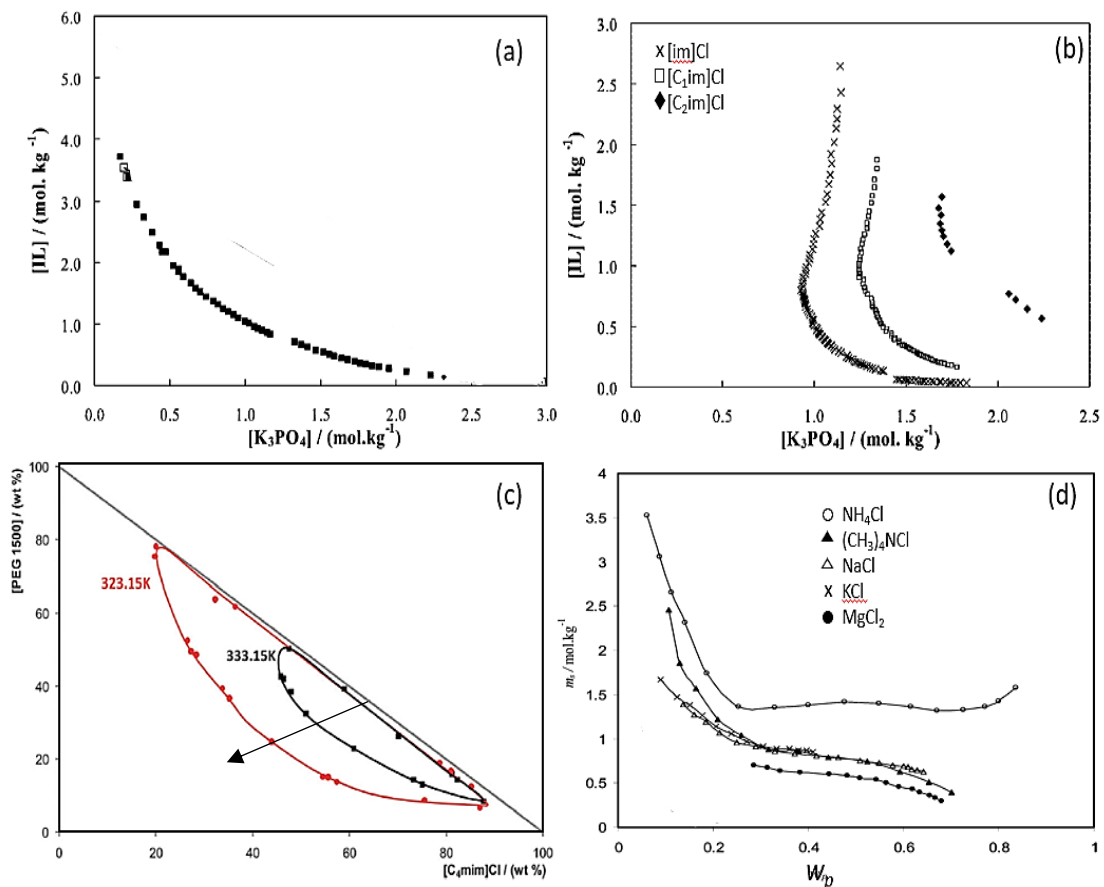
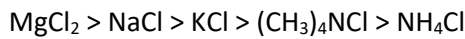


Figure 29. Different binodal curves from bibliography. The arrow in figure c indicates the decrease in temperature in the system.<sup>14,15,87</sup>

In conclusion, it can therefore be stated that by varying certain working conditions such as pH or temperature, it is possible to favour the phase demixing of different systems and thus extend the biphasic area of investigation.

## 4.2. Metal repartition in polymer and IL-based ABS

In this thesis, the investigation focused mainly on the repartition of metals in ABS. Two types of ABS were considered, those based on polymers and those based on ionic liquids. In the next section, a selection of articles will be presented in order to understand the mechanism behind the metal partitioning processes.

### 4.2.1. Polyglycol-based ABS.

Among the polymers known to date, the polyether family, in particular PEG and PPG, seems to play a leading role in the metal extraction in the ABS. In Table 3, is showed a list of publications in chronological order of ABS consisting of polymer/salt/H<sub>2</sub>O tested for metal extraction and in the following lines, will be presented the metals extraction mechanisms proposed by the various researchers.

Date of publication	System	Aim	First author and University	Ref.
1996	PEG-2000 / metals & salts / H <sub>2</sub> O	Partitioning behaviour of metals in polymer-based ABS	<i>R. D. Rogers and S. T. Griffin, USA.</i>	<sup>6</sup>
2000	PEG-2000 / (NH <sub>4</sub> ) <sub>2</sub> SO <sub>4</sub> / Na <sub>2</sub> CrO <sub>4</sub> / H <sub>2</sub> O	Recovery of Cr(III)	<i>H. F. Koch from Texas Tech University, USA.</i>	<sup>7</sup>
2007	PEG-1550 / (NH <sub>4</sub> ) <sub>2</sub> SO <sub>4</sub> / cadmium iodide / H <sub>2</sub> O	Extraction of Cd(II)	<i>L. Bulgariu from Technical University of Romania.</i>	<sup>8</sup>
2009	L35 / Li <sub>2</sub> SO <sub>4</sub> / Ni–Cd batteries leachate / H <sub>2</sub> O	Separation of Cd(II) and Ni(II)	<i>V. C. Lacerda from Grupo de Química Verde Coloidal, Brazil</i>	<sup>88</sup>
2011	L35 (or PEO-1500) / (NH <sub>4</sub> ) <sub>2</sub> SO <sub>4</sub> (or Li <sub>2</sub> SO <sub>4</sub> ) / chloride salt of Fe(III), Co(II) / Ni(II) / H <sub>2</sub> O	Selective extraction of Fe(III), Co(II) and Ni(II)	<i>P. da R. Patrício from Grupo de Química Verde Coloidal e Macromolecular, Brazil.</i>	<sup>89</sup>

2013	PEG-1500 / (NH <sub>4</sub> ) <sub>2</sub> SO <sub>4</sub> (or Na <sub>2</sub> SO <sub>4</sub> ) / sulfatesalts of Hg(II), Cd(II), Zn(II) / H <sub>2</sub> O	Selective extraction of Hg(II), Cd(II), Zn(II)	<i>L. Bulgariu from Technical University of Romania.</i>	<sup>90</sup>
2016	L64 (or PEO-1500) / electrolyte (sulfatebased) / metallic chromium / K <sub>2</sub> Cr <sub>2</sub> O <sub>7</sub> / H <sub>2</sub> O	Chromium speciation	<i>P. da R. Patrício from Grupo de Química Verde Coloidal e Macromolecular, Brazil.</i>	<sup>91</sup>
2016	PEG-400 / Na <sub>2</sub> SO <sub>4</sub> / K <sub>2</sub> Cr <sub>2</sub> O <sub>7</sub> / H <sub>2</sub> O	Recovery of Cr(III)	<i>J. Liu from Chinese Academy of Sciences</i>	<sup>92</sup>
2017	PEG-6000 / Na <sub>2</sub> CO <sub>3</sub> / nitrate salts of Co(II), Zn(II) / chloride salt of Hg(II) / H <sub>2</sub> O	Selective extraction of Hg(II), Co(II), Zn(II)	<i>A. Hamta from Thermodynamics Research Laboratory, Iran</i>	<sup>93</sup>
2017	L64 (or PEO-1500) / Ni-MH battery leachate / electrolyte / H <sub>2</sub> O	Extraction of La	<i>W. C. M. de Oliveira from Departamento de Química, FACET, Brazil</i>	<sup>94</sup>
2018	PEG(1000/2000/4000) / Na <sub>2</sub> SO <sub>4</sub> / Na <sub>2</sub> MoO <sub>4</sub> / H <sub>2</sub> O	Extraction of Mo(VI)	<i>P. Wang from School of environmental and chemical engineering, China.</i>	<sup>9</sup>
2018	PEG-400 / Na <sub>2</sub> SO <sub>4</sub> / Cr(VI) / H <sub>2</sub> O	Cr(VI) repartition in polymeric phase	<i>P. Sun from Chinese Academy of Sciences</i>	<sup>16</sup>
2019	PEG and PPG / CuSO <sub>4</sub> / Re / Mo / H <sub>2</sub> O	Selective extraction of Mo and Re, and Mo stripping	<i>L. Muruchi from Universidad de Antofagasta Chile and CICECO Portugal.</i>	<sup>10</sup>
2019	(PPG-PEG-PPG) / Na <sub>2</sub> SO <sub>4</sub> / Mo / H <sub>2</sub> O	Extraction of Mo and regeneration of tri-block polymer	<i>L. Das from Department of Chemistry- Calcutta, India</i>	<sup>95</sup>

Table 3. List of ABS, in order of date of publication, used for metal ions extraction. L35 is the tri-block polymer: EO-PO-EO, Mw=1900; L64 is the tri-block polymer PPO-PEO-PPO, Mw= 2900.

One of the first research group to use polymers for metal extraction through ABS was the one of Robin D. Rogers and co-workers<sup>6</sup>. They<sup>6</sup> investigated the separation of Tc, Th, Cd and Pb by using ABS

composed of polymer / salt / H<sub>2</sub>O, specifying the existence of three different mechanisms at work: (1) partitioning by the PEG-rich phase alone; (2) extraction of anionic metal complexes; and (3) extraction using a water soluble complexant agent. The polymer considered in their investigation is PEG-2000 and the metals to be extracted are Cd, Tc, Th, Pb.

- In the first mechanism, Rogers and co-workers showed that Tc is successfully extracted when using ABS consisting of PEG-2000 / sulfate salts / H<sub>2</sub>O. Furthermore, in their paper it is shown that by using sodium sulfate, the repartition of Tc in the polymer phase is more efficient than by using ammonium sulfate. Rogers and co-workers identified that the main reason for this variation is due to the ability of sodium sulfate to have a higher salting-out capacity than ammonium salt. From the values of  $\Delta G_{\text{Hyd}}$  collected in the bibliography by Rogers' group, it appears that sodium sulfate has higher values of  $\Delta G_{\text{Hyd}}$  and therefore it can be confirmed that it has a greater salting-out effect than the other sulfate salts considered.
- In the second extraction mechanism proposed, it has been shown that soft metals with high formation constants of halide complexes can be partitioned from an aqueous to a polymeric phase. In particular, the extraction refers to Cd<sup>2+</sup> and Pb<sup>2+</sup> while the halides considered as extractants are Cl<sup>-</sup>, Br<sup>-</sup> and I<sup>-</sup>. They state that the larger the halides, the greater its polarizability and therefore the stronger the complexation with soft metals. Therefore, Rogers et al. observe an increase in the distribution ratio ( $D_M$ ) by considering the following trend of the halide's contribution Cl<sup>-</sup><Br<sup>-</sup><I<sup>-</sup>. Moreover, the  $D_M$  of Cd<sup>2+</sup> is always greater than  $D_M$  of Pb<sup>2+</sup> in Rogers' experiments. The species that is extracted from the polymer in these experiments is MX<sub>4</sub><sup>2-</sup> (M=metal, X=halide).
- The third category of extraction involves hard metals. They used water-soluble ligands to extract them. The task of the ligand is to give a sphere of hydrophobicity to the metal species to be extracted, and it is through the formation of this new complex that the metal can pass into the polymeric phase, the most hydrophobic phase of the system.

Koch *et al.*<sup>7</sup> used PEG as a medium for the phase transfer and recovery of chromium from aqueous salt solutions. They demonstrated that it was possible to transfer Cr(VI) from a polymer solution containing PEG-2000 to an aqueous phase and *vice versa*. The working pH is between 6 and 8 and the temperature is not defined in the article. They proposed two mechanisms, the proton switch, and the redox switch. They refer to the mechanism based on the proton switch for the process that used ammonia to move Cr(VI) from the polymer phase to the aqueous phase, and for the process that has used carbon dioxide to return Cr(VI) to the polymer phase. While it refers to the redox switch method when it uses iron(II) sulfate to reduce Cr(VI) to Cr(III), and the latter passes into the aqueous phase. They also observed that after the reduction process, the polymer is degraded by oxidation. Koch *et al.*<sup>7</sup>

state that this mechanism for the phase transfer and recovery of chromium is related to the fact that PEG is to be regarded as a crown ether open chain, and thus exploits the complexing properties with metal ions of Group 1 of the periodic table typical of crown ethers. In addition, they assert that PEG has a sequence of oxygen ether functionalities available for hydrogen bonding with the oxo groups of Cr(VI) anions, or for coordination with alkali metal cations in the  $\text{Na}_2\text{CrO}_4$  or  $\text{K}_2\text{Cr}_2\text{O}_7$  salts.

Bulgariu *et al.*<sup>8</sup> demonstrated the extraction of Cd(II) with iodide species (such as NaI) using an ABS composed of PEG-1550/ammonium sulfate/ $\text{H}_2\text{O}$ , considering a pH range between 2 and 7. They acknowledge that the acidity brought by the ammonium sulfate does not cause protonation of the oxygens present in the ether groups of the polymer but is nevertheless responsible for the decrease in water content in the polymer phase. They also state that the "fixation" of the metal in the polymer phase occurs through specific interactions that depend on the metallic species present in solution and the polymer and this is related to pH. The mechanism described by Bulgariu and co-workers is based on the degree of hydration of the different Cd(II)-iodide species formed in the pH range considered. More exactly, they recognise the formation of 3 predominant species:  $\text{CdI}_4^{2-}$  (pH=2.05),  $\text{CdI}_2$  (pH=4.53) and  $\text{CdI}^+$  (pH=7.12), which will have a degree of extraction respectively of: 99.17%, 89.39% and 34.43% in the polymer phase. In Figure 30, Bulgariu et al. precisely propose the mechanism for the extraction of the neutral or anionic species, where in the first case  $\text{CdI}_2$  is trapped between two polymer chains, while in the second case  $\text{CdI}_4^{2-}$  is 'fixed' to the positively charged oxygen in the ether groups of the PEG.

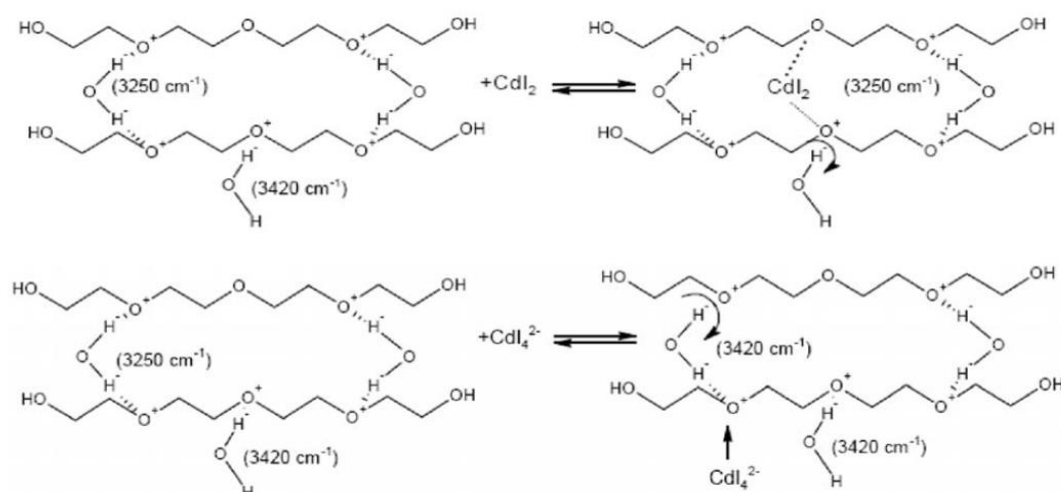


Figure 30. Mechanism proposed by Bulgariu for the extraction of the neutral species (top) and the anionic species (bottom) of Cd(II)-iodide in the PEG phase<sup>8</sup>.

Patricio *et al.*<sup>89</sup> studied the extraction behavior of the metal ions Co(II), Fe(III) and Ni(II) as a function of the amount of potassium thiocyanate used as extraction agent, using the following aqueous biphasic systems: PEO /  $(\text{NH}_4)_2\text{SO}_4$  /  $\text{H}_2\text{O}$ , PEO /  $\text{Li}_2\text{SO}_4$  /  $\text{H}_2\text{O}$ , L35 /  $(\text{NH}_4)_2\text{SO}_4$  /  $\text{H}_2\text{O}$  and L35 /  $(\text{Li})_2\text{SO}_4$  /  $\text{H}_2\text{O}$ . PEO is a polymer in the PEG class that has a molecular weight over 100,000 g/mol. They used the

triblock copolymer L35, HO-(EO)<sub>11</sub>(PO)<sub>16</sub>(EO)<sub>11</sub>-H, with an average molar mass (MM) of 1900 g/mol, or with poly (ethylene oxide) (PEO1500), with MM = 1500 g.mol<sup>-1</sup> for ABS formation. The investigation was carried out considering 4 working pH: 1.0, 1.5, 2.0, 4.0. The maximum extraction percentages obtained by Patricio and co-workers are: Co(II) (99.8%), Fe(III) (12.7%) and Ni(II) (3.17%) when the ABS was composed of PEO-1500 / (NH<sub>4</sub>)<sub>2</sub>SO<sub>4</sub> / H<sub>2</sub>O containing 1.4 mmol of KSCN at pH 4.0. Whereas, when the same ABS was used at pH 2.0, the maximum extraction percentages for iron and nickel were 99.5% and 4.34%, respectively, while for Co(II) it remained constant at (99.8%). The researchers then tried to find out what extraction mechanism was involved in their systems. It would appear that the thiocyanate ions form anionic complexes with Co(II). It is known that such complexes do not form easily in aqueous solution and therefore, they move to the upper phase of the system, which corresponds to the more hydrophobic phase and where the copolymer is present. In fact, according to Patricio *et al.*, it is precisely because of the hydrophobic and hydrophilic character of the two phases that this extraction mechanism is achieved. Furthermore, the difference in PEO1500 and L35 behavior is associated with the higher hydrophobicity of the copolymer macromolecule, which has propylene oxide (PO) units on its chain. Patricio and colleagues then add that, even though the macromolecules are solvated in the aqueous medium, there is less interaction between the PO units and the water molecules, thus favoring the intermolecular interactions of the PO units themselves, showing that this is the result of the so-called hydrophobic effect.

Wang *et al.*<sup>9</sup> analyzed the PEG(1000/2000/4000) / [Na<sub>2</sub>MoO<sub>4</sub> + Na<sub>2</sub>SO<sub>4</sub>]/ / H<sub>2</sub>O system without the addition of extractants, showing that the degree of molybdenum extraction varied according to the amount of polymer, sodium sulfate, molybdenum and temperature. In particular, they showed that the extraction increased as the concentration of sodium sulfate increased due to hydration of the latter. In addition, an increase in the molecular weight of the polymer also seems to be responsible for the increase in Mo(VI) extraction. Wang *et al.*, proposing the extraction mechanism, say that Mo(VI) is extracted in the PEG phase through electrostatic attraction between the polymolybdate anion and the protonated ether groups present in the polymer. In particular, they acknowledge that due to the hydrophobic character of the polymolybdate anion and the salting-out effect of sodium sulfate, the extraction mechanism can take place.

Muruchi *et al.*<sup>10</sup> showed that it is possible to selectively separate Mo and Re from a copper concentrate mining effluent. Specifically, they exploited the potential of the ABS composed of polymer/Cu<sub>2</sub>SO<sub>4</sub> /H<sub>2</sub>O to separate Mo(VI) and Re(VII) from Cu(II), and then Mo was stripped with an ammonium salt, resulting in a high-purity hybrid polymetallate complex. The polymers tested by Muruchi and co-workers are PEG (molecular weight from 2000 to 20K) and a mixture of PEG-400 and PPG-400. The species extracted are the oxoanionic forms of Mo and Re, i.e. polyoxomolybdates and ReO<sub>4</sub><sup>-</sup>.

Speciation of the different elements was confirmed through molecular dynamic simulation. In addition, chloride salts were added to enhance the hydrophobicity of the polymer phase. The chloride salts were chosen based on two main characteristics, they must not induce a biphasic system when they come into contact with PEG-4000 and they must not complex with the metals present in solution. The research group obtained the following results when the mine effluent was treated with the simple system consisting of PEG-4000 /  $\text{Cu}_2\text{SO}_4$  /  $\text{H}_2\text{O}$  at 35 °C and pH=2:

- The addition of chloride salt confirmed the preferential extraction of Mo and Re and the degree of extraction increased when moving from NaCl to LiCl to KCl. They correlated this tendency to the hydration molar entropy values ( $\Delta S_{\text{Hyd}}^\circ$ ) of the salts considered, showing that the salts that interact most with water have a high  $\Delta S_{\text{Hyd}}^\circ$ , so they will also have a high salting-out capacity and will prefer to stay in the aqueous phase. In fact, the copper sulfate already present in solution, having low values of  $\Delta S_{\text{Hyd}}^\circ$ , is not able by itself to act as an effective salting-out agent. In all the research conducted by Muruchi et al., the extraction coefficients of Mo and Re are always  $K_{\text{Mo}} > K_{\text{Re}}$ .
- The lower charge density of polyoxometalate complexes (in particular of the species  $\text{H}_{11}\text{Mo}_7\text{O}_{28}^{-3}$ ) was associated with a higher affinity for the more hydrophobic polymer-rich phase in the ABS proposed so far. With this in mind, Muruchi et al. decided to also test polymers that could be more hydrophobic than PEG-4000. With this experiment they showed that by switching from PEG-2000 to PEG-20K the Mo extraction was markedly enhanced and the impact on the Re was less pronounced. However, using PEGs with a high molecular weight meant that the viscosity of the solution increased considerably, thus also reducing the kinetics of mass transfer. To avoid this problem, Muruchi and co-workers proposed to test a polymer mix consisting of different distributions of PEG-4000/PPG-400 respectively 1:0, 3:1, 1:1, 1:3, 0:1. The system seems to follow an increasing trend for Mo extraction when going from 1:0 to 1:3 (PEG-4000/PPG-400) and reaches a maximum in the last case. At 0:1 (PEG-4000/PPG-400) the Mo partition coefficient decreases. As for Re, starting at 1:0 and reaching 0:1 (PEG-4000/PPG-400), the extraction efficiency follows a slightly decreasing trend.
- Finally, the precipitation of Mo from the PEG phase with an efficiency greater than 97% was carried out using ammonium salts.

The entire Muruchi et al. <sup>10</sup> process is shown in Figure 31.

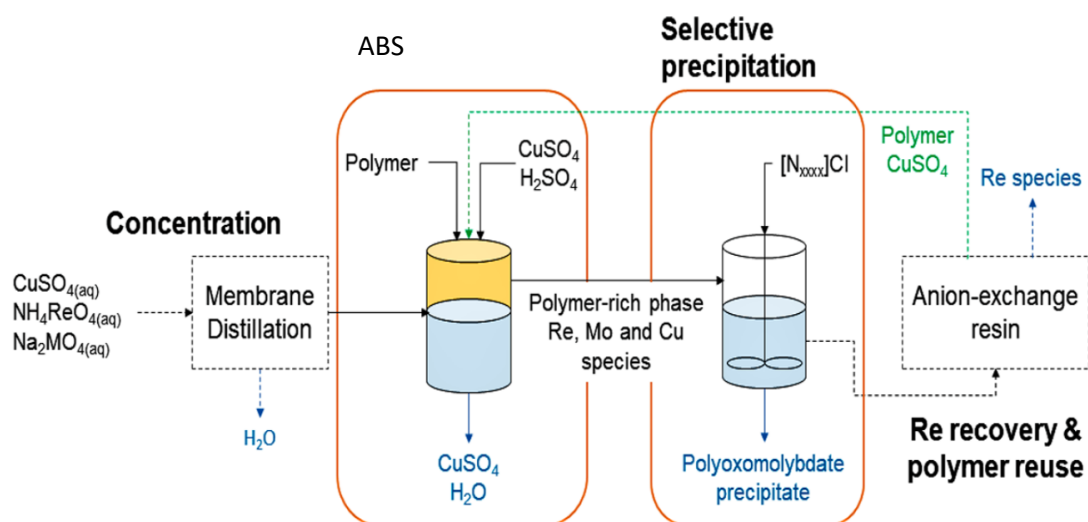


Figure 31. Potential process proposed by Muruchi et al. <sup>10</sup>

They concluded their research by saying that the effluent solution analyzed has the advantage of already containing within it further dissolved species based on metal sulfates, to be exact: 7.0 g/L of  $\text{Al}^{3+}$ , 5.0 g/L of  $\text{Mg}^{2+}$ , 0.8 g/L of  $\text{Mn}^{2+}$ , and 0.4 g/L of  $\text{Fe}^{2+/3+}$ ; the presence of these species accentuates the salting-out phenomenon allowing phase separation. In addition, the fact that copper is in  $\text{Cu}^{2+}$  form at the investigated pH (pH=2) while Re and Mo are in oxoanionic form allows the polymer to preferentially extract the latter two species.

Lie *et al.*<sup>92</sup> in 2016 demonstrated that it was possible to reduce Cr(VI) to Cr(III) by using PEG with different molecular weights (400 to 10,000) and under the sunlight irradiation. The investigation proved that the photo-reduction rate of Cr(VI) increased with decreasing pH of the solution and molecular weight of PEG, and increased with light intensity. Furthermore, the rate of Cr(VI) reduction increased with increasing amount of PEG and reached maximum values at pH below 3. Finally, both PEG and Cr(III) were recovered through the use of a highly concentrated solution of  $\text{Na}_2\text{SO}_4$  to induce the formation of a stable PEG- aqueous biphasic system. Experimentally, what Lie *et al.* did was to prepare a stock solution at a pH= 3, of PEG and Cr(VI), which was then left under the action of sunlight for a day. The Cr(VI) was then able to reduce to Cr(III). Then a very concentrated solution of  $\text{Na}_2\text{SO}_4$  was prepared and added to the previously mixed PEG and chromium. The four samples from these experiments are shown in Figure 32 (from the left to the right, figure directly linked with Lie *et al.*'s paper):

1. Chromium solution kept in the dark (without PEG).
2. PEG and chromium solution kept in the dark (with PEG).
3. Chromium solution exposed to sunlight (without PEG).
4. PEG and chromium solution exposed to sunlight (with PEG).

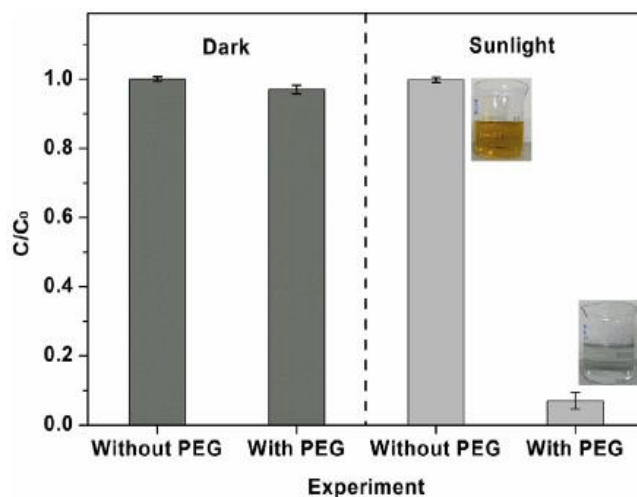
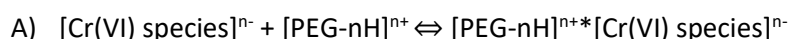


Figure 32. Comparison of Cr(VI) reduction in dark control and under solar irradiation with/without addition of

In each of experiments, the initial pH solution value is 3.0 and the light intensity tested by Lie *et al.* was  $50 \cdot 10^3$  lux and the working temperature was 25 °C. The added quantity of PEG 2000 used by these authors was 2 g and the initial Cr(VI) concentration was 100 mg/L. Reaction time was 20 min. Only sample number 4 showed decreasing concentration in chromium in the solution, confirmed by Lie and co-workers through ICP-MS analysis.

The mechanism proposed in this paper is based on the polymer-Cr(VI) interaction. They have shown that all Cr(VI) species present in solution are photochemically inert when they are not in contact with PEG. When the contact with the polymer occurs, in the presence of light, the photo-reduction of Cr(VI) to Cr(III) also takes place. At this point the oxygens in the polymer chain protonate giving  $[\text{PEG-nH}]^{n+}$  while the chromium will be found in an anionic form in solution  $[\text{Cr(VI) species}]^{n-}$  (pH =3). Lie *et al.*<sup>92</sup> stated that in solution the chromium complexes with the polymer according to the following reaction:



It is assumed that the reaction goes through intermediate stages with formation of radicals. The second step involves the formation of aldehydic groups in the PEG structure; this was confirmed by them through FTIR analysis, <sup>1</sup>H NMR and <sup>13</sup>C NMR, and the reaction proposed is:



They conclude by saying that the higher the acidity of the solution, the more favorable is the protonation of PEG and the reduction of Cr(VI) to Cr(III).

More recently in 2018, Sun et al.<sup>16</sup> proposed the same mechanism but with some variation and without considering the light. The first difference between the two experiments was in the way the solution was prepared. Whereas Lie et al. had successively added Na<sub>2</sub>SO<sub>4</sub> solution to an initial solution of PEG and Cr(VI), in this case, Sun and co-workers start with a solution of Cr(VI) and sodium sulfate and then add the polymer. In both cases the working temperature is 25 °C. Here again, it is shown that the repartition of Cr(VI) is related to the amount of protons in the solution. If the pH is low enough to protonate the polymeric oxygens and thus give a PEG-H<sup>+</sup>, then Cr(VI) will be extracted in an anionic form. An important point added by Sun's *et al.* study is that it defines the process of extraction by electrostatic interactions between the polymer cation and the metal anion. Sun and co-workers also highlight the fact that in a sodium sulfate solution, the polymer can also form the PEG-Na<sup>+</sup> structure, and not just the PEG-H<sup>+</sup> structure. The main Cr(VI) species considered by re HCrO<sub>4</sub><sup>-</sup> for pH below 4 and CrO<sub>4</sub><sup>2-</sup> for pH above 4.

Furthermore, by using dynamic molecular simulation (Figure 33), Sun *et al.* demonstrated that almost all HCrO<sub>4</sub><sup>-</sup> was distributed in the inner sphere of the PEG aggregates, some Na<sup>+</sup> was kept in the PEG aggregates, while the majority of SO<sub>4</sub><sup>2-</sup> and CrO<sub>4</sub><sup>2-</sup> was distributed in the aqueous solution outside around the PEG aggregates. The inner part corresponds to a polymeric phase similar to the one studied in the present work and the outside part is the aqueous phase of the biphasic system. Therefore, from molecular dynamic simulation, Sun and co-workers deduce that HCrO<sub>4</sub><sup>-</sup> interacts with PEG-Na<sup>+</sup>, but did not exclude that also CrO<sub>4</sub><sup>2-</sup>, having a larger negative charge, could interact with PEG-Na<sup>+</sup>. The fact that they do not interact is due to the hydrophilic/hydrophobic character of these compounds.

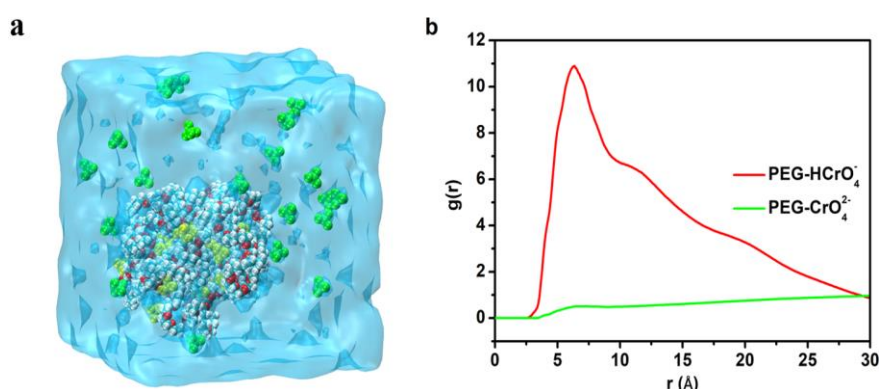


Figure 33. (a) Snapshot of the simulation box at equilibrium state (CrO<sub>4</sub><sup>2-</sup> is represented by the green spheres. HCrO<sub>4</sub><sup>-</sup> is represented by the yellow spheres. The carbon, hydrogen, and oxygen atoms in PEG molecules are represented by the cyan, white, and red spheres, respectively.) (b) The radial distribution of the chromium atoms of HCrO<sub>4</sub><sup>-</sup> or CrO<sub>4</sub><sup>2-</sup> around all of the monomers of PEG molecules in the aggregates.

Sun *et al.* also considered the radius distribution function of water around Na<sup>+</sup>, CrO<sub>4</sub><sup>2-</sup>, SO<sub>4</sub><sup>2-</sup>, HCrO<sub>4</sub><sup>-</sup>, and PEG, thus introducing the concept of hydrophobicity and hydrophilicity in a biphasic aqueous system. The radius distribution function, denoted in equations by g(r), defines the probability of finding a species at a distance r from another tagged species. In our case the common particles are the water

molecules, and these are compared to the molecules listed above. Figure 34 shows the results obtained by Sun and co-workers through molecular dynamics calculations, and proves that, considering the graph A of Figure 34 of the sodium-water interaction, there will be a high probability of finding the sodium ions close to the water molecules (characteristic peak at  $r=2.5\text{\AA}$ ) (a - Figure 34). While considering the graph B of Figure 34, by the same principle, there will be a high probability of finding  $\text{CrO}_4^{2-}$  and  $\text{SO}_4^{2-}$  close to water molecules and a lower probability for PEG and  $\text{HCrO}_4^-$ . This means that  $\text{Na}^+$ ,  $\text{SO}_4^{2-}$  and  $\text{CrO}_4^{2-}$  are more hydrophilic than PEG and  $\text{HCrO}_4^-$ , so the first species will prefer to be in the non-polymeric phase and the PEG and  $\text{HCrO}_4^-$ , in the polymer phase.

Moreover, Sun and co-workers also used the concept of polarizability, which is linked to the hydration properties of the ions. In particular, they say that, compared to the chromate  $\text{CrO}_4^{2-}$  which has a double charge,  $\text{HCrO}_4^-$  with a single charge has a higher polarizability. This also explains why the hydration of chromate is larger than  $\text{HCrO}_4^-$ .

As can be seen from the articles just described, one of the points in common between the studies is precisely the ability of this class of polymers, regardless of molecular weight, to change attitude when they come into contact with a salt, in ABS. Most of these articles deal with the hydrophobic/hydrophilic character of ABS components. In particular, it appears that the polymer loses its hydrophilic character when a compound with a higher affinity for water is added to the system, such as  $\text{Na}_2\text{SO}_4$ . It is on this evidence that ABS formation and metal extraction is demonstrated.

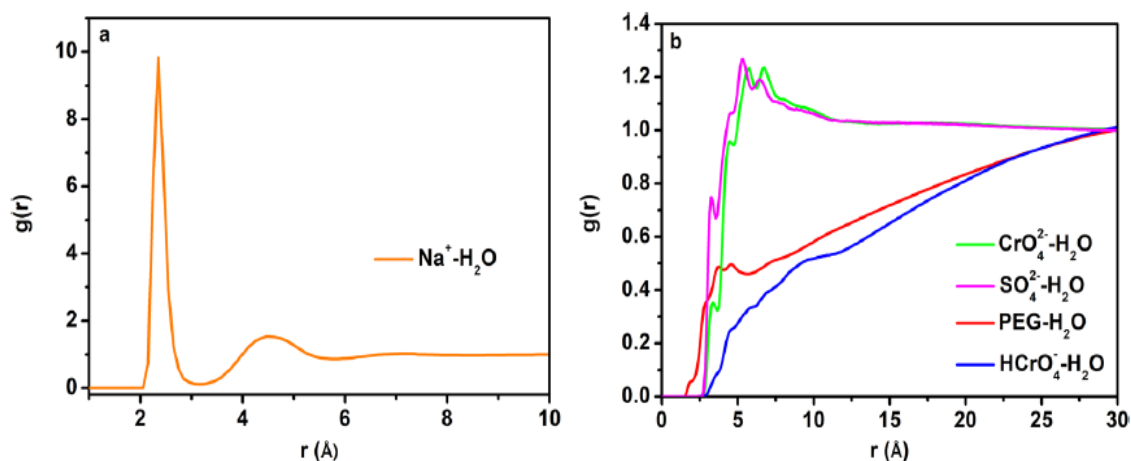


Figure 34. Radius distribution function of water around  $\text{Na}^+$ ,  $\text{CrO}_4^{2-}$ ,  $\text{SO}_4^{2-}$ ,  $\text{HCrO}_4^-$ , and PEG molecules.

#### 4.2.2. IL-based ABS

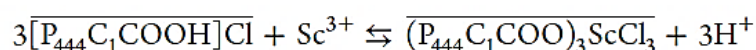
When ionic liquids started to be considered by the scientific community as greener solvents than organic ones, they quickly found their way into ABS applications. Table 4 shows IL-based ABS used for metal extraction. The articles are listed in chronological order. In addition, the following lines will outline how the scientific community has described the various mechanisms of action of ionic liquid-based ABS for metal extraction.

Date of publication	System	Aim	First author and University	Ref.
2000	TBAB / (NH <sub>4</sub> ) <sub>2</sub> SO <sub>4</sub> / metal ions solution [Cd(II) / Co(II) / Cu(II) / Fe(III) and Zn(II)] / H <sub>2</sub> O	Selective separation of Cd(II) from Co(II), Cu(II), Fe(III) and Zn(II)	<i>Y. Akama from University of Chemistry, Tokyo - Japan.</i>	49
2002	TBAB / (NH <sub>4</sub> ) <sub>2</sub> SO <sub>4</sub> / Cr(VI) solution / H <sub>2</sub> O	Selective extraction of Cr(VI)	<i>Y. Akama from University of Chemistry, Tokyo - Japan.</i>	50
2013	[C <sub>x</sub> mim]Br / Rb <sub>2</sub> CO <sub>3</sub> / Cs <sub>2</sub> CO <sub>3</sub> / H <sub>2</sub> O	Understanding of the phase diagram at different T	<i>G. Yin from Key Laboratory of Macromolecular Science China</i>	96
2014	[Bmim]Cl / K <sub>2</sub> HPO <sub>4</sub> / silver target / H <sub>2</sub> O	Separation of Cd from silver target	<i>K. Ghosh from Chemical Sciences Division, India</i>	45
2015	[P <sub>4.4.4.1</sub> C <sub>1</sub> COOH]Cl / NaCl / ScCl <sub>3</sub> / H <sub>2</sub> O	Selective extraction of Sc(III)	<i>D. Depuydt from KU Leuven, Department of Chemistry, Belgium (Binnemans Group)</i>	97
2015	[P <sub>4.4.4.14</sub> ]Cl / NaCl / CoCl <sub>2</sub> /NiCl <sub>2</sub> / H <sub>2</sub> O	Selective extraction of Co(II) from Ni(II)	<i>B. Onghena from KU Leuven, Department of Chemistry, Belgium (Binnemans Group)</i>	98
2018	[C <sub>4</sub> C <sub>1</sub> im]triflate / NaCl (or CsCl) / SrCl <sub>2</sub> / EuCl <sub>3</sub> ) / H <sub>2</sub> O	Understanding of ABS formation by molecular dynamic simulation	<i>R. Schurhammer Chimie de la Matière Complexe, UMR CNRS, Strasbourg – France</i>	54

2018	[P <sub>44414</sub> ]Cl / HCl (or NaCl) / NiMH leachate batterie / H <sub>2</sub> O	Selective extraction of Co(II) from Ni(II)	N. Schaeffer from CICECO-Aveiro Institute of Materials, Department of Chemistry, Portugal (Coutinho Group)	<sup>13</sup>
2020	[P <sub>44414</sub> ]Cl / Mn(II), Co(II), Ni(II) / synthetic solution mimic leached battery / H <sub>2</sub> O	Selective separation of Mn, Co, and Ni in a Fully Aqueous System	N. Schaeffer from CICECO-Aveiro Institute of Materials, Department of Chemistry, Portugal (Coutinho Group)	<sup>99</sup>

Table 4. List of IL-based ABS, in order of date of publication, used for selective metal ions extraction. TBAB is tetrabutylammonium bromide.

Akama *et al.*<sup>50</sup> used ionic liquid ABS to extract Cr(VI). The system they considered is composed of TBAB / (NH<sub>4</sub>)<sub>2</sub>SO<sub>4</sub> / H<sub>2</sub>O where TBAB is tetrabutylammonium bromide. Sigma Aldrich refers to TBAB as a quaternary ammonium salt with characteristics similar to ionic liquids. It has been placed in this part because it behaves like an ionic liquid in the ABS. In Akama *et al.*'s article<sup>50</sup>, the extraction efficiency of TBAB for Cr(VI) was shown to be greater than 90% and the mechanism governing the extraction is based on the formation of the HCrO<sub>4</sub><sup>-</sup>-TBAB<sup>+</sup> ion pair. In 2015, Depuydt *et al.*<sup>97</sup> demonstrated the extraction of Sc(III) using an ABS based on [P<sub>444</sub>C<sub>1</sub>COOH]Cl / NaCl / H<sub>2</sub>O at 25°C. In their paper they also demonstrated the stripping of Sc(III) from the ionic liquid phase using oxalic acid. The pH was always kept below 4 to avoid hydrolysis of Sc(III). Finally, they showed that more than 90% of Sc(III) is extracted in the ionic liquid phase according to the following reaction:



where Sc(III) forms a chloro-complex and this is extracted from towards the ionic liquid. The same group of researchers<sup>98</sup> then demonstrated how to separate Co(II) from Ni(II) using an ABS consisting of [P<sub>44414</sub>]Cl / NaCl / H<sub>2</sub>O. In this second study Co(II) is separated from Ni(II) with an efficiency of more than 90% when only 11 wt% NaCl is used in the ABS. More recently, N. Schaeffer *et al.*<sup>99</sup> proposed the separation and recovery of Mn(II), Co(II) and Ni(II), characteristic elements of nickel metal hydride and lithium ion batteries. In this paper<sup>99</sup>, the researchers first recovered Mn(II) by oxidizing it by ozone, then treated the Co(II) and Ni(II) solution with ionic liquid [P<sub>44414</sub>]Cl, extracting Co(II) in the ionic liquid phase by exploiting the ability of Co(II) to form chloro-complexes. Finally, Co(II) was precipitated with sodium carbonate. ABS based on ionic liquids therefore exploits the formation of a new ionic pair and it is thanks to the ionic exchange between species that the extraction mechanism that occurs for metal ions can also be demonstrated.

### 4.3. Acid-based ABS

Over the past 30 years, ABS based on ionic liquids and polymers have proved to be particularly useful for metal extraction. Only recently a big step forward in the ABS world has been made for the extraction of metals in highly acidic conditions for the treatment of spent batteries liquor, mining waste stream or stainless-steel spent processing baths. The interest in dealing with these former solutions, where the metals are under simplest form, gave rise to acid-based ABS (AcABS). AcABS<sup>100</sup> are aqueous biphasic systems where the inorganic salt of classic ABS is replaced by an inorganic acid. Regarding the ionic liquids, in 2011, Claudio *et al.*<sup>101</sup> investigated the impact that acid has in ABS based on IL. However, the concept of AcABS was only born in 2018 when Gras *et al.*<sup>101</sup> proposed these systems for metal extraction. In particular, Gras and co-workers<sup>101</sup> from LEPMI laboratory in collaboration with CICECO, examined AcABS composed of  $[P_{44414}][Cl]$  / HCl / H<sub>2</sub>O to demonstrate the partitioning of the metals Co(II), Fe(III), Ni(II) and Pt(IV) in hydrochloric acid solution. In addition, in this article, great attention was given to the temperature investigation in AcABS. Figure 35 shows the influence of temperature on the system studied by Gras *et al.*<sup>101</sup>.

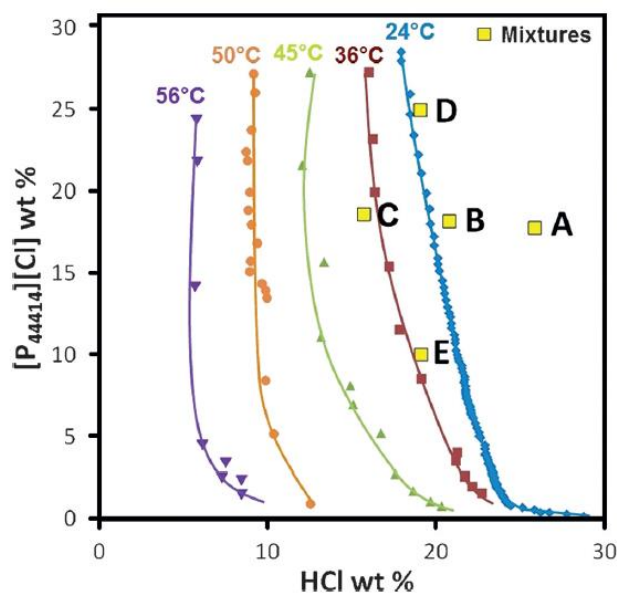


Figure 35. Binodal curves for the system  $[P_{44414}][Cl]$ -HCl-H<sub>2</sub>O at various temperatures and the composition of mixture points A–E studied. Lines are guides to the eye<sup>101</sup>.

In Figure 35 it can be seen that by considering the system  $[P_{44414}][Cl]$  / HCl / H<sub>2</sub>O and going from 24 to 56°C, the binodal curve shifts from right to left, and thus the biphasic area increases. In addition, the five experimental points shown in Figure 35 were analyzed by Gras *et al.*<sup>101</sup> to understand the distribution of metals under these experimental conditions. The experiment showed that Co(II), Fe(III) and

Pt(IV) are extracted in the ionic liquid rich phase, both at 24 and 50°C. Ni(II) remains in the acidic aqueous phase. Gras and co-workers<sup>101</sup> state that this selective character of the ionic liquid is related to the species present in solution. At high HCl concentrations, the predominant species for Fe(III) is  $\text{FeCl}_4^-$ , for Pt(IV) is  $\text{PtCl}_6^{2-}$ , for Co(II)  $\text{CoCl}_3^-$  and  $\text{CoCl}_4^-$  while Ni(II) hardly exists as a negatively charged chlorine-complex in water. Hence they<sup>101</sup> confirm the tendency of the ionic liquid to preferentially extract Fe(III), Co(II) and Pt(IV). Finally, Gras *et al.*<sup>101</sup> applied the investigated system to a real HCl leachate solution of NiMH batteries and obtained the same results.

This investigation opened the door to the use of AcABS for the separation of metals in highly acidic environments. The acid considered in Gras *et al.*<sup>101</sup> research was HCl, but it is well known that often, especially when dealing with solutions from the metallurgical industries, they<sup>101</sup> exploit the capabilities of several acids (HCl,  $\text{H}_2\text{SO}_4$  or  $\text{HNO}_3$ ) for their production and finishing processes. A thorough investigation of acid and temperature contribution in AcABS was carried out by Mogilireddy *et al.*<sup>11</sup>. Figure 36 shows the phase diagrams for the investigation with different acids and the investigation of temperature influence. They demonstrated the great impact that HCl,  $\text{H}_2\text{SO}_4$  and  $\text{HNO}_3$  acids have on the position and shape of the binodal curve in  $[\text{P}_{44414}]\text{Cl}/\text{acid}/\text{H}_2\text{O}$  system and thus on the phase separation and demixing. When passing from HCl to  $\text{H}_2\text{SO}_4$  and finally arriving at  $\text{HNO}_3$ , for the system  $[\text{P}_{44414}]\text{Cl}/\text{acid}/\text{H}_2\text{O}$  the binodal curve shifts from right to left, and thus the biphasic area increases in the order  $\text{HNO}_3 < \text{H}_2\text{SO}_4 < \text{HCl}$ . In addition, for the  $[\text{P}_{44414}]\text{Cl} / \text{HCl} / \text{H}_2\text{O}$  system, they showed that the binodal curve of the system took on a characteristic “onion shape”, which became more pronounced the higher the temperature was raised.

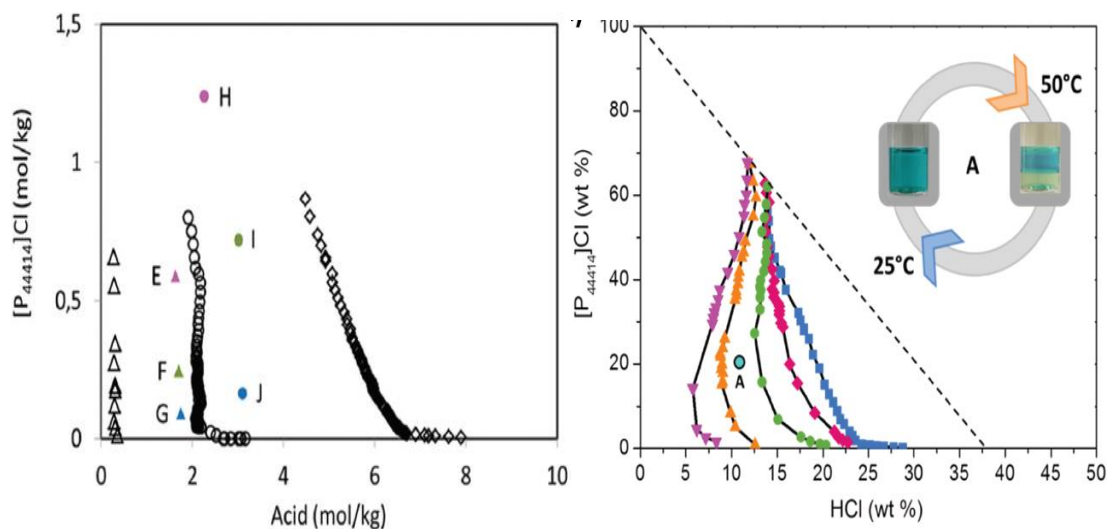


Figure 36. On the left, phase diagrams of AcABS composed of  $[\text{P}_{44414}]\text{Cl}$ , water and the acids HCl ( $\diamond$ ),  $\text{H}_2\text{SO}_4$  ( $\circ$ ) and  $\text{HNO}_3$  ( $\Delta$ ). The mixture points E, F and G belong to  $\text{HNO}_3$ -based system and H, I and J to  $\text{H}_2\text{SO}_4$ -based system. On the right, 2D representation of the binodal curves, starting from the blue and arriving to the purple at :25 °C, 36 °C, 45 °C, 50 °C and 56 °C; illustration of phase behavior for the mixture point of composition A (11.5 wt% acid; 20 wt% IL; 68.5 wt%  $\text{H}_2\text{O}$ ) at 25 and 50 °C; metal solutions were used for visual distinction of phases<sup>11</sup>.

In addition, to combine the usefulness of the previous ABS with the new AcABS, N. Schaeffer *et al.*<sup>100</sup> proposed the concept of synergistic aqueous biphasic systems to indicate a mixed ABS-AcABS approach, where in an AcABS consisting of a biphasic inducer/acid/H<sub>2</sub>O, the salt is added. The researchers state that the usefulness of using the two systems together is to be able to treat acidic solutions from industrial waste where the amount of Cl<sup>-</sup> is not sufficient to induce an AcABS system. Adding more HCl would result in more corrosion in the process equipment and more cost to neutralize the solution. For this reason, one part of HCl was replaced by NaCl. Reducing the acid concentration also makes it possible to promote the electrodeposition of metals, which would otherwise be impossible due to the high acidity. Three systems were analyzed N. Schaeffer and co-workers<sup>100</sup>:

- AcABS: [P<sub>44414</sub>] Cl / HCl / H<sub>2</sub>O
- ABS: [P<sub>44414</sub>] Cl / NaCl / H<sub>2</sub>O
- ABS-AcABS: [P<sub>44414</sub>] Cl / HCl / NaCl / H<sub>2</sub>O

A mixed metal ion solution containing 0.1 mol/L CoCl<sub>2</sub>·6H<sub>2</sub>O, 0.1 mol/L NiCl<sub>2</sub>·6H<sub>2</sub>O, and 0.1 mol/L MnCl<sub>2</sub>·4H<sub>2</sub>O was used for all the experiments, the working temperature is 25°C and the impact of NaCl was investigated in 3 different amounts in the third system, at 1, 2 and 4 wt%. They demonstrated<sup>100</sup> how the addition of a small concentration of NaCl leads to a large decrease in the corresponding HCl concentration required to induce phase separation. Finally, as far as metals are concerned, the AcABS-ABS system proposed by Schaeffer *et al.*<sup>100</sup> show that Co(II) is extracted in the ionic liquid phase, Mn(II) is divided between the two phases, while Ni(II) is not extracted.

In the chapter related to the investigation on the UGCO bath, will be described the AcABS composed of [P<sub>44414</sub>] Cl / [metal + HCl] / H<sub>2</sub>O. As far as the polymer based AcABS is concerned, to the best of my knowledge, there is no scientific research on it, and a large chapter of the thesis will be devoted to the new developments obtained for these systems.

#### 4.4. Can ABS based on PEG, PPG or [P<sub>44414</sub>] Cl be a useful and green alternative to classical liquid-liquid extraction systems with organic solvents?

Many parameters have to be considered in order to understand whether PEG, PPG and [P<sub>44414</sub>] Cl can be considered as a green alternative to the organic solvent. Among them, there are handling, economy, toxicity, ability to be recovered etc. However, to answer the "green" question, it must first be understood whether these compounds meet the standards promoted by green chemistry.

Anastas and Warner<sup>102</sup> in “Green chemistry: Theory and Practice” (Oxford 1998) stated that:

*“Green chemistry is the utilization of a set of principles that reduces or eliminates the use or generation of hazardous substances in the design, manufacture, and applications of chemical products.”*

Among the main objectives of green chemistry, there are those of minimizing or eliminating the production of waste material, avoiding the use of toxic and / or dangerous reagents and solvents, and developing technologies that exploit renewable materials. Reactions that use mineral acids or inorganic bases often in stoichiometric quantities, represent the major source of inorganic waste, difficult to recycle and dispose of. The elimination of this type of waste, together with the replacement of dangerous and toxic reagents such as phosgene or dimethyl sulfate, is one of the greatest achievements/goals of green chemistry.

William M. Nelson in 2002 proposed<sup>103</sup> an interesting table, answering some questions about the 'green' nature of ionic liquids (Table 5).

Greening of ionic liquids	G	P	U
• Does the solvent use lead to less energy expenditure?		*	
• Does the solvated species react more efficaciously and selectively?	*		
• Does the solvent improve atom-economy?	*		
• What is solvent distribution into environment?			*
• Will the solvent be absorbed by organism and how will it affect them?			*
• Is the solvent toxic? Can it be detoxified?			*

Table 5. William Nelson's table. G: good; P: poor; U: unknown.

What makes ILs attractive compared to the organic solvents is the possibility of changing their physical properties simply by changing their structure or one of their ions. This allows them to be adapted to the specific purpose for which they are intended (“tunability”), and they are therefore referred to as 'designer-solvents'. In fact, in ILs, the two components, cation and anion, give the compound different characteristics, so only by choosing different combinations of ions, it is possible to change the chemical-physical properties of the compound such as extraction selectivity, hydrophobicity, viscosity, etc. As far as polymers in the liquid form are concerned, these can also be referred to as a kind of engineering solvent, if the idea that a polymer can be synthesized by choosing various repetitive units is considered. These repeating units, which may for example contain a hydroxyl group instead of a nitric

one, or a bulkier group such as an aryl group, or a long alkyl chain which decreases the solubility in water, can vary the selectivity of the polymer extraction and its activity in ABS. A second common point between these biphasic inducers concerns the workability of these two compounds. In our project, for the majority of cases, the working temperature is around 70-80°C. In this condition, the IL and the polymer are both in the liquid state, and this is an essential aspect for the industrial scale. In addition, at this temperature the two biphasic inducers are not volatile, unlike most organic solvents. Moreover, both the ionic liquid and the polyglycols used in this work can be regenerated by simple distillation.

Another parameter for determining whether it is safe to work with these products is their degree of toxicity. The World Health Organization INCHEM (Internationally Peer Reviewed Chemical Safety Information) classified the pure polyethylene glycols with inverse toxicity to molecular weights. Absorption from the gastrointestinal tract decreases with increasing molecular weight<sup>104</sup>. Polyethylene glycol is employed extensively in pharmaceutical and biomedical areas. For the Agency of Toxic Substances & Disease Registry, in contrast to ethylene glycol, a potent cause of acute toxicity in humans, propylene glycol is a “generally recognized as safe” (GRAS) additive for foods and medications. Propylene glycol rarely causes toxic effects, and then only under very unusual circumstances. Propylene glycol is widely used in food and tobacco products, pharmaceuticals, and cosmetics. Concentrations in foods range from <0.001% in eggs and soups to about 15% in some seasonings and flavorings. Regarding the degree of toxicity of [P<sub>444n</sub>] Cl, Petkovic and co-workers<sup>105</sup> investigated the relationship between the length of the alkyl chain and the toxicity of alkyl tri-butyl phosphonium chlorides IL on a specific group of fungi, *Aspergillus nidulans* conidia. They stated that the toxicity of ionic liquid increases with increasing the alkyl chain length<sup>106</sup>. The question of toxicity to aquatic life remains in case of release by accident.

A difference between the two biphasic inducers lies in their extraction mechanism. As shown in section 4.2 of this chapter, the ionic liquid forms complexes with the metal ion while the polymer acts with different interaction forces (such as hydrogen bonds, electrostatic interactions, etc.) to capture them. It can be deduced from this that the ionic liquids and polyglycols considered have different selectivity because they extract different metal clusters.

Price is probably the most interesting parameter at industry level. As concern the polyglycols, 1 kg of PEG-200 costs €50-150 and 1 kg of PPG-425 costs €150-250 (source: Sigma Aldrich). The price increases with the molecular weight of the polymer. Furthermore, compared to the price indicated above for PEG and PPG, the [P<sub>44414</sub>] Cl has a much higher price of about 1500 euros per kg. However, for both polyglycols and ionic liquid, as the quantity of polymer or IL purchased increases, the price in

relation to the quantity of product also decreases, which can be interesting news for industrial purposes.

So it can be said that both ionic liquids and polymers are a good alternative to common organic solvents, but to understand which of the biphasic inducers is the best, their efficiency in the extraction process linked to their chemical-physical characteristics and finally their eco-sustainable character has to be considered.

## 5. Conclusions

The environmental impact of spent pickling liquor (SPL) from stainless steel refining processes has led Aperam to look for alternative methods to regenerate it. In addition, the techniques used today to treat SPL are often expensive (pyro-hydrolysis) or cause problems in the disposal of their waste by-products (neutralization). The alternative proposed to Aperam is ABS.

The extensive investigation carried out by the scientific community over the last 30 years on ABS based on polymers and ionic liquids for metal partitioning has achieved interesting results demonstrating the usefulness of these systems. The group's decision to continue working with ABS was based on the successful results of using these highly specific systems. Many separation mechanisms are now well known, such as those for oxoanions by polyglycols or the formation of a new ionic pair by the ionic liquid [P<sub>44414</sub>] Cl. In addition, a big step forward in the development of these systems was achieved in recent years, when AcABS were introduced. These systems have proven to reach very high separation efficiencies for metals dissolved in acidic solutions.

The research proposed in this work has developed in two strands, a more fundamental one dealing with the understanding of the mechanisms and experimentation in the laboratory, and a more applied one that has allowed us to work with a micro-pilot for the development of ABS. To date, ABS have been tested mainly in systems containing low concentrations (mg/L) of metals, and only in a few cases AcABS have been proposed to deal with larger concentrations (g/L) of metals (battery recycling). In this work, metals dissolved in acid solutions reach concentrations of up to 10 g/L.

However, ABS systems also have limitations, partly due to the fact that, as regarding to AcABS, they are fairly new systems and still need further investigation. Moreover, as ABS is water-based, the biphasic inducers have to be hydrophilic, drastically reducing the number of inducers to be used. The issue of the toxicity of certain ionic liquids also cannot be underestimated.

The next chapter will describe the analytical methods, instruments and protocols used during my investigation.

*Picture presented in the ©"Nordic Coastal Clean Up" project which aims to raise awareness among young people about the cleaning of the coasts of Norway, Sweden, and Finland after a shipping accident in 2017.*

# B. Material and methods





# 1. Introduction

This chapter will provide the information needed to understand and reproduce the experiments carried out during the PhD. After giving an exhaustive list of the chemical compounds used, the two methods for obtaining binodal curves will be presented. The last section will describe the different analytical techniques used during my research. For each technique, a brief description of the apparatus, the principle of the different techniques and the methods of analysis used will be presented. A schematic procedure of the investigation is shown in Figure 37 where the sample, which presents a phase repartition, is first displayed in a phase diagram (point A in the biphasic area) and to its right all the analysis techniques used for its characterization can be found.

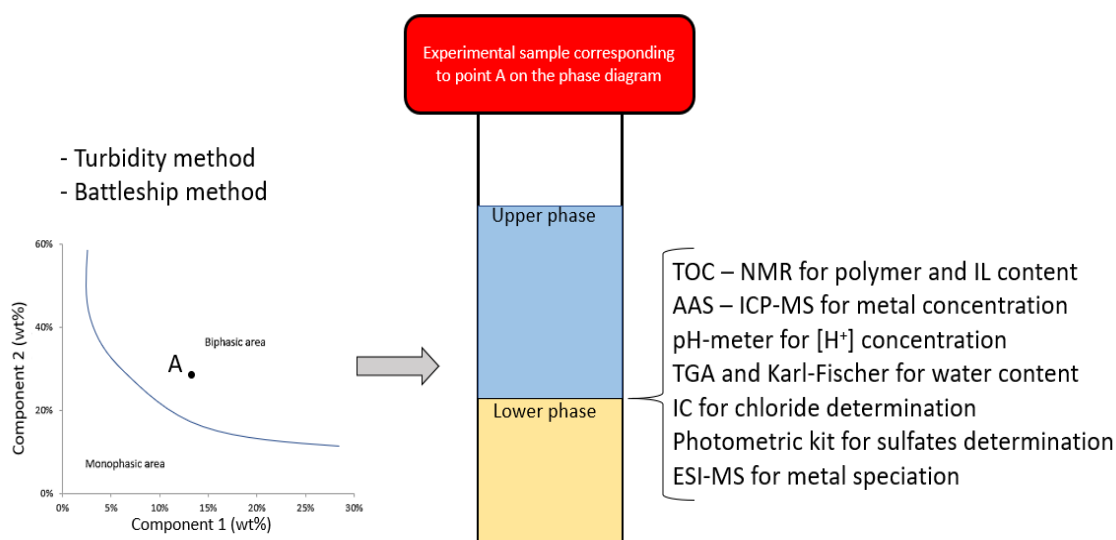


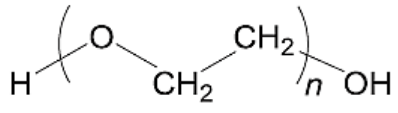
Figure 37. Procedure for determining an ABS and characterizing it using analytical tools.

# 2. Chemicals

Table 6 lists all the chemical compounds used during the PhD. The table is divided into four columns corresponding to the chemical formula, commercial name, supplier, and purity grade indicated by the supplier. Regarding the water used in the experiments, it was passed through a Milli-Q apparatus purification system commercialized by Merck (18M $\Omega$ ). Table 7 shows a list of biphasic inducers used during the PhD. In the next chapters the results of the experiments carried out with the biphasic inducers listed in Table 7 will be presented.

Compound	Commercial name	Supplier	Purity
HCl	Hydrochloric acid	Sigma-Aldrich	37% = 12 mol/L, in water
H <sub>2</sub> SO <sub>4</sub>	Sulfuric acid	Carl Roth	96% in water
HNO <sub>3</sub>	Nitric acid	Carl Roth	65%
Na <sub>2</sub> SO <sub>4</sub>	Sodium sulfate	Carl Roth	98%
NaCl	Sodium chloride	Merck	99%
Na <sub>2</sub> CO <sub>3</sub>	Sodium carbonate	Carl Roth	98%
NiCl <sub>2</sub> ·6H <sub>2</sub> O	Nickel chloride hexahydrate	Rectapur	98%
CrCl <sub>3</sub> ·6H <sub>2</sub> O	Chromium chloride hexahydrate	Fluka	98%
FeCl <sub>2</sub> ·4H <sub>2</sub> O	Ferrous chloride tetrahydrate	Merck	98%
FeCl <sub>3</sub> ·6H <sub>2</sub> O	Iron chloride hexahydrate	Merck	99%
Mo <sub>2</sub> (O <sub>2</sub> CCH <sub>3</sub> ) <sub>4</sub>	Molybdenum acetate dimer	ChemLab	97%
CuSO <sub>4</sub> ·5H <sub>2</sub> O	Copper sulfate pentahydrate	Rectapur	98%
Na <sub>2</sub> MoO <sub>4</sub> ·2H <sub>2</sub> O	Sodium molybdate dihydrate	Merck	97%
NaMnO <sub>4</sub> ·1H <sub>2</sub> O	Sodium permanganate monohydrate	Merck	98%
KMnO <sub>4</sub>	Potassium permanganate	Rectapur	98%
MnSO <sub>4</sub> ·1H <sub>2</sub> O	Magnesium sulfate monohydrate	Carl Roth	98%
Fe <sub>2</sub> (SO <sub>4</sub> ) <sub>3</sub>	Ferric sulfate	Fluka	98-99%
NiSO <sub>4</sub> ·6H <sub>2</sub> O	Nickel sulfate hexahydrate	Acros	98-99%
Na <sub>2</sub> Cr <sub>2</sub> O <sub>7</sub> ·2H <sub>2</sub> O	Sodium dichromate hexahydrate	Alfa Aesar	98-99%
Cr <sub>2</sub> (SO <sub>4</sub> ) <sub>3</sub>	Chromium sulfate anhydrous	Alfa Aesar	98-99%
CuSO <sub>4</sub> ·5H <sub>2</sub> O	Potassium sulfate pentahydrate	Alfa Aesar	98-99%

Table 6. Chemical compounds used during the PhD.

Commercial name	Molecule	Providers	Chemical structure
PEG	Polyethylene glycol	Chem-lab	
DBP	Di-block polymer composed of PEG-PPG	Sigma Aldrich	
TBP	Tri-block polymer composed of PPG-PEG-PPG	Sigma Aldrich	

3EGDE	Tri-ethylene glycol dimethyl ether	Sigma Aldrich	
4EGDE	Tetra-ethylene glycol dimethyl ether	Sigma Aldrich	
PE	Polyethylene	Sigma Aldrich	
PPG	Polypropylene glycol	Sigma Aldrich	
POxES	Polyoxyethylene stearate	Sigma Aldrich	
[P <sub>44414</sub> ] Cl	Tributyl-tetradecyl phosphonium chloride	Interchim	

Table 7. Polymers tested during the PhD.

### 3. Methods for obtaining binodal curves

During my PhD, two different methods were used to obtain binodal curves, the turbidity method and the battleship method. In the next section we will see how to obtain the curves using these methods and especially the advantages and disadvantages of each of them.

#### ❖ Turbidity method

The binodal curves for the systems, listed in Table 8, were obtained using the turbidity method, also known in literature as the cloud point titration method.<sup>107,108,109</sup> I will use all over the manuscript the first term, turbidity method, to refer to this procedure. The table is divided into two main parts, relating to the use of ionic liquid and polymer. Further sub-categories are present, and the division was made considering the medium in which the ABS was obtained: HCl, HNO<sub>3</sub>, H<sub>2</sub>SO<sub>4</sub> and Na<sub>2</sub>SO<sub>4</sub>/H<sub>2</sub>SO<sub>4</sub>.

For the last medium ( $\text{Na}_2\text{SO}_4/\text{H}_2\text{SO}_4$ ), it is important to note that sodium sulfate is the most common component and sulfuric acid was only added to bring the pH to 1.8. All experimental points of the binodal curves presented are given in the section Annex - HCl and  $\text{Na}_2\text{SO}_4$  medium investigation. A more detailed investigation has been carried out considering the influence of temperature (mainly from  $25^\circ\text{C}$  to  $50^\circ\text{C}$ ) and the contribution of the metal ion concentration (mainly from  $1\text{g/L}$  to  $40\text{g/L}$ ) for some of the system listed above.

Ionic liquid	Polymer
HCl medium	
[P <sub>44414</sub> ] Cl/[HCl 37 wt%]/H <sub>2</sub> O	PEG-600/[Fe(III)+HCl 37 wt%]/H <sub>2</sub> O
[P <sub>44414</sub> ] Cl/[Cr(III)+HCl 37 wt%]/H <sub>2</sub> O	M.S.
[P <sub>44414</sub> ] Cl/[Fe(II)+HCl 37 wt%]/H <sub>2</sub> O	M.S.
[P <sub>44414</sub> ] Cl/[Fe(III)+HCl 37 wt%]/H <sub>2</sub> O	M.S.
[P <sub>44414</sub> ] Cl/[Ni(II)+HCl 37 wt%]/H <sub>2</sub> O	M.S.
HNO <sub>3</sub> medium	
[P <sub>44414</sub> ] Cl/[HNO <sub>3</sub> 65 wt%]/H <sub>2</sub> O	
H <sub>2</sub> SO <sub>4</sub> medium	
[P <sub>44414</sub> ] Cl/[H <sub>2</sub> SO <sub>4</sub> 98 wt%]/H <sub>2</sub> O	
Na <sub>2</sub> SO <sub>4</sub> / H <sub>2</sub> SO <sub>4</sub> medium	
	PEG-400/Na <sub>2</sub> SO <sub>4</sub> bath
	PEG-400/[Na <sub>2</sub> SO <sub>4</sub> salt]/H <sub>2</sub> O
	PEG-400/[Ni(II)+ H <sub>2</sub> SO <sub>4</sub> + Na <sub>2</sub> SO <sub>4</sub> ]/H <sub>2</sub> O
	PEG-400/[Fe(III)+ H <sub>2</sub> SO <sub>4</sub> + Na <sub>2</sub> SO <sub>4</sub> ]/H <sub>2</sub> O
	PEG-400/[Cr(III)+ H <sub>2</sub> SO <sub>4</sub> + Na <sub>2</sub> SO <sub>4</sub> ]/H <sub>2</sub> O
	PEG-400/[Cr(VI)+ H <sub>2</sub> SO <sub>4</sub> + Na <sub>2</sub> SO <sub>4</sub> ]/H <sub>2</sub> O
	PEG-400/[Cu(II)+ H <sub>2</sub> SO <sub>4</sub> + Na <sub>2</sub> SO <sub>4</sub> ]/H <sub>2</sub> O
	PEG-400/[Mo(II)+ H <sub>2</sub> SO <sub>4</sub> + Na <sub>2</sub> SO <sub>4</sub> ]/H <sub>2</sub> O
	PEG-400/[Mn(II)+ H <sub>2</sub> SO <sub>4</sub> + Na <sub>2</sub> SO <sub>4</sub> ]/H <sub>2</sub> O
	PEG-400/[Mo(VI)+ H <sub>2</sub> SO <sub>4</sub> + Na <sub>2</sub> SO <sub>4</sub> ]/H <sub>2</sub> O

Table 8. Binodal curves obtained in different media. The table is divided in ionic liquid systems on the left and polymer systems on the right. M.S. = systems investigated but provided a monophasic behavior.

The setup used to obtain the binodal curve via the turbidity method is shown in Figure 38. It consists of a double wall vessel with a maximum volume of 10 mL that is wrapped in a thermal mesh to control the temperature. The temperature is regulated by water circulating in the double wall system and controlled by a thermo-cryostat. The vessel is lidded to keep the solution at a constant temperature

inside and to prevent evaporation. The solution is also kept under constant agitation through a magnet (400 rpm). The components required to obtain the binodal curve were added using glass pipettes.

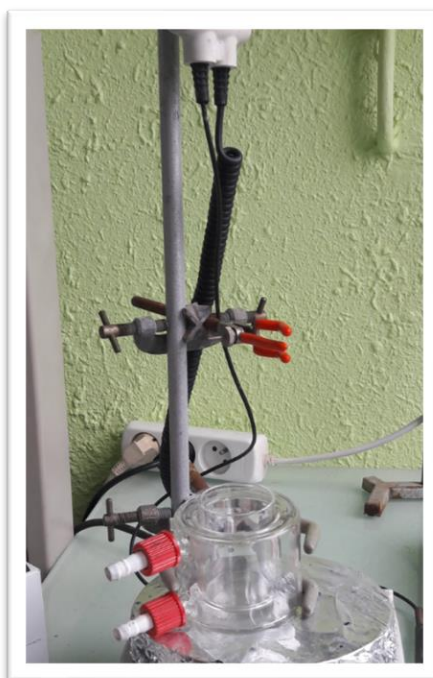


*Figure 38. Apparatus for cloud point titration method at LEPMI laboratory.*

The protocol used is as follows. The first step consists of preparing the biphasic inducers. For experiments conducted at room temperature, the ionic liquid [P<sub>44414</sub>] Cl which is a solid, has been left for few minutes under agitation with several drops of water, to allow the ionic liquid to pass in the liquid state. The amount of water was taken into account in the final calculations and considered as "added water" to the total water amount of the system. On the other hand, for experiments conducted at T above 35°C, it was not necessary to dissolve the ionic liquid since it is then liquid. Regarding PEG-600, it is in the solid state at room temperature but at 25 °C it becomes liquid; while as far as PEG-400 is concerned, this has been used directly as it is already in a liquid state at room temperature. With regard to their melting temperatures, this corresponds to 11°C for IL, 4-8°C for PEG-400 and 22°C for PEG-600, (Sigma Aldrich website) which can easily explain the need to dilute the compound with water in some cases. The working temperature was one of the most challenging parameters to control because the room temperature varied depending on the season. Moreover, some of the systems presented above are extremely sensitive to temperature variation and their state changes quickly (from monophasic to biphasic, and vice versa) namely if they pass from the inside to the outside of the thermal vessel. After preparing the biphasic inducer, this was weighed and introduced into the thermal vessel. The experiments were carried out starting from a known amount of ionic liquid or polymer between 3 and 5 g. This decision was taken to reduce the consumption of biphasic inducers used during the experiment.

The second step consists of preparing the other two components of the ABS: water and acid (or salt) solution with or without metals. A section of this chapter will be devoted to the preparation of metal stock solutions. A known quantity of UPW has been weighed and placed inside a beaker. For the solution containing only acid, the procedure is the same as for water. The acid was taken directly from its bottle, put in the beaker, covered with a plastic film, the pipette was inserted and the whole was weighed. The insertion of the acid into the beaker was carried out under fume hood. Once the three components of ABS, biphasic inducer, acid (or salts) solution with or without metals and water have been prepared, the experiment begins.

The third step consists of obtaining the binodal curve. Starting from the component 2 (may it be polymer or IL), which is free from component 1 (acid or salt solution with or without metals) and component 3 (water), this is represented by point A on the phase diagram in Figure 39. The point A is never to be found at 100 wt% since both the added water and the purity of the component 2 decrease this value. For clarification, it is important to state the difference between "added water" and component 3 (water). Added water is only used to dilute the biphasic inducer in order to pass it into a liquid phase and prepare it for the experiment, as already defined in previous sections. Component 3 is the water necessary to return the samples to the homogeneous state and then used to investigate the experimental points in the monophasic area of the phase diagram. In order to obtain the binodal curve, which is to be considered as a border line between the monophasic and the biphasic area, it is necessary to modify the solution that corresponds to point A by varying its composition. The point B obtained after this variation is experimentally presented as a turbid sample and corresponds to the step before reaching the biphasic area. The better the operator's ability to recognize the turbid sample, the more accurate the binodal curve will be. So, to arrive at point B, drops of component 1 have to be added to the initial sample A. The position of B is to be considered on line AC<sub>1</sub>, where C<sub>1</sub> is the point that corresponds to the composition of the solution of component 1. Experimentally, the more drops are added, the more the distance AB increases. Figure 39 also shows the AW-WZ case where the operator does not recognize the turbid point B during the experiment, there may be a case for reaching the W point, or any point on the line between A and C<sub>1</sub> in the biphasic area. Since the aim of the experiment is to define a binodal curve, in this extreme case, the operator can obtain the point Z by adding component 3 to the system, following the direction towards the origin of the axes. Thus, the difference in distance AB and AW lies in the number of drops of component 1 used in the two cases, and this will be higher for AW than for AB. If, however, the operator can immediately recognize the turbidity of the sample at point B, by adding a few drops of component 3, this leads to point C, where

the solution is back to the monophasic state. Point C will therefore lie on the line linking B and the origin of the axes. In addition, in the procedure of going from A to B, C, D etc., I have waited some minutes after adding the acid, because in such small volumes even a few drops of acid trigger an exothermic reaction which has two disadvantages, the first is the evaporation of the solution and the second is the need to re-establish the working temperature. To avoid these, a lid can be placed on the working beaker and a thermometer was used to monitor the temperature variation.

The last step is to process the data obtained. Experimentally, what is measured is the quantity in g of component 1 (acid or salt solution with or without metals) and component 3 (UPW), which are added gradually when passing from A to B to C etc. Each time component 1 and 3 are added to the system, the 2 beakers are reweighed and so on until the end of the experiment. The loss in weight of the beaker in component 1 and 3 represents the drops of the components respectively used to pass from one side of the binodal curve to the other. The values in the figure are expressed in wt% through the use of the following equations:

$$[(g_{\text{Component 1}}/g_{\text{tot}}) + (g_{\text{Component 2}}/g_{\text{tot}}) + (g_{\text{Component 3}}/g_{\text{tot}})] * 100 = 100 \text{ g/g}_{\text{tot}} \quad (1)$$

$$g_{\text{tot}} = \sum g_{\text{Component } x \text{ (} x=1,2,3)} \quad (2)$$

$$g/g_{\text{tot}} = \text{wt\%} \quad (3)$$

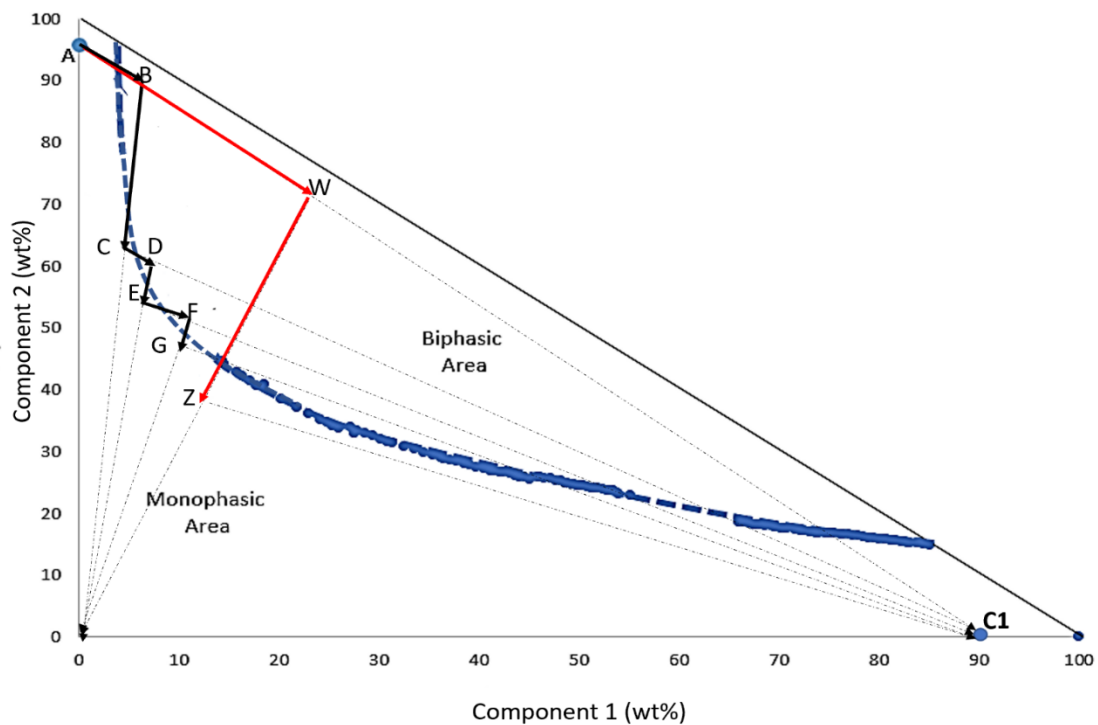


Figure 39. Binodal curve for system composed by a biphasic inducer, acidic solution, and water. The point A, B, C, D, E, F, G, W, Z, are experimental points found through turbidity method. The black arrows represent the ideal case where the operator immediately recognizes the turbid solution. The red arrows indicate the case where the operator does not recognize the turbid solution. The dotted lines are eye guides indicating the direction that the arrows will follow, and this coincides with the origin of the axes for monophasic samples, while it will coincide with the C1 point for biphasic samples.

The turbidity method is the most common method used in the literature. The main advantage of using this method is that a low concentration of biphasic inducers is used, thus avoiding their waste. However, it has not always been convenient for my investigation. First of all, this method relies on the ability of the operator to well distinguish the turbidity point which is more difficult when the used solutions are strongly colored like the ones which have been investigated during this thesis. In fact, the uncertainty of the turbidity method is related to the ability of the operator to well-distinguish between the biphasic or the monophasic behavior of the sample within the binodal curve vicinity. This is even linked to the number of drops (1 or 2) to pass from one region to the other. Another disadvantage of using this method is the acquisition time of the curves. To obtain a minimum of 40 experimental points, 4 hours of work are required. The time is even longer when the treated systems are very sensitive to temperature, i.e. when the system changes from monophasic to biphasic or vice versa without any change in components. In general, the investigation of the change of binodal curves as a function of temperature was the main reason that prompted me to look for an alternative method to the turbidity one, the battleship method.

#### ❖ Battleship method

During my PhD, an alternative method for preparing binodal curves was developed. The battleship method allowed us to obtain phase diagrams more quickly for temperature investigation and especially in cases where it was not possible to recognize the turbidity point during the cloud point titration method (e.g. solutions too dark as for the UGCO bath).

For the “battleship” method, several samples were prepared in glass vials (Figure 40) by mixing different amounts of polymer or IL, water and stock solutions of acid and metal salts. Then the temperature of the vials was controlled in the range 25 °C – 50 °C by the use of a water bath. At the given temperature, a visual observation easily allowed sorting the samples as either monophasic or biphasic. The temperature of the bath was controlled through the use of a thermometer.



Figure 40. Samples obtained by the battleship method.

As with the turbidity method, also for the battleship method there are pros and cons. The main advantage of using this method is the considerable reduction in time required for investigation when performing temperature-dependent experiments. Disadvantages include, for example, the case where samples are left in continuous contact between the upper and lower phase, this contact must not cause mass transfer in the system during the extended time spent in contact between the two phases. In addition, the samples must be stored in a place protected from light, in case the system is photosensitive, closed, to prevent the samples from absorbing water from the surrounding environment and at a constant temperature, to prevent evaporation at high temperature. In addition, great care must be taken when samples are left at very high temperatures, especially it is recommended not to close the sample cap, as working with acids, at high temperatures may cause gas formation and therefore explosion. For the battleship method, the uncertainty is due to the reasonable number of samples prepared by the operator to confirm with exactitude the border of the binodal curve.

The two methods have been proven to give coherent experimental results as shown in Figure 41 where the experimental points (black and white circles) obtained with the battleship method are exactly in the area of the graph corresponding respectively to the biphasic and monophasic part delineated by the binodal curve (triangles) and obtained through the turbidity method.

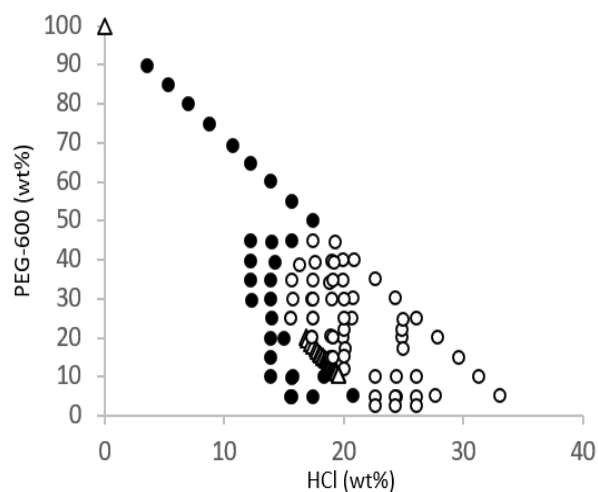


Figure 41. Phase diagram of the system PEG-600/HCl (37wt%)/Metal ions. The black dots and the empty circles are experimental points obtained through the battleship method and indicate the monophasic and the biphasic part of the graph respectively. The triangles correspond to the experimental points of the binodal curve obtained by the turbidity method.

## 4. Analytical techniques for element characterization in liquid state

### ❖ TOC determination through CO<sub>2</sub> detection

Total organic carbon (TOC) analysis was performed to determine the polymer content in a system composed of polymer / acid / H<sub>2</sub>O. Carbon-based compounds are known to be able to form countless bonds. However, it is possible to divide carbons into two large groups, inorganic carbon, and organic carbon. Inorganic carbon forms bonds directly with oxygen, as in carbon dioxide, bicarbonates or carbonates and other ions such as cyanides, cyanates and thiocyanates (for example, limestone is a calcium carbonate, a form of inorganic carbon). Organic carbon, on the other hand, can form bonds with various elements such as hydrogen, nitrogen, or other carbon atoms and in general with organic compounds. The inorganic carbon together with the organic carbon form the total carbon according to the following diagram:

$$TC = TIC + TOC \quad (4)$$

where TC = total carbon

TIC = total inorganic carbon

TOC = total organic carbon

It is also possible to find volatile organic compounds (VOC) among the various types of carbons. In general, volatile organic compounds have low vapor pressure at a given temperature and can be removed from a solution by bubbling a gas through a sample.

TOC is based on the determination of CO<sub>2</sub> produced by oxidation of organic compounds. The oxidation can be carried out in two ways<sup>110</sup>:

- *By thermal combustion*

The sample containing the carbon is acidified with phosphoric acid to transform the inorganic carbon into CO<sub>2</sub> by the following reaction:



The first half of the acidified sample is sent to an analyzer for CO<sub>2</sub> measurement by infra-red detector. This is how the TIC is measured. The other half is injected into a combustion chamber where the temperature is raised to 600-700 °C, and in some cases up to 1200 °C. Here all the carbon (TC) reacts with oxygen to form carbon dioxide. The sample is then sent to a cooling chamber and finally to the infra-

red detector. Usually, the detector used is a non-dispersive infra-red spectrophotometer. The TOC (total organic carbon) is determined by subtracting to the total carbon (TC) obtained from the burnt sample, the total inorganic carbon (TIC) obtained from the acidified sample (equation 4).

- *By wet oxidation*

The first part of the protocol is similar to the thermal combustion; the sample is acidified with phosphoric acid and in this case also ammonium persulfate is added. Half of the acidified sample goes into an infra-red detector (TIC measurements) and the other half is sent to an oxidation chamber where it is irradiated with ultraviolet rays by a mercury vapor lamp. In this way free radicals are formed from persulfate which react with all available carbon to form carbon dioxide. Both samples are then passed over membranes to determine the amount of CO<sub>2</sub> present. The TOC was determined following equation (4).

The thermal combustion method was used to perform my investigations. The instrument used is a TOC-Vcsn, SHIMADZU. The experiment was carried out with the help of the Mme D. Tisserand, in charge of the TOC setup at ISTERre laboratory, UGA (University of Grenoble Alpes).

#### ❖ pH-meter for acidity determination and titration with NaOH or HCl (37%)

The acidity of different samples has been determined either by direct pH measurement using a pH electrode or by acid-base titration. According to the definition:

$$\text{pH} = -\log_{10} [\text{H}_3\text{O}^+] \quad (6)$$

it is possible to evaluate the concentration of [H<sub>3</sub>O<sup>+</sup>] (or [H<sup>+</sup>]) in the tested solution.

**A pH meter**<sup>111</sup> is an electric device used to measure the quantity of H<sup>+</sup> which gives the measure of the acidity or alkalinity of the solution.

Fundamentally, a pH meter consists of a combined glass electrode, which is composed of several parts. The first part is a reference electrode and the second is a system able to measure the equilibrium of H<sup>+</sup> inside and outside the glass aperture of the electrode. The electrode consists in the measurement of an equilibrium which in electrochemistry is associated with a given potential, calculated through the Nernst's equation:

$$E = E^\circ - \frac{0.059}{n} \log \frac{[\text{Red}]^n}{[\text{Ox}]^m}$$

(7)

which depends on the activity of the reactants and products. Depending on the activity of the  $H^+$  in the outside solution, the internal system reaches a given potential. As it is not possible to measure a potential alone (we always measure a tension which is a difference of potentials) the tension is measured compared to an included reference electrode which has a known potential, so from the tension it is possible to deduce the potential of the electrode and find back the concentration of  $H^+$ .

The calibration curve was performed with stock solutions of pH= 4, 7 and 10. The pH is measured at LEPMI laboratory, with SI Analytics, Titration Titroline® 6000/7000.

### ❖ Polymer and water determination by TGA and Karl-Fischer

The thermogravimetric analysis (TGA) has been used for two main purposes: the measurement of the polymer content in the two phases after obtaining an ABS and the measurement of the water content in the ionic liquid [P<sub>44414</sub>]Cl. TGA is a method of a thermal analysis in which the evolution of the sample weight is recorded while its temperature is progressively increased.<sup>112</sup> In order to optimize the polymer determination, several samples of water / HCl mixtures of different proportions, PEG-600 / HCl / water and PEG-600 / metal ions / HCl / water were tested. The objective of analyzing three different types of mixtures was to understand the effect that the polymer or metal ions have on the water and HCl matrix solution. As for the determination of the water content into the ionic liquid, this was taken directly from the bottle and analyzed with the TGA. The crucible used for all the experiments was made from alumina. The instrument is a Mettler Toledo, with an accuracy of 0.0025% and the analyses were performed thanks to the help of Mr. Vincent Martin, responsible of the TGA device, situated at Leumi laboratory, UGA (University of Grenoble Alpes).

The water content of the ionic liquid [P<sub>44414</sub>]Cl has been determined also by **coulometric** Karl Fischer titration<sup>113</sup> where the iodine is electrolytically generated. During the titration, iodine is added to the sample and the amount of iodine used to consume all the water contained in the sample is determined by measuring the current needed for the electrochemical generation of the iodine. When reacting with water, the brown iodine is reduced to the colorless iodide. The ionic liquid samples were prepared under a glove box. The detection upper limit of the apparatus is 300ppm water. The sample was injected through a syringe and the maximum volume used is 2-3 mL. The Karl-Fischer apparatus used is a TITROLINE, 7500 KF placed at LEPMI laboratory - UGA.

#### ❖ Determination of metals concentration by AAS and ICP-MS

The atomic absorption (AA) and emission (AE) spectrometer was used to determine the concentration of metals in APERAM baths, synthetic solutions and the distribution of metals in biphasic systems. AAS is an analytical technique used for both quantitative and qualitative determination of metal ions in solution. The atomic absorption spectroscopy<sup>114</sup> is so named because a flame is used to atomize a sample. The atoms then interact with photons from the hollow cathode lamp and these photons are absorbed by the samples under certain conditions. The chemical-physical principle on which photon absorption is based on the fact that the atomic energy levels are discrete, therefore the electronic transitions allowed by radiative excitation are characteristic for each atom. Unlike molecules, atoms do not contain rotational or vibrational sub-structures and, therefore, the absorption of an electromagnetic radiation by excitation at a higher energy level does not occur for a frequency band but at a discrete wavelength. This implies that for each wavelength to which a electronic transition corresponds, quantitative measurements can be made by applying Beer Lambert's law:

$$A = \log_{10} I_0/I \quad (8)$$

$$A = - \log_{10} T \quad (9)$$

Where the absorbance ( $A$ ) is equal to the logarithm to the 10 of the ratio of the incident intensity,  $I_0$  over the transmitted intensity,  $I$ .  $T$  corresponds to the transmittance. The measurements were accomplished by calibration using single metal standard solutions. All calibration curves were based on six standards, including blank. The calibration ranges were selected in between 1 mg/L and 50 mg/L (1 – 4 – 10 – 25 – 50 mg/L). Standard solutions for AAS analyses were prepared by diluting a 1000 mg/L single element solution in 250 mL of total volume for each calibration point for each metal. The samples to be analyzed were diluted so that the concentration range for each metal could be between 5 and 50 mg/L.

Atomic emission spectroscopy<sup>115</sup> (AES) measurements were also possible with the same instrument. In fact, Na(I) was determined by this method, where the thermal energy of the flame excites the atoms of the injected compound into excited electronic states which will emit light once they return to their fundamental state (photon emission). Each element therefore has its own characteristic emission light with a given photon energy. Also, in this case it was necessary to use a calibration curve; for Na(I) the range of the selected calibration curve was between 0 and 2 mg/L. The AAS/AES instrument is a Perkin Elmer Pinaacle 900F with an accuracy of  $\pm 0.5\%$ .

Inductively coupled plasma mass spectrometry (ICP-MS) has been used to determine the purity of the water recovered at the end the process proposed in the Patent chapter. The inductively coupled plasma-mass spectrometry (ICP-MS) is an analytical technique based on the use of inductively coupled plasma combined to mass spectrometry. It is a very sensitive technique capable of determining various inorganic metallic and non-metallic atoms present in concentrations as low as one part per billion (ppb). It uses an ICP plasma torch to ionize the sample and a mass spectrometer for separation and detection of the ions produced. The apparatus used is a ICP-MS (PerkinElmer NexION 2000), located at Phelma department – G-INP. The experiment was carried out by engineer Vincent Martin, of the Lepmi laboratory, responsible for the apparatus.

#### ❖ Ion chromatography for chloride determination

Through the ion chromatography (IC) it was possible to estimate the concentration of free  $\text{Cl}^-$  in the UGCO bath. Ion exchange chromatography, or simply ion chromatography (IC), separates ions and polar molecules based on their affinity to the ion exchanger. At the column outlet the conductivity detector 1 (881 Compact IC pro1) is placed allowing the concentration determination, the recording time is 40 minutes, the integration is done automatically by the instrument, and the type of column is a Metrosep A. Supp 15-250/4. The composition of the eluent is 3mM  $\text{NaHCO}_3$  + 3.5mM  $\text{Na}_2\text{CO}_3$ . The working temperature is 45 °C. The model used is METROHM, 881 Compact IC PRO.

#### ❖ Sulfates determination by photometric kit

A photometric kit was used to measure sulfates through colorimetric analysis. In colorimetry a white light, natural or artificial, is used as the source of rays and the analysis is carried out with an instrument called a colorimeter or photometer. A colorimetric analysis is based on the principle that many substances reacting with a chemical compound produce a color change whose intensity will be proportional to the concentration of the substance being measured. When a substance is exposed to a source of rays of intensity ( $I_0$ ), part of the radiation is absorbed by the substance. The remaining light is transmitted to a detector. The difference in intensity is used to determine the concentration of the specie in the colored solution. The amount of absorbed radiation is given by the Lambert-Beer law. The absorbance is also given by:

$$A = \epsilon_{\lambda} * C * l \quad (10)$$

where:

A is the absorbance and is dimensionless;

$\epsilon_{\lambda}$  is the proportionality constant, called the molar extinction coefficient; it is a constant for a given substance, provided at a given temperature and wavelength [L/(mol.cm)];

C is the concentration of the substance (moles/liter);

l is the optical path length, i.e. the distance the light beam travels through the sample (cm).

Therefore, by knowing these factors, the concentration (C) can be calculated from the absorbance of the substance in relation to the transmitted radiation (I).

For the sulfates determination, standard solutions containing barium ions were used. The latter react with the sulfates to give the poorly soluble barium sulfate at pH between 2 and 10 (pH range to be observed)<sup>116</sup>. The resulting turbidity is measured by the photometer. Samples containing sulfates are pre-diluted in a concentration range of 100 to 1000 mg/L. The standard deviation of the method is 10.3 mg/L  $\text{SO}_4^{2-}$ . The instrument used is a Spectroquant Nova 60 A supplied by Merck.

#### ❖ PEG and IL concentration determination by NMR

Proton nuclear magnetic resonance ( $^1\text{H-NMR}$ ) was used to quantitatively determine the concentration of the polymer and the ionic liquid in the different phases of the ABS obtained during the investigations. In addition, the presence of organic impurities in the ionic liquid [P<sub>4 4 4 14</sub>] Cl was verified using NMR too. NMR is a technique based on the measurement of the precession of the spin of protons or other nuclei characterized by magnetic moment when subjected to a magnetic field. In particular, the  $^1\text{H-NMR}$  protocol for PEG-400 and [P<sub>4 4 4 14</sub>] Cl quantification has been carried out. It is based on D<sub>2</sub>O and DMSO (dimethyl sulfoxide) as solvent. The solvent was prepared mixing 200  $\mu\text{L}$  of DMSO and 8,75mL of D<sub>2</sub>O. The position of the DMSO chemical shift is located close to that of the two compounds of interest, without interfering with them, while previous attempts demonstrated that by using C<sub>6</sub>H<sub>6</sub>, its chemical shift was located too far from that of polymer signal, so the data treatment leads to curve distortions detrimental to the calibration accuracy. The sample was prepared considering a total volume of 450  $\mu\text{L}$  where 358  $\mu\text{L}$  is in solvent (DMSO + D<sub>2</sub>O) and about 95  $\mu\text{L}$  is in phase to be analyzed. Depending on the type of phase from an ABS, when considering first the polymeric one, this has to be diluted by a factor of 10, while the non-polymeric phase was used directly without dilution. The diluted

solution must be present in a homogeneous phase By mixing PEG/water with composition from 10-90wt% to 55-45wt%, the calibration curve showed in Figure 42 was obtained.

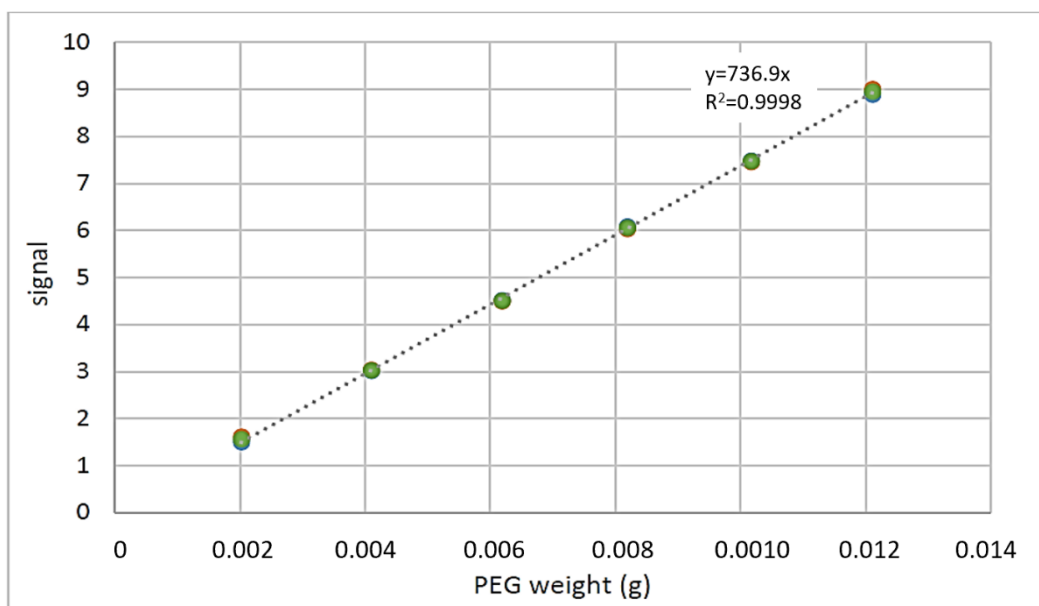


Figure 42. Calibration curve for NMR protocol for PEG determination.

The apparatus used is an NMR 400MHz, BRUKER, Advance III HD located at LEPMI laboratory – UGA. The experiment was carried out by me.

❖ **ESI-MS for metal speciation determination and distribution of molecular weight of PEG-400**

Electrospray Ionization– Mass Spectrometry (ESI-MS)<sup>117,118</sup>, was used to determine the speciation of the metals in solution. ESI does not fragment the macromolecules into smaller charged particles, rather it turns the macromolecule being ionized into small droplets by converting a solution-phase analyte into gas-phase ions. These droplets will then be further de-solvated into even smaller droplets,

Metallic ions ↓	[HCl] (M) →	5	12	5	12	5	12
Ni(II)		✓	✓				
Cr(III)		✓	✓				
Fe(II)				✓	✓		
Fe(III)		✓	✓			✓	✓
Metal ions concentration (g/L)→		5	20	5	20	5	20

Table 9. Stock solutions of metal ions used for ESI-MS analysis.

which creates molecules with attached protons. These protonated and de-solvated molecular ions will then be passed through the mass analyzer to the detector, and the mass of the sample can be determined. The solvent used in this investigation is water. Other solvents were tested like ethyl acetate or dichloromethane, however the last one presented complex molecule with the metals in the solution. The intensity of the peaks is not considered in this protocol. Even if the concentration of injection of the apparatus (5 $\mu$ /L) and the dilution factor to prepare the solution are known parameters, it would have been necessary to have a calibration curve to define the concentration of the species. Therefore, the results are only for a qualitative interpretation. Different samples were analyzed by ESI-MS (Table 9). Among these, stock solutions of Ni(II), Cr(III), Fe(II) and Fe(III) at 5 and 12M of HCl and at different concentrations of metal ions were analyzed.

Furthermore, the UGCO bath was analyzed by ESI-MS alone and after mixing it with 20 wt% of PEG-600, the two phases were characterized by the instrument. The experiments were performed at different dilution factors (d = 50,100). Only the first part of each ESI-MS spectrum is related to the metal ions of interest (from 0 to 200 m/z). After 200 m/z the source provokes an ionization process creating a dimerization of the metal ions, from that point it is not possible to understand if the presence of the dimer is due to the source or it is a real dimer in the solution, or both the cases. A further experiment was performed thanks to ESI-MS to investigate the degradation of PEG-600 and its ability to complex with metal ions. The apparatus is a Bruker Amazon Speed. The source is the electrospray ionization source connected to a mass spectrometer. The experiment was carried out in collaboration with Laure Fort, Rodolphe Gueret and Amelie Durand from the Molecular Chemistry Department of Grenoble.

### ❖ Fe(II)/Fe(III) speciation through colorimetric technique

The concentration of Fe(II) species in a mix solution of Fe(II) and Fe(III) in HCl medium (37 wt%) was determined by titration with KMnO<sub>4</sub>. This protocol is applicable for a concentration of Fe(II) from 5g/L to 80 g/L.

The reaction occurring during the colorimetric technique, consists of the oxidation of Fe(II) in Fe(III):



Five moles of Fe(II) were oxidized in Fe(III) using one mole of MnO<sub>4</sub><sup>-</sup>.

The stock solution containing Fe(II/III) species was diluted by a factor of 10. Two milliliters of the diluted solution were adjusted with an arbitrary volume for the analyses (this last volume was not a

parameter to be considered due to the general equation taken into account where are considered the moles and not the concentration of the stock solution). The solution of permanganate was prepared with an exact normality and introduced in a volumetric flask for the titration. Drop by drop the solution was mixed with the clear stock solution of Fe(II/III). The process finished when the stock solution starts to have a pinkish color.

The equation used for the calculation of Fe(II) (g/mL) is:

$$[\text{Fe}^{2+}] = V(\text{KMnO}_4)_{\text{eq}} \times [\text{KMnO}_4] \times M(\text{Fe}) \times \text{FD} / V_{\text{pe}} \quad (12)$$

$V(\text{KMnO}_4)$  = the volume (mL) of permanganate used for the titration.

$[\text{KMnO}_4]$  = the normality of the permanganate ( $n_{\text{eq}}$ /mL, precise value).

$M(\text{Fe})$  = molecular weight of Fe (55,85 g/mol)

FD = dilution factor x used for the preparation of the stock solution diluted

$V_{\text{pe}}$  = volume (mL) used of the diluted stock solution

## 5. Composition of different sulfate and chlorinated baths

During the PhD, different samples of UGCO and  $\text{Na}_2\text{SO}_4$  baths were sent from Aperam for analysis and metal extraction purposes. The metal composition of the aliquots was determined through AAS.

Regarding the samples from UGCO bath (Figure 43), they were sent in three different periods 2017, 2018 and 2019. For the samples received in 2017 and 2018, the concentrations of Fe(III) (78 g/L) and Cr(III) (20 g/L) are the same in all the samples, however, in the bath of 2019 Fe(III) is presented at almost 95 g/L. While the concentration of Ni(II) is higher in the bath of 2017 (almost 15 g/L), it is about 5 g/L in the bath received in 2018 and 2019. The density was found to be the same in all baths samples received, equal to 1.3. While the  $\text{H}^+$  concentration is 5.7 mol/L for the 2017 bath, 3.4 mol/L for the 2018 bath and 5.6 mol/L for the 2019 bath.

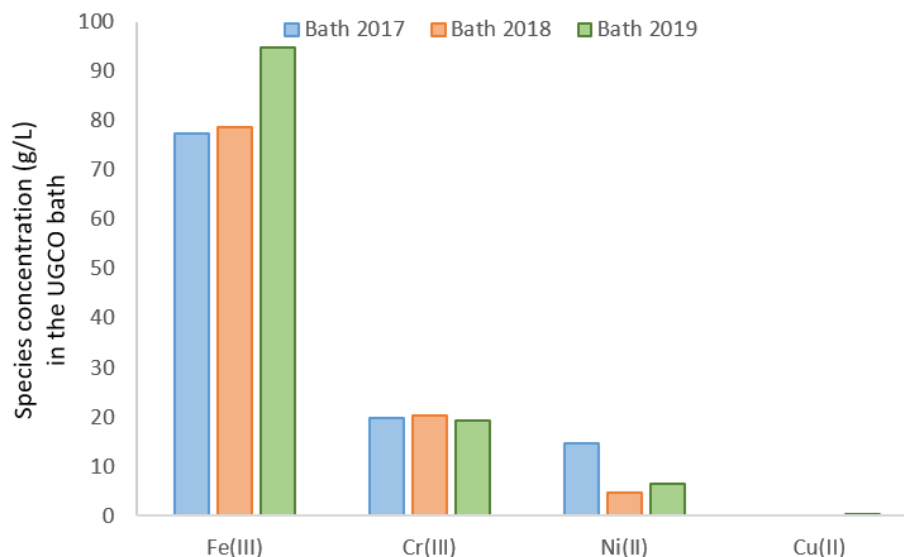


Figure 43. UGCO bath composition of three different aliquots sent by Aperam.

Regarding the aliquots of  $\text{Na}_2\text{SO}_4$  bath (Figure 44), three aliquots were received during 2018, two coming from the Isbergues site, received at the beginning of 2018 and at the end of 2018, and one coming from the Gueugnon site and received at the end of 2018. As far as the concentrations of Cr(VI), Fe(III) and Ni(II) in these samples are concerned, they are approximately the same, about 12 g/L of Cr(VI), and less than 1 g/L of Fe(III) and Ni(II). As far as the concentration of Na(I) is concerned, it remains constant in the baths from Isbergues (about 47 g/L) while it is present in greater quantity when considering the bath received from Gueugnon (about 67 g/L). The same happens for  $\text{SO}_4^{2-}$ , in the two baths coming from Isbergues it is found at 105 g/L, while in the bath coming from Gueugnon it is present for about 155 g/L. The density of the samples is between 1.15 and 1.18, while the pH is about 1.8-1.9 for the samples from Isbergues and rises to 2.4 for those from Gueugnon.

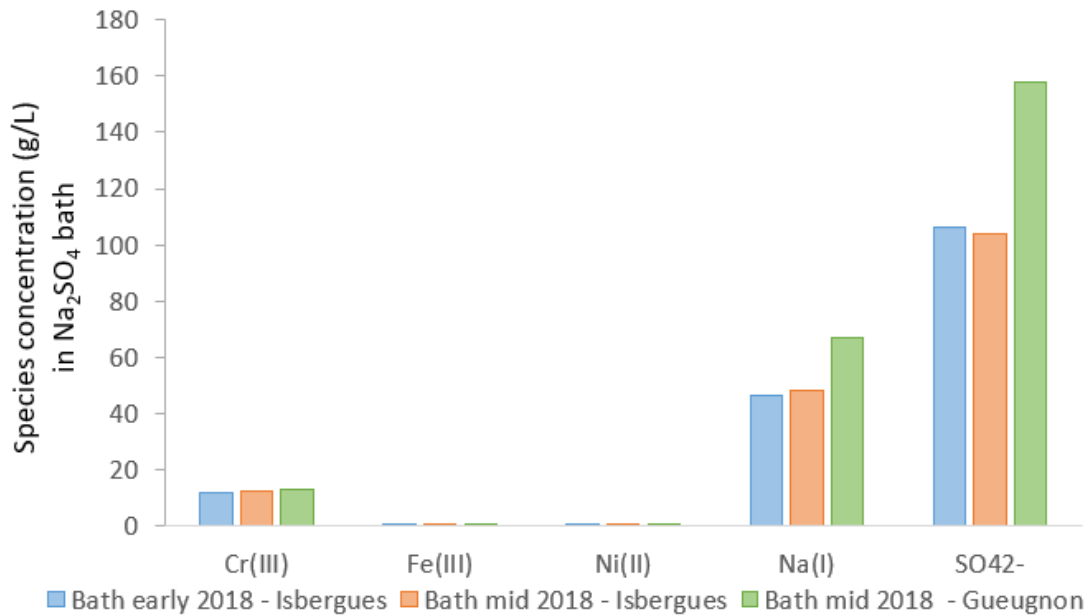


Figure 44. Na<sub>2</sub>SO<sub>4</sub> bath composition of three different aliquots sent by Aperam.

In both cases, the samples from the UGCO bath and the Na<sub>2</sub>SO<sub>4</sub> bath were taken and sent at different times of the pickling processes. The pickling process is a continuous process, the baths are never re-made from zero, and to enable the baths to work continuously, they are regenerated with fresh baths containing water, acids or salts. From this can be deduced that the concentration of acids, for example, always fluctuates over a range of values. For the dissolved metals, it is the same principle, the metals are coming from the pickled alloy, however, there are several types of stainless steel and also several campaigns of treatment where the types of steel are separated. So, if the samples have been taken during the pickling of austenitic steel, the pickling bath used for this treatment should have a high quantity of nickel because of the dissolution of this grade. However, if the sample was taken at the end of a ferritic campaign (ferritic have no Ni in their composition), the content in Ni in the bath will be lower. Hence, the different concentration levels of freshly sampled baths are showing the variability of composition of the industrial baths.

During the PhD, it was decided to work with baths that had close concentrations in order to be able to compare the obtained results. In the following chapters, for the purposes of analysis, the composition of the baths that was considered is as presented in Table 10, for the UGCO bath and in Table 11 for the Na<sub>2</sub>SO<sub>4</sub> bath.

Components and parameters	UGCO bath
Fe (II) (g/L)	50
Fe (III) (g/L)	50
Cr (III) (g/L)	19.3

Ni (II) (g/L)	4.6
Cl <sup>-</sup> (g/L)	200
[H <sup>+</sup> ](mol/L)	4-5
density (g/mL)	1.28

Table 10. Composition, pH and density of UGCO bath.

Components and parameters	Na <sub>2</sub> SO <sub>4</sub> Bath
Cr (VI) (g/L)	11.8
Ni (II) (g/L)	0.4
Fe (III) (g/L)	0.5
Na (I) (g/L)	46.7
SO <sub>4</sub> <sup>2-</sup> (g/L)	106
pH	1.8
density (g/mL)	1.14

Table 11. Composition, pH and density of Na<sub>2</sub>SO<sub>4</sub> bath.

## 6. Stock solution single or multi-metal to mimic the UGCO bath and Na<sub>2</sub>SO<sub>4</sub> bath.

In order to better understand the partitioning mechanism that takes place in Aperam baths, single and double metal synthetic solutions were prepared using the same species concentrations as in the baths.

All the stock solutions made to mimic the Na<sub>2</sub>SO<sub>4</sub> bath (showed from Figure 46 to Figure 55) have been prepared by mixing a metallic salt and Na<sub>2</sub>SO<sub>4</sub> in H<sub>2</sub>O and the pH has been adjusted with H<sub>2</sub>SO<sub>4</sub>. First of all, a known quantity of metallic salt was added to the beaker. Consequently, the acid was added and everything was stirred overnight to allow the total dissolution of the salt in an acidic environment.

The next day the sample was left under agitation in contact with a heat source for 30 minutes at a given temperature to prepare the compound for the working conditions of the process. The preparation and weight of the acid/metallic salt mix was carried out under a fume hood, and also in this case the beaker was covered with a plastic film. All the solutions have been prepared to contain approximately 5g/L of metal ion, 105 g/L of SO<sub>4</sub><sup>2-</sup>, 50 g /L of Na(I) and pH around 1.8. The decision to prepare these solutions in this

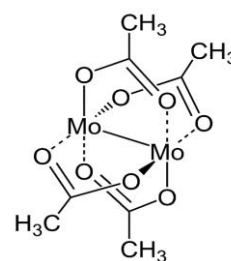


Figure 45. Mo(II) acetate dimer

way was made to imitate the concentrations present in the  $\text{Na}_2\text{SO}_4$  bath and then to compare the obtained results. The 5 g/L concentration of the metals was chosen based on their solubility. All metals are soluble under the proposed conditions except Cr(III) and Mo(II). According to the analysis with AAS the concentration of Cr(III) and Mo(II) present in the stock solution is equal to 0.62 g/L for Cr(III) and 0.8 g/L for Mo(II). The salt used for the experiment with Mo(II) is a molybdenum acetate dimer (II) (Figure 45) because only in this form could this metal be found commercially. While, Cr(VI) and Mo(VI) come from their sodium salts, and the remaining metals from their corresponding sulfate salts. All the biphasic samples, considered to determine the extraction efficiency of PEG-400, were prepared following the same distribution in PEG-400/stock solution single-element: 20/80, 30/70, 40/60 wt%. At 10/90 wt% of PEG-400/stock solution all the systems are monophasic. With regard to the samples in Figure 53, it was not possible to determine the composition of the upper and lower phase because as soon as the PEG-400 was mixed to the stock solution of Mn(VII) a reaction occurred and a dark precipitate appears on the bottom of the flask. For establishing the extraction efficiency of PEG-400, all samples were prepared at room temperature (the room temperature in the laboratory at the time of the experiment was 19°C). For obtaining the binodal curves the working temperature has been set to 25°C, controlled using a thermal bath. The ABSs for the aforementioned solutions will be analyzed in Chapter D.



Figure 46. From the left to the right: Stock solution Cr(VI) in  $\text{Na}_2\text{SO}_4/\text{H}_2\text{O}$ ; biphasic samples: 20/80, 30/70, 40/60 wt% of PEG-400/stock solution. The stock solution is made by 5g/L of Cr(VI), from  $\text{Na}_2\text{Cr}_2\text{O}_7 \cdot 2\text{H}_2\text{O}$  salt, 105g/L of  $\text{SO}_4^{2-}$ , 52.3g/L Na(I), pH=1.80.

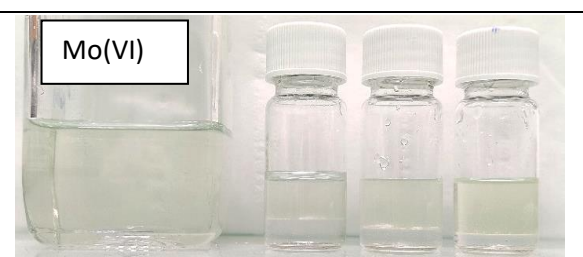


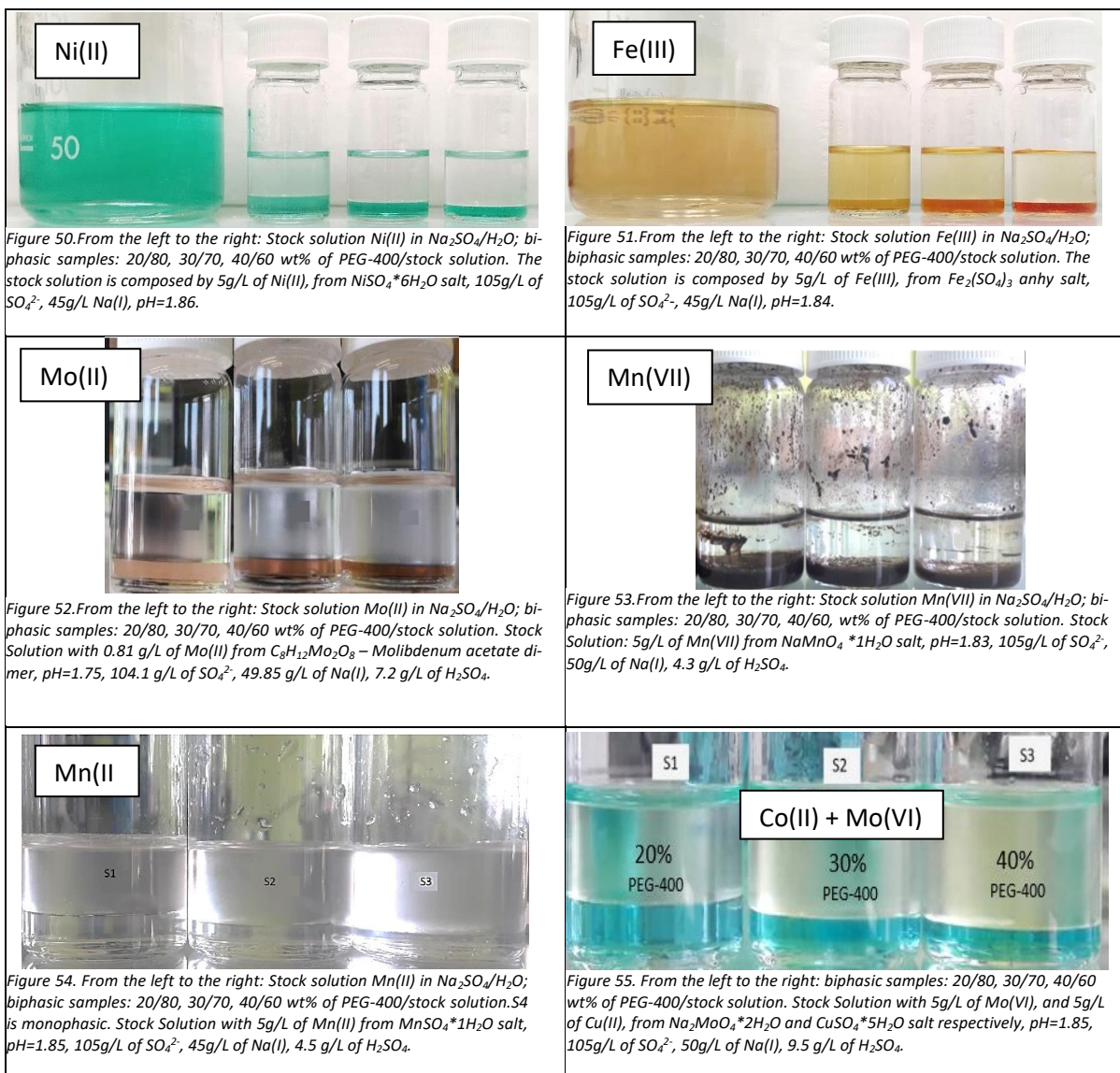
Figure 47. From the left to the right: Stock solution Mo(VI) in  $\text{Na}_2\text{SO}_4/\text{H}_2\text{O}$ ; biphasic samples: 20/80, 30/70, 40/60 wt% of PEG-400/stock solution. The stock solution is made by 5g/L of Mo(VI), from  $\text{Na}_2\text{MoO}_4 \cdot 2\text{H}_2\text{O}$  salt, 105g/L of  $\text{SO}_4^{2-}$ , 52.43g/L Na(I), pH=1.87.



Figure 48. From the left to the right: Stock solution Cu(II) in  $\text{Na}_2\text{SO}_4/\text{H}_2\text{O}$ ; biphasic samples: 20/80, 30/70, 40/60 wt% of PEG-400/stock solution. The stock solution is made by 5g/L of Cu(II), from  $\text{CuSO}_4 \cdot 5\text{H}_2\text{O}$  salt, 105g/L of  $\text{SO}_4^{2-}$ , 45g/L Na(I), pH=1.87.



Figure 49. From the left to the right: Stock solution Cr(III) in  $\text{Na}_2\text{SO}_4/\text{H}_2\text{O}$ ; biphasic samples: 20/80, 30/70, 40/60 wt% of PEG-400/stock solution. The stock solution is composed by 0.62 g/L of Cr(III), from  $\text{Cr}_2(\text{SO}_4)_3$  anhy. salt, 93 g/L of  $\text{SO}_4^{2-}$ , 43.63 g/L Na(I), pH=1.77



The concentration of metal ions used to prepare each stock solution made to mimic the UGCO bath was about 5 g/L. All different species investigated (Fe(II), Fe(III), Cr(III)) were soluble at the same working conditions, except for Ni(II) which some traces of non-dissolved salt remained solution. The concentration of this last element was determined by AAS and results to be 4 g/L. The decision to work with 5g/L and not more, comes from the difficulties to dissolve the species in HCl medium. The HCl concentration was equal to 5M. The preparation of these solutions is analogous to that for sulfate bath stock solutions.

## 7. Extraction and repartition efficiency

The extraction efficiency of the ionic liquid or the various polymers used in this manuscript, is determined by the following equation:

$$e.e.(U) \% = \frac{Me_{f(U)}}{Me_i} \times 100$$

$$e.e.(L) \% = \frac{Me_{f(L)}}{Me_i} \times 100$$
(13)

Where:

- $e.e.(U)\%$  corresponds to the extraction efficiency of the IL (or polymer), expressed in weight percentage, on the upper phase of an ABS.
- $e.e.(L)\%$  corresponds to the extraction efficiency of the IL (or polymer), expressed in weight percentage, on the lower phase of an ABS.
- $Me_i$  is the initial mass (in the stock or industrial solution) of metal, expressed in grams.
- $Me_{f(U)}$  is the final mass of metal in the upper phase of an ABS, expressed in grams.
- $Me_{f(L)}$  is the final mass of metal in the lower phase of an ABS, expressed in grams.

With regard to the repartition efficiency of metals in the upper and lower phases of an ABS, this was calculated according to the equations:

$$Me_{(U)} \% = \frac{Me_{(U)}}{Me_{(U)} + Me_{(L)}} \times 100$$

$$Me_{(L)} \% = \frac{Me_{(L)}}{Me_{(U)} + Me_{(L)}} \times 100$$
(14)

Where:

- $Me_{(U)}\%$  is the metal repartition expressed in weight percentage, in the upper phase of an ABS.
- $Me_{(L)}\%$  is the metal repartition expressed in weight percentage, in the lower phase of an ABS.
- $Me_{(U)}$  is the mass of metal expressed in grams, in the upper phase of an ABS.
- $Me_{(L)}$  is the mass of metal expressed in grams, in the lower phase of an ABS.

Both the extraction and repartition efficiency are influenced by a large number of factors, such as:

- the experimental error that occurs when measuring the volume distribution between two phases in an ABS;
- the formation of crystals that occurs during the investigation with temperature, which reduce the accuracy of AAS measurements;
- The dilution factors of the solutions analyzed were often found to be too high in relation to the corresponding calibration curves required by the instrument (e.g., d=10K to analyze Na(I) with AAS);

For these reasons, it was therefore very challenging to achieve a favorable mass balance, since it appeared that:

$$\text{Initial values} - \text{Final values} \neq 0 \quad (15)$$

Where initial values refer, in particular, to the grams of metal used to prepare a solution (or already present in an industrial solution), and final values correspond to the grams of metal in the upper and lower phase of an ABS.

Furthermore, in both cases the volume of the upper and lower phase in an ABS was a very important parameter taken into account during the calculations as it is known that:

$$\text{Me} = [\text{Me}] \times \text{Vol.}_{\text{phase}} \quad (14)$$

to obtain the mass of the metal (Me), expressed in g, the concentration of the metal [Me] obtained during the different analysis and expressed in g/L, must be multiplied by the volume of the phase (Vol.<sub>phase</sub>) where the metal is to be found, and this is expressed in L. Equation (14) also shows how the calculations were carried out to go from the concentrations (g/L), obtained in the various analysis techniques, to the mass (g) of metal and consequently to the repartition and extraction values.

## Conclusions

Both the turbidity and the battleship methods are effective in obtaining the experimental points necessary for the investigation of various three-components system. Through these methods it is then possible to represent a binodal curve on the phase diagram, for each system investigated, when this naturally provided an ABS. Each phase diagram and corresponding binodal curve for the different systems investigated will be presented in the following chapters. Once a biphasic sample has been obtained, this is to be considered as an individual ABS as it is characterized by unique set of working

conditions (concentration, pH, temperature, etc.). The sample is then analyzed using various instruments to determine its upper and lower phase compositions.

# C. ABS formation and metal extraction in hydrochloric media





## 1. Introduction

The UGCO bath is a patented pickling bath. It uses hydrochloric acid to dissolve the oxide layers and Fe(III) which reduces to Fe(II) and oxidizes the metals present on the surface of the stainless steel facilitating thus the dissolution process. The operating pickling conditions of the bath are maintained through the addition of a fresh acid and by oxidizing Fe(II) to Fe(III) *via* the addition of the hydrogen peroxide. The bath needs a continuous maintenance (i.e. adjustment of the composition), since its high aggressiveness allows the dissolution of large quantities of metals, which precipitate then in the form of a sludge. Moreover, the management of the settings of this bath is complicated by the relative low concentration of the commercial HCl acid (33w%) and a partial dumping of the bath is required in order to free tank volume for the addition of fresh acid. Nowadays the most common method used by Aperam is to neutralize the used pickling baths and send the sludge to a landfill. The best method to regenerate this bath would be the spray roasting followed by a distillation column to regenerate the acid, but the process is very expensive. The request of Aperam concerning this bath is to extract Cr and Ni from it, with only a low amount of iron co-extracted if possible, together with a dehydration of the bath and the removal of the present copper (which is an inhibitor of the pickling reaction). In

Table 12 it is possible to see the metal concentrations of the spent pickling liquor coming from the UGCO bath. Fe is the most present element in the bath, 89 g/L, followed by Cr and Ni, 18.87 g/L and 7.8 g/L respectively. Mn (1 g/L), Mo and Cu (<1g/L) are also present. In order to meet Aperam's demand for this bath and find an alternative to spray roasting, ABS systems based on ionic liquid or polymers were tested.

UGCO bath	
Type of Metal	Concentration (g/L)
Fe	88.86
Cr	18.87
Ni	7.88
Mn	1.08
Mo	0.36
Cu	0.35

Table 12. Metal concentration in UGCO bath.

## 2. Preliminary tests on ABS formation and metal extraction on SPL from UGCO bath

The first series of tests were aimed at obtaining ABS using the UGCO bath. For this purpose were chosen the ionic liquid [P<sub>44414</sub>]Cl and the polymer PEG-600. As described in the state of the art, both the biphasic inducers have already been widely used to obtain an ABS and extract metals. As for PEG-600, it was mixed with the UGCO bath according to a repartition of 30 / 70 wt% respectively at 25 °C, and this provides an ABS. The upper and lower phases, of the ABS, were analyzed by AAS. The polymer is mainly in the lower phase, and it extracts about 45% of iron, while nickel and chromium remain in the upper phase. Almost 40 wt% of H<sup>+</sup> is to be found in the polymer phase (Figure 56).

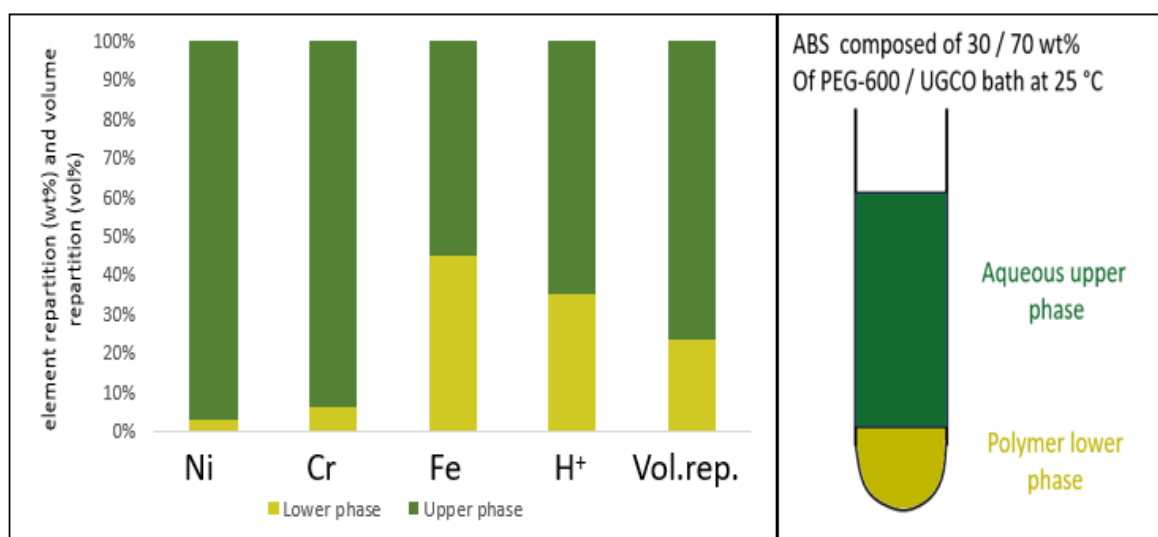


Figure 56. Element repartition (wt%) and volume repartition (vol%) for ABS composed of PEG-600 / UGCO bath (30/70 wt%) at 25°C.

As for the ionic liquid, it was mixed with UGCO bath in a ratio of 20 / 80 (wt%) respectively, at 20 °C, and the mix provide an ABS. When using more than 30 wt% of IL, a part of the IL remains in solid form under UGCO bath conditions. The IL is in this case in the upper phase of the system, and it extracts about 37 wt% of Fe while Cr and Ni remain in the bath (Figure 57).

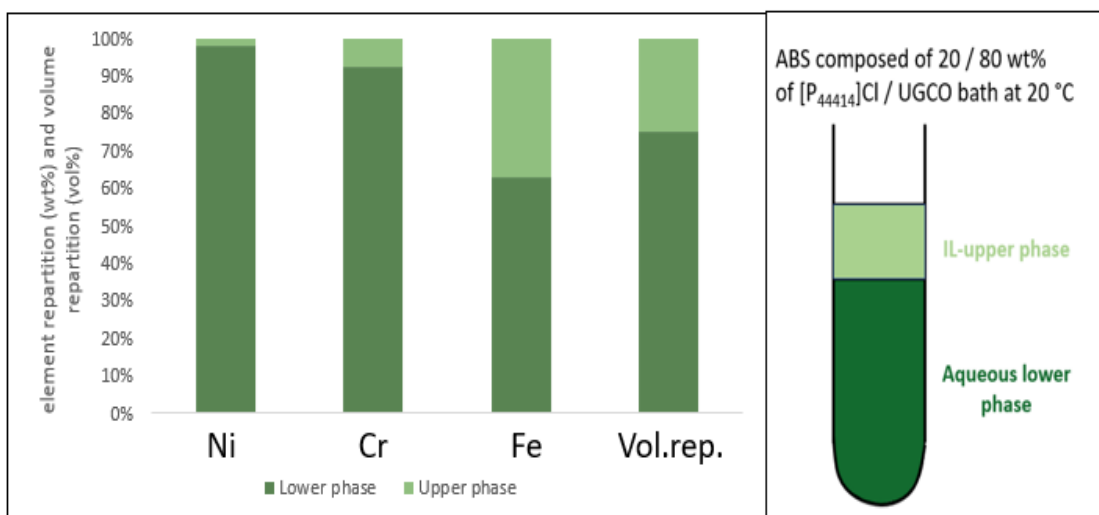


Figure 57. Element repartition (wt%) and volume repartition (vol%) for ABS composed of  $[P_{44414}]Cl$  / UGCO bath (20 / 80 wt%) at 20 °C.

This type of experimentations did not therefore lead to the fulfilment of Aperam's request to purify the UGCO bath from Ni(II) and Cr(III). However, the result obtained, in particular with PEG-600, was very surprising since an ABS was obtained using a polymer under very acidic conditions and high metal concentration.

### 3. Properties of ABS in HCl media

The following sections of this chapter have been supplemented by the article entitled "Uncommon biphasic behavior induced by very high metal ion concentrations in  $HCl/H_2O/[P_{44414}]Cl$  and  $HCl/H_2O/PEG-600$  systems", published on 30 September 2020.

#### 3.1. Systems without metals

The extraction efficiency of PEG-600 (45 wt% of iron extracted) or  $[P_{44414}]Cl$  mixed with UGCO bath when ABS was obtained did not allow to meet Aperam's initial request to clean the bath from all metals except the iron. For this reason, it was particularly challenging to continue working directly with the UGCO bath because the high number and concentration of species in it (metal ions, salts, acids, water) and above all the dark colour of the bath did not allow to further investigate. In particular, it has been tried to obtain a phase diagram and the corresponding binodal curve by using the turbidity method for the polymer / UGCO bath or IL / UGCO bath system, but it was very hard to understand

when the system turned from monophasic to biphasic due to the bath colour. The idea was therefore to simplify the real system, starting with the investigation of metal-free ABS. As far as the ionic liquid is concerned, Figure 58 shows the phase diagram and the binodal curve for the system  $[P_{4.4.4.14}]Cl/[HCl\ 37\ wt\%]/H_2O$  at  $T=25\ ^\circ C$  compared with the one already existing from Mogilireddy *et al.*<sup>119</sup>

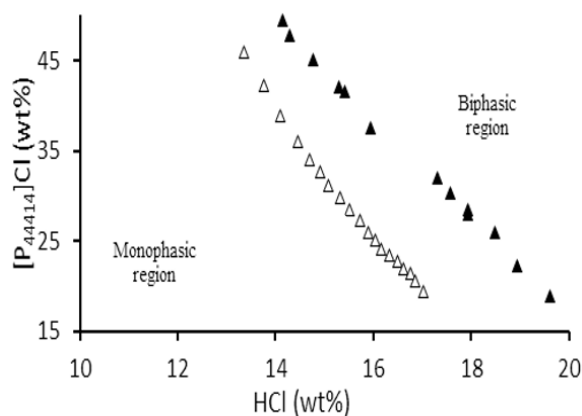


Figure 58. Binodal curves of the systems:  $[P_{4.4.4.14}]Cl/[HCl\ 37\ wt\%]/H_2O$  (IL = Cytec) (▲)<sup>10</sup>;  $[P_{4.4.4.14}]Cl/[HCl\ 37\ wt\%]/H_2O$  (IL = Interchim) – this work (Δ);

This difference between the two binodal curves without metal ions is ascribed to the different providers (*i.e.* Cyphos® IL 167- Cytec<sup>119</sup> versus Interchim, this work). According to the literature, phosphonium based ILs are prepared by nucleophilic addition of tertiary phosphines to haloalkanes.<sup>65,120</sup> The used phosphines can contain several isomers and other impurities (such as phosphine oxides) that can then be found in the resulting IL<sup>120</sup> and depending on their quantity influence the ABS formation. The different level of impurities is probably responsible of binodal curves shifts, although no information on this particular phenomenon has been found in the literature. Fortunately, this observation did not impact the results of this study as only Interchim's product has been used in this work. However, this part of the investigation requires more study, on understanding the causes that lead the two binodal curves to be in a different space of the phase diagram. In contrast, it has been checked that using different HCl providers (*i.e.* Fluka and Sigma Aldrich) does not induce discrepancies in the binodal determinations (Figure 137 - Annex).

As regards to the polymer, the system PEG-600 /  $[HCl\ 37\ wt\%] / H_2O$  did not provide an ABS. However, having obtained a biphasic system in the preliminary tests when the polymer was directly mixed with the UGCO bath, it was surprising that metal-free system did not behave in the same way. For this reason, the investigation went further, trying to understand the contribution of each metal present in the UGCO bath, and comparing the polymer-based ABS results with the IL-based ABS.

### 3.2. System with single metal

Synthetic stock solutions consisting of a single metal ion were prepared in order to understand which of the metals present in the bath is responsible for obtaining the biphasic system. The synthetic solutions have been investigated not only considering the contribution of PEG-600, but further experiments have been carried out considering the [P<sub>4 4 4 14</sub>] Cl ionic liquid contribution. For this purpose, four mono-element stock solutions of Ni(II), Cr(III), Fe(II) and Fe(III) were prepared in HCl (12M). Starting from the stock solutions of the given metal ion, by mixing them with the ionic liquid [P<sub>4 4 4 14</sub>] Cl and the polymer PEG-600 separately, the corresponding phase diagrams and binodal curves were investigated (only in case of ABS formation). The systems considered are the ones presented in the following table:

<b>Ionic liquid</b>
[P <sub>4 4 4 14</sub> ] Cl/[Ni(II)+HCl 37 wt%]/H <sub>2</sub> O
[P <sub>4 4 4 14</sub> ] Cl/[Cr(III)+HCl 37 wt%]/H <sub>2</sub> O
[P <sub>4 4 4 14</sub> ] Cl/[Fe(II)+HCl 37 wt%]/H <sub>2</sub> O
[P <sub>4 4 4 14</sub> ] Cl/[Fe(III)+HCl 37 wt%]/H <sub>2</sub> O
<b>Polymer</b>
PEG-600/[Ni(II)+HCl 37 wt%]/H <sub>2</sub> O
PEG-600/[Cr(II)+HCl 37 wt%]/H <sub>2</sub> O
PEG-600/[Fe(II)+HCl 37 wt%]/H <sub>2</sub> O
PEG-600/[Fe(III)+HCl 37 wt%]/H <sub>2</sub> O

Table 13. IL-based ABS and polymer-based ABS with metal contribution and HCl media.

All the experimental points obtained for the binodal curves listed above are presented in the tables in the Annex – HCl section.

The investigation was carried out considering a metal concentration range between 0 g/L and 15 g/L to mimic the UGCO bath conditions. The effects of metal salts observed by us are very uncommon in the literature. To the best of our knowledge, only two papers have evidenced changes in temperature of a system by addition of rather large amounts of a metal salt or an oxide: Rim et al.<sup>121</sup> evidenced the effect of large Cr(III) nitrate additions (from 0 to 10 g/L) in the cloud point of an aqueous/surfactant system while Fagnant and co-workers<sup>122</sup> got a decrease of the cloud point temperature by ca. 20 °C by adding up to 4 wt% of Nd<sub>2</sub>O<sub>3</sub> in the HbetTf<sub>2</sub>N/H<sub>2</sub>O system. The HbetTf<sub>2</sub>N is betainium bis (trifluoromethyl-sulfonyl) imide ionic liquid. However, these two systems are somewhat different from the current work. Our data address several aspects of the impact of high metal ion concentrations onto the

binodal curves for one [P<sub>44414</sub>]Cl-based and one PEG-based ABS. Considering two rather different systems consisting of [P<sub>44414</sub>]Cl and PEG-600, the latter being a neutral molecule while the former is formally a salt, the following description was divided into two parts, for these.

### 3.2.1. *IL-based systems*

The fact that metal salts could be part of IL-based ABS is not new. As reviewed by Freire and co-workers<sup>123</sup> some examples with Ca(II) and Mg(II) can be found in literature. Moreover, ABS containing Al(III) salts<sup>124</sup> have also been described. Yin *et al.* investigated ABS composed of ILs and either Rb(I) or Cs(I)<sup>96</sup>. The amounts of metal salts in such systems are in the range of *ca.* 5 to 45 wt% and the ILs used belong mainly to the imidazolium family, although ILs constituted by phosphonium and pyridinium cations can also be found. IL-based ABS induced by Sr(II), Eu(III) and Cs(I) have also been the topic of molecular dynamic simulations<sup>54</sup>. However, these systems can only bear metal ions that are not liable to hydrolysis because their working pH is close to neutrality, so the variety of metal elements composing them is somehow limited.

On the other hand, metal salts, introduced as traces in already formed ILs-based ABS, experience a partition between the upper and lower phases. This is in turn used to perform selective extraction, with numerous examples involving Sc(III)<sup>97</sup>, Cr(VI)<sup>50</sup>, Ru(III)<sup>125</sup>, Co(II) versus Ni(II)<sup>126</sup>, Ag(I) versus Cd(II)<sup>45</sup>, and Cd(II) versus Co(II), Cu(II), Fe(III) and Zn(II)<sup>49</sup>. Again, imidazolium, phosphonium and ammonium ILs' families are the most studied. Similarly, these systems are not compatible with metal ions suffering hydrolysis. More recently, the extraction of metal ions, *i.e.* Pt(IV) and Fe(III), at the trace levels, has been performed in novel AcABS<sup>127</sup>.

Our study differs markedly from these previous works for two main reasons: *i)* the presence of HCl does prevent hydrolysis of the metal ions; *ii)* the metal ions, present in large amounts, can be regarded as modifiers of the original ABS composed of [P<sub>44414</sub>]Cl, HCl (at 37 wt%) and H<sub>2</sub>O, and not as trace level solutes.

Figure 60 displays the binodal curves obtained for several initial Cr(III) concentrations ranging from 0 to 15 g/L. The addition of Cr(III) to the solution leads to an increase in the biphasic domain of the system, shifting the binodal curve to the left side (*i.e.* lesser amount of HCl is needed to promote biphasic regime), while the shape of the curves does not show any significant change.

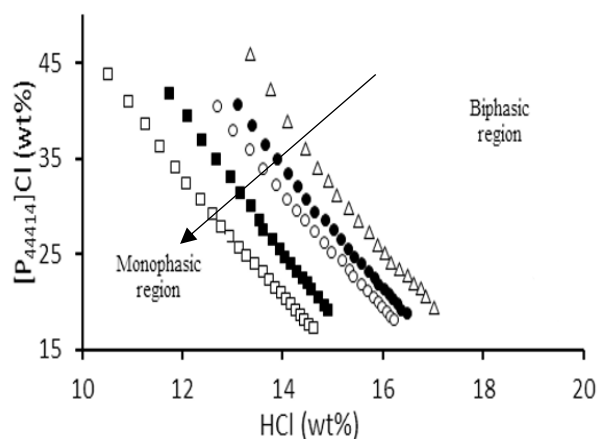


Figure 60. Binodal curves of the systems:  $[P_{44414}]Cl/[HCl\ 37\ wt\%]/H_2O$  (IL = Interchim) – this work ( $\Delta$ );  $[P_{44414}]Cl/[Cr(III)+HCl\ 37\ wt\%]/H_2O - [Cr(III)] = 2.5\ g/L$  ( $\bullet$ );  $[P_{44414}]Cl/[Cr(III)+HCl\ 37\ wt\%]/H_2O - [Cr(III)] = 5\ g/L$  ( $\circ$ );  $[P_{44414}]Cl/[Cr(III)+HCl\ 37\ wt\%]/H_2O - [Cr(III)] = 10\ g/L$  ( $\blacksquare$ );  $[P_{44414}]Cl/[Cr(III)+HCl\ 37\ wt\%]/H_2O - [Cr(III)] = 15\ g/L$  ( $\square$ ) at  $25^\circ C$ . The arrow indicates the increase in metal concentration.

Figure 59 displays the binodal curves obtained for several initial Ni(II) concentrations ranging from 0 to 15 g/L. The same behavior is observed for both Cr(III) and Ni(II) containing systems, *i.e.* an increase in the concentration of metals in the solution leads to a growth of the biphasic domain of the system.

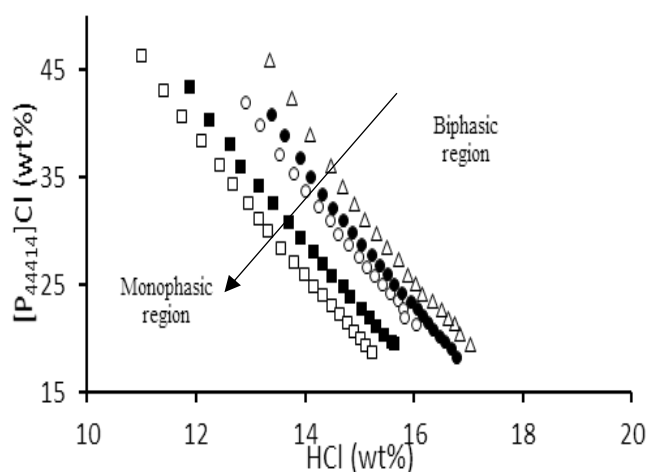


Figure 59. Binodal curves of the system:  $[P_{44414}]Cl/[HCl\ 37wt\%]/H_2O - [Me(x)] = 0\ g/L$  ( $\Delta$ );  $[P_{44414}]Cl/[Ni(II)+HCl\ 37\ wt\%]/H_2O - [Ni(II)] = 2.5\ g/L$  ( $\bullet$ );  $[P_{44414}]Cl/[Ni(II)+HCl\ 37\ wt\%]/H_2O - [Ni(II)] = 5\ g/L$  ( $\circ$ );  $[P_{44414}]Cl/[Ni(II)+HCl\ 37\ wt\%]/H_2O - [Ni(II)] = 10\ g/L$  ( $\blacksquare$ );  $[P_{44414}]Cl/[Ni(II)+HCl\ 37\ wt\%]/H_2O - [Ni(II)] = 15\ g/L$  ( $\square$ ) at  $25^\circ C$ . The arrow indicates the increase in metal concentration.

However, when comparing identical concentrations of Ni(II) and Cr(III) in the same graph, as shown in Figure 61 for 5 g/L and 15 g/L, it is relevant to notice significant differences in the increase of the binodal region when Ni(II) is changed to Cr(III). The experimental points corresponding to Cr(III) are always on the left of the points corresponding to Ni(II) for the same concentration of metals. It seems that chromium (III) has always a higher capacity than nickel (II) to induce the biphasic system.

The experimental curves also show that as the metal concentrations are increased, the difference between the curves of the two metals is more significant. Molecular weight of Ni (58.69 g/mol) is slightly

higher than the molecular weight of Cr (51.99 g/mol), so the difference is of *ca.* 11% and may explain part of the observed differences. However, this should induce a constant effect over the studied range of metal concentrations, which is not experimentally observed. Therefore, the difference cannot be solely ascribed to the difference of molar weight of the two studied components and other phenomena should be considered.

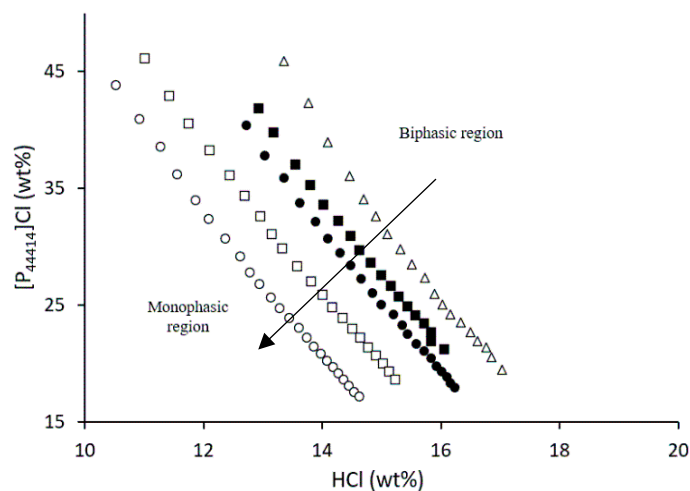


Figure 61. Binodal curves of the systems:  $[P_{44414}]Cl/[HCl\ 37\ wt\%]/H_2O$ ,  $[Me]=0\ gL^{-1}$  ( $\Delta$ );  $[P_{44414}]Cl/[Ni(II)+HCl\ 37\ wt\%]/H_2O$  at 5 g/L ( $\blacksquare$ ) or 15 g/L ( $\square$ ) of Ni(II);  $[P_{44414}]Cl/[Cr(III)+HCl\ 37\ wt\%]/H_2O$  at 5 g/L ( $\bullet$ ) or 15 g/L ( $\circ$ ) of Cr(III) at 25°C. Arrow indicates increase in metal concentration. The arrow indicates the increase in metal concentration.

Therefore, the addition of Ni(II) and Cr(III) salt, at 25 °C, leads to an enlargement of the biphasic area, in comparison with the system in the absence of metal ions (Figure 60 and Figure 59). It is possible to confirm that this effect is metal concentration-dependent, being more significant above *ca.* 1 g/L of metal ion, it increases with concentration and is more pronounced for Cr in comparison to Ni (Figure 61).

Figure 62 and Figure 63 display, respectively, the binodal curves for the systems  $[P_{44414}]Cl/[Fe(II)+HCl\ 37\ wt\%]/H_2O$  and  $[P_{44414}]Cl/[Fe(III)+HCl\ 37\ wt\%]/H_2O$  obtained for several Fe concentrations. A rather particular behavior is seen when Fe(II) or Fe(III) is used instead of Ni(II) or Cr(III). There is still an increase in the biphasic domain of the system when the Fe concentration is increased but there is also a substantial change in the shape of the curve as compared to curves obtained for Ni(II) or Cr(III).

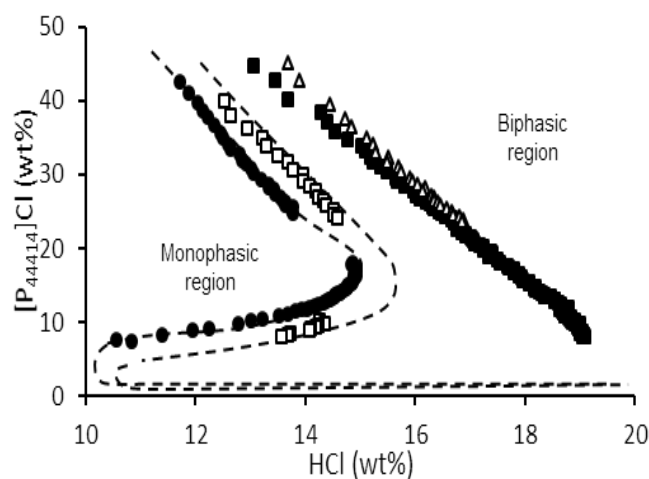


Figure 62. Binodal curves of the system  $[P_{44414}]Cl/[Fe(II)+HCl\ 37\ wt\%]/H_2O$  at:  $[Fe(II)] = 0\ g/L$  ( $\Delta$ ),  $[Fe(II)] = 1\ g/L$  ( $\blacksquare$ ),  $[Fe(II)] = 10\ g/L$  ( $\square$ ) and  $[Fe(II)] = 15\ g/L$  ( $\bullet$ ) at  $25^\circ C$ . Dashed lines (---) are only a guide for the eye.

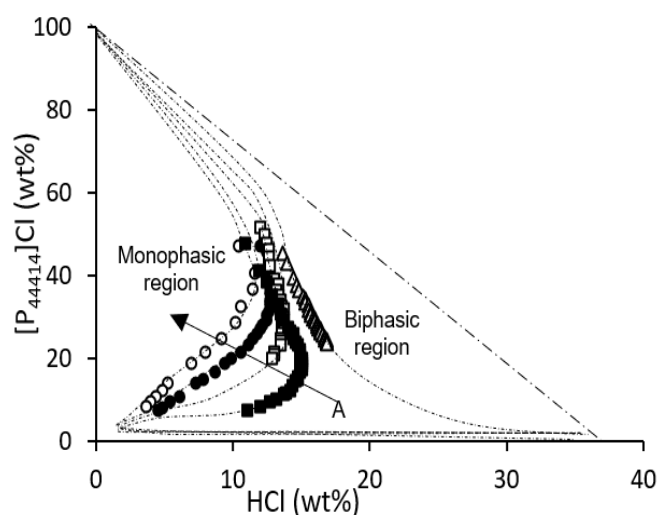


Figure 63. Binodal curves of the system  $[P_{44414}]Cl/[Fe(III)+HCl\ 37\ wt\%]/H_2O$  at  $[Fe(III)] = 0\ g/L$  ( $\Delta$ ),  $[Fe(III)] = 2.5\ g/L$  ( $\blacksquare$ ),  $[Fe(III)] = 5\ g/L$  ( $\square$ ),  $[Fe(III)] = 10\ g/L$  ( $\bullet$ ) and  $[Fe(III)] = 15\ g/L$  ( $\circ$ ) at  $25^\circ C$  (Point A position explained later in the discussion section).

In general, the binodal curves found in the literature are smooth decreasing curves, oriented from top left to bottom right. Curves presenting this kind of deformation have been scarcely reported in the literature. As explained in the state of the art chapter, two IL-based ABS binodal curves with this characteristic “onion shape” were reported by Neves *et al.*<sup>128</sup> and Mogilireddy *et al.*<sup>119</sup> However, in the former case the curves are deformed under the effect of the IL, namely by number of alkyl groups present at the cation, the cation side alkyl chain length and the presence of double bonds, aromatic rings and hydroxyl groups on this alkyl chain. In the latter case, the curves are deformed under the effect of the temperature of the system. By contrast, the deformation of the curves observed in Figure 62 and Figure 63 is simply obtained by raising the Fe concentration in the solution at fixed temperature. Moreover, the elbow of these curves is oriented towards right in an opposite direction compared to Mogilireddy *et al.*<sup>119</sup>, whose curves were oriented towards left.

Finally, Figure 64 (obtained *via* the battleship method explained in the Experimental analysis section) highlights the influence of the temperature in the system  $[P_{44414}] Cl/[Fe(II)+HCl\ 37wt\%]/H_2O$  at  $[Fe(II)] = 20$ .

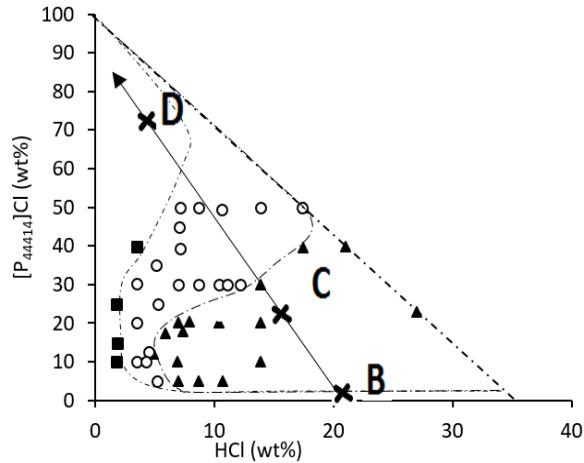


Figure 64. Phase diagram obtained with the battleship method for the system  $[P_{44414}] Cl/[Fe(II)+HCl\ 37wt\%]/H_2O - [Fe(II)] = 20$  g/L. Monophasic samples at both  $T = 25\ ^\circ C$  and  $50\ ^\circ C$  (■), biphasic samples at both  $T = 25\ ^\circ C$  and  $T = 50\ ^\circ C$  (▲) and samples that become biphasic passing from  $25\ ^\circ C$  to  $50\ ^\circ C$  (○). Experimental points B, C, D. The arrow (→) indicates the displacement direction of the point B, C, D increasing the wt% of IL (see text). Dashed lines (---) are only a guide for the eye.

One of the striking results of this work is the change in the shape of the binodal curves upon Fe(II) or Fe(III) addition (Figure 62 and Figure 63), which tends to disappear at a higher temperature (see Figure 64). At  $25\ ^\circ C$ , the effect of Fe(II) or Fe(III) addition onto the shape of the binodal curves is different from that observed for Ni(II) or Cr(III) (this work) or Na(I)<sup>83</sup>. It is evident that the physico-chemical mechanisms behind the effects of the salts in the phase demixing cannot be solely ascribed to the oxidation state of the metal and are far more complex.

Data displayed in Figure 62 and Figure 63 evidence a rather unusual phenomenon as soon as Fe ions are added to the system. In the absence of Fe ions, the sample (point A, Figure 63) is monophasic. Adding increasing amounts of pure IL to this sample will move the point towards a pure IL composition (reached upon infinite addition of pure IL only), along the arrow and the sample will remain in a monophasic state whatever the amount of added IL. By contrast, in case Fe(III) ions are added in HCl at 2.5 g/L, point A corresponds to a biphasic region and by addition of pure IL amounts, the sample will change from biphasic to monophasic along the arrow at *ca.* 15 wt% of HCl and 15 wt% of IL. Increasing the amount of Fe(III) ions will modify the values at which the sample will turn monophasic, stressing the complexity of the phenomena involved in such biphasic/monophasic behavior. There is another aspect of the binodal curves in the presence of Fe(III) ions that can be deduced from the plots in Figure

63. Extrapolations of the three binodal curves converge towards an equivalent point on the x-axis, corresponding to the chemical composition of *ca.* 2 wt% HCl and no IL (see dashed-dotted lines in Figure 63). However, such an intersection with the x-axis is chemically impossible, as it would mean that a sample composed of water and, for example, 5 wt% of HCl would be biphasic, which is not the case. Similar reasoning leads to the conclusion that the binodal curves cannot cross the y-axis either. As the binodal curves cannot present a critical point as for the gas-liquid equilibrium, the only possibility to extend any of the binodal curves in Fig. 5 in a chemically meaningful way is to have an onion-shaped curve as experimentally observed in Figure 64 for  $[\text{Fe(II)}] = 20 \text{ gL}^{-1}$  at  $T = 25^\circ\text{C}$ . In this case, starting from a monophasic sample composition corresponding to point B, adding increasing amounts of pure IL will first turn the sample to a biphasic state (C) and in a second step, back to a monophasic state (D), along the arrow B, C, D.

Many works have been devoted to the empirical fitting of classical binodal curves.<sup>129</sup> These empirical expressions have already been shown to be irrelevant for the fitting of onion-shaped curves as those evidenced in this work<sup>119</sup>.

On a more theoretical aspect, several papers have dealt with the formation mechanism of IL-based ABS. Some explanations focus on entropic reasons while others put the emphasis on Gibbs free energy. Recently, Schaeffer and co-workers<sup>130</sup> suggested an explanation for the ABS formation in the  $[\text{P}_{44414}] \text{Cl} / \text{HCl} / \text{H}_2\text{O}$  system and the effect of NaCl addition based on the comparison of entropy of hydration of NaCl and HCl. Using dynamic molecular simulations and experimental data, they supported the idea that the phenomenon is related to a competition for the water molecules between  $\text{Na}^+$ ,  $[\text{P}_{44414}]^+$  and  $\text{H}_3\text{O}^+$ , together with the relative interactions occurring between all these ions. For these authors,  $[\text{P}_{44414}] \text{Cl}$  forms micelles, the size of which is increased by the presence of  $\text{Na}^+$ . By contrast, the presence of  $\text{H}_3\text{O}^+$  has no direct effect on the micelles size but impacts micelles interactions, bringing water molecules to the micelles and thus being unfavorable to ABS formation. Due to these different interactions arising from NaCl or HCl addition, the system  $[\text{P}_{44414}] \text{Cl} / \text{HCl} / \text{H}_2\text{O}$  is less prone to ABS formation than ABS containing other chloride salts, in particular, NaCl. Indeed, Schaeffer *et al.*<sup>100</sup> proposed to use a mixture of NaCl and HCl instead of a pure AcABS only with HCl. In this way, the metal extraction efficiency is preserved and a lower amount of HCl is used. To summarize, additions of NaCl induce a shift of the binodal curve of the system  $[\text{P}_{44414}] \text{Cl} / \text{HCl} / \text{H}_2\text{O}$  to the left, with no change in the shape of its binodal, while keeping a reasonable amount of HCl allows extraction of metal ions prone to hydrolysis.

In our work, chloride salts of Ni(II), Cr(III), Fe(II) and Fe(III) were used instead of Na(I). Based on literature data<sup>131</sup>, the order of conventional standard molar entropies of hydration of the studied ions

( $\Delta_{\text{hydr}}S_i^\circ$ , at 25°C and expressed in  $\text{JK}^{-1}\text{mol}^{-1}$ ) is as follows:  $\text{Na(I)} \gg \text{Ni(II)} \geq \text{Fe(II)} > \text{Cr(III)} \geq \text{Fe(III)}$ . As suggested by Schaeffer *et al.*<sup>100</sup>, the purpose of our work was to extend the range of chloride salts and to evaluate their effect on the phase separation. However, as demonstrated in Figure 61, at the same concentration the ABS formation is favored in the case of Cr compared to Ni. Moreover, the unusual shape of Fe containing system is not well explained by this parameter either and hydration entropy parameter fails thus to explain our experimental results.

For example, the binodal curve of the system with 5 g/L of Fe(III) is an almost vertical linear curve (see Figure 63), which crosses the onion-shaped binodal curve of the Fe(II)-based ABS. It is important to note that the  $\Delta_{\text{hydr}}S_i^\circ$  values for Ni(II) and Fe(II) are very similar ( $-307 \text{ JK}^{-1}\text{mol}^{-1}$  for Ni(II) and  $-318 \text{ JK}^{-1}\text{mol}^{-1}$  for Fe(II)), as well as both Cr(III) and Fe(III) ions ( $-448 \text{ JK}^{-1}\text{mol}^{-1}$  for Cr(III) and  $-490 \text{ JK}^{-1}\text{mol}^{-1}$  for Fe(III)), but the shapes of the corresponding binodal curves are fully distinct, either between Ni(II) and Fe(II) or between Cr(III) and Fe(III). These differences in the shape of respective binodal curves indicate that  $\Delta_{\text{hydr}}S_i^\circ$  is not the only parameter to be considered.

The second type of explanation for the ABS formation is related to the Gibbs free energy of hydration of ions ( $\Delta_{\text{hydr}}G^\circ$ ). Marcus *et al.*<sup>132</sup>, in 1991, determined the  $\Delta_{\text{hydr}}G^\circ$  of a wide range of ions and developed the concept of the hydration of metal ions. In 2007, Bridges and co-workers<sup>133</sup> formed salt/salt ABS composed of  $\text{K}_3\text{PO}_4$ ,  $\text{K}_2\text{CO}_3$ ,  $(\text{NH}_4)_2\text{SO}_4$ , and hydrophilic imidazolium-, pyridinium-, phosphonium-based ILs. They demonstrated that, like in the polymer-salt ABS, the salting-out strength of the highly charged inorganic salts (*i.e.* water-ion interaction stronger than water-water interactions) follows the Hoffmeister series which can be related to the ions' Gibbs free energy of hydration ( $\Delta_{\text{hydr}}G^\circ$ ). The molar Gibbs energy of hydration of the studied ions ( $\Delta G_{\text{hydr}}^*$ ) differs ( $\text{Ni}^{2+} = -1980$ ;  $\text{Cr}^{3+} = -4010$ ;  $\text{Fe}^{2+} = -1840$ ;  $\text{Fe}^{3+} = -4265$ , all expressed in  $\text{kJmol}^{-1}$ ) and the values follow the order:  $\text{Fe(II)} > \text{Ni(II)} > \text{Cr(III)} > \text{Fe(III)}$ . The order of this series is identical to the one of the series based on entropy considerations, except for Ni(II) and Fe(II), which are inverted. As a consequence, the points raised above (shape of the binodal curves and atypical behavior of Fe(II) *versus* Fe(III)) remain unexplained, and thus the conclusion is that Gibbs free energy consideration is not sufficient to explain our whole data set.

Apart from the  $\Delta_{\text{hydr}}S_i^\circ$  or Gibbs free energy possible involvement in the formation of ABS, the chloride ion is another important partner in the systems under study which role should not be minimized. Onghena *et al.*<sup>126</sup> worked with  $[\text{P}_{44414}]\text{Cl}/\text{NaCl}/\text{H}_2\text{O}$  while Gras *et al.*<sup>127</sup> used  $[\text{P}_{44414}]\text{Cl}/\text{HCl}/\text{H}_2\text{O}$ , both of them to separate Co(II) and Ni(II). These two studies pinpoint the decisive effect of Co(II)-Cl<sup>-</sup> complexation and anionic species formation for its extraction to the IL-rich upper phase via an anion exchange, while Ni remains in the aqueous phase as a cation due to its limited coordination with chloride anions. In these works, the concentrations of Co and Ni were in the traces range<sup>127</sup> or *ca.*  $1 \text{ g/kg}$ <sup>126</sup>, to be

compared to our maximum value equal to *ca.* 12.5 g/kg. We have also used chloride salt and can thus confirm, that the increased concentration of Ni used in our work does not affect the observed results, which are similar to the previous ones, *i.e.* Ni remains in the lower aqueous phase and is not extracted.

Therefore, one possible additional phenomenon at work in the formation of [P<sub>44414</sub>] Cl / [Me(x)+HCl 37 wt%] / H<sub>2</sub>O ABS is the complexation of metals with chloride and evolution of their chemical speciation caused by concentration and temperature changes of the system. Values for the first complexation constant,  $K_1$ , for various metal ions and several temperatures can be found in the literature.<sup>134</sup> Unfortunately, there's a lack of reliable data related to the chloride systems, namely when the influence of increasing temperature is looked for. We have only been able to find these values for perchlorate based systems: for Fe(III) in 1 mol/L HClO<sub>4</sub>, values range from  $K_1 = 0.36$  (14.3-16.3 °C); 0.46 (25 °C); 0.49 (30.1 °C) until 0.68 (44.3 °C). The  $K_1$  increases with the temperature, which can be correlated with the enlargement of the biphasic region, *i.e.* when the temperature was changed from 25 to 50 °C. As a consequence of the formation of FeCl<sub>4</sub><sup>-</sup>, the new compound [P<sub>44414</sub>][FeCl<sub>4</sub>] is thus theoretically formed, although there is no proof yet that the two ions are associated. Other iron-containing ILs, based on dialkylimidazolium cations, have been shown to display a thermomorphic behavior in pure water, with a Lower Critical Solution Temperature (LCST)<sup>135</sup>. To the best of our knowledge, a LCST behavior for [P<sub>44414</sub>] [FeCl<sub>4</sub>] has not been reported but could be involved in the change of the binodals we observed. Similarly, considering Cr(III) in 4.4 mol/L HClO<sub>4</sub> medium, following values evidence an increase in  $K_1$ :  $K_1 = -0.62$  (30 °C); -0.42 (46.3 °C); -0.19 (63.5 °C) until 0.16 (95.4 °C). Finally, comparing the chloride complexation constants of Cr(III) and Ni(II) in almost identical media ( $K_1$  for Cr(III) = 0.18 measured in 1 mol/L NaClO<sub>4</sub> medium and  $K_1$  of Ni(II) = -0.25 measured in 1.5 mol/L NaClO<sub>4</sub> medium), it is observed that it also correlates with the ability of Cr(III) to display a larger biphasic area than Ni(II) (Figure 61). However, the involved physico-chemical phenomenon remains unclear.

Moreover, the differences in complexation constants do not explain the particular shape of binodal curves for iron containing systems. The deformation may be related to the extraction phenomenon, but it should be further investigated. These comparisons are thus only limited ones and are not substantiated by a deeper theoretical approach.

### 3.2.2. Polymer-based systems

By using PEG-600 instead of the ionic liquid [P<sub>44414</sub>] Cl, no biphasic behavior is observed for the system PEG-600/HCl 37 wt%/H<sub>2</sub>O whatever its composition, as ranges from 0 wt% to 99 wt% of PEG-600 and from 0 wt% to 37 wt% of HCl have been explored. Similarly, the systems PEG-600 / [Me(x)+HCl 37wt%] / H<sub>2</sub>O with Fe(II), Ni(II) and Cr(III) are monophasic at 25 °C and at 50 °C, whatever the composition. By contrast, the systems PEG-600/[Fe(III)+HCl 37 wt%]/ H<sub>2</sub>O with [Fe(III)] = 10 g/L and 40 g/L (Figure 65) display a large biphasic area, being this area increased with the increase of [Fe(III)] concentration at both temperature.

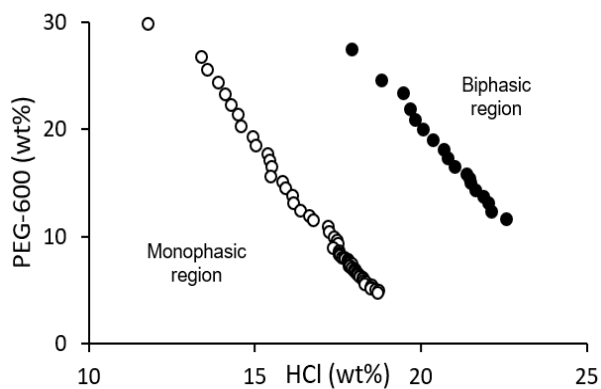


Figure 65. Phase diagram obtained by turbidity method for the systems PEG-600/[Fe(III)+HCl 37wt%]/H<sub>2</sub>O – [Fe(III)] = 10 g/L (●) and 40 g/L (o) at 25 °C.

As well as in the case of the IL-system, the binodal curves obtained for the polymer-system with Fe(III) at 50 °C (Figure 66) present a different shape compared to the classical binodal curves found in the literature.<sup>51,136,137</sup>

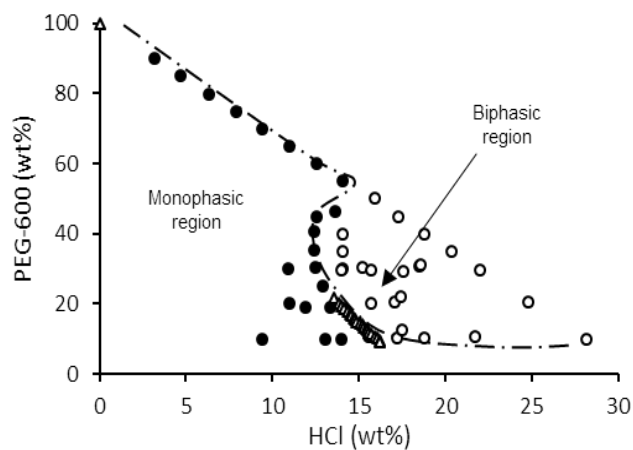


Figure 66. Phase diagram obtained by battle ship and turbidity method for the system PEG-600/[Fe(III)+HCl 37wt%]/H<sub>2</sub>O – [Fe(III)] = 40 g/L at 50°C. Monophasic region (●), biphasic region (o), binodal curve obtained by the turbidity method (Δ). The dashed line (---) is only a guide for the eye.

Figure 67 compares binodal curves of the system PEG-600/[Fe(III)+ HCl 37wt%]/H<sub>2</sub>O ([Fe(III)] = 10 g/L and 40 g/L) obtained at  $T = 25\text{ °C}$  and  $T = 50\text{ °C}$  (Please note that only a small portion of the binodal

curve from Figure 5- triangles - is shown in Figure 67 – empty squares). These results evidence, independently of Fe(III) concentration, a widening of the biphasic area when the temperature increases.

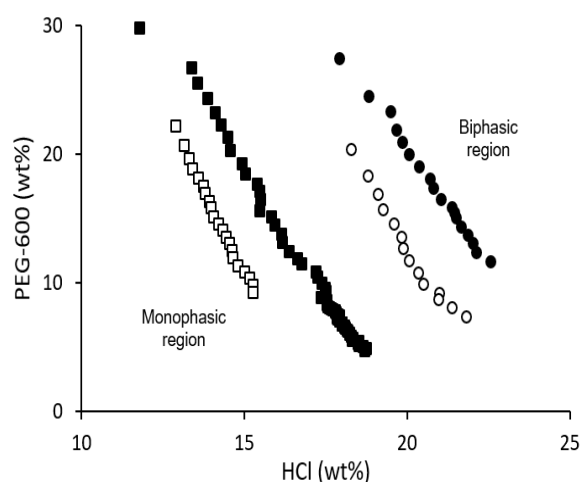


Figure 67. Binodal curves obtained by turbidity method for the system PEG-600/[Fe(III)+HCl 37wt%]/H<sub>2</sub>O – [Fe(III)] = 40 g/L at 50°C (□) and at 25°C (■) and for the systems PEG-600/[Fe(III)+HCl 37wt%]/H<sub>2</sub>O – [Fe(III)] = 10 g/L at 50°C (○) and at 25°C (●).

Our data have already pinpointed Fe(III) as specific IL-based ABS inducer (owing to the shape of the binodal curves, Figure 63) and this ion is also peculiar in the case of PEG-based ABS. However, one can notice differences between the PEG-based and IL-based systems involving Fe(III) ions as far as the temperature is concerned. Actually, as T increases from 25°C to 50°C, the onion shape behavior becomes more obvious for the IL-based systems (Figure 63). As already discussed for the IL-based systems, these data cannot be described by using traditional empirical models, owing to the onion shape of the binodal curves. This remark is also valid for the Setschenow equation (Ni *et al.*<sup>78</sup>), another empirical function that is nevertheless related to some physicochemical parameters of the system and has been proposed for the mutual solubility of an electrolyte and a polymer.

By contrast to the IL-based ABS, one can find many works devoted to PEG-based ABS and the possible reasons behind the formation of the biphasic state or its absence, as in the case of PEG-600/[HCl 37 wt%]/H<sub>2</sub>O. Among the proposed hypotheses can be cited those referring to the changes in the hydration of the polymer or to the existence of strong interactions between multivalent cations, particularly metal ones, and ether oxygens of PEG and will be discussed below under the light of our data.

First, the absence of biphasic state for mixtures of PEG-600, HCl and water should be explained. Huddleston *et al.*<sup>138</sup> stated that the formation of a biphasic regime by dissolving water-soluble polymer and inorganic salts results from the competition for hydration between the polymer and the salts. This is dependent on the relative hydrophobicity of the polymer (based on polymer type or average molecular weight) and the salting-out strength of the inorganic salt ions, *i.e.* ions' Gibbs free energies of hydration<sup>139</sup>. Water is the main component in this system and PEG-600 is highly hydrophilic, interacting

actively with 2 or 3 water molecules per each ethylene oxide (EO) unit. As most ionic species,  $\text{Cl}^-$  anions are also highly water-soluble. Therefore, to induce a phase demixing, the salt should exhibit a salting-out aptitude enough to dehydrate, at least partially, the PEG-600. Although hydrogen chloride (HCl) when dissolved in water behaves as a strong electrolyte, its preferential hydration is not strong enough to dehydrate and expel the hydrophilic PEG-600 to another incompatible phase. Thus, all compounds are remaining dissolved in a monophasic aqueous solution. Additionally, as demonstrated by Tomé *et al.*<sup>140</sup>, it has also to be considered that  $\text{Cl}^-$  anions can establish an equivalent of hydrogen bonds with the -OH end group of the PEG polymers, favoring their mutual solubility in water. Therefore, in addition to the water solvation of the ether groups of the oxygen chain, the formation of ABS when mixing aqueous solutions of PEG and chloride-based salts is also a result of the ability of the PEG terminal groups to preferably interact with water or the chloride anion (Pereira *et al.*<sup>141</sup>).

Second, the biphasic inducing property of Fe(III) should be examined, together with the inefficiency to do so of the other metal ions tested in our work. As already discussed for the IL-based data, it is known that the complexation constant<sup>133</sup> of Fe-Cl is higher than the Ni-Cl or the Cr-Cl complexation constants. The charge density<sup>142</sup> of the metal ions is also quite different ( $\text{Ni}^{2+} = 82$ ;  $\text{Cr}^{3+} = 261$ ;  $\text{Fe}^{2+} = 181$ ;  $\text{Fe}^{3+} = 349$ , all expressed in  $\text{C}\cdot\text{mm}^{-3}$ ) and follows the order:  $\text{Ni(II)} < \text{Fe(II)} < \text{Cr(III)} < \text{Fe(III)}$ . If the behavior is influenced by the charge density, then the ABS formation “ability” would follow this order (in both cases, *i.e.* IL and PEG), which is not the case. Moreover, it does not explain the iron case particularities. Finally, the molar Gibbs energy of hydration of ions ( $\Delta G^*_{\text{hydr.}}$ ) values already given above differ markedly for the studied ions, whereas very close values are ascribed in the literature for Ni(II) and Fe(II) and then again for Cr(III) and Fe(III). So if the biphasic behavior and partition phenomenon were governed solely by this parameter, one could expect that Ni(II) and Fe(II) will behave similarly and then again Cr(III) and trivalent iron, which is clearly not the case.

To go a step further, one has to recall that the formation of a biphasic state imposes electro-neutrality to both the upper (PEG and iron-rich) and lower phases. From the electrospray ionization – mass spectrometry (ESI-MS) analyses, the main species present in the acidic solution of Fe(III) and HCl (37 wt% = 12 mol/L) is  $[\text{Fe(III)Cl}_4]^-$  (Figure 139 - Annex). This implies that the  $[\text{Fe(III)Cl}_4]^-$  species, which is responsible for the biphasic formation, is accompanied by a positively charged species during the phase separation. In our system, the only available cation is the  $\text{H}^+$ . Therefore, one has to consider at the same time the ability of  $\text{H}^+$  and  $[\text{FeCl}_4]^-$  to be trapped in the PEG-rich phase.

Regarding the cationic moiety, Sartori *et al.*<sup>143</sup> described PEG's ability to absorb ions from solutions containing an alkali-metal cation ( $\text{Li}^+$ ,  $\text{Na}^+$ ,  $\text{Rb}^+$ ,  $\text{K}^+$  and  $\text{Cs}^+$ ) and a series of anions including  $\text{Cl}^-$ . Furthermore, they showed that the polymer strongly interacts with the cations they examined. This leads to

the formation of a positively charged surroundings that “attracts the anions (...) to the vicinity of the PEG molecule”<sup>143</sup>. Although H<sup>+</sup> was not studied in the work of Sartori *et al.*, it is reasonable to assume that the proton plays the role of an alkali metal cation in our system.

However, this first hypothesis does not exclude the strong contribution of the anion to the system partition. Bulgariu *et al.*<sup>144</sup> suggested that chloride anionic species based on Zn(II), Hg(II) and Cd(II) are “fixed” by the O-groups present in the ether chain of the PEG by ionic forces. It could thus be envisioned that the same phenomenon occurs with [Fe(III)Cl<sub>4</sub>]<sup>-</sup>.

As shown in Figure 68, the chemical structure that can be proposed is the intramolecular bonding between two polymer chains of PEG that are connected *via* the water molecules.

The anionic iron species interacts then with the oxygens present within the polymer. It is important to underline that the interaction between Fe and O is not based on a covalent bond but is rather an ionic interaction due to the differences in the electronegativities of the two atoms. This is supported by the ESI-MS results that showed the absence of a stable covalent bond between the PEG and the metal ions (Figure 136 - Annex). In this sense the schematic view, as displayed in Figure 68 is in line with the comment of Sartori and co-workers<sup>143</sup>, who pinpointed that “the anions remain mainly outside the polymer coil”. Furthermore, it seems that in a high concentrated HCl medium, the structure of the Fe(III) is an equilibrium between an octahedral (Figure 68-C) and a tetrahedral structure (Figure 68-D)<sup>145</sup>.

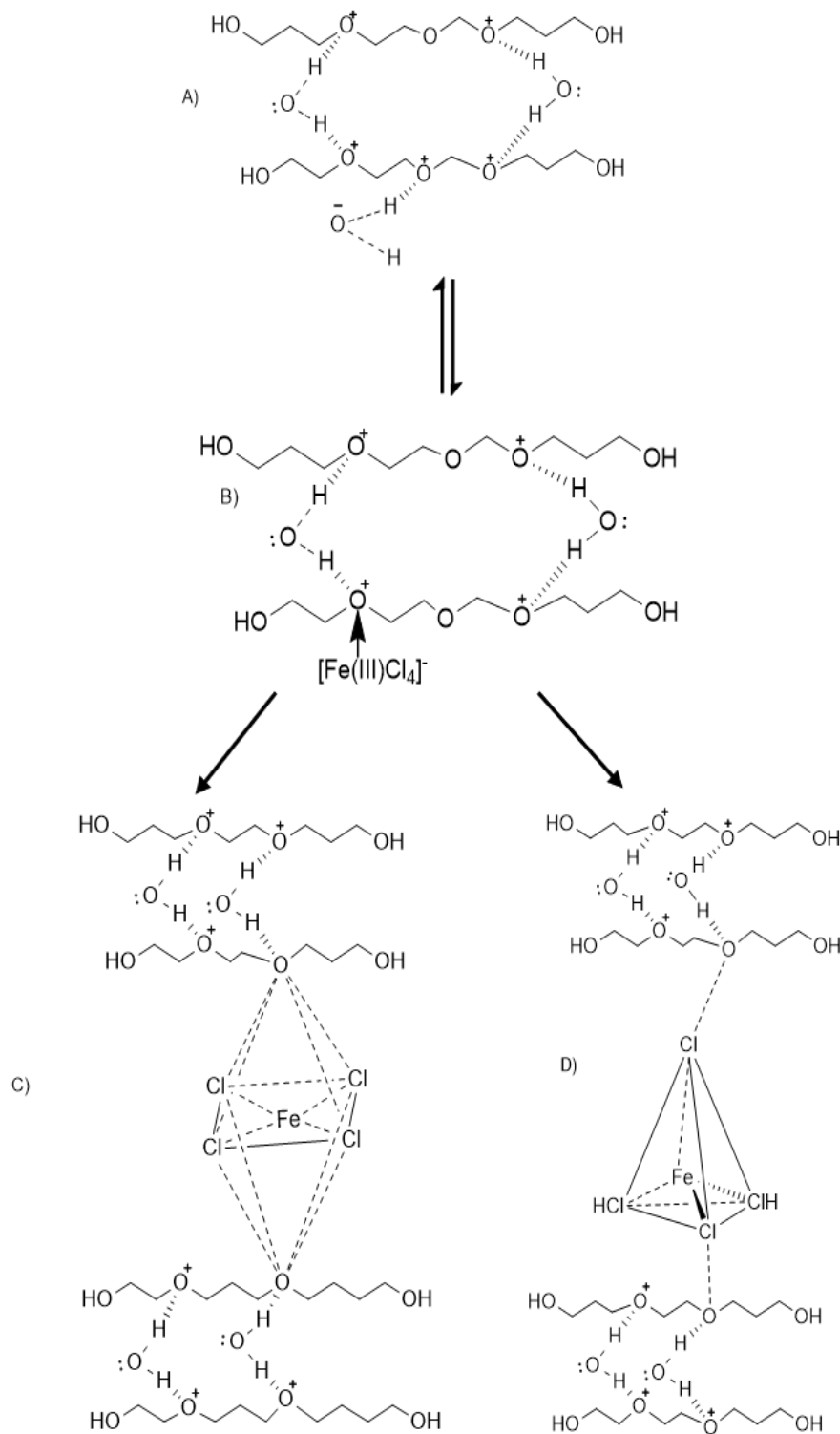


Figure 68. Mechanism of PEG extraction of Fe(III). 10-A: inter-chain connection proposed by Bulgariu et al.<sup>43</sup>; 10-B: Fe(III) connection with the ether group of the polymer; 10-C: octahedral structure of the species (Fe(III)Cl<sub>4</sub>); 10-D: tetrahedral structure of the species (Fe(III)Cl<sub>4</sub>); Adapted from ref. Bulgariu et al.<sup>43</sup>.

## 4. ABS and metal extraction in UGCO bath

The fascinating ability of the PEG-600 to act as a biphasic inducer when mixed with a 12M HCl solution and in the presence of high concentrations of Fe(III) prompted further investigation in order to understand whether there were other PEG-like biphasic inducers that could promote ABS formation in acidic medium and with the presence of metals. For this reason, it was considered, on occasion, PEG with different molecular weights (PEG-400, PEG-8000), secondly different polymer blocks (di and tri-block polymer), then the monomers (3EGDE, 4EGDE) and finally a compound with some functional groups different from PEG (POxES). A test was also carried out with (EG+CCI), which belongs to the family of deep eutectic solvents. Table 14 lists the compounds just mentioned above, and it is also indicated which of them can give an ABS.

<b>Sample</b>	<b>Commercial name</b>	<b>Molecule</b>	<b>ABS</b>
<b>S1</b>	PEG-400	polyethylene glycol 400Mw	Yes
<b>S2</b>	PEG-600	polyethylene glycol 600Mw	Yes
<b>S3</b>	PEG-8000	polyethylene glycol 8000Mw	No
<b>S4</b>	DBP	di-block polymer	No
<b>S5</b>	TBP	tri-block polymer	No
<b>S6</b>	3EGDE	triethylene glycol dimethyl ether	Yes
<b>S7</b>	4EGDE	tetraethylene glycol dimethyl ether	Yes
<b>S8</b>	PE	polyethylene	No
<b>S9</b>	EG+CCI	Ethylene glycol + choline chloride	No
<b>S10</b>	POxES	polyoxyethylene stearate	No

*Table 14. List of polymers used to induce a biphasic system with the UGCO bath.*

All samples were prepared with a ratio of 20 / 80 wt% of polymer / UGCO bath. In order to uniform the results with the other biphasic inducers, which are soluble up to a maximum of 20 wt%, the experiment concerning PEG-600 / UGCO bath, already proposed in the preliminary tests, has been repeated considering the same repartition of the other systems.

As far as PEG with different molecular weights is concerned, the polymers appear in three different states at 20 °C, considering the different molecular weights, PEG-400 is in the liquid state, PEG-600 is jelly-like towards solid, while PEG-8000 is in the solid state. The ability of PEG-400 to be in a liquid state at 20 °C makes this polymer easier to use than PEG-8000, while many researchers<sup>9,92</sup> have

described the great ability of PEG with high molecular weight to promote the ABS formation. However, increasing the molecular weight of the polymer is not always an advantage, in fact, increasing the molecular weight of the PEG also means decreasing its solubility, due to the hydrophobic character of the  $-CH_2-$  groups in the chains (State of the Art – PEG solubility in water). Consequently, since ABS consists of at least 3 components, where one is water and the other two must be water-soluble, if we increase the molecular weight of the polymer considerably, at this point, a classical liquid-liquid extraction instead of an ABS is favored. In short, it is necessary to find the suitable polymer that can be soluble in water, be in a liquid state to be more easily processed at room temperature, but which also has a good ability to provide a biphasic system and at the same time a good extraction efficiency. In fact, PEG-8000 provided an ABS, but the polymeric phase is very viscous and therefore impossible to work with, so it has not been considered, while PEG-400 interacted optimally by providing an ABS, with the two phases having a water-like viscosity. The polymeric blocks considered are DBP (di-block polymer) consisting of PEG-PPG and TBP (tri-block polymer) consisting of PPG-PEG-PPG with different distribution ratios. The idea of using these polymeric blocks comes from a careful bibliographic research<sup>10</sup> that shows how these polymers can combine the chemical-physical properties of the corresponding components, the PEG and the PPG. In fact, on the one hand we have PEG characterized by the hydroxyl groups responsible for the solubility of this polymer in the aqueous phase, on the other hand we find the branched structure of PPG which presents a tertiary methyl group in the repetitive unit responsible for the steric encumbrance of the polymer. Finally, neither DBP nor TBP were suitable for the investigation because DBP provided a solid mix after coming into contact with UGCO bath, while TBP behaved like PEG-8000, i.e. once the biphasic sample was obtained, the lower phase was too viscous to work with. As far as the monomers 3EGDE and 4EGDE are concerned, these were considered for their attractive price. In fact, 250g of these monomers cost exactly half of the same amount of PEG-600 (Sigma Aldrich website). The DES composed of ethylene glycol plus choline chloride (1:1) does not provide a biphasic system, and the same occurred with polyethylene (PE) and polyoxyethylene stearate (POxES).

To sum up, only 4 of these compounds induce an ABS (Figure 69), and these are polyethylene glycol with different molecular weight (PEG-400, PEG 600), tri ethylene glycol dimethyl ether (3EGDE) and tetra ethylene glycol dimethyl ether (4EGDE). After analysis with AAS, in Figure 69 it is possible to see that monomers and polymers extract from 15% to 40% of iron, and more than 90% of nickel and chromium remain in the Aperam bath. The position of the biphasic inducer in the various systems was made by approximately considering the density of these in relation to that of the UGCO bath and the color. The 3EGDE and 4EGDE are to be found the upper phase of the biphasic sample, while PEG-400 and PEG-600 in the lower phase.

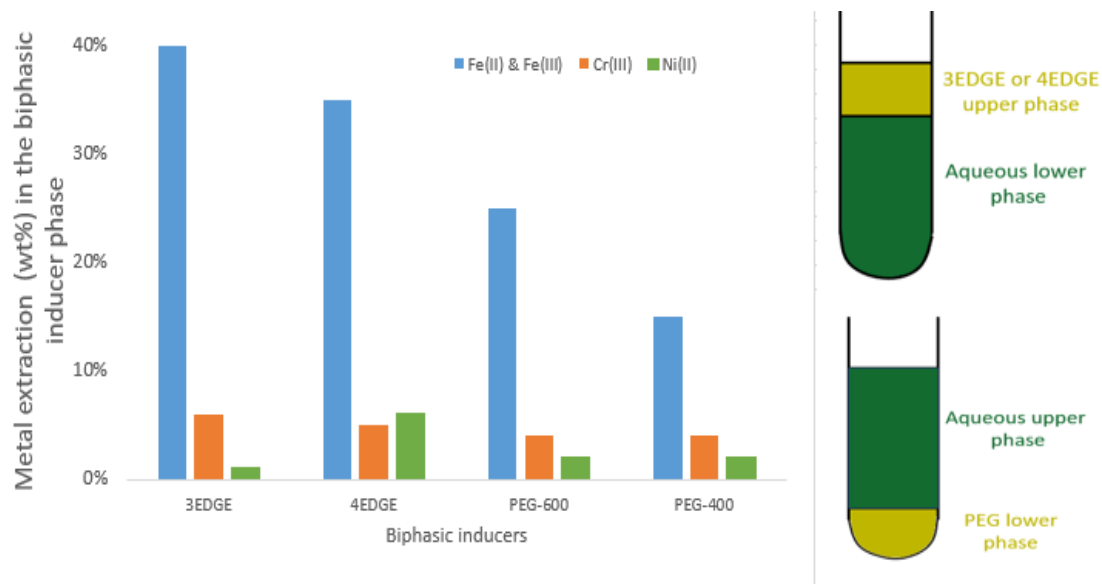


Figure 69. Metal ions repartition in the biphasic inducer phase for samples: 3EDGE, 4EGDE, PEG-600 and PEG-400. The samples on the left indicate the volume repartition and the position of the biphasic inducers and the aqueous phases after ABS formation.

On the one hand, the new biphasic inducers responded very well to obtaining ABS with the UGCO bath, but on the other hand they confirmed the same extraction trend of promoting iron recovery over other metals.

Aperam's attention then shifted to Cu(II), which is present in the UGCO bath in concentrations of less than 1 g/L, but which would be a problem if present in larger quantities as it would inhibit the pickling process in this bath. The sample considered for this investigation was prepared with a distribution in [P<sub>44414</sub>] Cl / UGCO bath of 30/70 wt% respectively at 20 °C (Figure 70). The ionic liquid is in the upper phase of the ABS. The trend of metals investigated so far remains the same, Ni(II) and Cr(III) are not extracted while Fe(II) and Fe(III) are extracted at 80/100%, while Cu(II) goes into the ionic liquid phase at 55%.

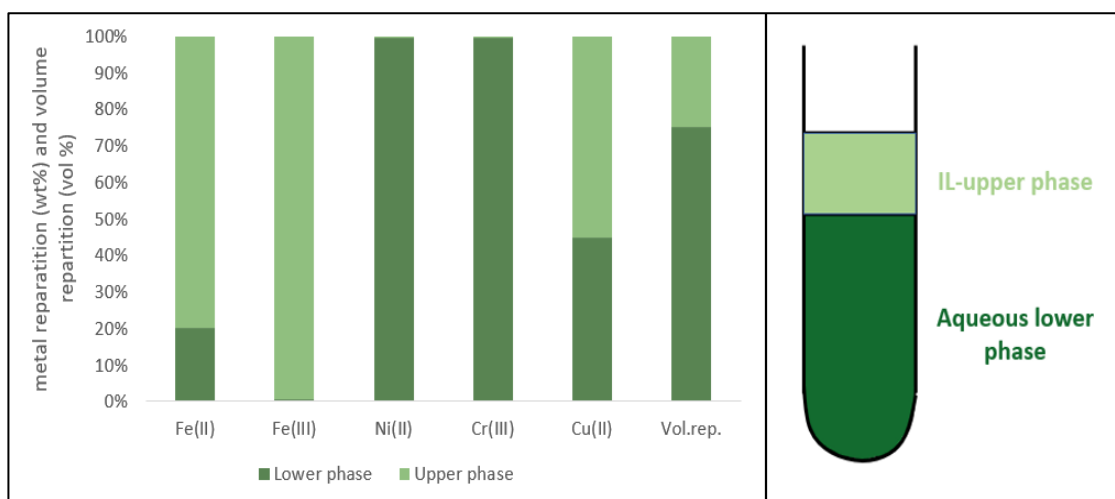


Figure 70. Metallic ion extraction mixing 30 / 70 wt% of [P<sub>44414</sub>] Cl / UGCO bath.

The study of Cu(II) extraction requires more investigation; one must first understand the tendency of ILs to extract the metal as a function of their concentrations, investigate different working temperatures, and test other compounds that may favour Cu(II) extraction. In this connection, a short-term research project on the extraction of this metal was carried out with the collaboration of Master's student Patricia Folio. She tested some deep eutectic solvents and defined their extraction efficiency on the UGCO bath. As DES is not the subject of my thesis, for a global understanding of the work, a summary of Folio's project is presented in Section HCl, Annex.

## 5. Conclusions

For metal-free systems and in 12 M HCl, the mixture [P<sub>44414</sub>] Cl / [HCl 37 wt%] / H<sub>2</sub>O is an ABS, while the corresponding system with PEG-600 is not. In addition, further investigation is required regarding the difference in the position of the binodal curves for ionic liquid supplied by different providers. It turns out that for the [P<sub>44414</sub>] Cl supplied by Interchim (used in this work) the biphasic region is larger than for the same ionic liquid supplied by Cytec<sup>119</sup>.

The challenging treatment of UGCO bath led us to shift our attention to a more fundamental study on the understanding of the mechanisms that drive mainly the polymer and the ionic liquid to prefer iron extraction over the other elements. For this reason, we start working with systems containing only one metal at a time, and the result was surprising. In particular, we investigate the impact of 4 different types of metal ions: Fe(II), Fe(III), Ni(II) and Cr(III). In the case of IL, it was possible to obtain a biphasic system with all four different metal ions, separately. The peculiarity of these systems lies in the particular anion shape form that presents the binodal curve of the system with Fe(II)/(III). Regarding PEG-600-based systems, only Fe(III) can induce a biphasic system in the presence of HCl, and also in this case the binodal curve has an atypical shape.

The investigation of the influence of factors such as the presence of metals and the temperature on the binodal curves of ABS is important at the fundamental level for the understanding of these systems. In particular, close to the elbow of the onion-shaped binodal curve, addition of PEG will turn the system from monophasic to biphasic and finally back to monophasic for rather small amounts of polymer. This means that the sample is susceptible to mono/bi phasic state changes upon small concentration changes, and this could be an interesting experimental and theoretical point to study in the near future.

For a more practical aspect, these investigations have also a very pronounced benefit, given the high potential for industrial use of this knowledge. There are many industrial aqueous liquid wastes that contain a very high concentration of iron. Our work demonstrates that there is an economic and efficient way to significantly reduce the amount of iron ions in these wastes by adding PEG polymer. A clear advantage is that the more concentrated the iron is, the lower amount of PEG is required to remove this element from its solution. Once iron is extracted, it should be easier to recover the other minor but valuable elements possibly present, either by traditional means (electrodeposition, precipitation etc.) or by inducing the formation of another ABS system. Furthermore, it is already known<sup>146</sup> that increasing the molecular weight of the polyethene glycol, the biphasic area increases but at the same time the solubility in water of the polymer decreases, so this is another parameter to play with. Work on these lines is currently under progress in our laboratory.

Therefore, for the matrix solutions containing metal ions, acid, and water, such as the spent pickling liquor from UGCO bath, and for the stock solutions of single metals, both the polymer and ionic liquid provided an ABS, but the extraction trend obtained in the preliminary tests with the two biphasic inducers did not fulfill the company's request to extract all the metals from the bath. In addition, Aperam's initial request concerning the possibility of dehydrating the UGCO bath did not see full fulfilment when using ABS. In fact, as far as IL is concerned, its use made it possible to extract a small volume of water from the bath (5vol%), since the volume of the ionic liquid-rich phase increased in relation to the amount of IL used for the ABS. In contrast, when the polymer was used, it was distributed in both phases of the ABS, and it was not possible to notice whether the polymer had absorbed some of the water from the UGCO bath.

It was only later that attention turned to copper, which was shown to be extracted from [P<sub>44414</sub>] Cl with an efficiency of 55 wt%. Promising results were also obtained by the master student Patricia Folio, (Section HCl – Annex), which used DES for the extraction of this element. For this reason, this research needs further investigation by developing a method that can selectively extract Cu(II) from the UGCO bath.



# D. ABS formation and metals extraction in $\text{Na}_2\text{SO}_4$ media





## 1. Introduction

The  $\text{Na}_2\text{SO}_4$  bath is an electrolytic bath used by Aperam during the pickling process to remove oxides on the surface of the stainless steel. As can be seen in Table 15, the sulfate bath contains mainly Cr (mostly in the form Cr(VI)) but also Fe, Ni, Mn and Cu. The bath must contain a minimum amount of Cr(VI) of 5 g/L, as this minimum concentration will inhibit the dissolution of the metal surface. However, when the value of Cr(VI) reaches approximately 20 g/L, the pickling efficiency of the bath drops. Thus, a fraction of the Cr(VI) loaded pickling bath is discarded and a new metal-free sodium sulfate solution is added to the bath. The loaded pickling bath fraction is sent to the neutralization plant, and the sludge obtained at the end of the process is sent to the landfill. The high amount of S present in the sludge prevents it from being treated by pyrometallurgical procedures. Aperam's request on this bath is to remove all metals dissolved in it, recover them in metallic form or in sludge not containing S, so as to regenerate the sulfate bath and reuse it in the pickling process.

Na <sub>2</sub> SO <sub>4</sub> bath	
Type of metal	Concentration (g/L)
Cr	13.510
Fe	0.620
Ni	0.380
Mn	0.097
Cu	0.048

Table 15. Metal concentration in  $\text{Na}_2\text{SO}_4$  bath.

The alternative to the neutralization process proposed for the treatment of the spent pickling liquor (SPL) fraction is ABS. In the chapter "State of the art" it has been shown how it was possible to obtain an ABS by using a system composed of polyglycols /  $\text{Na}_2\text{SO}_4$  /  $\text{H}_2\text{O}$  at a given temperature and pH and the high efficiency of this system in extracting metals. This type of ABS will be investigated throughout the chapter, considering also the contribution of the metals into it.

## 2. Preliminary tests on ABS formation and metal extraction on SPL from $\text{Na}_2\text{SO}_4$ bath

The biphasic inducers tested on the  $\text{Na}_2\text{SO}_4$  SPL to induce an ABS and extract metals are PEG (of different molecular weights) and PPG-425. The composition of the SPL used for this series of investigations is shown in chapter Materials and methods, section 3. In the chapter "State of the art" it has been shown that the ability of these polymers to extract metals was linked by the presence of a salt, where both are playing the role of biphasic inducers and are necessary for obtaining an ABS. Due to the composition of the sulfate bath, this facilitates the formation of ABS, as the high concentration of sodium sulfate creates a suitable environment for testing polymer-based ABS. Regarding the ionic liquid used in the UGCO bath,  $[\text{P}_{44414}]\text{Cl}$ , this was not taken into account in the experiments on SPL from the  $\text{Na}_2\text{SO}_4$  bath, because it involves the addition of  $\text{Cl}^-$ , which are not recommended as they reduce the efficiency of the pickling process.

A first series of tests were carried out by treating the SPL from the sulfate bath with PPG-425. Four samples were prepared with different repartitions of SPL of  $\text{Na}_2\text{SO}_4$  bath and polymer at  $80^\circ\text{C}$ . As can be seen from Figure 71, the appearance of ABS was noted under all experimental conditions tested, however according to the AAS analysis the extracted amounts of metals, in particular of  $\text{Cr(VI)}$ , in the polymeric phase, were very low (less than 5 wt%). Therefore, the PPG-425 investigation was not continued further.



Figure 71. Samples prepared for demonstrating the PPG-425 extraction efficiency on the  $\text{Na}_2\text{SO}_4$  bath. Starting from the left to the right: 10/90-20/80-30/70-40/60 wt% of PPG-425/  $\text{Na}_2\text{SO}_4$  bath.

A second series of test was carried out to determine the contribution of PEG to the ABS formation and metal extraction. Initially, PEG with a  $M_w=600$  was tested, which is in the solid state at room temperature, then it was decided to continue the experiments with PEG-400, which exists in a liquid form at room temperature. Better results, compared to PPG-425, have been obtained when PEG-400 was tested. The sample in Figure 72 shows an ABS prepared starting from a repartition of 50/50 wt% in

PEG-400 / SPL from  $\text{Na}_2\text{SO}_4$  bath. More than 99.7% of Cr is extracted in the polymer upper phase while Ni, Fe and  $\text{Na}_2\text{SO}_4$  salts remain in the aqueous phase. The polymer is to be found in the upper phase for more than 99%.



*Figure 72. Sample prepared to demonstrate the PEG-400 extraction efficiency on the  $\text{Na}_2\text{SO}_4$  bath. Repartition used 50/50 wt% of polymer/bath.*

The results obtained in preliminary tests with PEG-400 made it possible to meet two of Aperam's initial requests for this bath:

- to clean it of most metals, and in this specific case of chromium
- the recovered metal solution contains the lowest concentration of sulfate

For these reasons, it was decided to continue the investigation with this polymer.

### 3. Properties of ABS in $\text{Na}_2\text{SO}_4$ media

#### 3.1. System without metals

First of all, the system without metal was studied. In Figure 73 it is possible to see the phase diagram and the corresponding binodal curve for the ABS consisting of PEG-400 /  $\text{Na}_2\text{SO}_4$  /  $\text{H}_2\text{O}$  at  $T=25^\circ\text{C}$ . The binodal curve was prepared in this specific case, starting from a stock solution of sodium sulfate ( $\text{Na}_2\text{SO}_4 = 150 \text{ g/L}$ ) and adjusted to  $\text{pH}=2$  with  $\text{H}_2\text{SO}_4$ . These values have been chosen to mimic the conditions of the SPL from the sulfate bath. The experimental points of the curve can be found in Section  $\text{Na}_2\text{SO}_4$ , Annex, table 26 -30.

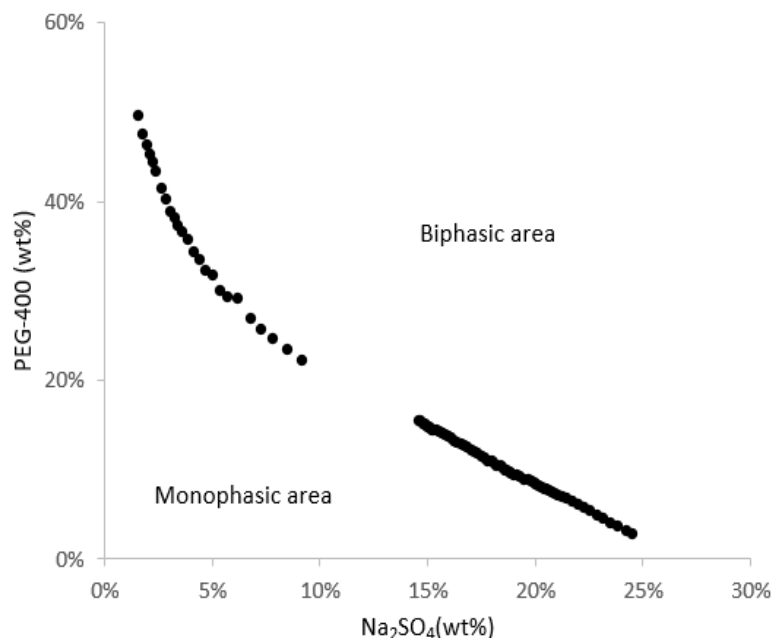


Figure 73. Binodal curve for ABS composed of PEG-400 / Na<sub>2</sub>SO<sub>4</sub> / H<sub>2</sub>O

Sodium sulfate, and PEG-400, act as biphasic inducers in the PEG-400 / Na<sub>2</sub>SO<sub>4</sub> / H<sub>2</sub>O system, in contrast to the PEG-400 / HCl 37 wt% / H<sub>2</sub>O system presented in the previous chapter, where HCl did not play the role of a biphasic inducer and therefore did not enable the formation of ABS. The contribution of sodium sulfate and different additives in polymer-based ABS has been widely discussed in the bibliography over the years<sup>147,148,82</sup>. The free energy of hydration<sup>132</sup> of Na<sub>2</sub>SO<sub>4</sub> is large enough ((absolute value),  $\Delta G^{\circ}\text{hyd}(\text{Na}^+) = -365 \text{ kJ mol}^{-1}$ ,  $\Delta G^{\circ}\text{hyd}(\text{SO}_4^{2-}) = -1080 \text{ kJ mol}^{-1}$  at 298.15 K) that gives to the salt a high affinity for the non-polymeric phase. Moreover, for biological systems, the cation and anion contribution in the inorganic salt for polymer-based ABS systems follows the Hoffmeister series. With various approximations that are beyond the scope of the present investigation, this series can also be applied to the repartition of metals.

### 3.2. System with single metal

Single metal stock solutions were prepared to investigate the contribution of metals in the system PEG-400 / Na<sub>2</sub>SO<sub>4</sub> / H<sub>2</sub>O. The solutions used are described in section 4 of the Materials and Methods chapter. The metals considered for investigation are: Ni(II), Mn(II), Cu(II), Mo(II), Fe(III), Cr(III), Cr(VI) and Mo(VI). The concentration of each metal in the solutions is around 5 g/L, except for Cr(III) and

Mo(II), which were only soluble at concentrations below 1 g/L. Na<sub>2</sub>SO<sub>4</sub> is to be found at concentration of about 150 g/L and the pH is around 2.

### 3.2.1. Element contribution and their distribution in the system PEG-400 / [Me + Na<sub>2</sub>SO<sub>4</sub>] / H<sub>2</sub>O

Six binodal curves have been prepared for the corresponding system PEG-400 / [Me + Na<sub>2</sub>SO<sub>4</sub>] / H<sub>2</sub>O at 25°C (Figure 7):

1. PEG-400/[Fe(III)+Na<sub>2</sub>SO<sub>4</sub>]/H<sub>2</sub>O
2. PEG-400/[Ni(II)+Na<sub>2</sub>SO<sub>4</sub>]/H<sub>2</sub>O
3. PEG-400/[Cr(III)+Na<sub>2</sub>SO<sub>4</sub>]/H<sub>2</sub>O
4. PEG-400/[Cr(VI)+Na<sub>2</sub>SO<sub>4</sub>]/H<sub>2</sub>O
5. PEG-400/[Mo(VI)+Na<sub>2</sub>SO<sub>4</sub>]/H<sub>2</sub>O

The binodal curves with metals were compared to the one already obtained for the metal-free system (Figure 73). As can be seen in Figure 74, the binodal curves are all in the same position in the phase diagram and they present the same shape. It can therefore be deduced that the binodal curves are not affected by the different types of metals, or their oxidation number (Cr(III) - Cr(VI)). The binodal curves obtained for systems composed of PEG-400 in sulfate medium are therefore stable whatever the T and metal concentration, which is an advantage for its use in industrial conditions (which can vary) compared to the binodal curves obtained in hydrochloric medium that depend on all parameters (T, C...) and are therefore less friendly to use in industrial processes.

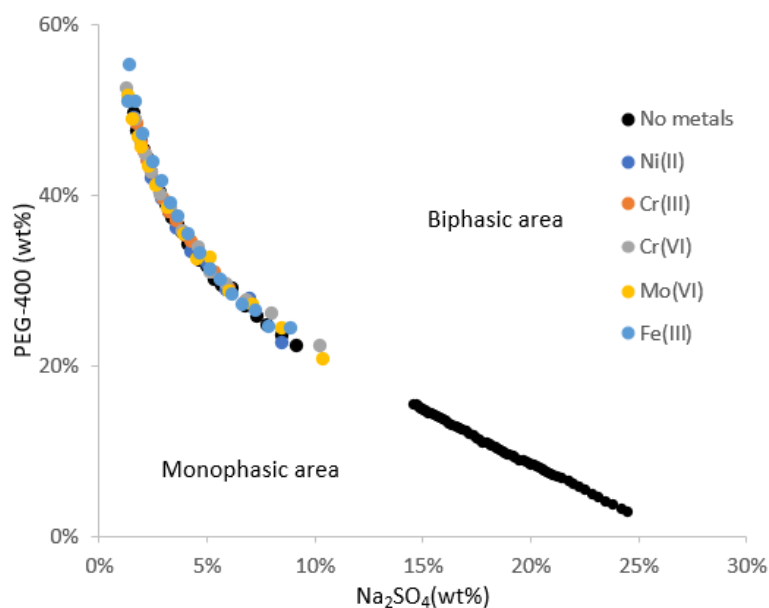


Figure 74. Binodal curve for ABS composed of PEG-400 / Na<sub>2</sub>SO<sub>4</sub> / H<sub>2</sub>O and metals.

Figure 75 shows the results obtained when determining the polymer extraction efficiency in PEG-400 / [Me + Na<sub>2</sub>SO<sub>4</sub>] / H<sub>2</sub>O system at 25°C. For each metal considered in the investigation, three ABS were

prepared with a polymer/ synthetic single metal solution partition of 20 / 80 - 30 / 70 - 40 / 60 wt% respectively. In all cases, 99 wt% of the polymer is present in the upper phase of the ABS. The extraction of Cr(VI) is constant at around 99 wt%, in the three ABS composed of different amounts of PEG-400 (wt%). For Mo(VI), an evolution can be seen from 92 wt% to 99 wt% of extracted metal when the amount of polymer used in the systems increases from 20 wt% to 40 wt%. For the remaining tested species, a decreasing trend of extraction can be observed as the amount of polymer used in the systems increases. In particular, Fe(III) decreases from about 70 wt% to 30 wt%, Mo(II) decreases from about 65 wt% to 38 wt%, Cr(III) goes from 55 wt% to 15 wt%, while Cu(II), Ni(II) and Mn(II) go from about 30 wt% to 10 wt% in the polymer phase when the amount (wt%) of PEG-400 used for ABS increases from 20 wt% to 40 wt.

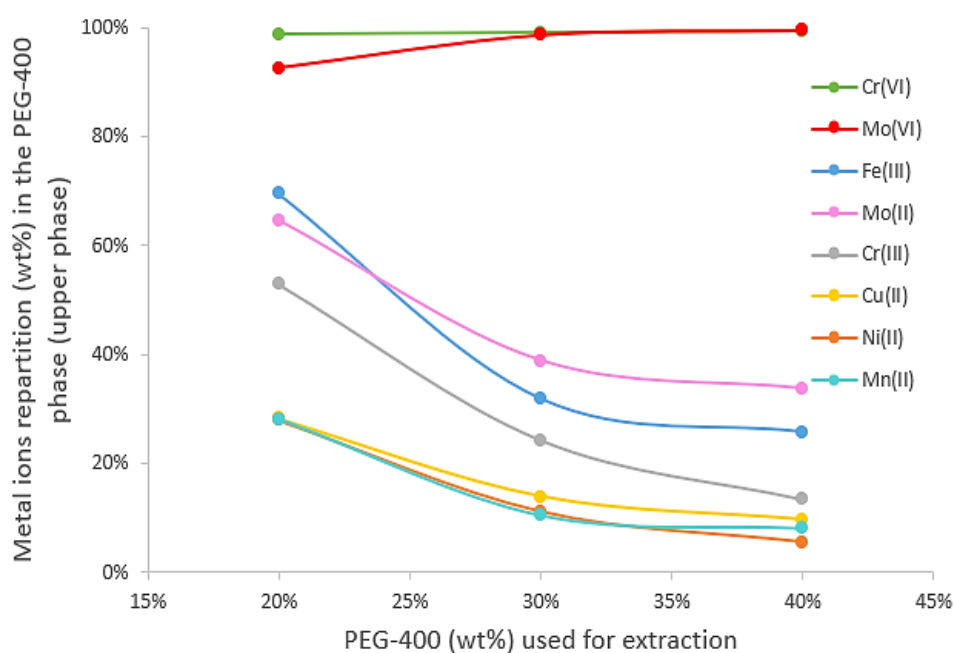


Figure 75. Metal ions extracted in the upper PEG-400 phase in  $\text{Na}_2\text{SO}_4$  media starting from synthetic solutions mono-element.

As regards to the partitioning of sodium in the different stock solution single metal (Figure 76), it appears to follow a common and decreasing trends for all the systems. This analysis certainly requires more investigation, to confirm the values obtained. In addition, the determination of sulfate in different synthetic solutions is ongoing and this would allow a better understanding of the extraction mechanisms.

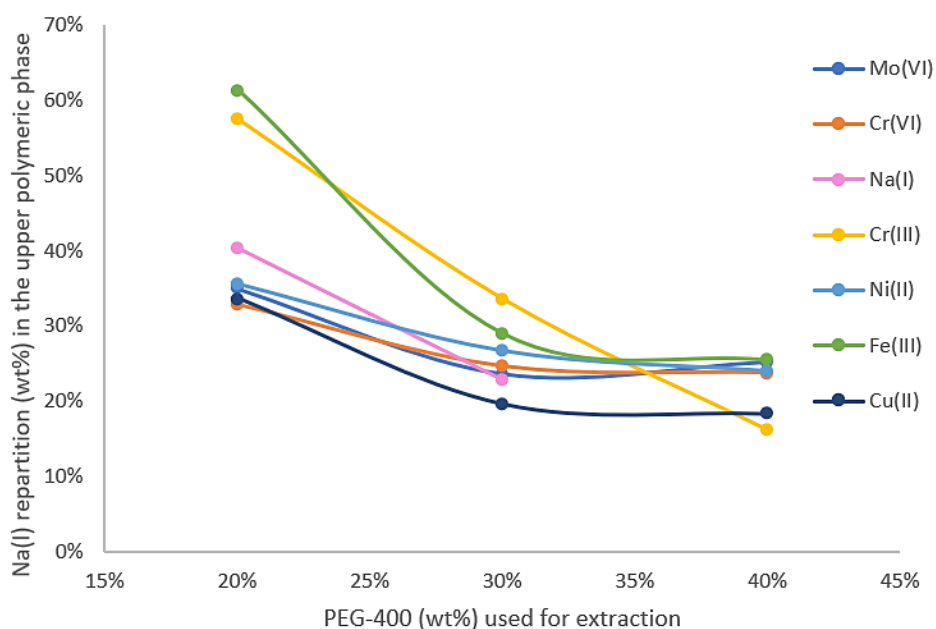


Figure 76. Na(I) repartition (wt%) in the polymer phase for the systems of Fe(III), Ni(II), Cu(II), Cr(VI) and Cr(III).

Figure 77 shows that the volume of the upper polymeric phase for the examined ABSs increases as the amount of polymer used for extraction increases, except for Fe(III). When the wt% of PEG in the initial mixture increases, then the final volume of the PEG-phase increases, and this can be explained also by considering the binodal curves of the systems proposed in Figure 7. In fact, when increasing the PEG content in the mixture, the position of the mixture on the graph moves towards the direction of the PEG. With regard to Fe(III), at 20 wt% of PEG-400, the volume of the upper phase is around 80 wt%, when the 30 wt% polymer is used, the volume of the upper phase drops below 80 wt% and then when the amount of polymer used in the system increases to 40 wt%, the volume in the upper phase exceeds the value of 80 wt%. More experiments are needed to give an explanation of the behavior of Fe(III). Finally, it is interesting to note that the distribution volumes between one metal and another do not superimpose but seem to be influenced by the different type of metal. This part would deserve a dedicated study, as it was not carried out during the project.

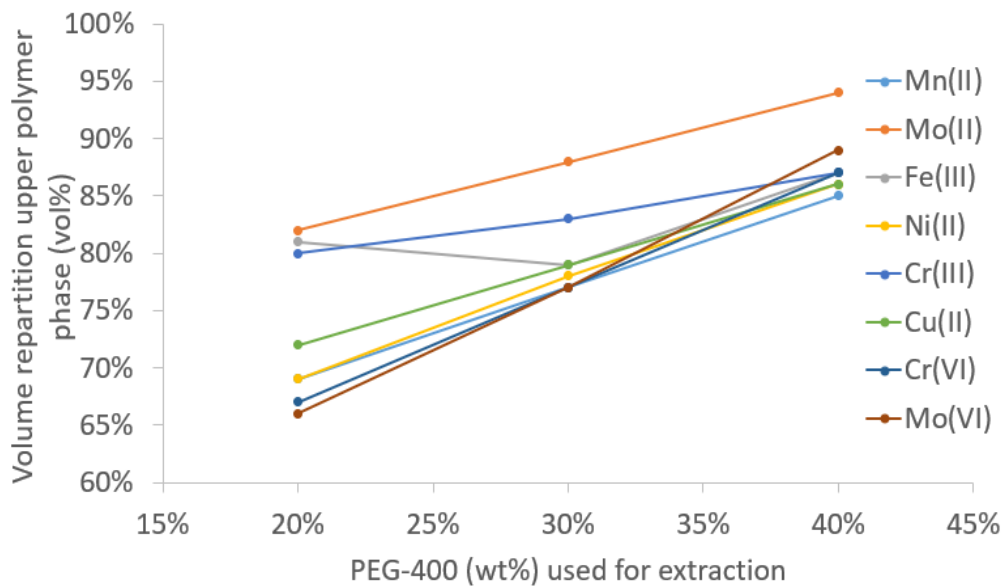


Figure 77. Volume distribution for each stock solution mono-element.

While the binodal curves are superimpose, and there is no influence of metals on their position, the extraction efficiency of PEG-400 seems to be particularly affected by the type of metal and by its form (oxidation number, speciation). Regarding the metals speciation, the different studies in literature deal more with describing methods that determine the presence of one species over another in an aqueous solution, and it has been difficult to find concordant results when considering a complex system. What can be said for sure is that considering our stock solutions with pH around 2 and concentration of 5 g/L in metals, the species with number of oxidation +II and +III, will be found mainly in their cationic dissociated form ( $Me^{n+}$ ), as confirmed by the Pourbaix diagrams in Figure 78.

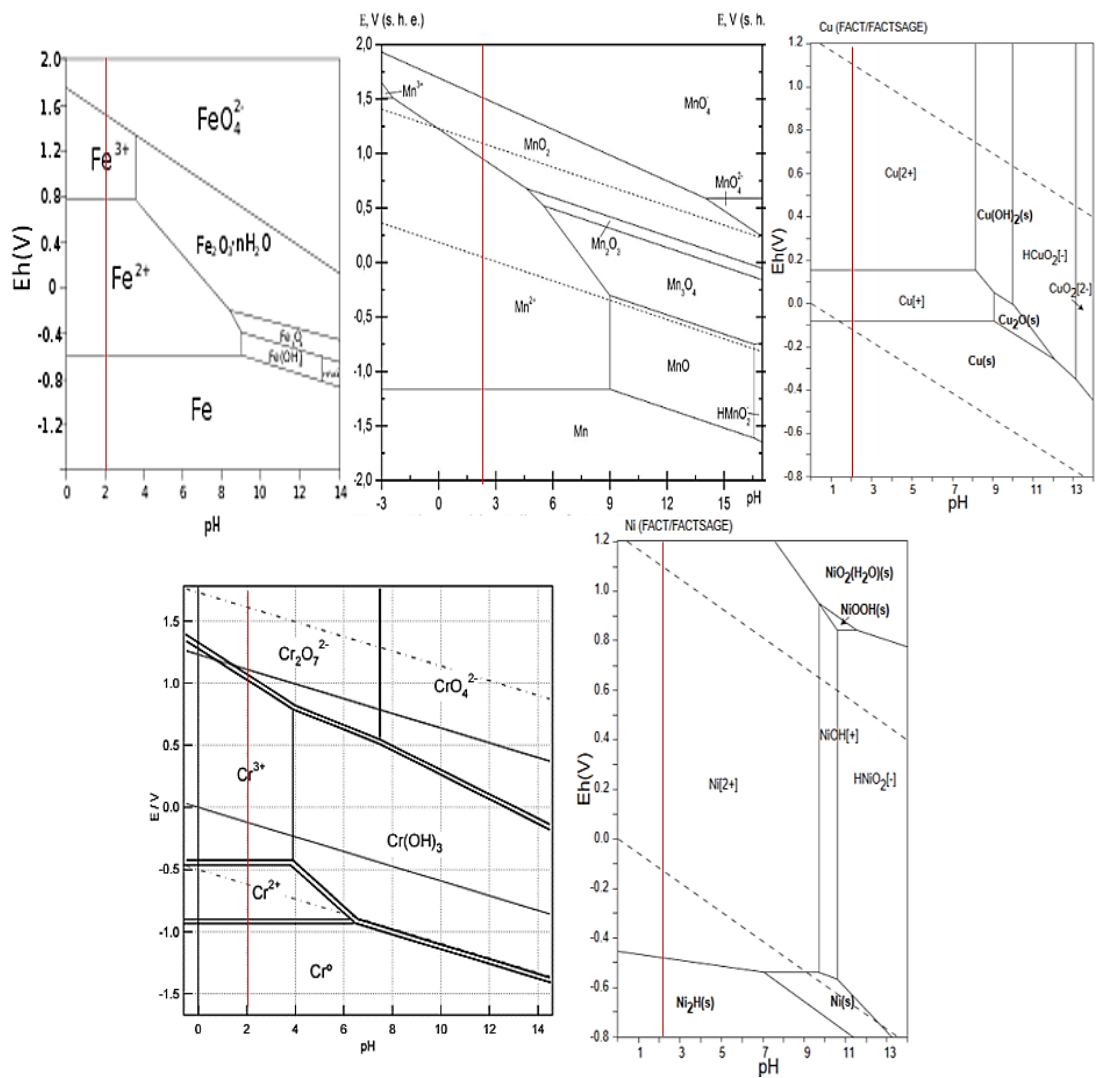


Figure 78. Pourbaix diagrams for Fe, Mn, Cr, Ni and Cu at T=25°C. Red lines have been inserted at pH=2 to allow the reader to more easily identify the species present in the solutions investigated in this work.

Regarding Cr(VI), it exists mainly in two forms, as chromate ( $\text{CrO}_4^{2-}$ ) and dichromate ( $\text{Cr}_2\text{O}_7^{2-}$ ) (Figure

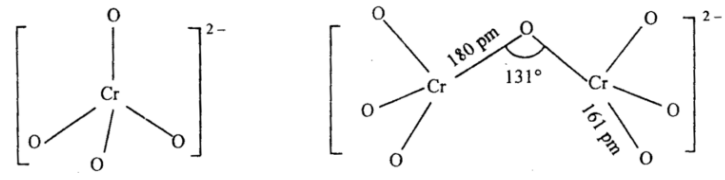


Figure 79. Chemical structures of chromate (left) and dichromate (right)

79).

In the stock solution prepared from  $\text{Na}_2\text{Cr}_2\text{O}_7 \cdot \text{H}_2\text{O}$  salt, it is possible to assume that the metal is mainly present as dissociated salt, dichromate ( $\text{Cr}_2\text{O}_7^{2-}$ ) as anion and  $\text{Na}^+$  as cation:



The predominance of dichromate is confirmed also in this case by the diagram in Figure 80. Focusing on the red line, which corresponds to the concentration (5g/L) used in my investigation, at pH around 2, the predominant species is  $\text{Cr}_2\text{O}_7^{2-}$ .

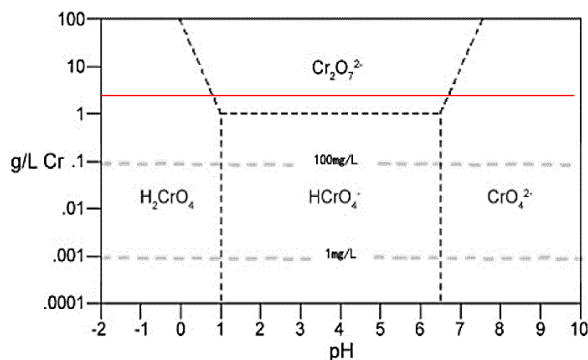


Figure 80. Speciation diagram of Cr(VI) at different pH and concentration (g/L). The red line indicates the concentration considered during my investigation (5g/L).

Moreover, taking into account the variation in color in the ABS consisting of PEG-400 /  $[\text{Cr(VI)}+\text{Na}_2\text{SO}_4]$  /  $\text{H}_2\text{O}$  at 25 °C presented in Figure 81, it can be noticed that, starting from A, which corresponds to the initial stock solution, adding PEG-400 at a ratio of 20/80 wt% of polymer/stock solution leads to sample B. Sample B shows that the dichromate ions (orange) are located in the polymeric upper phase while the chromate ions (yellow) are mostly in the lower aqueous phase. After 24 hours, under exposure to sunlight, the lower phase of sample C, turns green, probably due to the reduction of Cr(VI) in Cr(III).

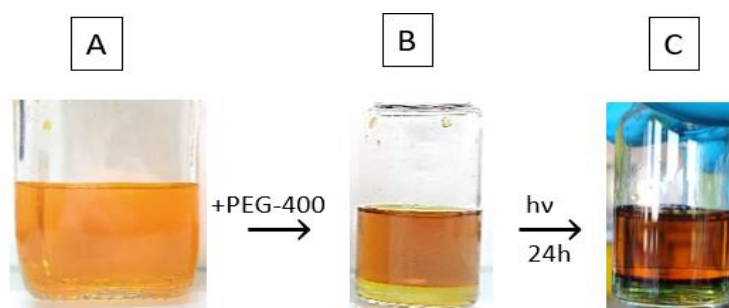


Figure 81. Reaction that occurs when PEG-400 is mixed with Cr(VI) stock solution in partition 20/80 wt% of polymer/stock solution Cr(VI). A) stock solution; B) Biphasic system as soon the polymer encounters the stock solution; C) samples after 24h, left in direct contact with light.

Considering the color distribution in ABS, the repartition of Cr(VI) in the upper phase PEG-400 is almost 100% on the dichromate (orange color). For chromate (yellow), however, the repartition was not considered in this investigation. What is certain is that chromate is distributed less than 100% in the polymer phase and is largely present in the lower phase of the system.

As far as Mo(VI) is concerned, in Table 16 is possible to see that above pH=2.5, the most common species is the oxoanionic one in polyanionic form (Yongqiang et al.<sup>149</sup>).

pH	<1.8	<2.5	<4	<5	<7	>7
Species	MoO <sub>2</sub> <sup>2+</sup>	H <sub>2</sub> Mo <sub>7</sub> O <sub>24</sub> <sup>4-</sup>	HMo <sub>7</sub> O <sub>24</sub> <sup>5-</sup>	Mo <sub>7</sub> O <sub>24</sub> <sup>6-</sup>	Mo <sub>2</sub> O <sub>7</sub> <sup>2-</sup>	MoO <sub>4</sub> <sup>2-</sup>
z /n	0.6667	0.1212	0.1562	0.1935	0.2222	0.4
z /M	0.01562	0.003774	0.004726	0.005682	0.006579	0.0125

Table 16. Ratio of charge, mass and charge density of Mo(VI) under different pH. |z| is the absolute value of ions charge, n is atomic number of ions, M is molar mass of ions. |z|/M is the charge density<sup>149</sup>.

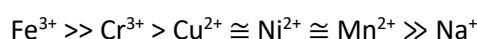
Another oxoanionic species that is present in all the stock solutions is SO<sub>4</sub><sup>2-</sup>. The sulfates, dichromates and polymolybdates will then interact with the cationic species present in solutions to maintain the neutrality in both the upper and lower phases.

In particular, considering the values of the stability constants (log K) of sulfate (SO<sub>4</sub><sup>2-</sup>) of some cations with oxidation number +I, +II and +III present in solution (Table 17):

Species	log K
Na <sup>+</sup>	0.70
Cr <sup>3+</sup>	2.60
Mn <sup>2+</sup>	2.26
Fe <sup>3+</sup>	4.04
Ni <sup>2+</sup>	2.32
Cu <sup>2+</sup>	2.36

Table 17. Stability constant of the species with SO<sub>4</sub><sup>2-</sup>.

It can be said that Fe(III)-sulfate complex is the most stable (log K = 4.04), followed by Cr(III) (log K = 2.60), while Ni(II), Cu(II) and Mn(II) have values very close to each other (log K between 2.26 and 2.36). In last place is present Na(I) (log K = 0.70). The more stable the compound, the less dissociated it will be in solution. It is possible to conclude that the trend of stability will be as follows:



It is important to mention that PEG is well known to promote interactions with groups 1 and 2 of the periodic table, in our case we refer in particular to Na(I). In fact, as demonstrated by Rogers et al.<sup>150,151</sup> PEG behaves like crown ether ligands. The latter have proven to be valuable compounds due to their known size selectivity for hard metal ions, as well as for their successful use in conventional solvent extraction systems of elements of groups 1 and 2 of the periodic table. Furthermore, the extraction

efficiency of PEG is also well known with respect to oxoanionic molecules, and in particular, Sun *et al.*<sup>16</sup> showed that PEG could extract Cr(VI) through Na(I) interaction (State of the Art).

By combining the polymer extraction efficiencies obtained during the investigation and the information derived from the literature research, in Figure 82 is proposed an mechanism extraction that describes what occurs in the ABS composed by PEG-400 / [Me + Na<sub>2</sub>SO<sub>4</sub>] / H<sub>2</sub>O. The figure is divided into a polymeric upper phase and a salt-rich lower phase. In the polymeric phase it is possible to find two PEG chains linked together by water molecules, as also proposed by Bulgariu *et al.*<sup>8</sup>. Moreover, it is assumed that water molecules can also be found outside the chains (A), and their presence indicates the affinity that the polymer has with the aqueous biphasic system in which it is located. Next poly-molybdates (B) and dichromates (C), are extracted as oxoanionic structures and interact with the polymer chain via Na(I), as stated by Sun *et al.*<sup>16</sup> Then we find the sulfates, which also interact with the polymer chain via Na(I). Next are all those structures that are more or less stable under the present working conditions, Fe(III), Cr(III) etc., which will be extracted as sulfate salts and will always interact with the polymer via Na(I). Dissociated cationic species and water-solvated structures of the metals investigated will be found in the salt-rich lower phase of the ABS.

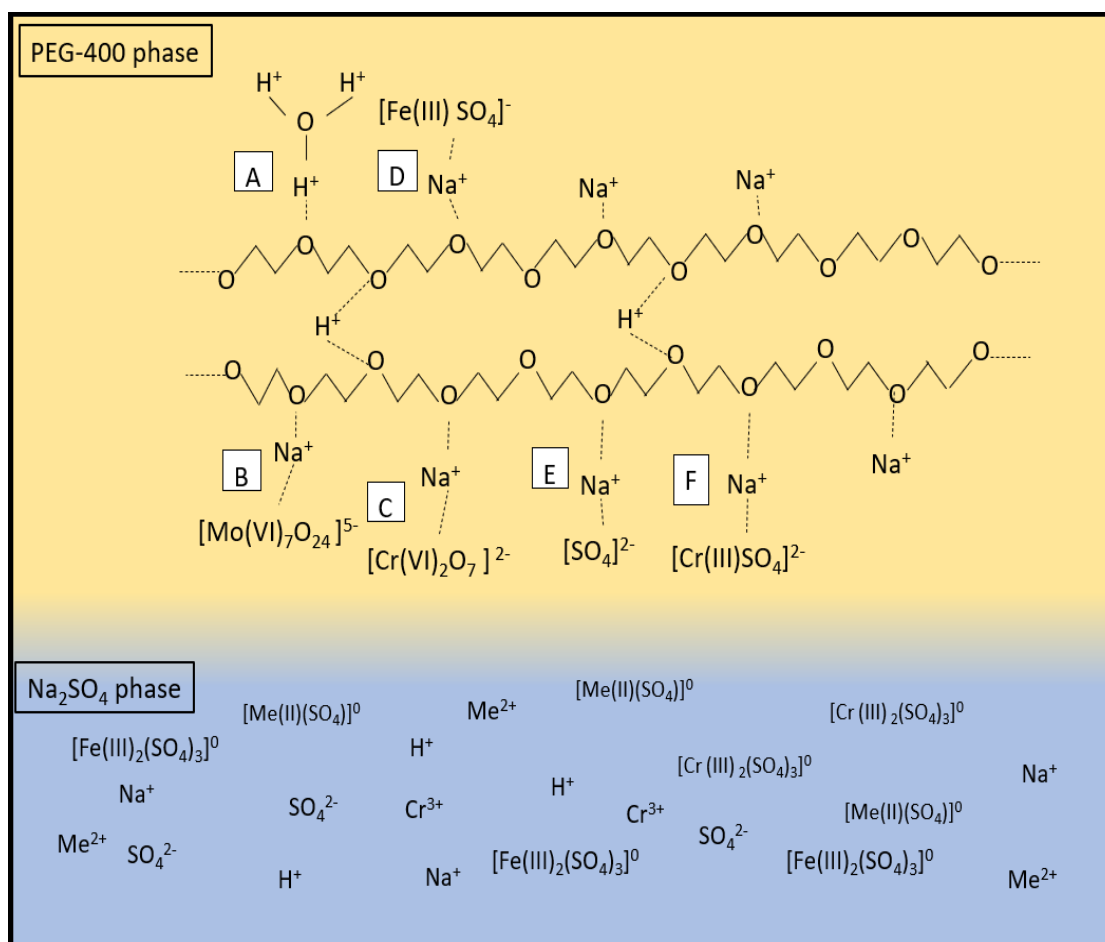


Figure 82. Extraction mechanism of PEG-400 proposed in this work.

The results just presented for the system PEG-400 / [Me + Na<sub>2</sub>SO<sub>4</sub>] / H<sub>2</sub>O differ considerably from those obtained with the system PEG-600 / [Me + HCl<sub>37 wt%</sub>] / H<sub>2</sub>O presented in the previous chapter. In particular, for the PEG-600 / [Me + HCl<sub>37 wt%</sub>] / H<sub>2</sub>O system, an ABS could only be obtained by considering Fe(III) contribution. While, in the case of PEG-400 / [Me + Na<sub>2</sub>SO<sub>4</sub>] / H<sub>2</sub>O system, it provides an ABS also when different other metals such as Ni(II), Cr(III), Cr(VI), Mo(VI) etc., are considered. In addition, the system PEG-400 / [Fe(III) + HCl] / H<sub>2</sub>O provides an unusual binodal curve, which we have named "onion-shape", while with PEG-400 / [Fe(III) + Na<sub>2</sub>SO<sub>4</sub>] / H<sub>2</sub>O presented in Figure 63, the binodal curve shows a classical form, which can be found already in several publications. The mechanism of Fe(III) extraction using PEG in hydrochloric medium is also different from the sulfate extraction proposed in this chapter. In the previous chapter, Fe(III) was presented in an anionic form with Cl<sup>-</sup> in solution, so a mechanism was proposed whereby FeCl<sub>4</sub><sup>-</sup> interacts directly with the O<sup>+</sup> present on the polymer chain, as also proposed by Rogers and co-workers<sup>6</sup> and Bulgariu et al.<sup>8</sup>

### 3.2.2. *Metal concentration and temperature influence*

The investigation continued by obtaining binodal curves for systems composed of different concentrations of the same metal (Cr(VI)) and at different temperatures (25 °C and 40 °C). The results presented in Figure 83 show that the binodal curves, by varying the concentration or temperature, are not influenced by the studied experimental conditions and so they do not move in the phase diagram.

By comparing the results obtained for the temperature investigation with the one presented by Das et al.<sup>95</sup>, (State of the Art) where the research group used a copolymer consisting of PEG-PPG they demonstrated that in the ABS composed of PEG-PPG / Na<sub>2</sub>SO<sub>4</sub> / H<sub>2</sub>O, the binodal curve shifts to the left as the temperature increases. Therefore, it can be deduced that the choice of polymer plays a key role in the investigation.

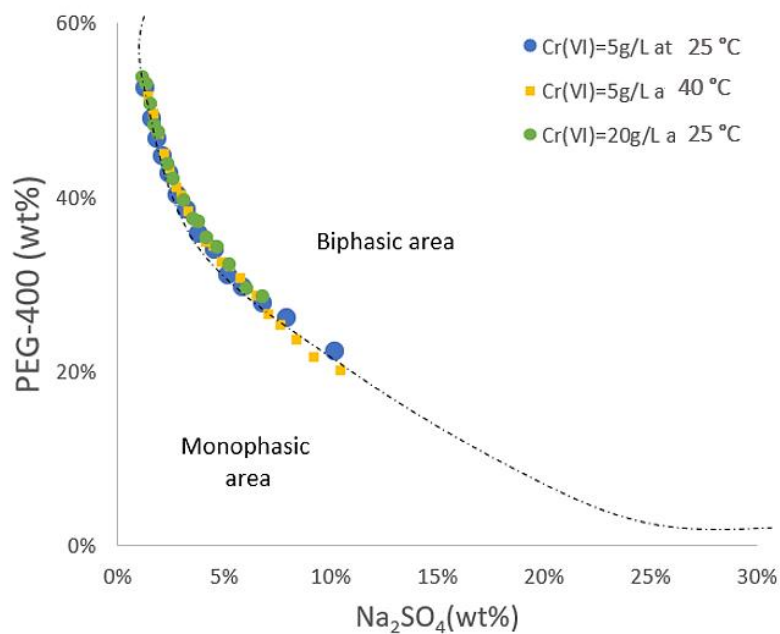


Figure 83. Binodal curves for the systems PEG-400 / [Cr(VI) + Na<sub>2</sub>SO<sub>4</sub>] / H<sub>2</sub>O, considering (blue) [Cr(VI) = 5 g/L and T = 25 °C, (yellow) [Cr(VI) = 5 g/L and T = 40 °C, (green) [Cr(VI) = 20 g/L and T = 25 °C.

Although the temperature impact on ABS formation is negligible, this was a challenging parameter to control, in fact, as can be seen in Figure 84, at 15°C, the systems promoted crystal formation or solid precipitation after the ABS was obtained.

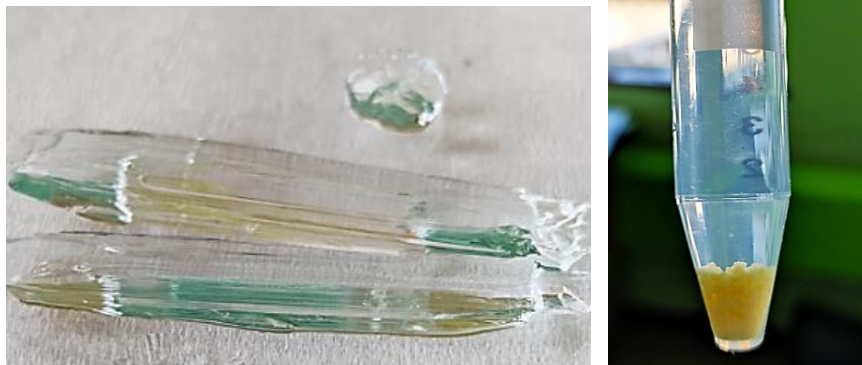


Figure 84. (left) Crystal's formation at T=15°C in the upper and lower phase of the samples composed by 20/80 wt% of PEG-400/stock solution of Cr(III) 0.64 g/L.(right) Precipitation effect on the upper and lower phase of sample containing 20/80 wt% of PEG-400/Stock solution of Fe(III) 5 g/L after exposition at 15°C.

Navarro et al.<sup>152</sup> demonstrated how in a Na<sub>2</sub>SO<sub>4</sub>-H<sub>2</sub>O system, anhydrous Na<sub>2</sub>SO<sub>4</sub> is reported to precipitate directly from solution at temperatures above 32.4°C (curve 3 - Figure 85). Below 32.4°C, the stable phase is mirabilite (Na<sub>2</sub>SO<sub>4</sub>\*10H<sub>2</sub>O in curve 1 - Figure 85), which rapidly dehydrates below 20°C to form anhydrous Na<sub>2</sub>SO<sub>4</sub>. Furthermore, as discussed in section 2.4. State of the art, Taboada et al.<sup>82</sup> also recognize the formation of different types of solids when located to the right of the binodal curve.

A practical disadvantage of working with these systems was the impossibility of storing the solutions for long periods, since a variation in temperature (higher or lower than room temperature) favored the formation of crystalline salts. Furthermore, solid formation was found to be irreversible in these systems. For this reason, the optimum working temperature range was between 20 °C and 25 °C. Finally, it is important to underline that the investigated systems contain 10 g/L of H<sub>2</sub>SO<sub>4</sub> which increased the solubility of the metallic salts and reduced the formation of crystals. Therefore, the crystallization temperature proposed by Navarro et al.<sup>152</sup> is perhaps not totally applicable to my systems.

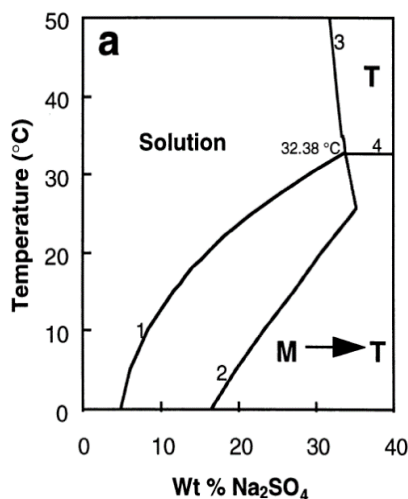


Figure 85. Na<sub>2</sub>SO<sub>4</sub>-H<sub>2</sub>O system. Temperature vs. concentration diagram (M= mirabilite= Na<sub>2</sub>SO<sub>4</sub>\*10H<sub>2</sub>O; T= the-  
nardite= Na<sub>2</sub>SO<sub>4</sub> anhydrous; 1 = solubility curve for Na<sub>2</sub>SO<sub>4</sub>\*10H<sub>2</sub>O; 2 = solubility curve for Na<sub>2</sub>SO<sub>4</sub>\*7H<sub>2</sub>O; 3 = solu-  
bility curve for Na<sub>2</sub>SO<sub>4</sub> anhydrous; 4=Na<sub>2</sub>SO<sub>4</sub>/Na<sub>2</sub>SO<sub>4</sub>\*10H<sub>2</sub>O boundary system),

Crystal formation and solid precipitation is also promoted when working at room temperature. As discussed in the State of the art, Taboada et al.<sup>82</sup> presented the existence of different regions for the PEG-400 / Na<sub>2</sub>SO<sub>4</sub> / H<sub>2</sub>O system at 20 °C, and they stated that the formation of a third solid phase is favored when the wt% of polymer exceeds 40 wt%. In particular, in my investigation, the Fe(III)-sulfate system showed a larger tendency compared to other solutions to form crystals under the same working conditions, after ABS formation. Thus, it can be assumed that the crystal formation can also impact the volume repartition, indeed, it is thought that the presence of crystals prevents a linear increase in the volume of the upper phase when increasing the amount of polymer used in the system. (Fe(III) in Figure 77). It can be assumed that the formation of the solid (or crystalline) phase may be due to competition between the polymer and the salt in attracting water. Since we are in an aqueous biphasic system, both the phases contain water. Although PEG-4000, used by Taboada and co-workers<sup>82</sup>, is less soluble than PEG-400 used in my investigation, both they have high affinity with the aqueous medium. If the salt-rich phase is depleted of water, the salt concentration will increase and thus a precipitate will appear, and so it becomes a question of solubility.

### 3.3. System with double element

The investigation of synthetic solutions continued by examining whether the matrix effect between metals could influence their distribution in the ABS. The matrix effect is also to be related to the sulfate bath, where several metals are present at the same time. For this purpose, a comparison has been made between the extraction efficiency of PEG-400 in the single-element stock solutions (Cu(II) and Mo(VI) separately) and in a stock solution containing both Cu(II) and Mo(VI). The stock solution is made by 5g/L of Cu(II), 5g/L of Mo(VI), pH=1.85, 100g/L of SO<sub>4</sub>, 50g/L of Na, 10 g/L of H<sub>2</sub>SO<sub>4</sub>. Three biphasic samples were obtained by mixing different amounts of PEG-400 and synthetic Cu(II)+Mo(VI) solution. The samples after the phase separation are shown in Figure 86 and they consist respectively of 20/80, 30/70 and 40/60 wt% polymer/double-element stock solution.



Figure 86. Samples obtained by mixing different wt% of PEG-400 + stock solution Cu(II)+Mo(VI); s1 = 20/80, s2 = 30/70, s3 = 40/60, in wt%, of PEG-400/stock solution.

Figure 87 shows the polymer extraction efficiency considering single metal stock solution (dotted lines) and double metal stock solution of Mo(VI) and Cu(II) (solid lines). It appears that the polymer's extraction efficiency is higher when the metals are together in double-element stock solution starting from 20 wt% of PEG-400 used to obtain a biphasic system. The extraction efficiency has closer values when 30 wt% of PEG-400 is used for extraction and reaches equal values for 40 wt% of PEG-400. This is a preliminary experiment that needs to see further research to be confirmed. In fact, it would be interesting to see the contribution of other metals as well, and to understand whether there is a common trend that leads PEG-400 to increase its extraction efficiency when the different species are all found together or vice versa.

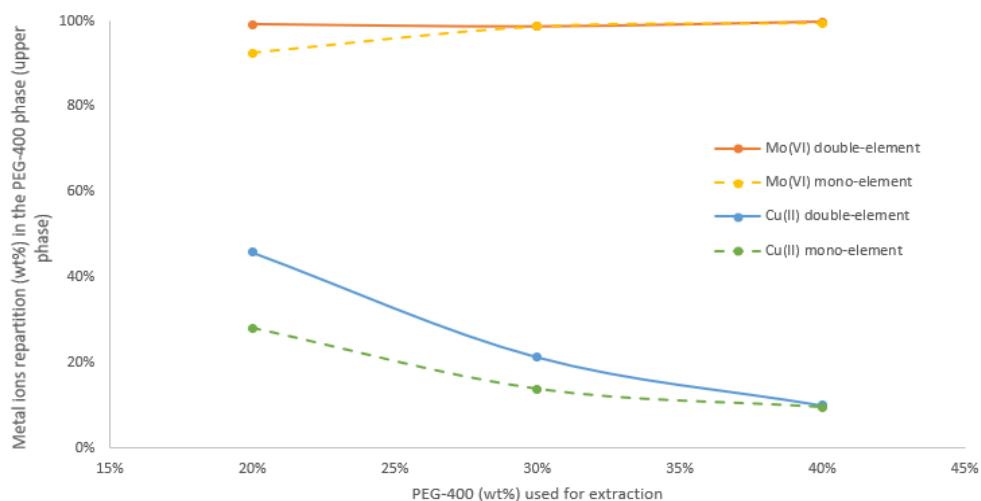


Figure 87. PEG-400 extraction efficiency considering Cu(II) and Mo(VI) in the same stock solution (straight line) or separately (dotted line).

#### 4. Binodal curve with Na<sub>2</sub>SO<sub>4</sub> bath

A further investigation was made to compare the binodal curve for the two previously presented ABS consisting of PEG-400 / Na<sub>2</sub>SO<sub>4</sub> salt / H<sub>2</sub>O and PEG-400 / [Cr(VI) + Na<sub>2</sub>SO<sub>4</sub> salt] / H<sub>2</sub>O and the PEG-400 / Na<sub>2</sub>SO<sub>4</sub> bath system at 25 °C. The metal concentration of the sulfate bath used to obtain the binodal curve is shown in section 3.5. State of the art. The main differences between the solutions are in the concentration of Cr(VI), which is present at about 5 g/L in the synthetic solution and about 11 g/L in the sulfate bath, and the presence of other metals in the bath. The binodal curves presented in Figure 88 are nearly superimpose on the phase diagram. It can therefore be confirmed that the type of metal, their concentrations, and also the combination of several metals does not influence the ABS properties.

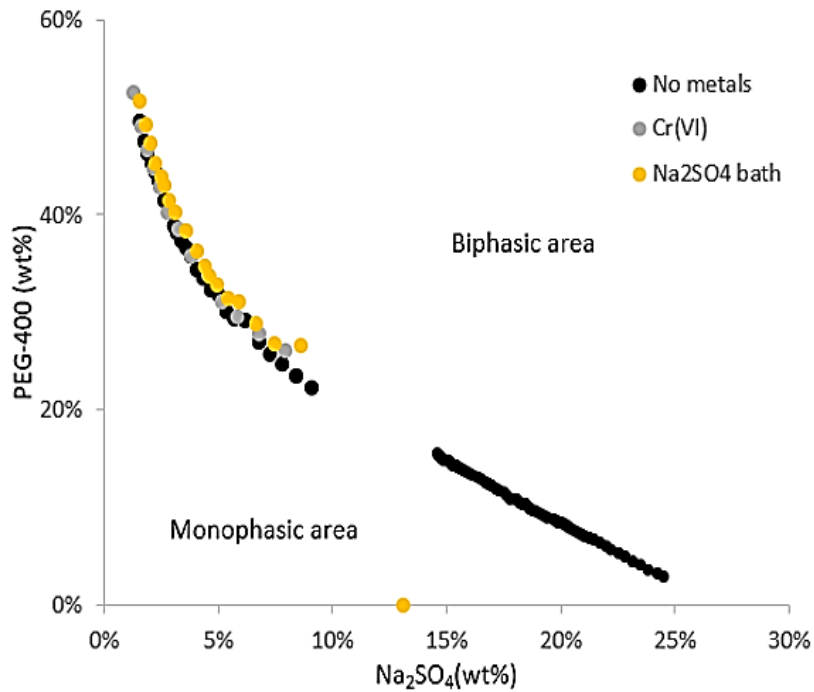
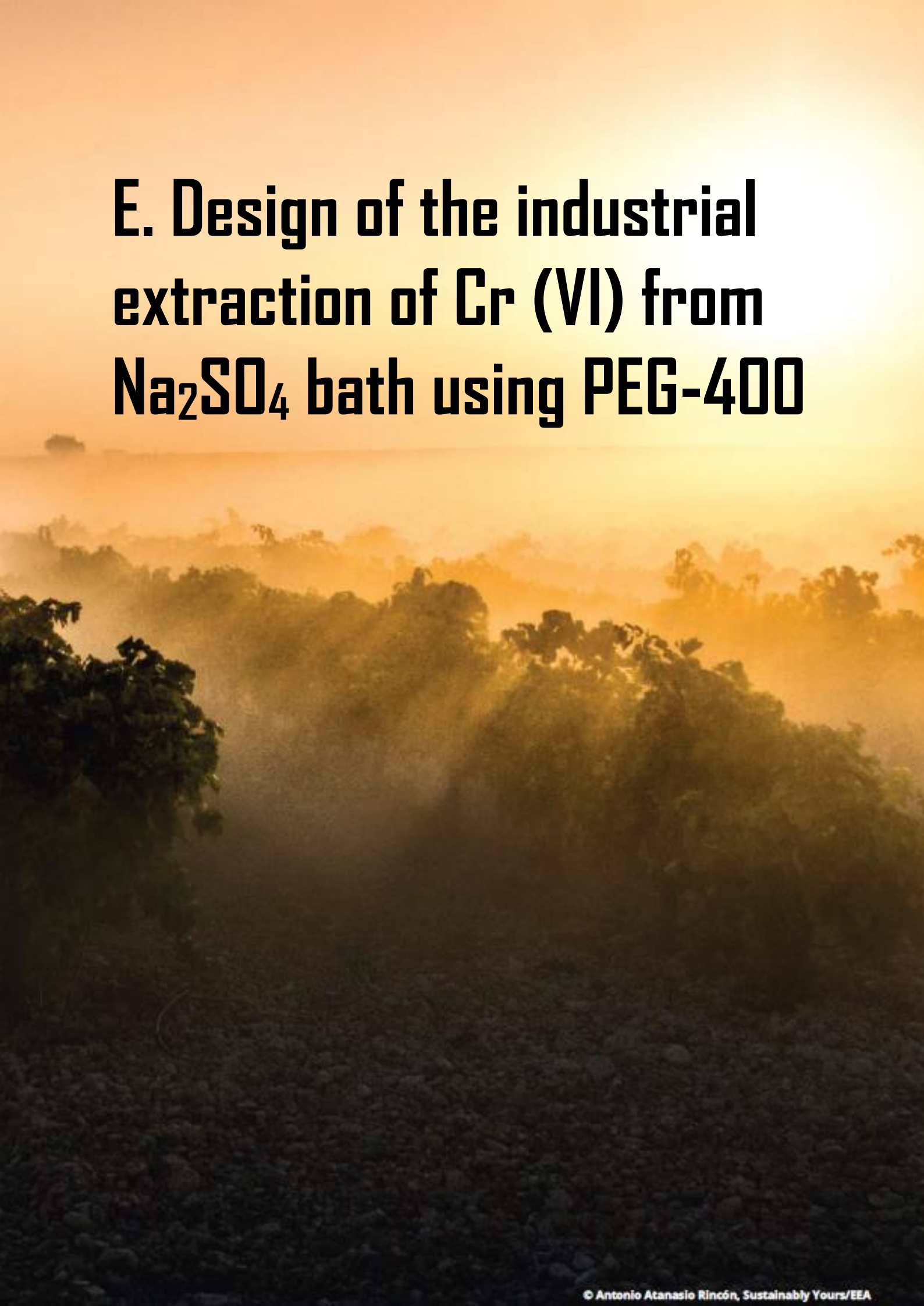


Figure 88. Binodal curves for the ABS composed of: (yellow) PEG-400/ $\text{Na}_2\text{SO}_4$  bath; (grey) PEG-400/[Cr(VI) -  $\text{Na}_2\text{SO}_4$  salt] /  $\text{H}_2\text{O}$ ; (black) PEG-400/  $\text{Na}_2\text{SO}_4$  salt /  $\text{H}_2\text{O}$  at 25 °C.

## 5. Conclusions

Both the preliminary tests and the experiments carried out on the single metal stock solutions seem to respond perfectly to Aperam's request to clean a solution similar to the sulfate bath of metals, in this specific case from Cr(VI) which is the most abundant species in the Aperam bath. It has also been demonstrated in this chapter that the extraction mechanism of PEG-400 favors the extraction of oxoanionic compounds over cationic species in solution. For this reason, in the next chapter will be shown all the experiments carried out directly on the sulfate bath, and the ABS obtained for the PEG-400 /  $\text{Na}_2\text{SO}_4$  bath/water will be integrated in a global loop for the development of the extraction process of Cr(VI) through the use of PEG-400 in the Aperam bath.



# **E. Design of the industrial extraction of Cr (VI) from $\text{Na}_2\text{SO}_4$ bath using PEG-400**



# 1. Introduction

The high amount of spent pickling liquor (SPL) produced by steel refining processes is one of the main causes of pollution for metallurgical companies. Nowadays, Aperam treats the SPL coming from the  $\text{Na}_2\text{SO}_4$  bath and characterized by a high amount of Cr(VI) (20 g/L) *via* neutralization processes. Cr(VI) is first reduced to Cr(III) with bisulfite or Fe(II), then lime is added to the mixture to raise the pH and form hydroxide, which precipitates. The hydroxides are then separated from the liquid part by filtration. The sludge is landfilled, and the liquid part (mainly water) is poured into the river. The sludge obtained at the end of the neutralization process are loaded with sulfate ions, which prevents them from being revalorized through pyrometallurgical treatments. Aperam's request for this bath is to clean the bath of metals, to recover them either in metallic form or in a form not contaminated by sulfates, and to reuse the cleaned bath in the pickling process. The ABS proposed in Chapter D seems to be a good alternative to the neutralization processes used so far by Aperam, since through the PEG-400 /  $\text{Na}_2\text{SO}_4$  /  $\text{H}_2\text{O}$  system it was possible to clean the sulfate bath from Cr(VI), the most abundant species in this type of SPL. This chapter will first describe the various experiments carried out aimed at implementing the extraction process proposed in chapter D. Finally, the ABS will be inserted into the general loop of the chromium extraction and recovery process. Each stage of the loop will be presented in this chapter using the term: step 1, step 2, step 3 etc.

## 2. Step 1: extraction of chromium with a PEG-400 based-ABS

### 2.1. Optimization of the Cr(IV) extraction process

The influence of experimental parameters such as working temperature, amount of polymer used for extraction and kinetics of chromium extraction was considered during the investigation to evaluate their impact on the extraction process.

The first aspect analyzed was the working temperature. The aim of investigating temperature is to understand whether it can influence the repartition of metals or the volume distribution during the extraction process. Two samples were prepared for the experiment with a constant repartition of PEG-400 /  $\text{Na}_2\text{SO}_4$  bath of 27/73 wt% respectively. They were then placed in a thermal bath, one at 25 °C and the other at 75 °C. Once the biphasic system was achieved, the two phases of each sample were separated, and the concentration of metals was determined by AAS. Figure 89 shows the repartition

of elements and of volumes expressed in wt% in the polymeric upper phase of the system. As the temperature increases, the extraction efficiency of the polymer decreases for the elements considered (Cr(VI), Ni(II), Fe(III), and Na(I)), and the same occurs for the volume (wt%) of the polymer upper phase.

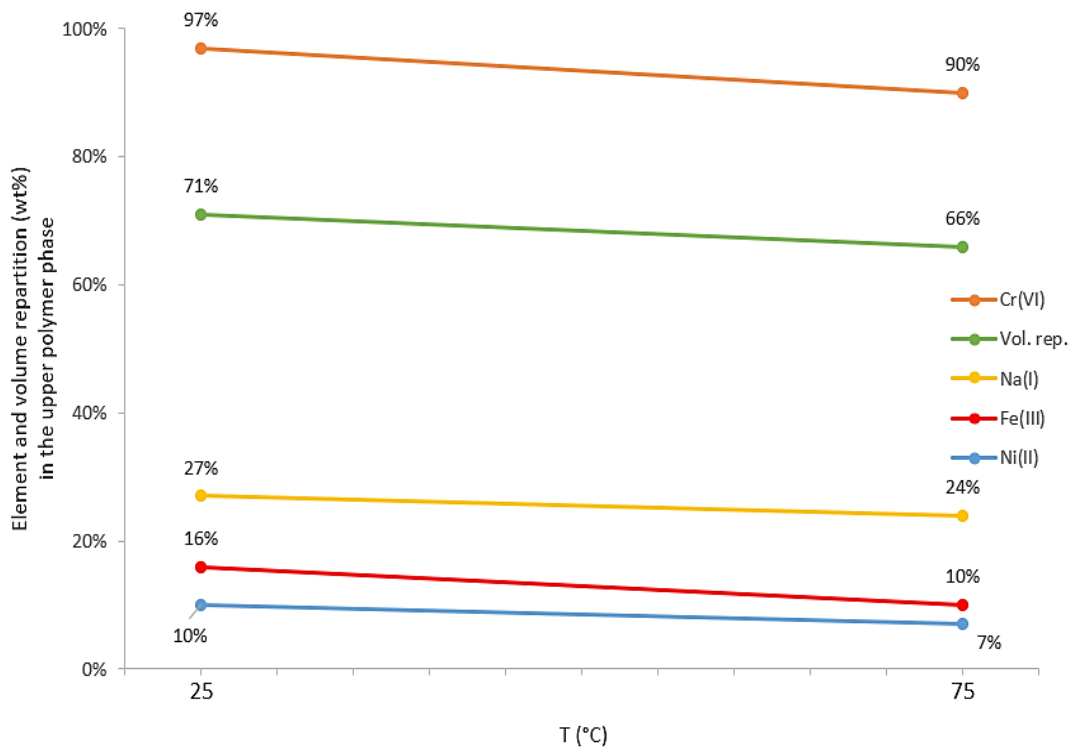


Figure 89. Element and volume repartition (wt%) for the system composed by 27 wt% of PEG-400 and 73wt% of  $\text{Na}_2\text{SO}_4$  bath at two different given temperatures, 25°C and 75 °C.

The working temperature chosen throughout the investigation was 70 - 80 °C, as this also corresponds to the working temperature to which the sulfate bath is exposed during the pickling process (70 - 80 °C), thus creating a continuous working line between the pickling process and the regeneration of the temperature-depleted bath.

The second series of experiments conducted concerned the influence of different amounts of polymer used in the extraction process. For this purpose, 5 samples were prepared with a PEG-400 / $\text{Na}_2\text{SO}_4$  repartition of 20/80 - 25/75 - 30/70 - 40/60 - 50/50 (wt%) at 80 °C. Figure 90 shows the repartition for the polymeric upper phase. As the amount of polymer (wt%) used to obtain a biphasic system increases, the amount (wt%) of chromium extracted in the polymer phase increases while the amount (wt%) of nickel and iron decreases. The concentration expressed in wt% of  $\text{Na}_2\text{SO}_4$  salt also decreases in the polymer upper phase when the amount of PEG used in the mixture increases.

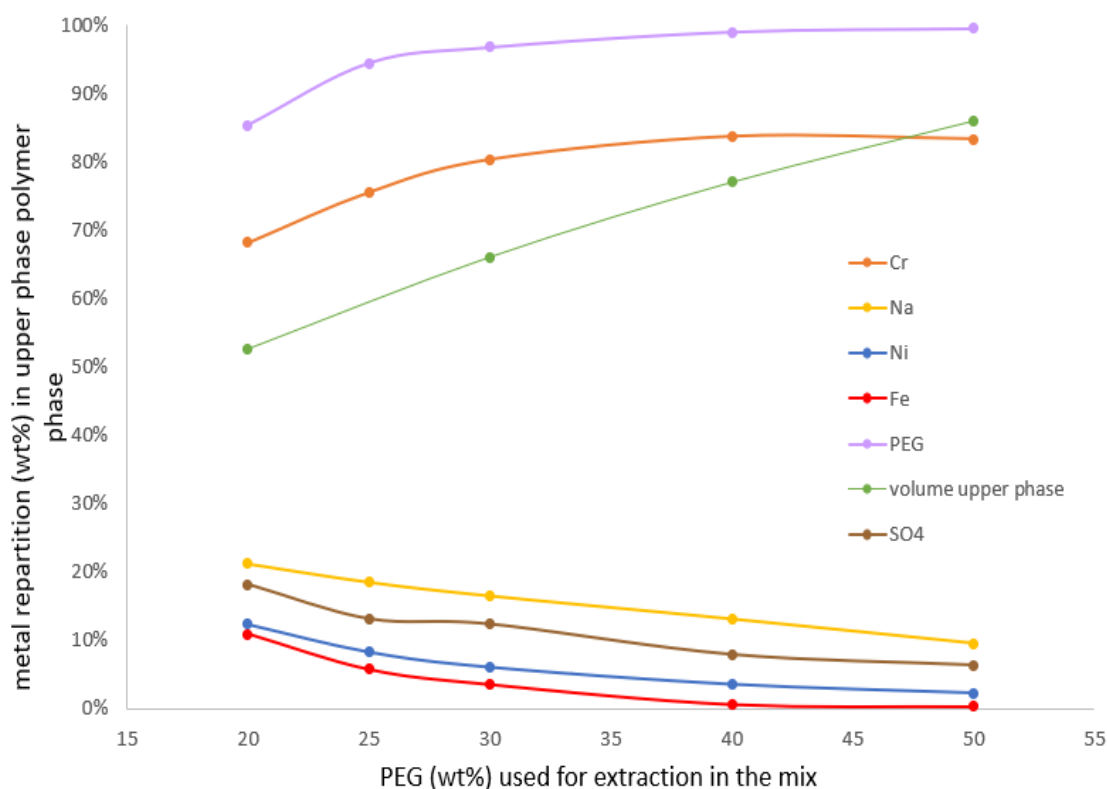


Figure 90. Extraction efficiency of PEG-400 considering different samples made up respectively of 20%, 30%, and 40% of PEG-400 and the difference in  $\text{Na}_2\text{SO}_4$  bath. Values taken from table 23.

The amount of polymer used for the remainder of the investigation is 40 wt%, as this value was found to be a good compromise between the extraction efficiency for Cr(VI), the amount of sulfates present in the polymer phase and the volume of bath regenerated.

The extraction kinetics was examined by measuring the Cr(VI) concentration after mixing 60 wt% of  $\text{Na}_2\text{SO}_4$  bath and 40 wt% of PEG-400 at  $T=80^\circ\text{C}$ . As soon as a distinctive upper and lower phase separation was visible in the sample, characterized by the formation of a meniscus, 8 aliquots were taken every 0.5 minutes in a total time interval of 5 minutes. The result shown in Figure 91 demonstrates that more than 8 g/L of Cr (initial Cr concentration 11 g/L) was extracted from PEG-400 at the time of  $t=0.5$  minutes and after few seconds the Cr(VI) value reaches a stable concentration

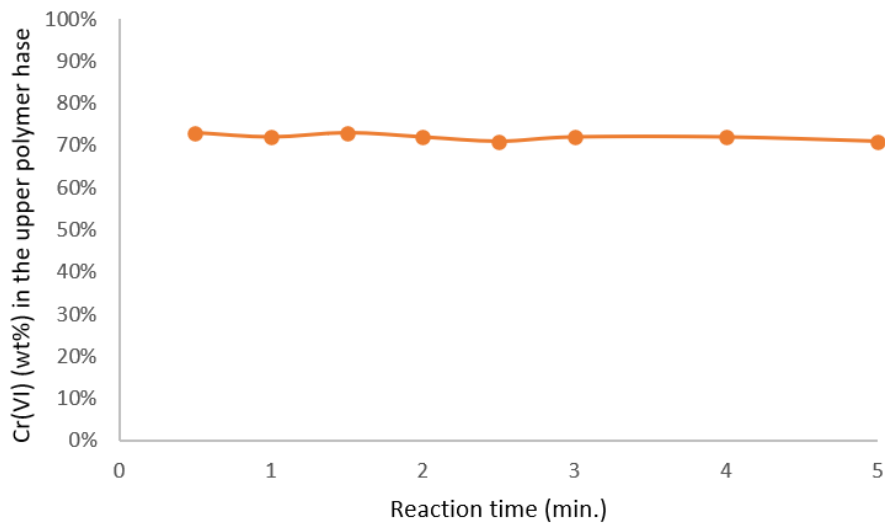


Figure 91. Extraction kinetics of Cr(VI) in the extraction process by using PEG-400

In addition, the mixing time of the polymer and the sulfate bath was approx. 1 - 2 minutes. The quiet time for phase separation was found to be 0.5-1min.

## 2.2. Test using laboratory pilot scale

The ABS proposed in the previous section consisting of 40wt% PEG-400 / 60wt% Na<sub>2</sub>SO<sub>4</sub> bath at 70/80 °C for the extraction of Cr(VI) from the sulfate bath prepared in the laboratory with a weight of 200 g was repeated on a larger scale of 10 kg (Figure 92).

The sulfate bath used for the experiment was first analyzed with AAS for the determination of metals' concentrations; the values are shown in Table 18. Chromium is the most abundant metal (11.6 g/L), nickel and iron are present at less than 1 g/L, while sodium sulfate is present at high concentrations ( $\text{Na(I)} = 48 \text{ g/L}$  and  $\text{SO}_4^{2-} = 104 \text{ g/L}$ ).

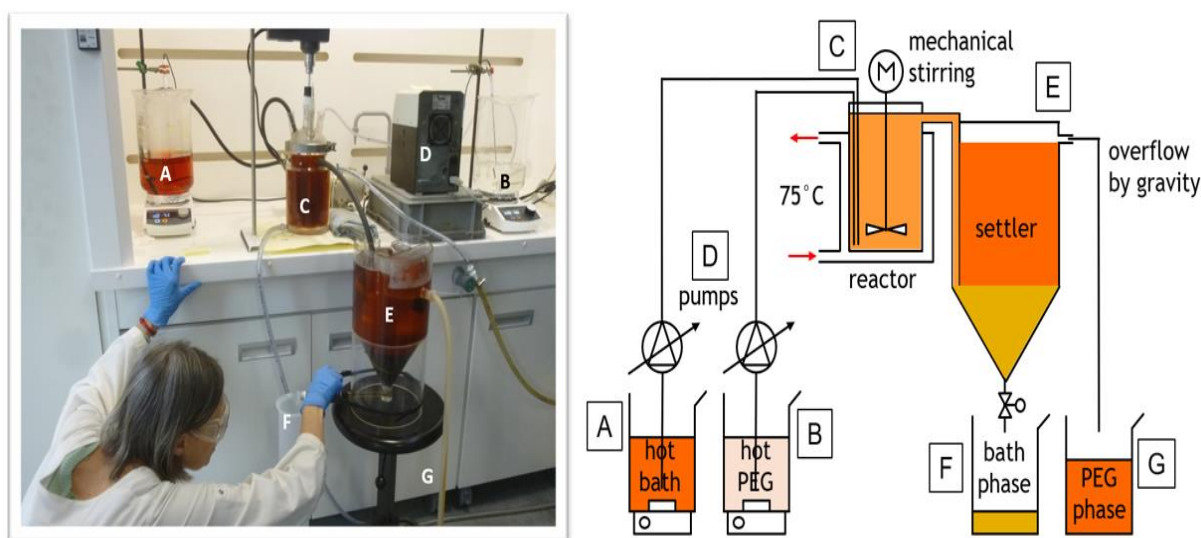


Figure 92. Snapshot of the process (on the right) and schematic diagram of step 1 big volume (10 kg) (on the left).

Density	1.145
pH	1.95
[Cr] (g/L)	11.6
[Fe] (g/L)	0.7
[Ni] (g/L)	0.3
[Na] (g/L)	48
[ $\text{SO}_4^{2-}$ ] (g/L)	104

Table 18. Composition, pH, and density of the  $\text{Na}_2\text{SO}_4$  bath filtrated.

The working temperature chosen is 70 - 80 °C. Large-scale reproduction was possible after the acquisition of a stirring system (C), a separation reactor (E) and the pumps (D). The two inputs A and B, respectively  $\text{Na}_2\text{SO}_4$  bath and PEG-400, are both introduced into the mixing reactor through two pumps (D) which inject the components in the correct ratio for extraction (40 wt% of PEG-400 and 60 wt% of the bath). The mixing solution has been carried out in the reactor C called jacketed reactor that maintains the temperature around 70 – 80 °C. The reactor is composed of a mixer which allows mixing and continuous contact between the two primary components (A and B). When this reactor is filled, the PEG solution is transferred by overflow into the reactor E. The separation reactor has a typical funnel shape, where the phase separation is operated. The phase composed of PEG-400 and

chromium, located in the upper part of the reactor, is evacuated by overflow into the container F, while the aqueous phase with the other elements, situated in the lower part of the reactor, goes into the container G.

Almost 6 kg of  $\text{Na}_2\text{SO}_4$  bath and 4 kg of PEG-400 were required for the implementation of step 1 in a large scale. With 5.2 kg of the initial mixture it was possible to fill the separation reactor, while the remaining 4.8 kg allowed the continuous process (of which 2.88 kg bath and 1.92 kg PEG-400) to be carried-out. The total time of the operation was 18 minutes, of which 11 minutes were spent on filling the reactor and 7 minutes on the continuous treatment.

The mass balance calculations proposed in Table 19 show that all the input values correspond to the output ones; only sodium seems to give divergent values, probably due to the determination method necessitating excessive dilutions.

Element	Input (g)	Output (g)	Balance
Cr	29.1	28.3	-3%
Fe	1.7	1.6	-7%
Ni	0.8	0.8	-3%
Na	121	143	18%
$\text{SO}_4$	246	221	-10%

Table 19. Mass balance step 1 big volume (10 kg).

As soon as the formation of the upper and lower phases of the system was achieved, three aliquots were taken every 2 minutes and analyzed to determine their composition in metals,  $\text{Na(I)}$ ,  $\text{SO}_4^{2-}$  and polymer. Figure 93 shows that the composition distributions remain constant throughout the process, with a slight increase in  $\text{Na(I)}$  at  $t = 4$  minutes. It is also important to emphasize that the polymer extracts a low amount of sulfates (around 15 wt%), so that the chromium passing into the polymer phase is not contaminated by the latter. Furthermore, at the end of the process the volume partition was 67 (wt%) upper phase and 37 (wt%) lower phase.

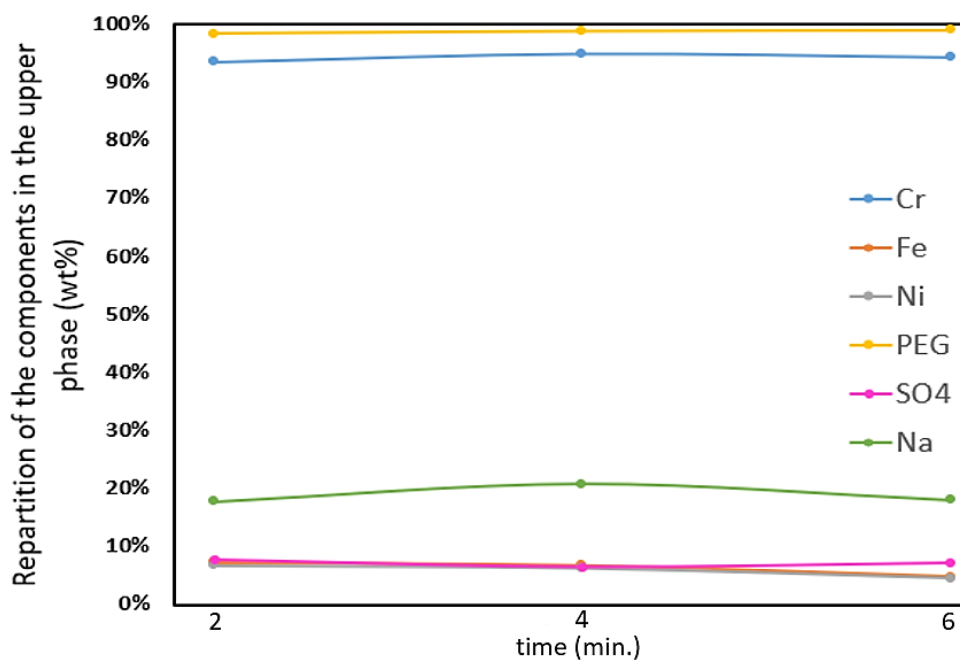


Figure 93. Metal extraction values for step 1 big volume.

One of the most challenging parameters to control during the investigation was the temperature. The polymer and the sulfate bath were pre-heated at  $T=40\text{ }^{\circ}\text{C}$  before being fed into the mixing reactor. This temperature was chosen mainly because at  $50\text{ }^{\circ}\text{C}$  a precipitation of solid phases occurred in the  $\text{Na}_2\text{SO}_4$  bath (Figure 94 on the left). Moreover, we tried to keep the temperature constant in the reactor between  $70\text{ }^{\circ}\text{C}$  and  $80\text{ }^{\circ}\text{C}$ , because as shown in the Figure 94 (on the right), if the temperature exceeded  $80\text{ }^{\circ}\text{C}$  due to a temperature control error, the system would promote the formation of crystals or solid precipitation. In particular, the solid was only detected during the cooling down step of the process since this had no opportunity to settle as the process was in continuous flow and under stirring. As discussed in chapter 4 of the thesis, the formation of crystals or solid precipitate must be avoided as this causes a change in the concentration of the species present in the  $\text{Na}_2\text{SO}_4$  bath. Moreover, it has been shown that the species that precipitates is mainly sodium sulfate, and the high concentration of this in the bath is essential for obtaining the biphasic system, as it plays the role of salting out agent in ABS. Finally, it should be noted that there is a considerable amount of  $\text{H}_2\text{SO}_4$  in the bath (about  $10\text{ g/L}$ ), which prevents the precipitation or the formation of crystals at lower temperature.



Figure 94. On the left - formation of crystal structures in the  $\text{Na}_2\text{SO}_4$  bath with a temperature superior of  $50^\circ\text{C}$ . On the right - solid precipitation occurred during the continuous process.

### 2.3. Extraction column for Cr(VI) partition

The results obtained with the mixing and settler reactor confirmed that the phase separation and homogenization is nearly instantaneous after stopping the mixing, and mixing is nearly instantaneous. For this reason, both the mixing reactor and the settler have been replaced by an extraction column (Figure 95). The selected column is made of glass, with a filling (glass Raschig rings) of about 160 mL of useful volume (about 60 cm long and 3 cm in diameter) operating in counter-current regime. With acknowledgement to Dr Nadine Commenges-Berrole for having performed the experiments with the extraction column.

The test was carried out by preheating the polymer and the sulfate bath at  $50^\circ\text{C}$ . The working temperature in the column was  $75^\circ\text{C}$ . The flow rates initially calculated to meet the optimum conditions defined in the process were  $m_{\text{PEG}} = 0.66 m_{\text{bath}}$ ,  $Q_{\text{bath}} = 100 \text{ mL/min}$  and  $Q_{\text{PEG}} = 62 \text{ mL/min}$ .

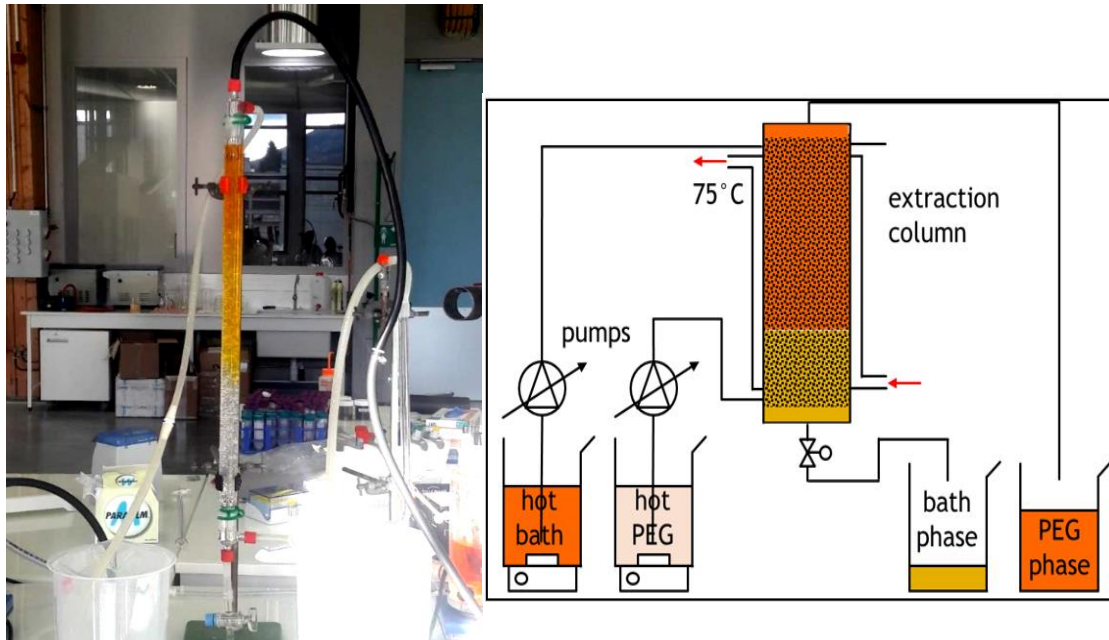


Figure 95. Snapshot of the extraction column process (on the left) and corresponding schematic diagram (on the right).

Although the column is practical to use and does not take up a lot of space in the process, compared to the mixing and the settler reactor, it was difficult to create the counter-current feed because of the very small difference in density between the bath and PEG-400. In fact, PEG-400 was not light enough and did not rise up the column, which made it difficult to create the ABS under the optimal and defined conditions for the operation of the process. It was impossible to recover the expected phases at the top and bottom of the column and the recovery of a bath-PEG mixture at the bottom of the column proved to be unusable. Therefore, the investigation with the extraction column was abandoned.

#### 2.4. Static mixer for Cr(VI) partition

Due to the density difference which is negligible for the polymer and sulfate bath on the extraction column, it was decided to retain the settler and replace the mixing reactor with a static mixer (Figure 96). The static mixer consists of a pipe with helical core inside, to ensure the strong *in situ* mixing of the 2 components. Three types of static mixers were tested, characterized by 24 or 36 elements, lengths: 276 - 334 - 552 mm, internal  $\varnothing$  7 or 10 mm, and different shape of the elements. The flow rates initially calculated to meet the optimum conditions defined in the process were  $Q_{\text{bath}} = 600\text{mL/min}$  and  $Q_{\text{PEG}} = 400\text{mL/min}$ , corresponding to 60 wt% in PEG-400 and 40 wt% of  $\text{Na}_2\text{SO}_4$  bath at 75°C.

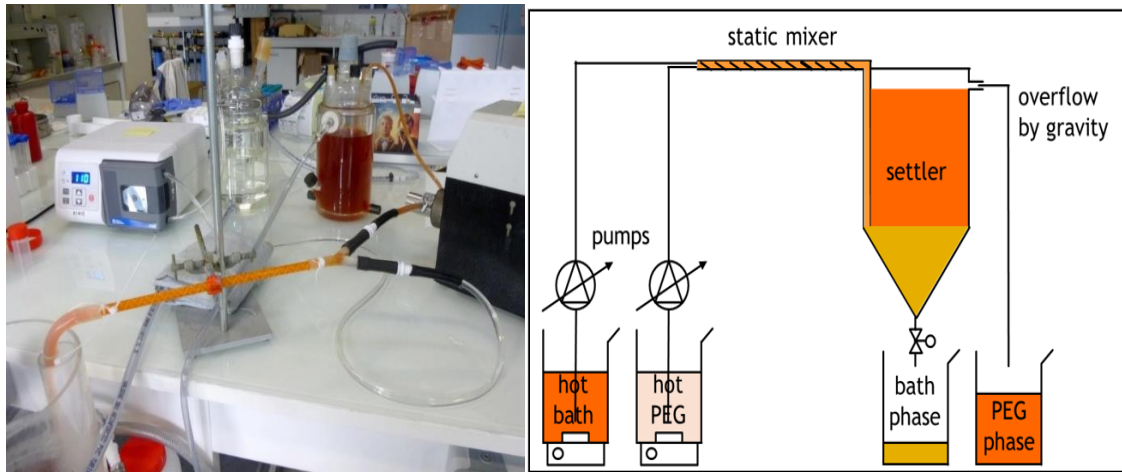


Figure 96. Snapshot static mixer process (on the left) and corresponding schematic diagram (on the right).

The results of the static mixers (green) are presented in Figure 97, and these are compared to the values obtained with the mixer and settler reactors (blue). Thanks to the static mixers, it is possible to extract a greater quantity (wt%) of metals in the polymer phase than the mixer and settler reactor. Moreover, the static mixers are very economical, not very complex, need only low maintenance and no footprint is required for their installation. On the other hand, the experiment conducted in the mixer and settler reactor provided a greater volume (vol%) of bath cleaned of metals than the static mixers.

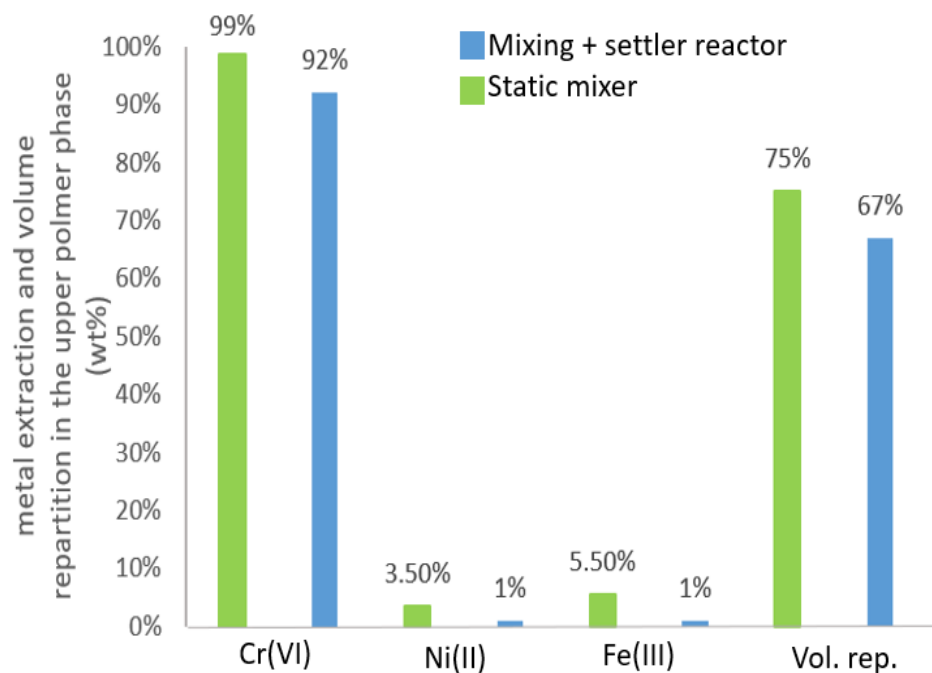


Figure 97. Extraction efficiency (wt%) of PEG-400 in the polymer phase, using a mixing and settler reactor (blues) and a static mixer (green).

## 2.5. What is the fate of Upper phase step 1 and the Lower phase step 1?

After treating the sulfate bath with the polymer, an upper phase step 1 (UPS1) rich in PEG-400 and Cr(VI), and a lower phase step 1 (LPS1) concentrated mainly in sodium sulfate were obtained (Figure 98). With regard to LPS1, Aperam checked the compatibility and the efficiency of the cleaned bath. The results indicated that LPS1 can be reinserted into the  $\text{Na}_2\text{SO}_4$  bath to be used for further pickling cycles after addition of water and correction of the pH. As for UPS1, different treatments will be proposed in the next section.

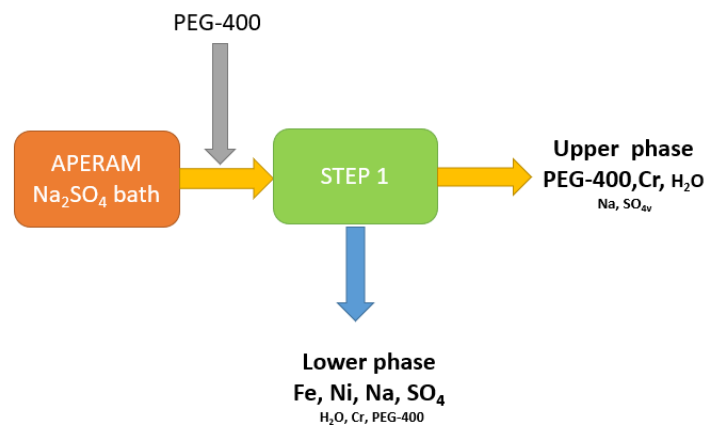


Figure 98. Step 1 of the process.

## 3. Step 2: separation of Cr(VI) from PEG-400 and Cr(III) recovery

### 3.1. UPS1 treatment with $\text{Na}_2\text{CO}_3$ and NaOH

The objective of step 2 is to separate the Cr(VI) in the polymer phase from UPS1, so that the polymer can be cleaned and used for further extraction processes, and the Cr(VI) recovered. As mentioned in the State of the Art, an ABS consisting of three components must have two biphasic inducers. UPS1 already contains PEG-400 which plays the role of the first biphasic inducer, so it was decided to add a salt to remove Cr(VI) from the polymer phase.  $\text{Na}_2\text{CO}_3$  was first tested on the UPS1 and then  $\text{Na}_2\text{SO}_4$ . As soon as the  $\text{Na}_2\text{CO}_3$  came into contact with UPS1, a biphasic system occurred and the same happened with  $\text{Na}_2\text{SO}_4$ . For what concerns  $\text{Na}_2\text{CO}_3$ , 4 samples were prepared at  $80^\circ\text{C}$ , with a  $\text{Na}_2\text{CO}_3$  decahydrate/ UPS1 repartition of 10 / 90 - 20 / 80 - 25 / 75 and 30 / 70 wt%.  $\text{Na}_2\text{CO}_3$  decahydrate was added in the UPS1 in the solid form. After the formation of an upper and lower phase which we will call UPS2 (upper phase step 2) and LPS2 (lower phase step 2) respectively, these were separated, and composition and volume repartition were determined. The values are shown in Figure 99. The polymer is to be found for more than 99% in the upper phase. By increasing the  $\text{Na}_2\text{CO}_3$  (wt%) used for the ABS

formation the amount of Cr(VI), Na(I) and  $\text{SO}_4^{2-}$  in the polymer phase increases (from 2 to 10 wt%). The volume of the polymer phase decreases (from 61 to 56 vol%) as the amount (wt%) of carbonate increases.

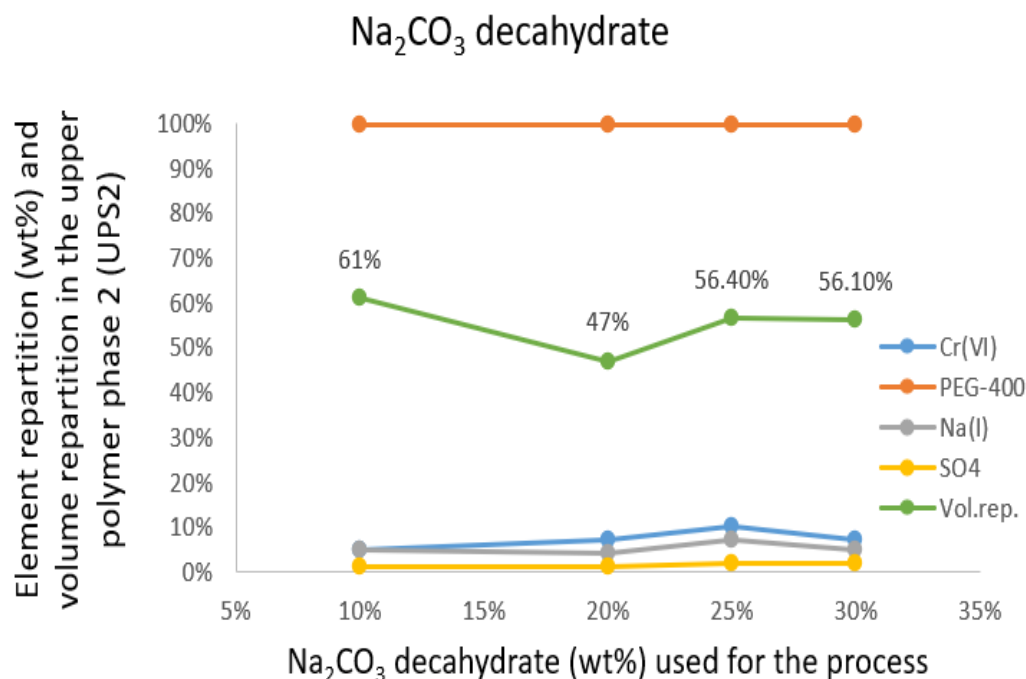


Figure 99. Extraction efficiency of  $\text{Na}_2\text{CO}_3$  decahydrate in the UPS1.

The decahydrate salt was then replaced by its anhydrous equivalent, as it was supposed that the  $\text{Na}_2\text{CO}_3$  decahydrate might dilute UPS1 too much.

For this analysis 4 samples were prepared at 80 °C, with  $\text{Na}_2\text{CO}_3$  anhydrous / UPS1 repartition of 5 / 95 - 6 / 94 - 7 / 93 - 8 / 92 wt% respectively.  $\text{Na}_2\text{CO}_3$  anhydrous has been added in the form of a solid and is soluble in UPS1 up to a maximum of 8 wt%. Figure 100 shows the repartition values of the Cr(VI), Na(I),  $\text{SO}_4^{2-}$  and PEG-400 and the volume repartition of the upper phase. The polymer is more than 99 wt% distributed in the upper phase. As the amount (wt%) of anhydrous  $\text{Na}_2\text{CO}_3$  used to obtain the biphasic system increased, the values of  $\text{SO}_4^{2-}$  and Na(I) remained low and constant in the polymer phase (around 5 wt%  $\text{SO}_4^{2-}$  and about 15 wt% Na(I)). Cr(VI) shows a slight decrease in the polymer phase as the amount (wt%) of anhydrous  $\text{Na}_2\text{CO}_3$  used increases. Finally, the volume repartition decreased (from 88 to 80 vol%) in the upper phase as the amount (wt%) of  $\text{Na}_2\text{CO}_3$  anhydrous increased.

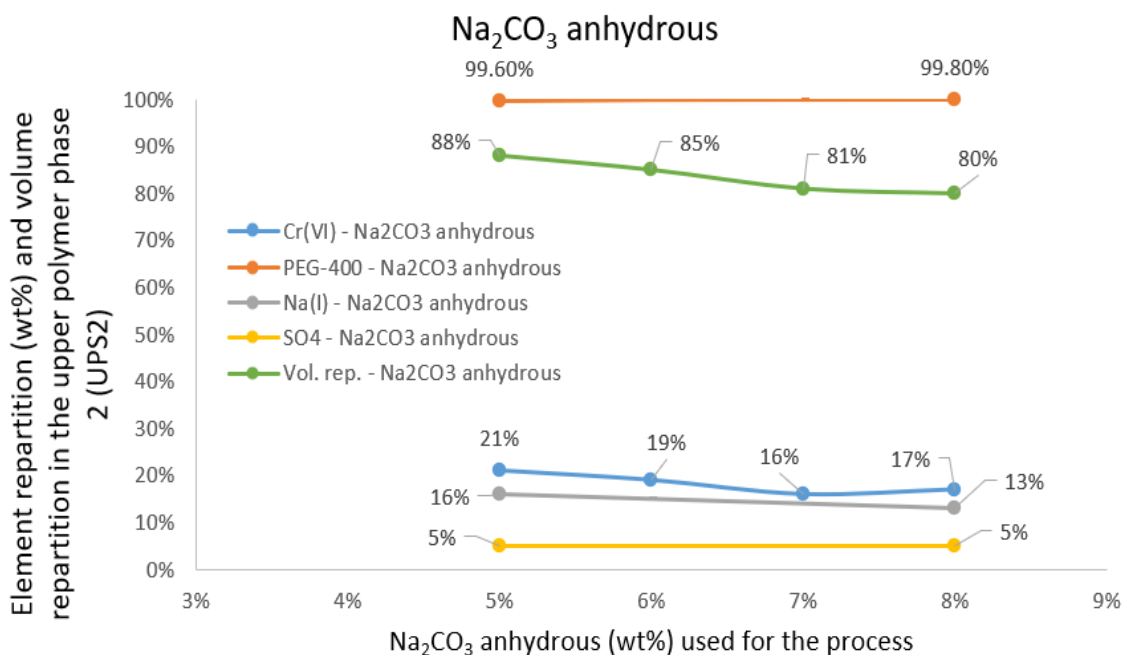


Figure 100. Extraction efficiency of Na<sub>2</sub>CO<sub>3</sub> anhydrous in the UPS1.

The main drawback we encountered with anhydrous salt was that we had to investigate a very limited concentration range (5 wt% to 8 wt%) for the salt since at higher quantities (wt%) the salt reached its solubility limit. It was decided to investigate the behavior of this system when a constant amount of salt (5wt%) was used and different amounts of water were added. For this purpose, 3 samples consisting of Na<sub>2</sub>CO<sub>3</sub> anhydrous / (added water) / UPS1 of 5 / 5 / 90 - 5 / 10 / 85 and 5 / 20 / 75 wt% respectively were prepared. Again, as can be seen in the Figure 102, more than 99 wt% of the polymer is in the upper phase, Na(I) is not particularly affected (about 20 wt%) by the increased addition of water to the system, the volume of the upper phase decreases slightly (from 85 to 81 vol%) with the addition of water, while both sulfate and Cr(VI) increase their concentration (wt%) in the polymer phase when 5 to 20 wt% of water is added.

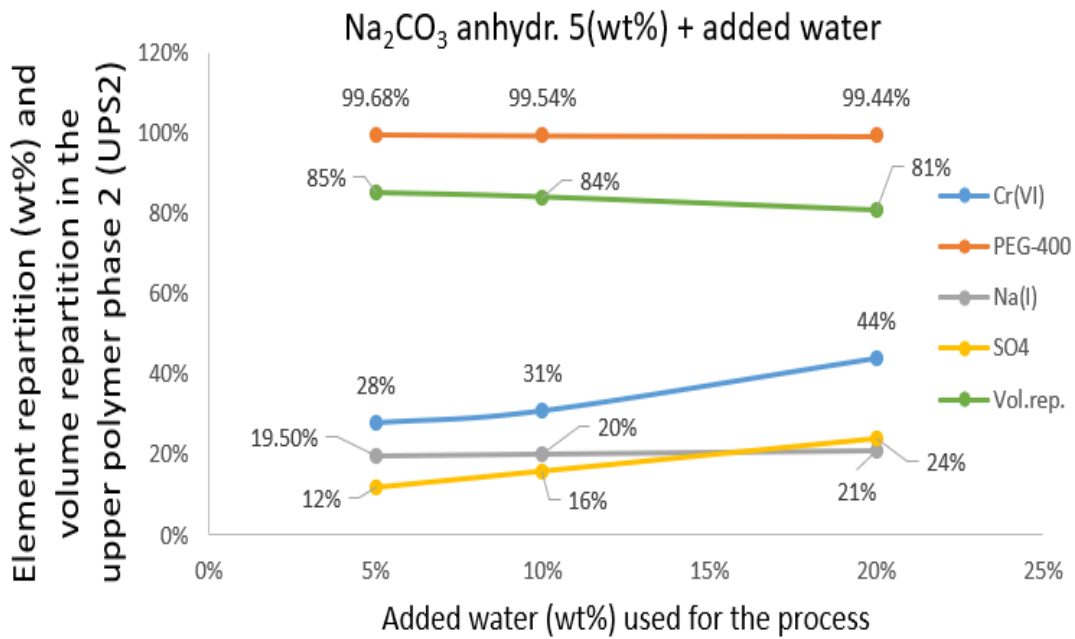


Figure 102. Extraction efficiency of Na<sub>2</sub>CO<sub>3</sub> anhydrous plus added water in the UPS1

Further tests were carried out considering anhydrous Na<sub>2</sub>SO<sub>4</sub> and with the addition of water. anhydrous Na<sub>2</sub>SO<sub>4</sub> was tested to see if it could fulfil the same role as anhydrous Na<sub>2</sub>CO<sub>3</sub>, i.e. to separate Cr(VI) from PEG-400. The results are shown in Figure 101, in both graphs are shown the values of Cr(VI) and volume repartition when on the left it is used the anhydrous salt, while on the right by using a constant concentration of anhydrous Na<sub>2</sub>SO<sub>4</sub> of 5 wt% and adding 10 or 20 wt% water to the system. In the first graph on the left, by increasing the amount (wt%) of anhydrous salt used to obtain the biphasic system, Cr(VI) slightly increases in the upper polymer phase (from 93 to 96 wt%) and the partition volume decreases (from 84 to 75 wt%). On the other hand, taking a constant amount of anhydrous salt (5 wt%) and adding 10 or 20 wt% of water (Figure 101 on the right), both the Cr(VI) and the partition volume do not show great variations (about 92-93 wt% of Cr(VI) remains in the polymer phase and the volume of the phase shown in the figure is about 84-86 vol%).

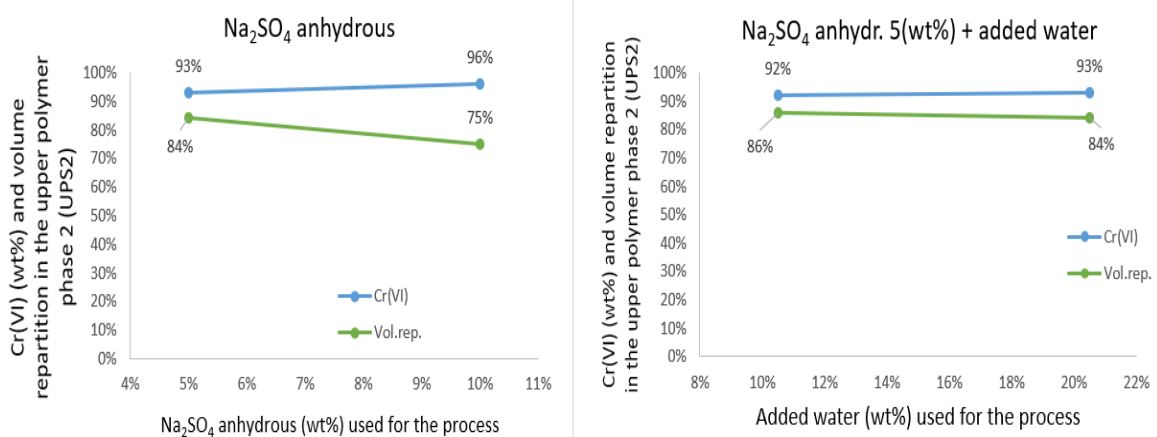


Figure 101. (left) Extraction efficiency using Na<sub>2</sub>SO<sub>4</sub> anhydrous on the UPS1. (right) Extraction efficiency using 5wt% of Na<sub>2</sub>SO<sub>4</sub> anhydrous and added water on the UPS1.

Summarizing the results obtained for the two types of salts investigated, sodium sulfate can firstly be excluded, as it does not play the intended role. Whereas for an optimum process, Na<sub>2</sub>CO<sub>3</sub> anhydrous salt at 7 wt% could be used, since in this way, the salt is soluble in UPS1, and the polymer phase obtained contains a low amount of Cr(VI) (16 wt%). Water should not be added to the system as this would reduce the amount of Cr(VI) extracted.

From an economic point of view, Na<sub>2</sub>CO<sub>3</sub> is one of the most affordable salts available (2 euros/kg). As for the new species that the salt introduces into the system, no various highly polluting halogens are involved, but the formation of carbonates must be taken into account. To further reduce the number of species introduced into the system, NaOH 30% was tested instead of Na<sub>2</sub>CO<sub>3</sub>.

The NaOH was taken from an aqueous solution NaOH 30%. Eight samples were prepared at 80°C, with a different distribution in NaOH 30% / UPS1 of 2 / 98 - 2.5 / 97.5 - 5 / 95 - 7.5 / 92.5 - 10 / 90 - 15 / 85 - 20 / 80 - 25 / 75 (wt%) respectively. As shown in Figure 103, by increasing the NaOH 30% concentration used for the extraction, the amount of Cr(VI) (wt%) and the volume (vol%) of the polymeric phase decrease.

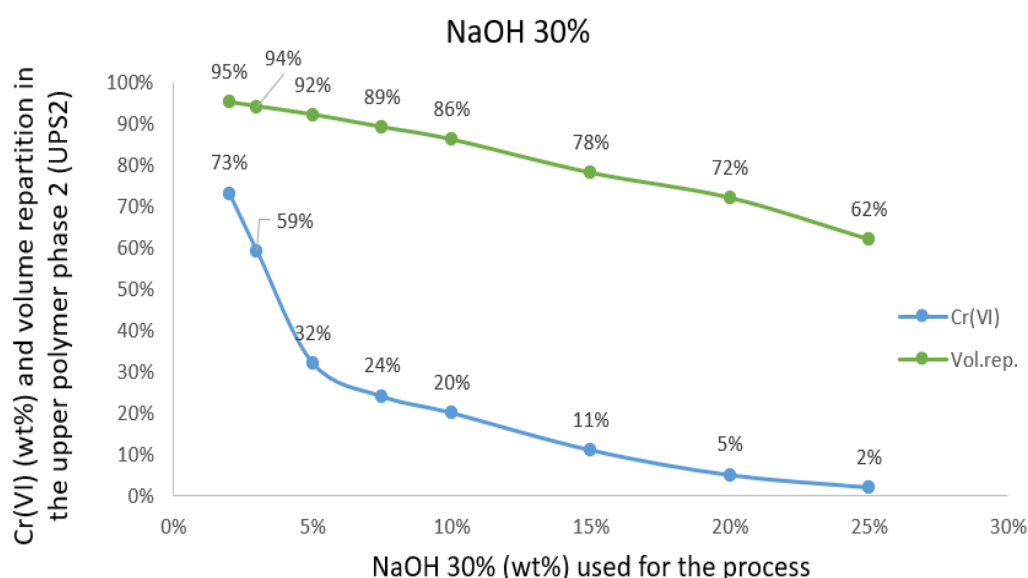


Figure 103. Extraction efficiency of NaOH 30% mixed with UPS1 at 80 °C.

When we consider the efficiency of anhydrous Na<sub>2</sub>CO<sub>3</sub> and NaOH 30% examined so far, the lower phase obtained with the soda is easier to process since it tends to remain liquid without crystallization even at room temperature, which is not the case for the lower phase obtained with Na<sub>2</sub>CO<sub>3</sub>. In addition, by using 25 wt% NaOH it is possible to remove from PEG-400 approximately 98 (wt%) Cr(VI).

A common disadvantage between NaOH 30% and anhydrous Na<sub>2</sub>CO<sub>3</sub> was the formation of a third phase when working with larger volumes (250mL) (Figure 104).

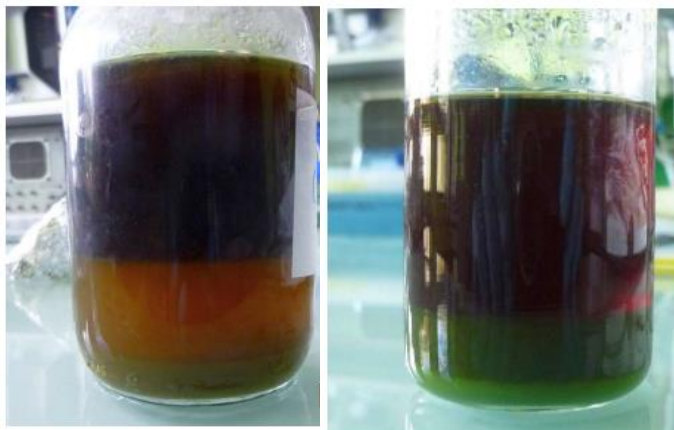


Figure 104. Triphasic systems when considering  $\text{Na}_2\text{CO}_3$  (left) and  $\text{NaOH}$  30% (right) to separate the chromium from the polymer in big volume.

The LPS2 (lower phase step 2), coming from the mixing of 7wt% anhydrous  $\text{Na}_2\text{CO}_3$  and UPS1 in small volume and containing mainly chromium separated from PEG-400, was then treated to precipitate  $\text{Cr(III)}$ .

The first series of tests consists of mixing LPS2 and  $\text{NaHSO}_3$  at different distributions 25 / 75 – 30 / 70 – 35 / 65 wt% respectively. The solution was left under stirring for 30 minutes at  $80^\circ\text{C}$  (samples A – B – C Figure 105). After centrifugation of the samples for 30 minutes at  $25^\circ\text{C}$ , the concentration of chromium remaining in the liquid phase was measured with AAS. The amount of chromium decreased in solution as the amount of  $\text{NaHSO}_3$  used for precipitation increased. Almost 40 wt% of  $\text{Cr(III)}$  precipitates in solid phase, while the rest stays in the liquid phase. This can be explained by the fact that bisulfite has the role of reducing  $\text{Cr(VI)}$  to  $\text{Cr(III)}$ , and its addition also changes the pH of the solution, which, by becoming more basic, allows  $\text{Cr(III)}$  to precipitate, probably in the form of  $\text{Cr(OH)}_3$ .

The second test was carried out by considering a variation of pH (sample D - Figure 105). The initial pH of the LPS2 solution is 10. The acidification of chromium solution (from LPS2) made by using always  $\text{NaHSO}_3$ , allows a good reduction of chromium from  $\text{Cr(VI)}$  to  $\text{Cr(III)}$ . However, the pH after the addition of a large amount of bisulfite had reached a range between 4-5. In order to reduce all the  $\text{Cr(VI)}$  to  $\text{Cr(III)}$  it was necessary to further decrease the pH; for this purpose,  $\text{H}_2\text{SO}_4$  was added to reach  $\text{pH}=2$ . The last step consists of precipitating the  $\text{Cr(III)}$  by using  $\text{NaOH}$  30%, (until  $\text{pH}=8$ ). The sample D in Figure 105 is composed by 70 wt% LPS2, 10 wt%  $\text{NaOH}$ , 5wt%  $\text{NaHSO}_3$  and 15 wt%  $\text{H}_2\text{SO}_4$ . The amount of chromium precipitated was around 30 wt%.

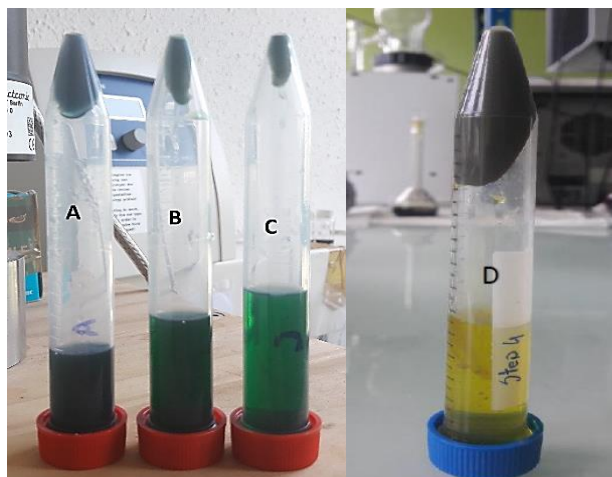


Figure 105. (left) Samples prepared for chromium precipitation through  $\text{NaHSO}_3$ . A) 25 wt%, B) 30 wt% and C) 35 wt% of sodium bisulfate used. (right) Second test for chromium precipitation.

Although the separation efficiencies of Cr(VI) using anhydrous  $\text{Na}_2\text{CO}_3$  or NaOH 30% were very high, the two compounds showed the disadvantage of crystallising at large volumes, and the proposed precipitation protocol also did not show a good recovery efficiency of Cr(III) (30 wt%). For these reasons, another method was proposed to separate and precipitate Cr(III) at the same time.

### 3.2. UPS1 treatment by light

During the treatment of ABS obtained by mixing the polymer and the sulfate bath, a particular behavior was noticed. In particular, when the UPS1 samples were left under the exposure of sunlight, the solutions became darker after few days and a precipitate was formed. The three samples are presented in Figure 106; they differ in their exposure time to light. The first sample on the left corresponds to the UPS1 immediately after the phase separation, the second corresponds to the UPS1 exposed to sunlight for 12 hours and the third one is the UPS1 that was left for more than 24 hours in contact with the sunlight.



Figure 106. UPS1 exposed to the sunlight. Starting from the left to the right: UPS1 as soon as was separated from the lower phase in the step 1, UPS1 exposed to the sunlight for 12 hours, UPS1 exposed to the sunlight for 24 hours.

This behavior was also described by Lie et al.<sup>92</sup> and Sun and co-workers<sup>16</sup> in their studies (State of the Art - section 4.2.1.). An attempt was made to understand whether the same mechanism proposed by

Lie *et al.* and Sun *et al.* could also be applied to these systems. Table 20 summarizes the working parameters and species used by Lie and collaborators and Sun *et al.* and those that concern to this investigation.

Working conditions	Lie <i>et al.</i>	Sun <i>et al.</i>	This work
Polymer used	400 < PEG < 10.000	PEG-2000	PEG-400
Metal investigated	Cr(VI)	Cr(VI)	Cr(VI)
Metal speciation	$\text{HCrO}_4^-$	$\text{HCrO}_4^-$	$\text{Cr}_2\text{O}_7^{2-}$
Concentration of metals	Cr = 0.02 mol/L	Cr = 0.02 mol/L	Cr > 0.15 mol/L
Temperature investigated	25 °C	25 °C	80 °C
pH investigated	0.5 - 6	0.5 - 6	3

Table 20. Working parameters proposed by Lie *et al.*, Sun *et al.* and this investigation.

While Lie *et al.* has shown that the light source is necessary for the reaction, Sun and co-workers do not consider any light source during their investigation. These two positions allowed us to arrive at a third option, which will be presented in the following lines.

Our investigation of Step 2 for Cr(VI) reduction and precipitation started by understanding the impact of the light source on the UPS1. We had noticed that sunlight could promote the reaction, but this resulted to be very long and challenging to control, so it was decided to irradiate the sample with different light sources. Preliminary tests with the UV spectrometer (Figure 107) also showed that Cr(VI) was reduced to Cr(III) within about seven hours of investigation. No additional light (sunlight or lamp) was directed at the sample. This was an experiment performed in the dark of the UV-vis spectrophotometer, so the only light was from the beam when measuring the sample.

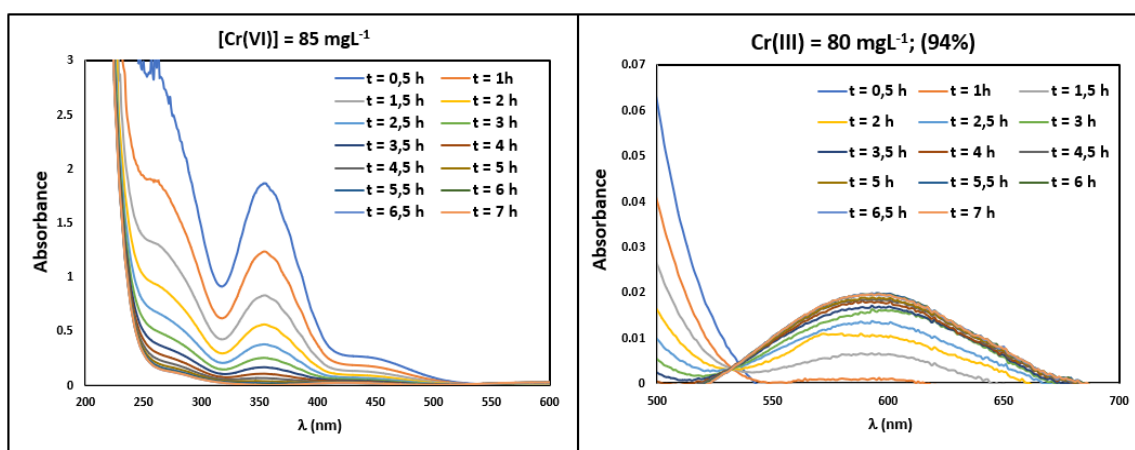


Figure 107. Conversion of Cr(VI) (left) to Cr(III)(right) by UV-visible spectrophotometer. Monophasic solution containing 85 mg/L Cr(VI), 560 g/L PEG-400, pH=2 obtained by the addition of  $\text{H}_2\text{SO}_4$ , working temperature 65 °C.

The light box used for this investigation is showed in Figure 108.



Figure 108. Light box used as UV source for step 2.

The different light sources examined are presented in Figure 109. As can be seen, the different sources have distinct parameters, particularly with regard to their contribution in UV or visible energy.

<i>mesures at 20cm</i>	UV-vis lab scale light box	UV dryer	garland	garland int.	big box neons
brightness in visible (lux)	12 000	< 2000	7 000	30 000	/
total energy (W/m <sup>2</sup> )	12	3	17	35	6
percentage in UV (%)	25%	45%	0%	0%	100%
energy in UV (W/m <sup>2</sup> )	3	2	0	0	6
energy in visible (W/m <sup>2</sup> )	9	2	17	35	0

Figure 109. Characteristics of the various apparatus used for the investigation.

Figure 110 shows the behavior of three samples containing UPS1:

- Grey curve, sample left in the dark.
- Green curve, sample exposed to sunlight.
- Yellow curve, sample exposed to UV light.

The graph in Figure 110 is obtained by measuring the Cr(VI) concentration in solution (UPS1) by using AAS, at different exposure times. The initial metal concentration in UPS1 is approximately 9.5 g/L. First of all, it is important to notice, that the reaction occurs even in the dark, or at least when the light source is very weak. Furthermore, the precipitation of chromium follows the same trend when the sample is in the dark and when it is exposed to sunlight. The slope of the curve is more negative more when the UPS1 sample is irradiated with a UV light source. Indeed, in this case, after about 3.5 hours of experiment, starting from 9.5 g/L, the concentration of Cr(VI) drops to almost 7g/L in the UPS1.

These series of experiments only showed that UV light could help accelerate the reaction to a certain extent. In general, however, the reaction occurs slowly in all three cases.

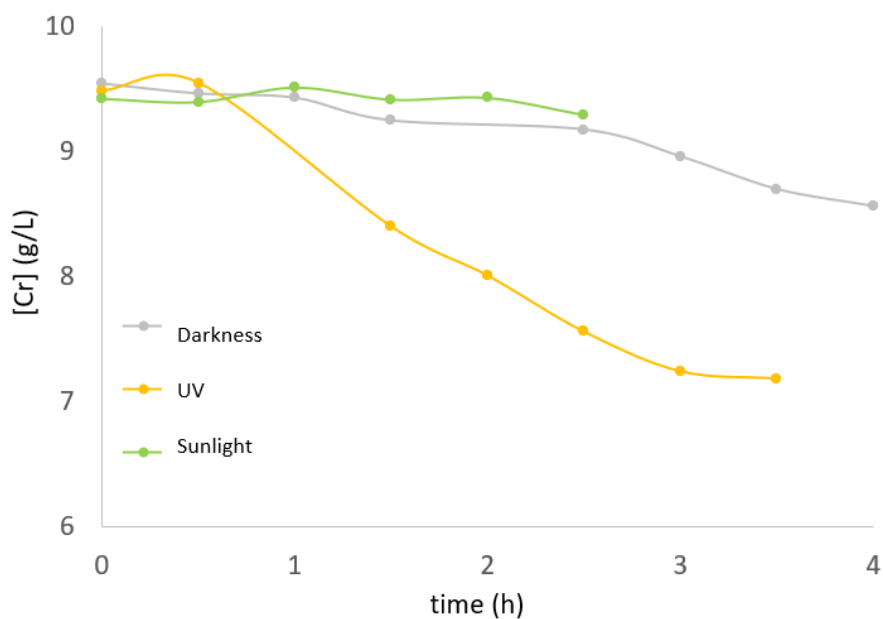


Figure 110. Cr(g/L) precipitation in function of the time at 2 different exposures of the light and at the darkness.

Further analyses were carried out to see which of the pure UV, UV-visible and pure visible sources would be most effective in reducing and precipitating chromium. A set-up consisting of a UV-visible source was used for both the UV-visible light and to obtain a purely visible source, where the UV radiation was blocked through the use of a membrane working as an anti-UV filter. These membranes were placed on top of the crystalliser where UPS1 is contained. The experiment was conducted at 80 °C. In Figure 111 it is possible to see the concentration of Cr(VI), measured by AAS in solution (UPS1), at different exposure times considering different light sources.

In 5 hours of experiment, the following results were obtained:

- using pure UV light, the amount of Cr(VI) in solution decreased from about 8 g/L to 6 g/L.
- using pure visible light, the amount of Cr(VI) in solution decreased from about 7 g/L to 3.5 g/L.
- finally, by using UV-visible light, the amount of Cr(VI) in solution decreased from about 8 g/L to 1 g/L.

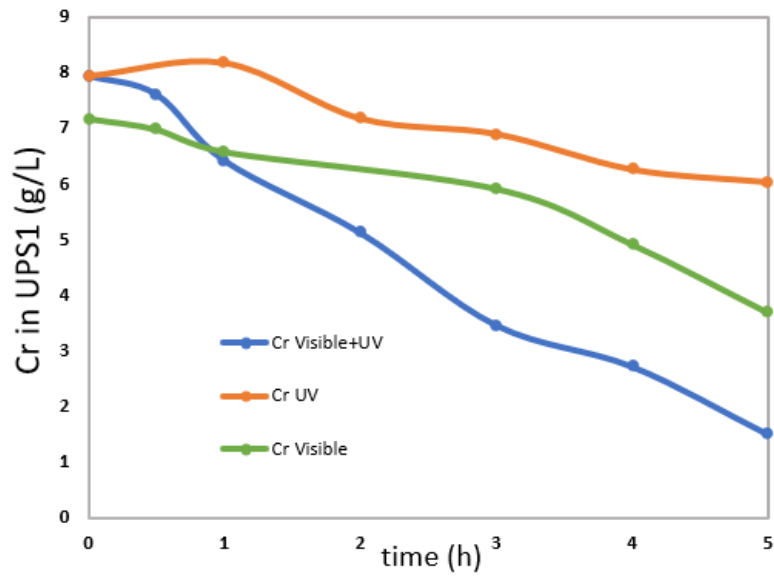


Figure 111. Cr(VI) precipitation in function of the time for three different light source: pure UV, UV-visible and pure visible light.

In order to compare the values in Figure 111, it is necessary to assume that some parameters, such as the intensity of the light source, are considered constant. We can therefore conclude that, UV-visible source is the one that allows to reduce the greatest amount of Cr(VI) in the same investigation time, compared to the other two light sources. However, this experimentation requires more investigation.

Considering the values in Cr recovery using different lamps, a series of tests was carried out to investigate the variation in pH in the UPS1 for the case of the UV-visible light source. Figure 112 shows that chromium concentration decreases from 8 g/L to about 1 g/L during the 5 hours of exposure to the light and at the same time the pH increases from 3 to 10.

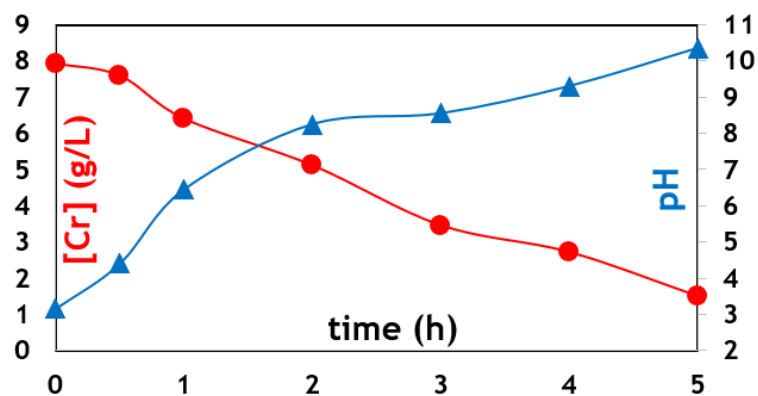
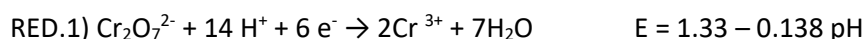
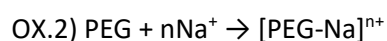


Figure 112. Cr precipitation in function of pH.

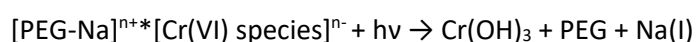
Following the pH change in the solution, it is possible to hypothesize the oxidation-reduction reaction that occurs during the action of light on Cr(VI). We assumed that the acidity of the solution favors the reduction of the dichromate to Cr(III) and this is demonstrated by the following reaction:



The  $\text{Cr}_2\text{O}_7^{2-}$  is considered to be as  $[\text{Cr(VI) species}]^{n-}$ . On the other hand, PEG is oxidized, as was also confirmed by Sun et al. The reaction is presented schematically in the following lines, but as already mentioned, it is considered that radicals are involved.



It is suggested that both Ox.1 and Ox.2 occur in solution, ox.1 is responsible for the hydrogen bonds between the polymer and water while ox.2 is the reaction responsible for the extraction process of Cr(VI). In UPS1 the polymer is to be found linked to the anionic  $[\text{Cr(VI) species}]^{n-}$  in the form of  $[\text{PEG-Na}]^{n+}[\text{Cr(VI)species}]^{n-}$ . Finally, through the use of a light source, the following reaction takes place:



Cr(III) precipitated *in situ* with free  $\text{OH}^-$  in the form of  $\text{Cr(OH)}_3$ . The final solution free most Cr(VI) is dark colored probably due to the low amount of Cr(VI) that still is to be found in polymer phase.

Figure 113 shows a graphical representation of what happens in step 2. At pH=3 the dichromate is bound to  $\text{PEG-Na}^{n+}$ . When UV light is applied and after the first hours of reaction, the pH arrives to 7 and the precipitate begins to form, as the Cr(VI) is reduced to Cr(III), and Cr(III) starts to bind to the low amount of  $\text{OH}^-$  present in solution. The product of the reaction starts to accumulate while the reaction keeps in progress. After 24 hours, all Cr(VI) was reduced to Cr(III). The Cr(III) is now to be found in  $\text{Cr(OH)}_3$  form. In this last step, moreover, the  $\text{Na}^+$  no longer having dichromate with which to achieve neutrality, will be in equilibrium with  $\text{OH}^-$ .

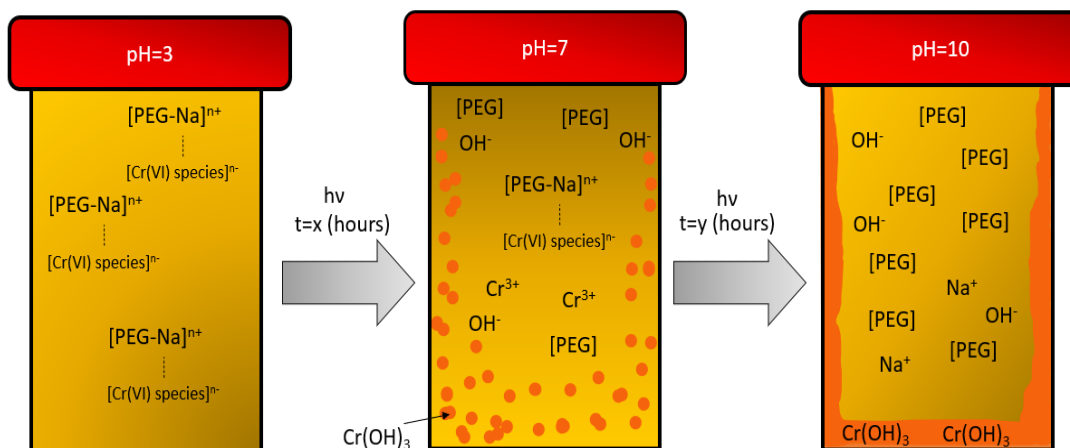


Figure 113. Graphical explanation of the mechanism of reaction of step 2.

Several other parameters were investigated by my colleague Jérôme Cognard for the implementation of step 2. These include namely the contact surface between UPS1 and the light source. It was confirmed that the greater the surface of exposure to light, the faster was the chromium hydroxide precipitation. The test was carried out by first working in a beaker with an exposure surface of 12 cm<sup>2</sup> and then with a crystallizer with an exposure surface of 95 cm<sup>2</sup>. Another parameter investigated was the number of filtrations to be carried out during step 2. The purpose was to prevent light absorption by the Cr(OH)<sub>3</sub> and so to promote the reaction process. It was finally demonstrated that by increasing the number of filtrations during step 2, the kinetics of reduction of chromium also increased. In detail, we will see in the next section how filtration was performed in order to recover the precipitated solid phase.

### 3.3. Recovery and characterization of solid precipitation

For small volumes, filtration of the liquid phase of UPS1, after light irradiation, was initially performed manually using a Büchner funnel. Subsequently, for large volumes, a filter press was used. The filter press consists of a stack of textile filter sheets, resistant to the injection of solid/liquid mixtures at high pressure and has been primarily used to provide simultaneously a large treatment flow rate and good efficiency. The advantages of using a filter press include efficiency, reliability, robustness and low maintenance. Figure 114 shows the filter press used in this investigation.

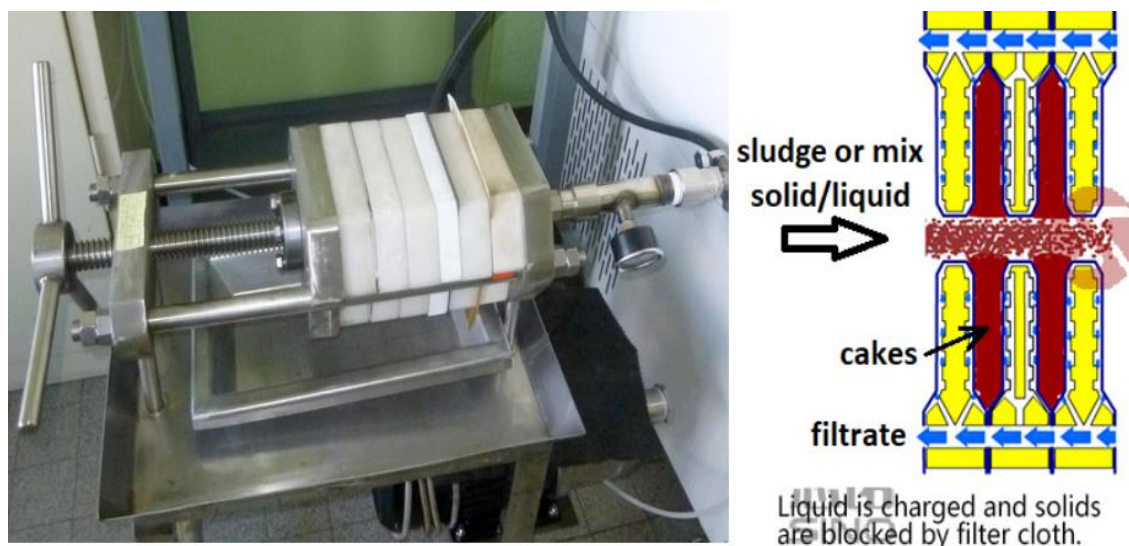


Figure 114. Filter press used for large volumes (left). Schematic working mechanism of the filter press (right)

Three different types of textile filter sheets were tested in different pore size:  $10\mu\text{m}$ ,  $25\mu\text{m}$  and  $46\mu\text{m}$ . After measuring the fluid pressure as a function of time, of the three membranes (Figure 115), the  $25\mu\text{m}$  membrane was chosen as it represented a good compromise between not too high pressure and the entrapment of medium-sized solids.

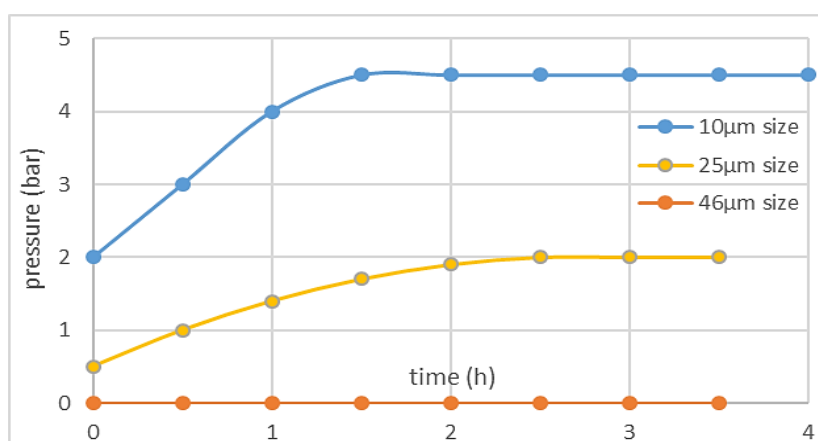


Figure 115. Pressure of the fluid in function of time of experiments for three different membranes used in the filter press.

The mechanism of action of the filter press equipped with a pump involves the injection of the solution exposed to the light source into the filter press, which retains the solid precipitate and sends the liquid solution back to the irradiation setup. This cycle ends when all the Cr(VI) has been reduced to Cr(III) and the solid precipitate is completely retained in the filter press sheets. Four different types of precipitate are shown in Figure 116:

- solid obtained from small volumes of sample exposed to UV-visible light
- solid obtained considering large volumes of sample exposed to UV-visible light
- solid obtained considering small volumes of sample exposed to pure visible light

D) solid obtained considering large volumes of sample exposed to pure visible light

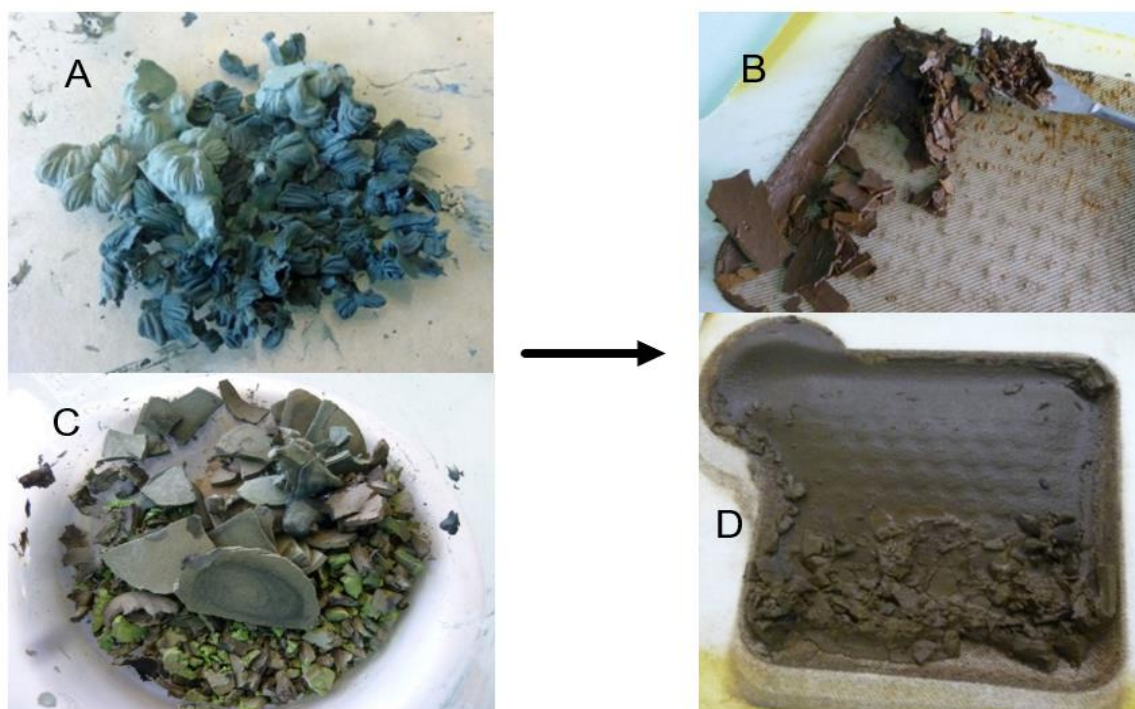


Figure 116. Four different types of precipitates obtained during the investigation.

Subsequently, the solid was collected, washed with water, dried, and finally characterized by different techniques for qualitative and quantitative investigation.

In Figure 117, it is possible to see the wide scan (or survey spectrum) on the top and the high-resolution spectrum on the bottom of the X-ray photoelectron spectroscopy (XPS) analysis for the solid (C in Figure 116). Thanks to XPS, it was possible to determine which types of elements (qualitative approach) are present in the precipitate (top graph in Figure 117) and their molecular structure (bottom graph in Figure 117). As the spectra indicate (top of the Figure 117), the major component of the solid is chromium. Due to the characteristic peaks of chromium (Cr2p) and oxygen (O1s) in the spectrum, and after bibliographic investigation<sup>153,154,155</sup>, it can be deduced that these peaks are obtained from the contribution of the following species:  $\text{Cr}(\text{OH})_3$ ,  $\text{CrO}_3$  and  $\text{Cr}_2\text{O}_3$ .

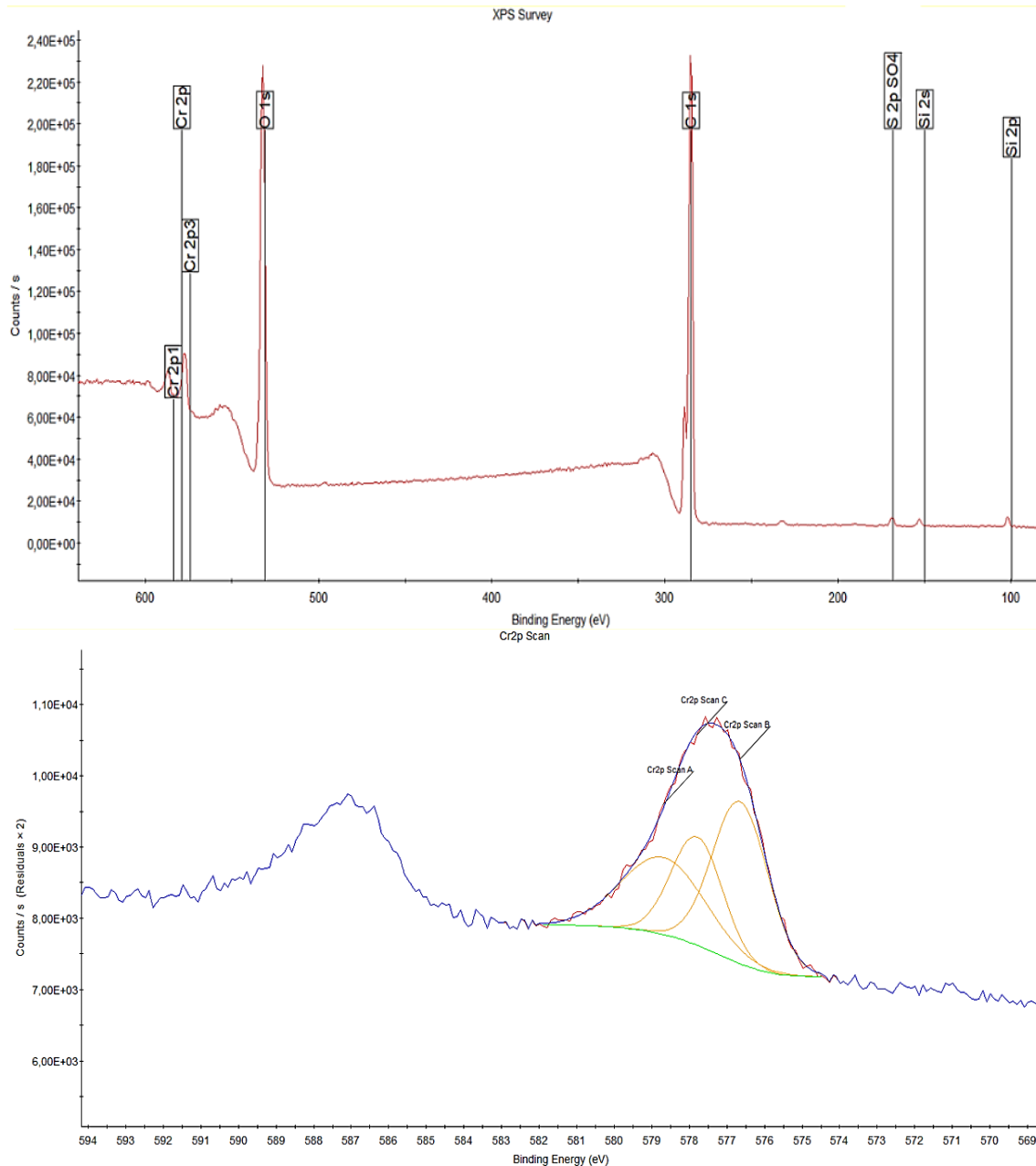


Figure 117. Wide scan or survey spectrum at the top and the high-resolution spectrum at the bottom of XPS analysis of the solid precipitation at the end of the step 2. Starting from the first band on the left to the third on the right there are  $\text{Cr}(\text{OH})_3$ ,  $\text{CrO}_3$  and  $\text{Cr}_2\text{O}_3$ .

The presence of chromium in the solid precipitate was further confirmed qualitatively by Energy Dispersive X-Ray Analysis (EDX). In fact, the 3 spectra in Figure 119 show predominantly the presence of chromium. The main difference between the 2 spectra is the washing procedure applied to the the solid. From bottom to top spectrum the solid was rinsed several times with water until the characteristic S peak disappeared.

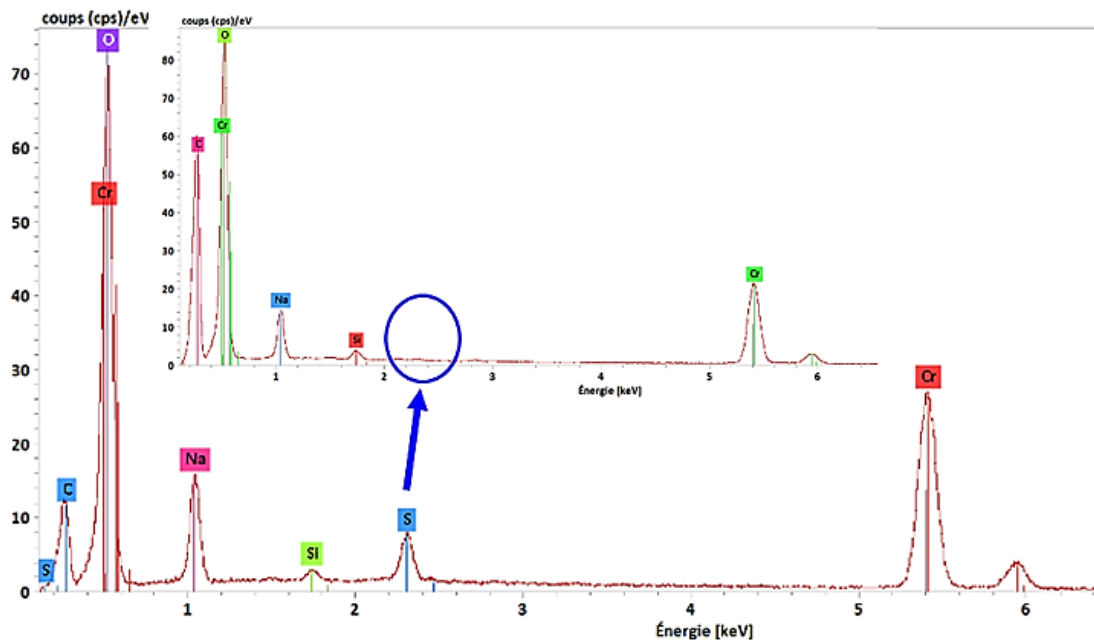


Figure 119. EDX spectrum for solid sample C in Figure 116. The main peaks in the spectra are characterized by the Cr, O, Na, C, Si and S. The blue arrow and the corresponding circle of the same color indicate the position of the sulfate.

Finally, the last qualitative analysis on sample C in Figure 116 was performed with X-Ray diffraction (XRD). The spectrum in red in Figure 118 shows the characteristic peaks of sodium sulfate, before washing the solid. The spectrum in blue corresponds to the same solid after washing. No peak for sodium sulfate appears in the latter case. No further crystal structures were noted in the solid. XRD is suitable for the detection of crystalline structures, and the absence of peaks in the blue band indicates that the compounds in the solid are in an amorphous state. The Snapshot in Figure 118 was obtained by Scanning Electron Microscopy (SEM) for the unwashed solid sample, and represents sodium sulfate.

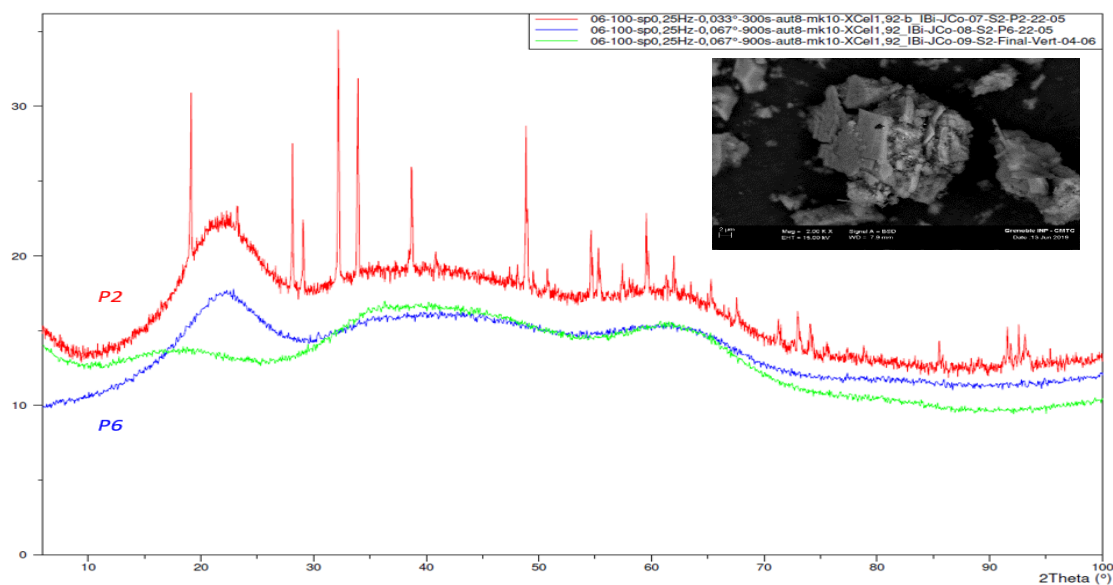


Figure 118. XRD and SEM for solid sample C in Figure 116.

### 3.4. The sort of solid precipitate and liquid phase step 2

The water-washing procedure was thus a crucial step for the quality of the final product, in fact, the precipitated chromium can be now treated by pyrometallurgy as it contains a low quantity of S. The liquid phase obtained from step 2 contains mostly polymer and water, and this will be sent to the next step of the process (Figure 120).

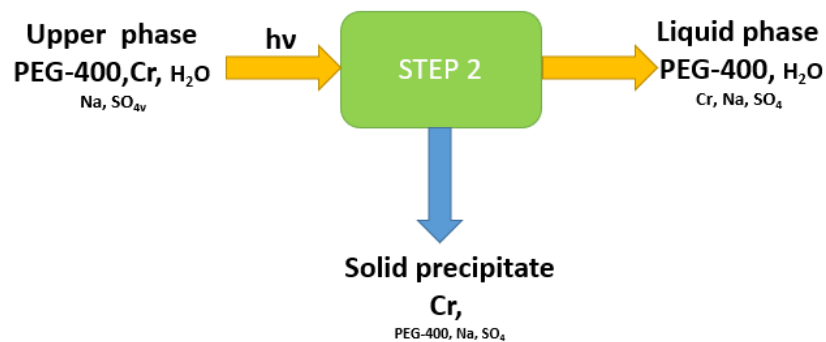


Figure 120. Step 2 of the process.

### 4. Step 3: PEG-400 recovery for further extraction cycles

The liquid phase containing mostly PEG-400 and water arrives at step 3 of the process, which concerns the dehydration of the polymer. This step allows the polymer to be concentrated and reused. When the polymer is regenerated and used for further extraction cycles, it must contain a minimum or zero amount of water, as this would change the working condition of extraction in the sulfate bath. A significant increase of water in the polymer in each extraction cycle would result in the disappearance of the biphasic system.

#### 4.1. Distillation process

Distillation has been proposed as a method of dehydration of PEG-400. The apparatus used is a common distillation column as shown in Figure 121.



*Figure 121. Step 3 - Distillation process proposed in this work (700g of polymer treated).*

Before starting the distillation process, TGA was carried out on the liquid phase step 2 (Figure 122). TGA allows the measurement of the weight of a substance while it is being heated with controlled temperature increase. As the temperature increases, the weight of the substance decreases. In our case, we can consider the liquid phase from step 2 as a matrix solution containing several substances. Therefore, the TGA graph will show as many stairs of the curve as there are substances in solution, that disappear at different temperatures. We will refer to evaporation temperature for volatiles compounds, degradation temperature for polymers and incineration temperature for metals, to indicate the temperature at which the compound starts to lose weight. In our specific case, in Figure 122 starting from the left, we find the first step of the curve, which corresponds to the most volatile elements present in the liquid phase. It has been assumed that the most volatile element in the liquid phase coming from step 2 is water so that step refers to the loss of water when the temperature in the apparatus increases. The TGA allows to make a quantitative analysis so it can be confirmed that between 50 °C and 100 °C of investigation, about 35% of water from the total weight of the solution has disappeared, that corresponds to almost 95% of the total water. As the temperature increases, the water will be completely removed from the tested sample. At about 200 °C we see a second step appear. From the literature, we know that PEG-400 starts to degrade at temperatures higher than 200 °C. Therefore, we can associate this second step to weight loss of the polymer. The totality of polymer disappears at 350 °C. After 350 °C the last elements (salts and metals) start to decompose.

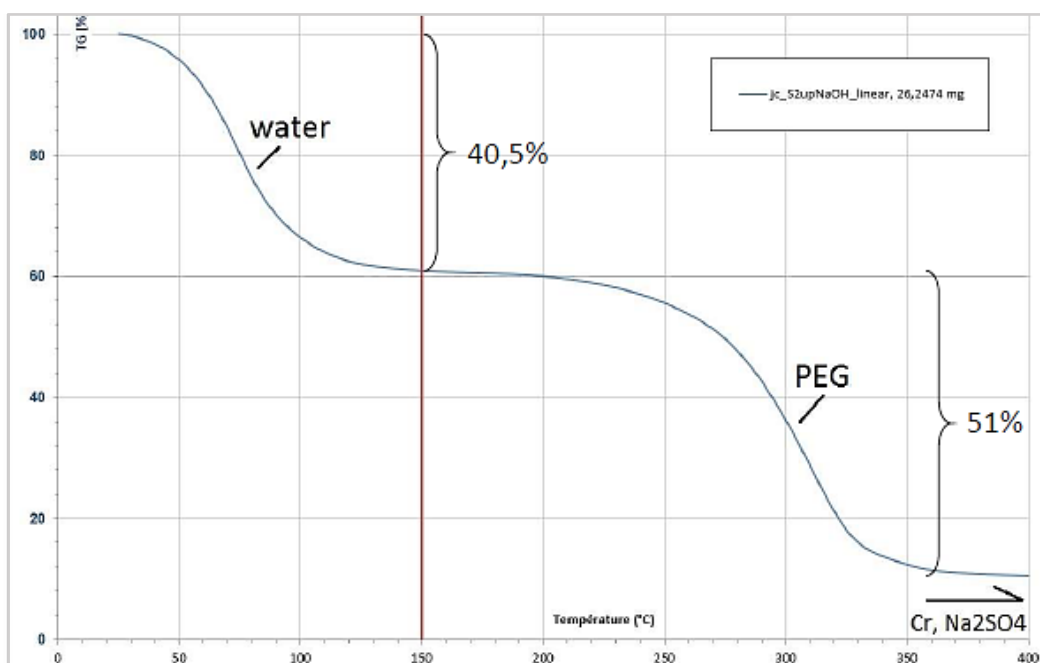


Figure 122. TGA analysis on the liquid phase from step 2.

From the results obtained with the TGA, a temperature between 120 °C and 150 °C was chosen for the distillation process in order to extract as much water as possible and to prevent the PEG-400 from being degraded.

More than 90 wt% of water was thus recovered and analyzed by ICP-MS. The water recovered from the process was highly pure (values shown in Table 21 expressed in  $\mu\text{g/L}$ ). The presence of zinc can be attributed to the instrument.

ICP-MS analyses on the water from distillation step 3 ( $\mu\text{g/L}$ )									
Na	Zn	Ni	Cr	Fe	Cu	Mn	Mo	Ag	Pb
85	20	8	2	2	2	1	0	0	0

Table 21. Metal concentration in  $\mu\text{g/L}$  in water recovered after step 3.

Moreover, the PEG recovered after distillation was analyzed by steric exclusion chromatography (SEC). SEC was used to determine the molecular weight distribution of the polymer. The spectrum is obtained by considering the retention time of the compound as a function of polymer concentration. As can be seen in Figure 123, the pure PEG (in red) and the PEG obtained at the end of the distillation (in blue) gave the same characteristic PEG-400 distribution. The difference in area is due to the presence of water, in fact, the PEG-400 used in the extraction results to be more concentrated.

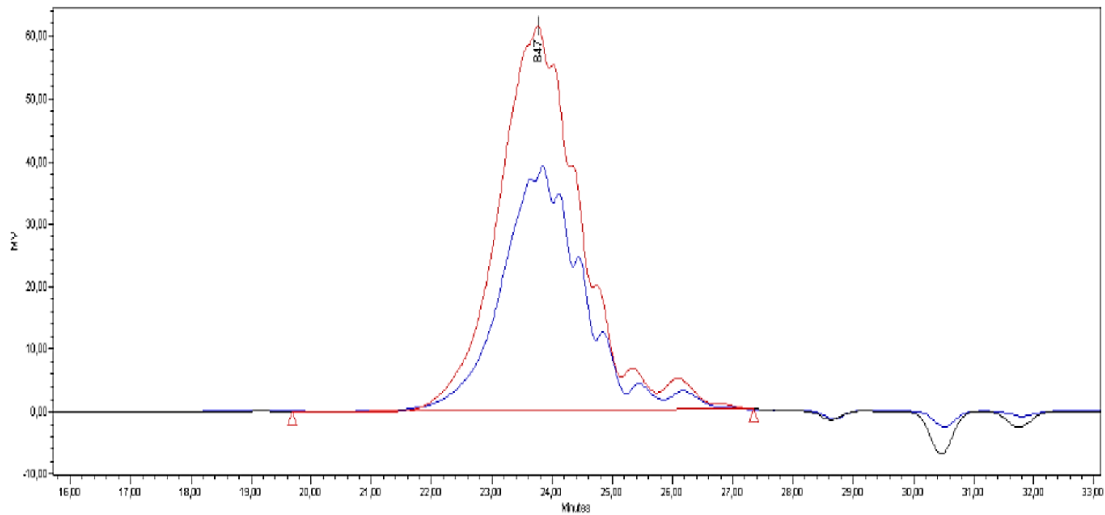


Figure 123. Steric exclusion chromatography spectrum for demonstrating PEG-degradation. Pure PEG in red and PEG after distillation step 3 in blue

We can therefore confirm that the PEG-400 obtained at the end of the process was not degraded, and the black color it exhibits may be due to traces of chromium and other metals (> 1 wt%) present in it.

#### 4.2. Recycled polymer and pure water

A schematic overview of step 3 is presented in Figure 124 where after distillation, PEG-400 continues the process, while pure water can be re-introduced into the sulfate bath for farther pickling processes.

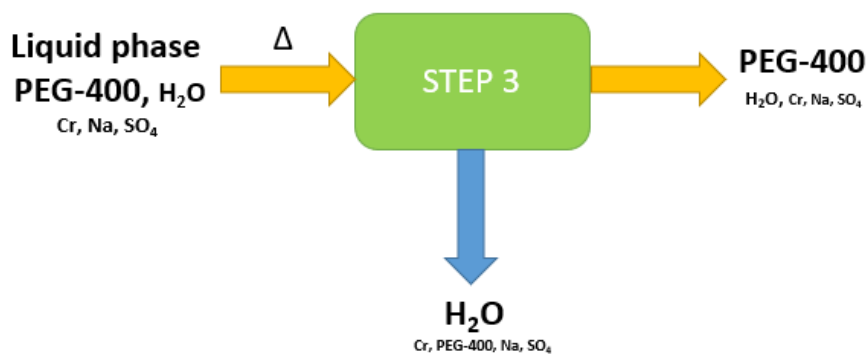


Figure 124. Step 3 of the process.

After being dehydrated the PEG-400 was tested directly on fresh  $\text{Na}_2\text{SO}_4$  bath. The experiment was carried out with the same polymer/sulfate bath partition (40 / 60 wt% respectively) and the same working conditions proposed in step 1 of the process ( $T = 80^\circ\text{C}$ ). The values presented in Figure 125 show that PEG-400 recycled after distillation maintains its high extraction efficiency (93 wt% of Cr(VI) extracted in the polymer phase) and this can be compared to fresh PEG-400 extraction efficiency (96 wt%). In both cases the polymer is 99 wt% in the upper phase. Approximately 6 wt% of Fe(III) and Ni(II)

pass into the polymer phase for both fresh and recycled PEG-400. The volume distribution is approximately the same, 80 vol% of upper phase is obtained when using fresh PEG-400 and 78 vol% of upper phase is obtained when using recycled PEG-400.

This is the last step to close the process loop and in the next section will be presented the process of extracting Cr(VI) from the sulfate bath in a global view.

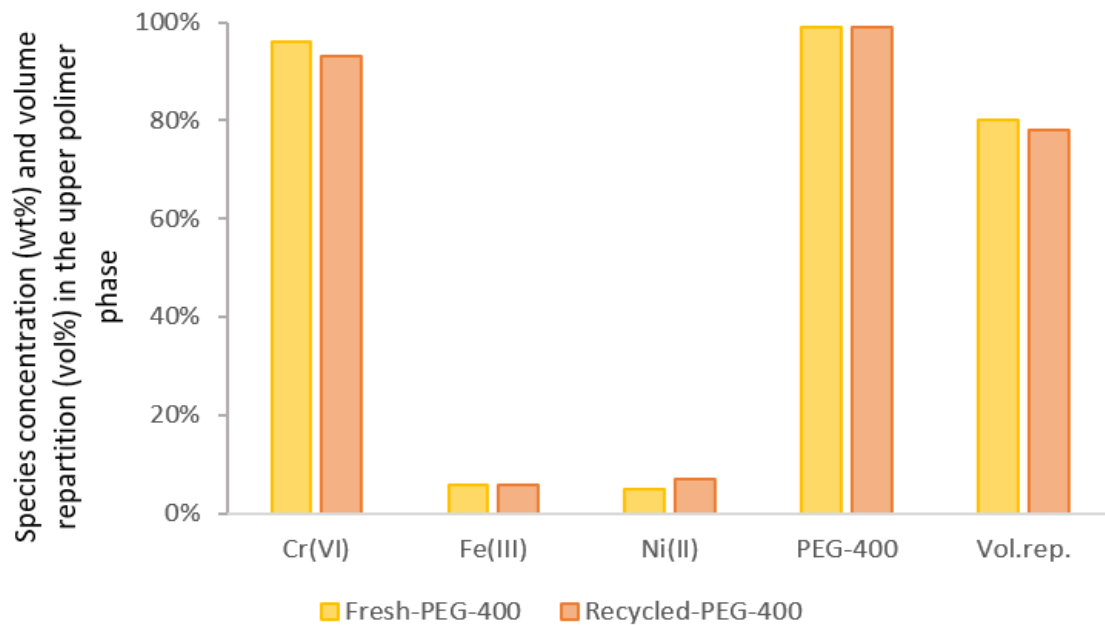


Figure 125. Species concentration (wt%) and volume repartition (vol %) in the upper polymer phase of ABS obtained by using 40 wt% of PEG-400 fresh (yellow) and recycled (orange) at 80 °C.

## 5. Global view of the process loop

Figure 126 outlines the sequence of operations to be carried out for optimal implementation of the process according to the 3 steps described so far in the chapter. The process can be carried-out continuously since the spent pickling liquor (SPL) fraction can be taken directly from the  $\text{Na}_2\text{SO}_4$  pickling bath or from any other container into which it would have been transferred (1). The SPL fraction arrives at the mixing reactor (or a static reactor) (2) where PEG-400 is added in the ratio of 40 / 60 wt% (polymer / SPL respectively) at  $T=80$  °C. The polymer is stored in a dedicated container (3). As soon as the polymer and SPL come into contact, an aqueous biphasic system is obtained, and the two phases end up in a gravity settler (4) where they are separated. At the upper part, we have the polymeric phase, and at the lower part, the non-polymeric phase. The non-polymeric phase can be re-used as a fresh bath in the pickling process, as it contains mostly  $\text{Na}_2\text{SO}_4$ , water and only traces of metals. The polymer phase is brought into contact with the light source (5), and *via* a photochemical reaction the

chromium precipitates under a solid form. The solid part is filtered (6), washed, collected in a tank (7) and finally sent for pyrometallurgical treatment, since the precipitate has low S content. The liquid part, on the other hand, which contains mostly PEG-400 and water, is distilled (8), resulting in a dehydrated PEG-400, which can be accumulated in the container (3) and reused for further extraction processes, and water, which is reinjected into the sulfate bath.

The overall process cycle was submitted (patent number CN102531139B 20131106) in September 2019.

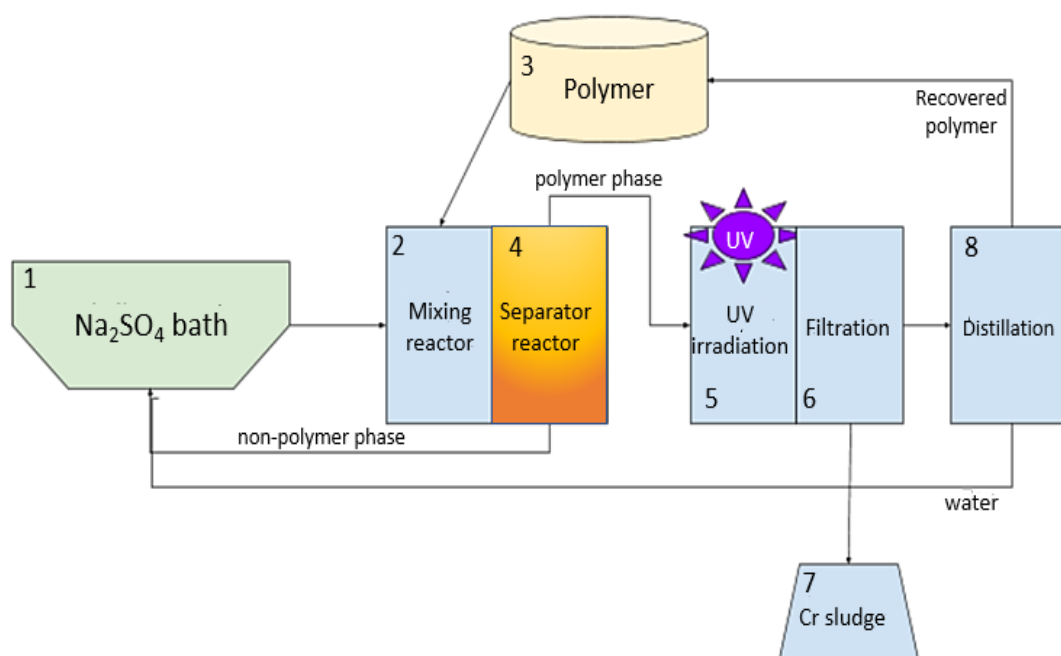


Figure 126. Schema of the patent for Cr(VI) recovery from  $\text{Na}_2\text{SO}_4$  bath.

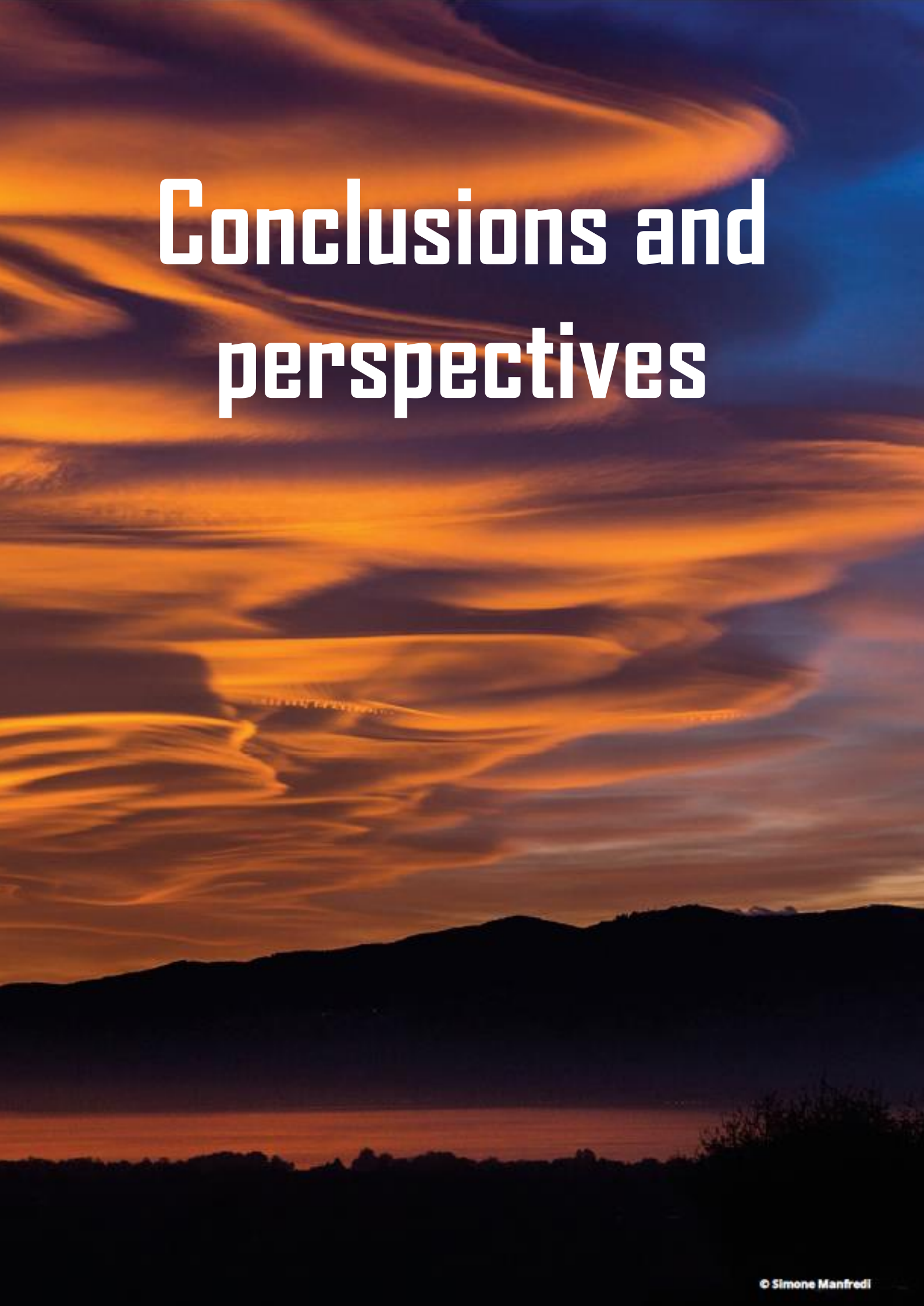
## 6. Conclusions

The process presented in this chapter is being continuously implemented, especially in terms of industrial design. Step 1 saw a more detailed analysis and development on both at micro and macro-industrial scale and the reproducibility of small and larger volumes (10 kg) was confirmed. Step 2 showed that, in about 5 hours of exposure to visible light, it was possible to reduce the concentration of Cr(VI) from 8 g/L to 1 g/L in the polymeric solution. However, this step needs more investigation to study the different light sources and to understand the photochemical reaction that takes place. Finally, in step 3, 90 wt% of PEG-400 was recovered after distillation; the resulting water was very pure (traces of metals in ppm) and the recovered PEG-400 was used for one further extraction process obtaining 93 wt% of chromium extracted (efficiency value for fresh PEG-400 is between 89 and 94 wt%).

From an industrial point of view, the patent needs to see more implementation, and these are some of the next steps for industrializing the process:

- Scaling up the process loop in an industrial pilot to check the stability of the whole process on long running duration and also to verify the yield and consumption of the reagents.
- Meeting with external partners: engineering companies, suppliers, local authorities if required (legal or environmental organization).
- Definition of precise specifications for each equipment and each instrumentation (process sensors).
- Order, receive and set up equipment and instrumentation.
- Connection of all networks to existing site utilities (electricity, water, air, waste instrumentation etc.).
- Initiation of industrial tests for validation of equipment, instrumentation, and control of process efficiency.
- Written procedures and safety rules for workers / QHSE service.
- Organize logistics (timing, workers, supply of inputs, transport, storage, output management etc.)
- Planning of maintenance work

# Conclusions and perspectives





The urgency to act on the environmental sustainability challenge outlined in the latest European Environment Agency report (SOER 2020) has shifted the focus of most European companies to the new environmental regulations to be implemented by 2050.

Aperam, world leader in the production and treatment of stainless steel, has taken up the challenge by committing itself to reduce its environmental impact with the aim of being carbon neutral by the target date. To achieve this, the company has launched projects on topics such as air quality, waste reduction and reuse, CO<sub>2</sub> reduction and recycling.

It is precisely in the area of recycling that the thesis project was developed, in particular, it focused on the regeneration of acidic baths used for the pickling process. The pickling process consists of a metal treatment used to remove superficial impurities from the surface of a product. In particular, two different baths were considered during the investigation, the UGCO and Na<sub>2</sub>SO<sub>4</sub> baths. The process currently used by the company to treat used baths is based on the neutralization of acidity and precipitation of metals by using various chemicals. However, although neutralization is very efficient and interesting from an economic point of view, it causes problems with waste disposal. The alternative that has been proposed is the aqueous biphasic systems (ABS). ABS is a liquid-liquid extraction system, consisting of two biphasic inducers and water. In recent years, these systems have been shown to be particularly advantageous in metal extraction processes. Furthermore, the ABS are graphically represented by a phase diagram and the corresponding binodal curves. The company's demands on the two baths involved the cleaning of the baths of most dissolved metals, except for those essential for the efficiency of the pickling process.

For the UGCO bath, two ABS were investigated, one consisting of the ionic liquid [P<sub>44414</sub>]Cl and UGCO bath and the other of the polymer PEG-600 and UGCO bath. From an extraction selectivity point of view, the two systems did not meet the company's request, since both preferentially extracted only Fe, which is essential for the pickling process and must therefore remain in the bath.

However, what made these systems very interesting was the behavior that certain metals exhibited. To better understand this behavior and the phase repartition mechanisms that occurred in each ABS, single-metal systems mimicking UGCO bath conditions were investigated.

For the systems with the ionic liquid and only Ni (or Cr), the binodal curves obtained were similar to most of those found in the literature. However, the binodal curve had an uncommon shape, referred to in this manuscript as an "onion shape", when the system with ionic liquid, HCl and Fe was considered. The proposed extraction mechanism is that of ion exchange, between the parts that constitute the ionic liquid (anion and cation) and the species present in solution.

As regards the polymer system, no ABS has been demonstrated to date when PEG / HCl / H<sub>2</sub>O are mixed under certain conditions. Surprisingly, when Fe(III) was added to the system, it provided ABS. The new system consisting of PEG-600 / [Fe(III) + HCl] / H<sub>2</sub>O has proven to be unique in the ABS field. The proposed extraction mechanism in this case involves the extraction of the FeCl<sub>4</sub><sup>-</sup>, which binds with the oxygens in the polymer chain. Moreover, during the various tests carried out, the company's attention also shifted to other metals such as Cu(II) present in the UGCO bath, which at high concentrations causes issues with the pickling process. It was shown in the manuscript that the ionic liquid was able to extract about 50 wt% of Cu(II) from the UGCO bath. This study, however, requires further investigation. In addition, the issue of bath dehydration, one of the company's initial requests on the UGCO bath, was not considered, as the focus was mainly on the repartition of metals in ABS systems.

For the Na<sub>2</sub>SO<sub>4</sub> bath, the ABS mainly investigated was that consisting of PEG-400/ Na<sub>2</sub>SO<sub>4</sub> bath. The ABS was integrated into the general process of extracting Cr(VI) from the sulfate bath, and this consists of 3 main steps.

As far as step 1 is concerned, that consists of the ABS used to extract Cr from the Na<sub>2</sub>SO<sub>4</sub> bath, this was reproduced on a micro-pilot scale of 10 kg, through the use of a mixer-settler, or static mixer followed by a settler. The use of the static mixer brought better results than the mixer, considering the efficiency of extraction, the space it takes up in the installation, the ease of use and maintenance and the price of the equipment. Step 1 was also performed with synthetic single metal solutions. The systems investigated showed that, by varying the type of metal, its concentration or the working temperature, the obtained binodal curves were identical, unlike the systems in HCl medium for the UGCO bath where the systems were very sensitive to such variations. The stability of ABS in the sulfate medium makes these systems very advantageous from an industrial point of view. The extraction selectivity of PEG-400 towards Cr is linked to the form in which the metal is in solution. In fact, after a careful literature search, it has been shown that oxoanionic structures, such as the dichromate present in the Na<sub>2</sub>SO<sub>4</sub> bath, are the ones preferably extracted by (?)the polymer, and the latter will act as a crown ether.

In step 2 the separation of the chromium from the polymer phase accelerated by the presence of a light source occurred. However, in the manuscript, it was proven that the separation takes place also in dark conditions. Various types of light sources have been tested, but it is not yet certain whether the presence of UV light part in the source can promote or not the photochemical process.

Step 3 of the process involved the regeneration of the polymer and its re-use in the extraction process. The regeneration of the polymer consists of its dehydration through a distillation column in order to remove the polymer of the water absorbed during the process. The presence of water would in fact

dilute the sulfate bath and could prevent the formation of further ABS when the polymer is used for subsequent extraction cycles. The regenerated polymer was used only once to determine its extraction efficiency and was found to have the same efficiency as the fresh polymer. Further cycles of regeneration need to be investigated to determine how many times the PEG can be used.

The process of extracting Cr(VI) from the sulfate bath was successfully submitted in September 2019. To this day, it is being implemented continuously, especially in terms of industrial design. In fact, there is a need to scale up the process loop in an industrial pilot to check the stability of the whole process on long running duration and to verify the yield and consumption of the reagents.

In this work, ABS have been shown to be effective in meeting new requirements in terms of recycling and ecological processes. Moreover, the possibility of using specific biphasic inducers to replace the organic solvents required in the extraction process makes these systems even more environmentally friendly. It was also shown that it is possible to treat concentrated metal solutions under acidic conditions (AcABS), which makes these systems promising for various industrial applications, such as treatment of industrial wastes. Although the use of ABS for industrial applications still requires extensive investigation, especially with regard to the choice of biphasic inducers and their extraction mechanism for certain metal species, it is safe to say that the results obtained in the research carried out during the three years of my PHD allow me to recognize ABS as a good substitute for conventional extraction processes using organic solvents for the species investigated.



## Annex

### 1. HCl media and UGCO bath

#### 1.1. Free chloride in the UGCO bath

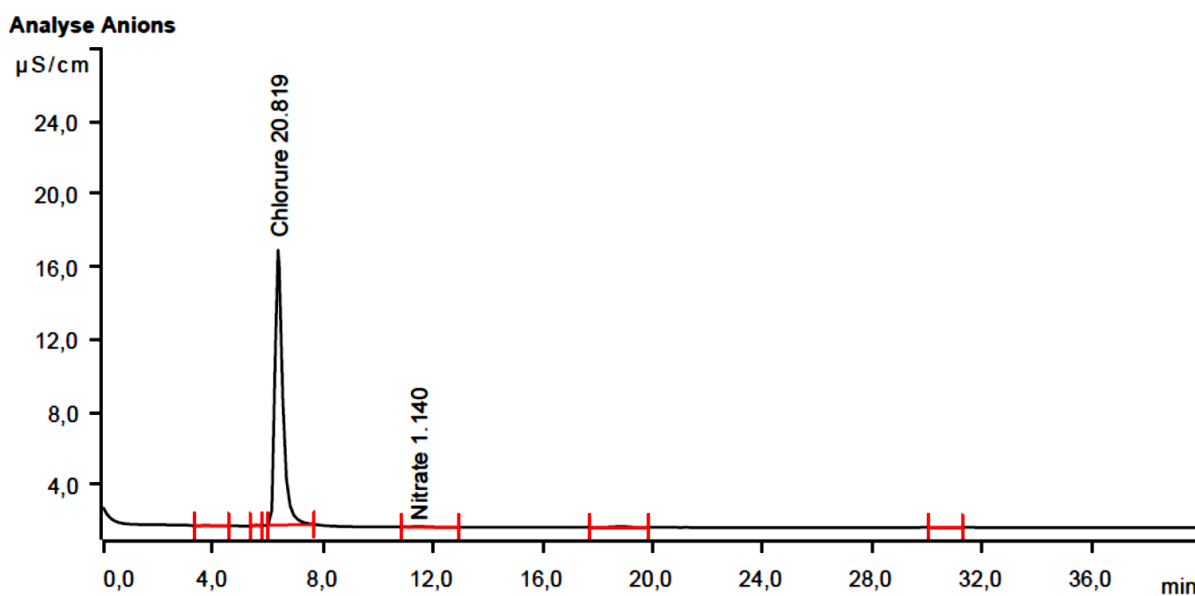


Figure 127. Cl<sup>-</sup> free determination through Ion Chromatography for the UGCO bath investigation. The value is given in mg/L

#### 1.2. PPG investigation on the UGCO bath – Victor Matia Fernandes Master's project

The student Victro Maia Fernandes conducted a study on the extraction efficiency of PPG-425 in the UGCO bath. Three samples were prepared by mixing 20/80, 30/70 and 40/60 wt% of polymer/ bath respectively. After obtaining the corresponding ABS, the upper and lower phase of the systems were analyzed. Figure 2 shows the composition of the upper polymer phases of the various systems. Only Fe(III) passes into the polymer phase between 30 and 40 wt% while Cr(III) and Ni(II) both remain in the bath. The volume of the upper phase increases as the amount of polymer used for extraction increases.

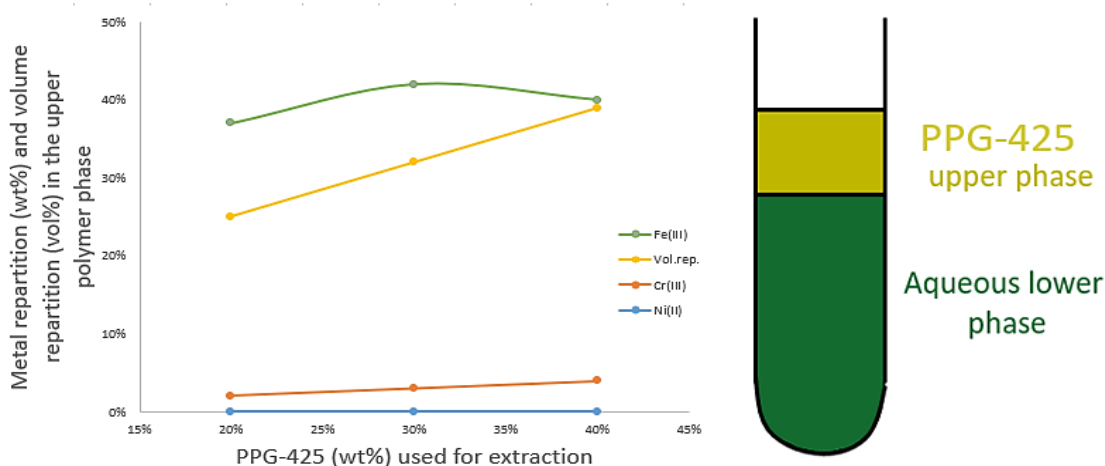


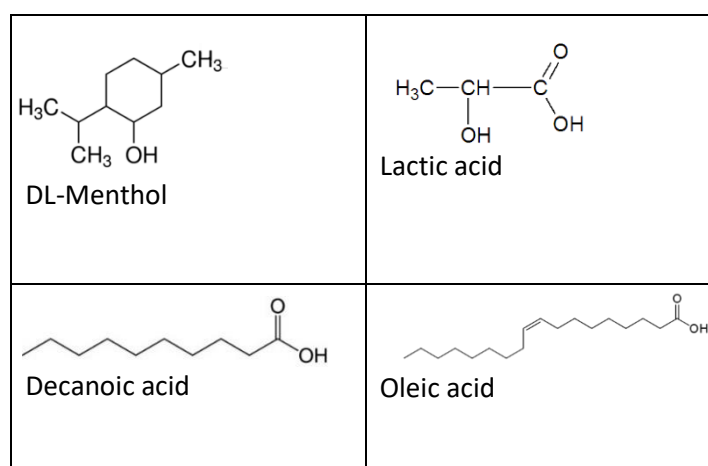
Figure 128. Metal repartitions and volume repartition for different systems composed of PPG-425 / UGCO bath.

### 1.3. DES investigation on the UGCO bath – Patricia Folio Master’s project

The priorities of the UGCO bath have changed over the years, afterwards it became interesting for the company to extract Cu(II) in order to reuse it for the production of other stainless steel. The investigation conducted by the Master student Patricia Folio was aimed at obtaining ABS using deep eutectic solvents (DES). DES are mixtures of two components mainly a quaternary ammonium halide salt and a hydrogen bond donor such as amines, alcohols or acids which form a low eutectic melt. Three different groups of DES were used as biphasic inducers: green DES, phosphorus-based DES, and ammonium chloride-based DES.

#### “Green” DESs

The different combinations of molecules presented in Table 22 resulted in the green DESs.



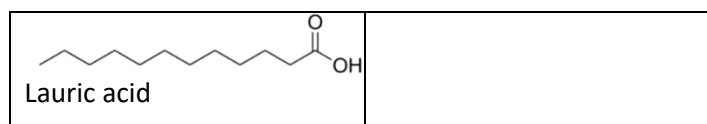


Table 22. List of “green” DES used for liquid-liquid extraction.

As shown in Figure 129, Most of the green DESs considered in the investigation extract mainly Fe, except for Lactic acid: DL-Menthol (1:2), which can extract also a part of all the other metallic ions. The Lactic acid is a shorter carbon chain than other organic acids and contains two hydroxyl groups. It has been shown that increasing the number of OH groups in the molecule the “extraction activity” of these molecules increases. Almost 40% of Fe is extracted using Lactic acid (2 OH groups) and less than 25% of Fe is extracted using molecules with just 1 OH group. By increasing the length of the acid chain, the extraction of Fe decreases (same molar ratio 2:1). Moreover, by increasing the molar ratio of DL-Menthol, Fe extraction increases. In Lactic acid: DL-Menthol (1:2), Ni and Cr are characterized by the same extraction efficiency (5-7%), Cu is extracted at 20% and Fe at 40%. In general, Fe is always extracted.

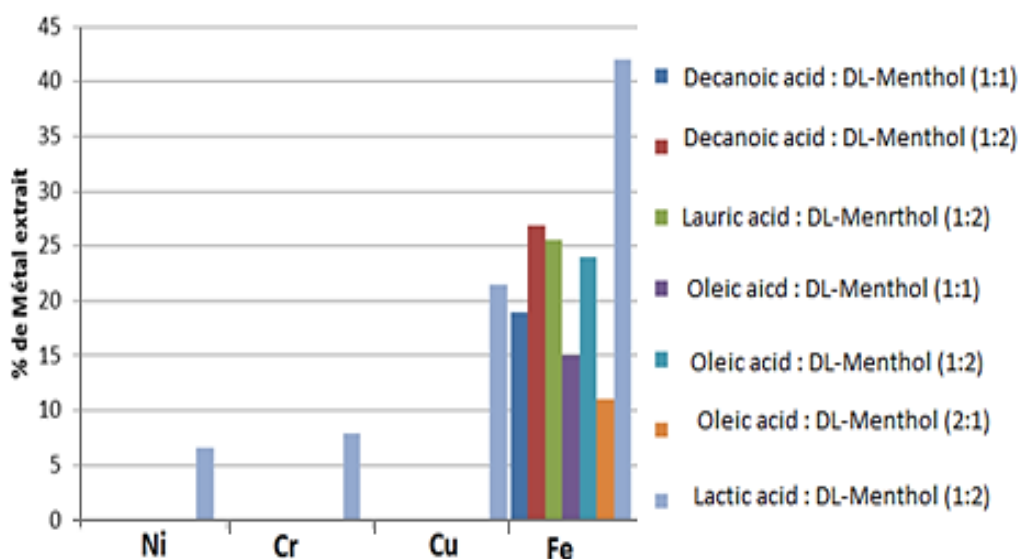


Figure 129. Metallic ions extraction with “green” DES from Table 9.

### Phosphorus based DES

The second group of DESs investigated are Cyanex 923<sup>®</sup> (Figure 130) and Tri-hexyl tetradecyl phosphonium chloride + Decanoic acid (Figure 131).

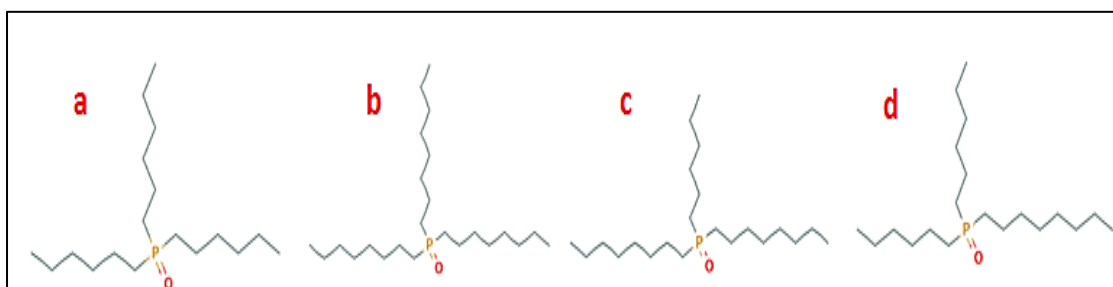


Figure 130. Cyanex 923<sup>®</sup>, mixture of trihexyl phosphine oxide (a), trioctyl phosphine oxide (b), dioctylhexyl phosphine oxide (c) and dihexyloctyl phosphine oxide (HBA).

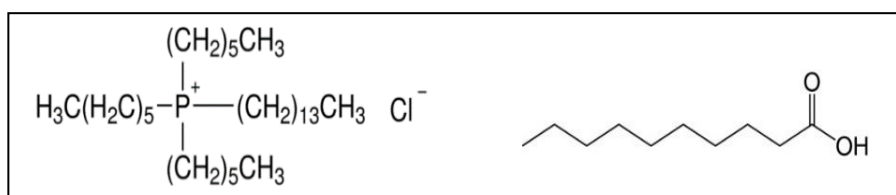


Figure 131. Trihexyl tetradecyl phosphonium chloride+ Decanoic acid.

As shown in Figure 132, by increasing the molar ratio of [P<sub>66614</sub>] Cl, Fe extraction increases (from 62% to 75%). By using Cyanex, almost the same extraction value in Fe and Cu is obtained compared with other DES. Moreover, by using the IL instead to DL-Menthol, the IL prefers the extraction of Fe (the DL-Menthol extracts around 20-25% of Fe and 0% of Cu while the [P<sub>66614</sub>] Cl extracts around 60% of Fe and almost 100% of Cu).

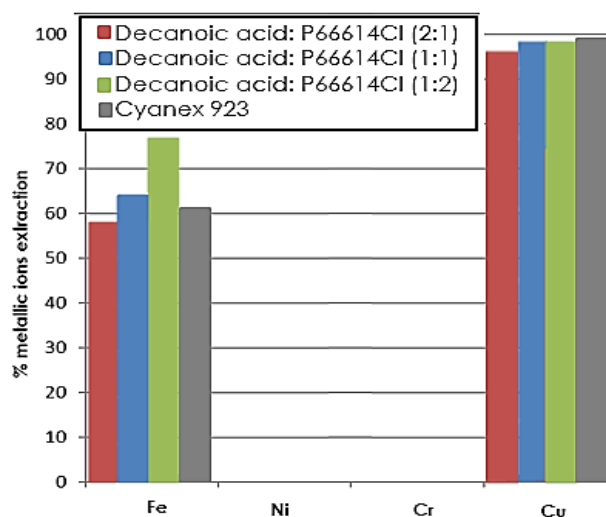


Figure 132. Metallic ions extraction for phosphorus-based DES.

## Ammonium chloride-based DES

From Figure 7 to Figure 9 is shown the extraction efficiency of different ammonium chloride based DESs.

DES composed of Tetra-heptyl ammonium chloride + oleic acid (2:1) has a low extraction efficiency for the metals considered (green - Figure 133). Testing DES composed of Tetra-heptyl ammonium chloride + decanoic acid (or lauric acid) gives the same extraction efficiency, so it can be said that increasing the carbon chain length of the acid part from 10 to 12 there is no significant change, and it is difficult to see a trend (blue and red - Figure 133).

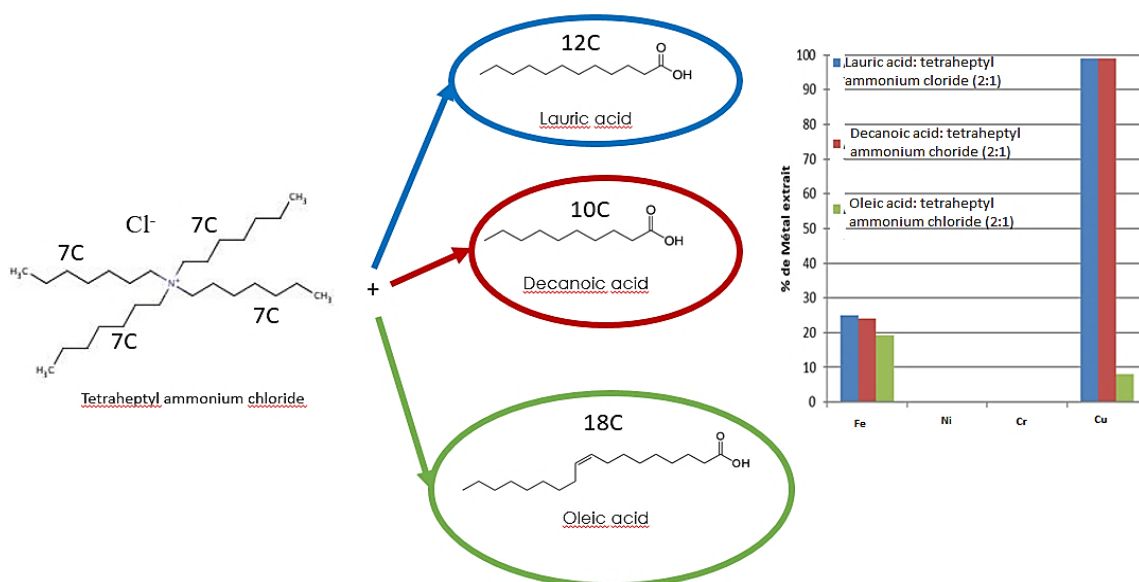


Figure 133. Extraction efficiency for ammonium chloride-based DES composed of Tetra-heptyl ammonium chloride with: (blue) Lauric acid (2:1), (red) Decanoic acid (2:1), (green) Oleic acid (2:1).

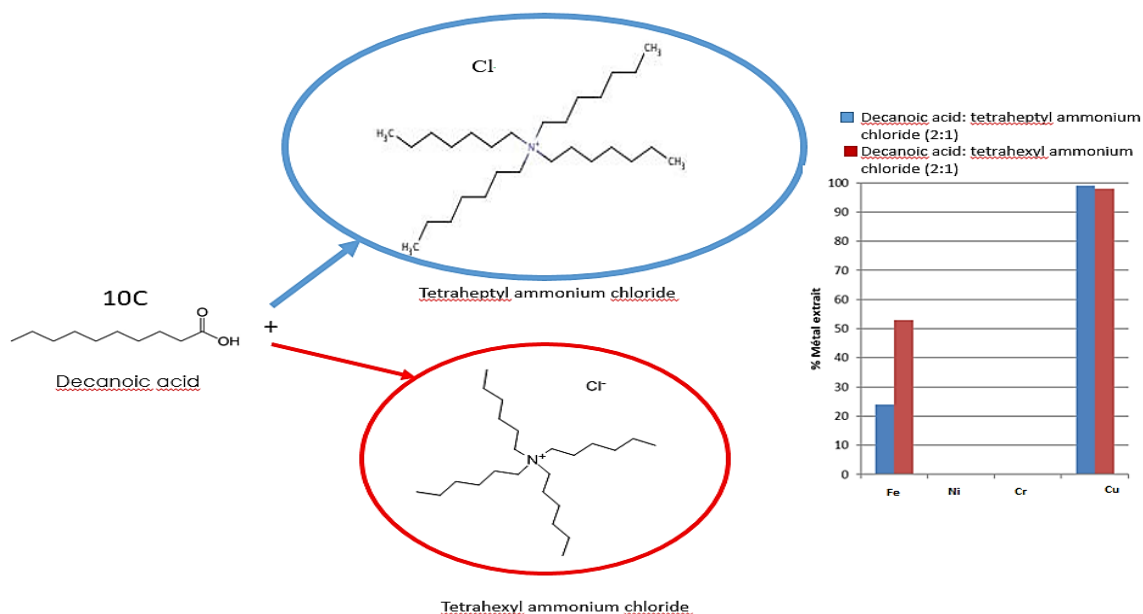


Figure 134. Extraction efficiency for ammonium chloride-based DES composed of Decanoic acid with: (blue) Tetra-heptyl ammonium chloride (2:1) and (red) Tetra-hexyl ammonium chloride (2:1).

The efficiency of DES composed of Tetra-heptyl ammonium chloride + decanoic acid (2:1) (blues - Figure 134) was compared to that of DES composed of Tetra-hexyl ammonium chloride + decanoic acid (2:1) (red - Figure 134). The extraction efficiency of Cu was found to be the same, while decreasing the length of the alkyl chains in the quaternary ammonium chloride salt (from heptyl to hexyl) the extraction efficiency of iron doubled.

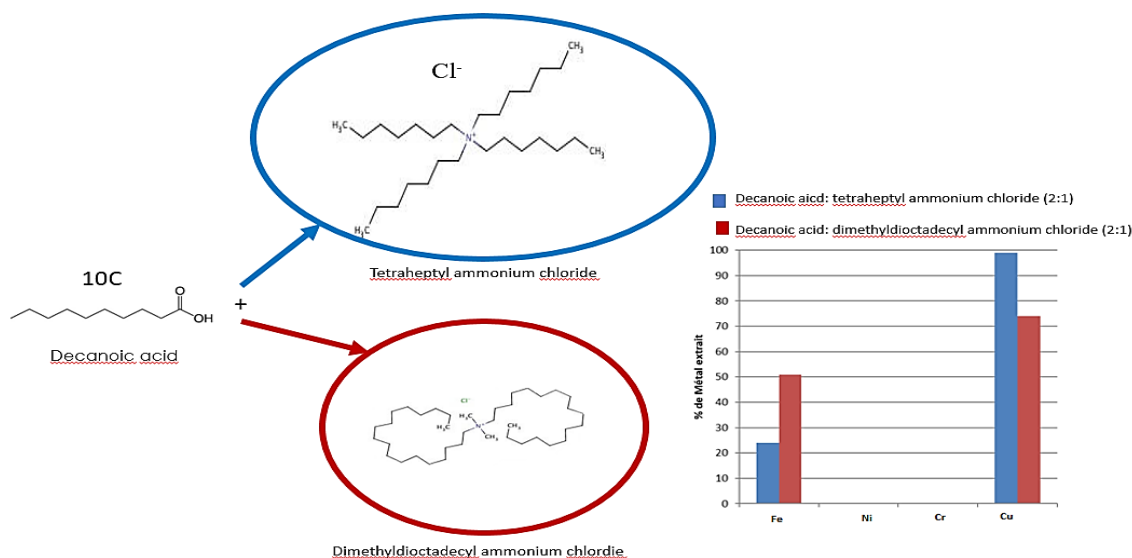


Figure 135. Extraction efficiency for ammonium chloride-based DES composed of Decanoic acid with: (blue) Tetra-heptyl ammonium chloride (2:1) and (red) Dimethyl dioctadecyl ammonium chloride (2:1).

DES composed of Tetra-heptyl ammonium chloride + decanoic acid (2:1) was then compared to DES composed of Dimethyl dioctadecyl ammonium chloride + decanoic acid (2:1) (Figure 135). It was found that by switching from a linear to a longer, curled structure of the alkyl chains in the quaternary salt, the extraction efficiency of Fe increased and that of Cu decreased.

To conclude, the results obtained during the investigation have shown that:

- Green DES (in particular, Lactic acid: DL-Menthol (1:2)) extracts almost 40% Fe(III) and 20% Cu(II).
- DES based on phosphorus (in particular, Decanoic acid: [P<sub>66614</sub>] Cl (2:1)) extracts almost 60% Fe(III) and 100% Cu(II).
- DES based on ammonium chloride (in particular, Decanoic acid (or Lauric acid) + Tetra heptyl ammonium chloride (2:1)) extracts almost 20% Fe(III) and 100% Cu(II).

This last result seems to be very interesting to meet the company's needs to extract Cu from the UGCO bath. For this, further investigation is necessary.

1.4. Binodal curves for systems composed of IL (or polymer) / synthetic solution single-metal that mimic the UGCO bath composition / water.

Table S1: [P<sub>44414</sub>]Cl / HCl / H<sub>2</sub>O at 25 °C (*turbidity method*)

HCl (wt%)	[P <sub>44414</sub> ]Cl (wt%)						
13.7	45.2	15.2	34.0	16.0	28.6	16.6	25.4
13.9	42.9	15.3	33.1	16.2	28.1	16.7	24.9
14.5	39.4	15.5	32.3	16.1	27.8	16.7	24.5
14.7	37.6	15.5	31.7	16.3	27.3	16.8	24.3
14.8	36.4	15.7	31.0	16.3	26.9	16.9	23.9
15.1	35.0	15.7	30.3	16.3	26.5	16.8	23.6
		15.9	29.5	16.4	26.2	16.9	23.3
		16.0	29.1	16.5	25.9		

Table S2: [P<sub>44414</sub>]Cl / HCl / CrCl<sub>3</sub> / H<sub>2</sub>O [Cr(III)] = 2.60 g/L at 25 °C (*turbidity method*)

HCl (wt%)	[P <sub>44414</sub> ]Cl (wt%)						
0.0	74.8	14.1	33.3	15.3	25.5	16.1	20.7
13.1	40.6	14.3	31.9	15.4	24.6	16.2	20.2
13.4	38.4	14.5	30.6	15.6	23.9	16.3	19.7
13.7	36.4	14.7	29.4	15.7	23.1	16.4	19.2
13.9	34.9	14.9	28.4	15.8	22.4	16.5	18.8
		15.0	27.4	15.9	21.8		
		15.2	26.4	16.0	21.2		

Table S2: [P<sub>44414</sub>]Cl / HCl / CrCl<sub>3</sub> / H<sub>2</sub>O [Cr(III)] = 2.60 g/L at 25 °C (*turbidity method*)

HCl (wt%)	[P <sub>44414</sub> ]Cl (wt%)						
0.0	74.8	14.1	33.3	15.3	25.5	16.1	20.7
13.1	40.6	14.3	31.9	15.4	24.6	16.2	20.2
13.4	38.4	14.5	30.6	15.6	23.9	16.3	19.7
13.7	36.4	14.7	29.4	15.7	23.1	16.4	19.2
13.9	34.9	14.9	28.4	15.8	22.4	16.5	18.8
		15.0	27.4	15.9	21.8		
		15.2	26.4	16.0	21.2		

Table S3: [P<sub>44414</sub>]Cl / HCl / CrCl<sub>3</sub> / H<sub>2</sub>O [Cr(III)] = 5.11 g/L at 25 °C (*turbidity method*)

HCl (wt%)	[P <sub>44414</sub> ]Cl (wt%)						
0.0	72.2	13.9	32.2	15.2	24.3	16.0	19.4
12.7	40.4	14.1	30.7	15.3	23.3	16.1	18.9
13.0	37.8	14.3	29.5	15.4	22.6	16.2	18.4
13.4	35.9	14.5	28.5	15.6	21.8	16.2	18.0
13.6	33.8	14.6	27.3	15.7	21.2		
		14.8	26.1	15.8	20.5		
		15.0	25.1	15.9	19.9		

Table S4: [P<sub>44414</sub>]Cl / HCl / CrCl<sub>3</sub> / H<sub>2</sub>O [Cr(III)] = 10.0 g/L at 25 °C (*turbidity method*)

HCl (wt%)	[P <sub>44414</sub> ]Cl (wt%)						
0.0	72.1	12.7	34.8	13.8	26.5	14.5	21.9
11.7	41.8	13.0	33.0	14.0	25.5	14.6	21.3
12.1	39.4	13.2	31.4	14.1	24.7	14.7	20.5
12.4	37.0	13.4	30.0	14.2	23.9	14.8	19.7
		13.5	28.5	14.3	23.2	14.9	19.1
		13.6	27.4	14.4	22.5		

Table S5: [P<sub>44414</sub>]Cl / HCl / CrCl<sub>3</sub> / H<sub>2</sub>O [Cr(III)] = 15.33 g/L at 25 °C (*turbidity method*)

HCl (wt%)	[P <sub>44414</sub> ]Cl (wt%)						
0.0	71.7	11.9	34.0	13.3	24.7	14.2	19.7
10.5	43.8	12.1	32.4	13.4	23.9	14.3	19.2
10.9	40.9	12.4	30.7	13.6	23.1	14.4	18.6
11.3	38.6	12.6	29.2	13.7	22.2	14.4	18.1
11.6	36.2	12.8	27.8	13.9	21.5	14.5	17.6
		12.9	26.8	14.0	20.9	14.6	17.2
		13.1	25.7	14.1	20.3		

Table S6: [P<sub>44414</sub>]Cl / HCl / NiCl<sub>2</sub> / H<sub>2</sub>O [Ni(II)] = 2.51 g/L at 25 °C (*turbidity method*)

HCl (wt%)	[P <sub>44414</sub> ]Cl (wt%)						
13.4	40.8	14.5	32.1	15.6	25.0	16.5	20.1
13.6	38.8	14.7	31.0	15.8	24.1	16.6	19.6
13.9	36.8	14.9	29.7	16.0	23.4	16.7	18.9
14.1	35.0	15.1	28.6	16.1	22.6	16.8	18.2
14.3	33.4	15.2	27.6	16.2	22.0		
		15.4	26.7	16.3	21.4		
		15.5	25.9	16.4	20.7		

Table S7: [P<sub>44414</sub>]Cl / HCl / NiCl<sub>2</sub> / H<sub>2</sub>O [Ni(II)] = 5.01 g/L at 25 °C (*turbidity method*)

HCl (wt%)	[P <sub>44414</sub> ]Cl (wt%)						
12.9	41.8	13.8	35.3	14.8	28.7	15.6	24.1
13.2	39.8	14.0	33.6	15.0	27.6	15.7	23.4
13.5	37.0	14.3	32.2	15.2	26.6	15.8	22.7
		14.5	30.9	15.3	25.8	15.8	22.0
		14.6	29.7	15.4	24.9	16.1	21.2

Table S8: [P<sub>44414</sub>]Cl / HCl / NiCl<sub>2</sub> / H<sub>2</sub>O [Ni(II)] = 10.00 g/L at 25 °C (*turbidity method*)

HCl (wt%)	[P <sub>44414</sub> ]Cl (wt%)						
11.9	43.5	13.2	34.2	14.5	25.9	15.5	20.3
12.3	40.4	13.4	32.5	14.7	24.8	15.6	19.7
12.6	38.0	13.7	30.9	14.8	23.9	15.6	19.6
12.8	35.9	13.9	29.3	15.0	22.8		
		14.1	28.1	15.2	21.9		
		14.3	27.0	15.3	21.1		

Table S9: [P<sub>44414</sub>]Cl / HCl / NiCl<sub>2</sub> / H<sub>2</sub>O [Ni(II)] = 15.05 g/L at 25 °C (*turbidity method*)

HCl (wt%)	[P <sub>44414</sub> ]Cl (wt%)						
11.0	46.1	12.4	36.2	13.8	27.0	14.8	21.4
11.4	42.9	12.7	34.4	14.0	25.9	14.9	20.7
11.7	40.5	13.0	32.6	14.2	24.9	15.0	20.0
12.1	38.3	13.2	31.1	14.3	23.9	15.1	19.3
		13.3	29.9	14.5	23.0	15.2	18.6
		13.6	28.4	14.6	22.2		

Table S10: [P<sub>44414</sub>]Cl / HCl / FeCl<sub>2</sub> / H<sub>2</sub>O [Fe(II)] = 1.05 g/L at 25 °C (*turbidity method*)

HCl (wt%)	[P <sub>44414</sub> ]Cl (wt%)						
13.1	44.7	13.5	42.7	14.4	37.0	15.0	33.9
		13.7	40.1	14.5	35.8	15.1	33.4
		14.3	38.5	14.8	34.7	15.1	33.2

15.2	32.3	16.9	22.0	18.3	14.2	19.0	9.8
15.2	31.7	16.9	21.8	18.3	13.9	19.0	9.7
15.4	31.1	17.0	21.5	18.4	13.7	19.0	9.6
15.5	30.4	17.0	21.3	18.4	13.5	19.0	9.6
15.7	29.6	17.1	21.1	18.5	13.4	19.0	9.5
15.7	29.1	17.1	20.8	18.5	13.2	19.0	9.4
15.8	28.5	17.2	20.4	18.5	13.0	19.0	9.4
16.0	28.1	17.2	20.2	18.6	12.8	18.9	9.3
16.0	27.8	17.2	19.9	18.6	12.6	19.0	9.2
16.1	27.5	17.4	19.6	18.6	12.4	19.0	9.1
16.0	27.1	17.4	19.3	18.6	12.2	19.0	9.0
16.1	26.7	17.4	18.9	18.8	12.0	19.0	9.0
16.2	26.3	17.5	18.4	18.6	11.7	19.0	8.9
16.3	26.0	17.6	18.0	18.7	11.6	19.0	8.8
16.3	25.7	17.7	17.6	18.7	11.4	19.0	8.7
16.4	25.4	17.7	17.3	18.7	11.3	19.0	8.7
16.4	25.0	17.8	17.1	18.7	11.1	19.0	8.6
16.5	24.7	17.8	16.8	18.7	11.0	19.0	8.5
16.5	24.3	17.9	16.6	18.8	10.9	19.0	8.5
16.7	24.0	17.9	16.4	18.8	10.8	19.1	8.4
16.7	23.8	18.0	16.0	18.8	10.6	19.1	8.3
16.7	23.4	18.0	15.8	18.8	10.5	19.1	8.2
16.8	23.1	18.1	15.4	18.8	10.3	19.1	8.2
16.8	22.9	18.1	15.1	18.9	10.2	19.1	8.1
16.8	22.6	18.2	14.8	18.9	10.1		
16.9	22.5	18.2	14.6	18.9	10.0		
16.9	22.2	18.2	14.4	18.9	9.9		

Table S11: [P<sub>44414</sub>] Cl / HCl / FeCl<sub>2</sub> / H<sub>2</sub>O [Fe(II)] = 10.0 g/L at 25 °C (turbidity method)

<b>HCl (wt%)</b>	<b>[P<sub>44414</sub>]Cl (wt%)</b>	13.7	31.7	14.4	25.8	14.1	9.1
12.5	39.8	13.8	30.7	14.5	25.2	14.1	8.9
12.6	38.1	14.0	29.9	14.5	24.6	13.7	8.5
13.0	36.3	14.0	29.2	14.6	24.1	13.7	8.2
13.2	35.0	14.1	28.4	14.3	10.2	13.6	8.0
13.3	33.9	14.2	27.8	14.4	9.8		
13.5	32.5	14.2	27.0	14.2	9.7		
		14.3	26.6	14.2	9.4		

Table S12: [P<sub>44414</sub>] Cl / HCl / FeCl<sub>2</sub> / H<sub>2</sub>O [Fe(II)] = 15.0 g/L at 25 °C (turbidity method)

<b>HCl (wt%)</b>	<b>[P<sub>44414</sub>]Cl (wt%)</b>	12.5	35.7	13.1	30.2	13.6	26.2
11.7	42.5	12.5	34.9	13.2	29.4	13.6	25.9
11.9	41.0	12.6	34.1	13.3	28.7	13.8	25.6
12.0	39.6	12.6	33.5	13.3	28.2	13.8	25.1
12.1	38.7	12.8	32.7	13.4	27.9	13.8	24.8
12.2	37.9	12.9	32.0	13.5	27.5		
12.3	36.7	12.9	31.4	13.6	27.0		
		13.0	30.8	13.6	26.6		

Table S13: [P<sub>44414</sub>] Cl / HCl / FeCl<sub>2</sub> / H<sub>2</sub>O [Fe(II)] = 20.0 g/L at transition temperature: 25 to 50 °C (bat-  
tle ship method)

HCl (wt%)	[P <sub>44414</sub> ] Cl (wt%)						
		10.4	20.0	8.7	30.0	3.5	20.0
		10.7	5.0	10.4	30.0	8.7	50.0
		7.9	20.4	12.2	30.0	5.2	5.0
27.0	23.0	7.0	5.0	11.1	30.0	17.4	50.0
13.9	10.0	7.4	17.9	3.5	10.0	13.9	50.0
6.9	10.0	5.4	18.5	7.1	44.9	4.2	10.0
13.9	30.0	17.5	39.6	3.5	30.2	1.9	14.9
13.9	20.0	21.0	39.9	5.2	24.8	3.5	39.9
17.5	50.0	7.1	49.8	5.1	35.1	1.8	24.9
4.9	12.0	7.0	30.0	7.1	39.3	1.8	10.0
7.0	20.0	4.5	12.5	10.6	49.5		

Always biphasic points: green

Transition points: yellow

Always monophasic points: blue

Table S14: [P<sub>44414</sub>] Cl / HCl / FeCl<sub>3</sub> / H<sub>2</sub>O [Fe(III)] = 2.5 g/L at 25 °C (turbidity method)

HCl (wt%)	[P <sub>44414</sub> ]Cl (wt%)						
		13.9	28.6	15.0	21.0	15.0	16.0
		14.2	27.4	15.0	20.3	14.9	15.2
10.9	47.3	14.3	26.1	15.1	19.7	14.8	14.5
12.0	41.0	14.5	25.3	15.1	19.0	14.7	13.8
12.6	37.9	14.5	24.4	15.1	18.4	14.4	12.7
13.0	35.0	14.7	23.5	15.1	18.0		
13.4	32.6	14.9	22.6	15.0	17.3		
13.5	30.4	15.0	21.8	15.1	16.6		

Table S15: [P<sub>44414</sub>] Cl / HCl / FeCl<sub>3</sub> / H<sub>2</sub>O [Fe(III)] = 5.17 g/L at 25 °C (turbidity method)

HCl (wt%)	[P <sub>44414</sub> ]Cl (wt%)						
		12.8	41.7	13.7	30.1	13.5	23.0
		13.1	38.8	13.8	29.3	13.1	21.4
		13.4	37.6	13.7	28.3	13.1	20.8
12.1	51.3	13.2	36.1	13.7	27.6	12.9	19.3
12.4	49.2	13.4	34.7	13.8	27.0	12.1	51.3
12.5	47.2	13.5	33.6	13.7	25.6	12.4	49.2
12.6	45.7	13.7	32.1	13.5	24.5		
12.7	43.9	13.8	31.4	13.6	23.9		

Table S16: [P<sub>44414</sub>] Cl / HCl / FeCl<sub>3</sub> / H<sub>2</sub>O [Fe(III)] = 10.2 g/L at 25 °C (turbidity method)

HCl (wt%)	[P <sub>44414</sub> ]Cl (wt%)						
		12.7	40.7	12.7	32.8	12.1	27.0
		12.6	38.7	12.6	31.3	11.7	25.7
		12.8	37.2	12.5	30.2	11.5	24.4
12.5	45.2	12.7	35.5	12.4	29.2	11.2	23.3
12.6	42.7	12.8	33.8	12.2	28.2	10.6	21.5

9.9	19.7
9.5	18.4
8.7	16.7

7.8	14.9
7.3	13.5
6.1	10.7

5.5	9.3
4.9	7.9
4.6	7.1

12.5	45.2
------	------

Table S17: [P<sub>44414</sub>]Cl / HCl / FeCl<sub>3</sub> / H<sub>2</sub>O [Fe(III)] = 15.1 g/L at 25 °C (turbidity method)

HCl (wt%)	[P <sub>44414</sub> ]Cl (wt%)
10.5	46.6
11.7	40.0
11.5	36.6
10.7	31.9
10.2	28.0

9.2	24.5
8.1	21.2
7.1	18.2
5.4	13.6
4.9	11.9
4.5	10.5
4.0	8.9

3.8	8.0
10.5	46.6
11.7	40.0
11.5	36.6
10.7	31.9
10.2	28.0
9.2	24.5

8.1	21.2
7.1	18.2
5.4	13.6
4.9	11.9
4.5	10.5
4.0	8.9

Table S18: PEG-600 / HCl / FeCl<sub>3</sub> / H<sub>2</sub>O [Fe(III)] = 10 g/L at 25 °C (turbidity method)

HCl (wt%)	PEG-600 (wt%)
17.9	27.5
18.8	24.5
19.5	23.4

19.7	21.9
19.8	20.9
20.0	20.0
20.4	19.1
20.7	18.1

20.8	17.4
21.0	16.5
21.4	15.9
21.5	15.5
21.5	15.1

21.6	14.4
21.9	13.7
22.0	13.1
22.1	12.4
22.6	11.7

Table S19: PEG-600 / HCl / FeCl<sub>3</sub> / H<sub>2</sub>O [Fe(III)] = 10 g/L at 50 °C (turbidity method)

HCl (wt%)	PEG-600 (wt%)
18.3	20.4
18.8	18.4

19.1	16.9
19.3	15.7
19.6	14.6
19.8	13.6

19.9	12.7
20.1	11.8
20.3	10.8
20.5	9.9

21.0	9.2
21.0	8.7
21.4	8.1
21.8	7.4

Table S20: PEG-600 / HCl / FeCl<sub>3</sub> / H<sub>2</sub>O [Fe(III)] = 40 g/L at 25 °C (turbidity method)

HCl (wt%)	PEG-600 (wt%)
11.8	29.8
13.4	26.7
13.6	25.5
13.9	24.4
14.1	23.3
14.3	22.3
14.5	21.4
14.6	20.3
14.9	19.3
15.0	18.5
15.4	17.7
15.4	17.2
15.5	16.5
15.5	15.6
15.8	15.2

15.9	14.5
16.1	13.8
16.2	13.2
16.4	12.5
16.6	11.9
16.7	11.6
17.2	10.9
17.2	10.5
17.4	10.0
17.5	9.6
17.5	9.4
17.3	8.9
17.5	8.6
17.5	8.4
17.5	8.3
17.6	8.2
17.6	8.1
17.7	8.0

17.7	8.0
17.8	7.9
17.8	7.8
17.8	7.7
17.9	7.6
17.9	7.5
17.8	7.3
17.9	7.2
17.9	7.1
17.9	7.0
18.0	7.0
18.0	6.9
18.0	6.8
18.1	6.7
18.1	6.6
18.1	6.5
18.1	6.4
18.2	6.3

18.2	6.2
18.2	6.0
18.3	5.9
18.3	5.7
18.3	5.6
18.5	5.5
18.5	5.3
18.5	5.2
18.6	5.1
18.7	5.0
18.7	4.8
11.8	29.8
13.4	26.7
13.6	25.5
13.9	24.4
14.1	23.3
14.3	22.3
14.5	21.4
14.5	21.4

14.6	20.3	17.2	10.9	17.8	7.8	18.1	6.4
14.9	19.3	17.2	10.5	17.8	7.7	18.2	6.3
15.0	18.5	17.4	10.0	17.9	7.6	18.2	6.2
15.4	17.7	17.5	9.6	17.9	7.5	18.2	6.0
15.4	17.2	17.5	9.4	17.8	7.3	18.3	5.9
15.5	16.5	17.3	8.9	17.9	7.2	18.3	5.7
15.5	15.6	17.5	8.6	17.9	7.1	18.3	5.6
15.8	15.2	17.5	8.4	17.9	7.0	18.5	5.5
15.9	14.5	17.5	8.3	18.0	7.0	18.5	5.3
16.1	13.8	17.6	8.2	18.0	6.9	18.5	5.2
16.2	13.2	17.6	8.1	18.0	6.8	18.6	5.1
16.4	12.5	17.7	8.0	18.1	6.7	18.7	5.0
16.6	11.9	17.7	8.0	18.1	6.6	18.7	4.8
16.7	11.6	17.8	7.9	18.1	6.5		

Table S21: PEG-600 / HCl / FeCl<sub>3</sub> / H<sub>2</sub>O [Fe(III)] = 40 g/L at 50 °C (*turbidity method*)

HCl (wt% )	PEG-600 (wt% )						
		13.6	18.2	14.3	14.1	15.1	10.4
		13.7	17.6	14.4	13.6	15.2	9.8
		13.8	17.0	14.5	13.1	15.3	9.3
12.9	22.2	13.9	16.4	14.6	12.6	12.9	22.2
13.1	20.7	14.0	15.9	14.6	12.0	13.1	20.7
13.3	19.7	14.1	15.2	14.8	11.4	13.3	19.7
13.4	18.9	14.2	14.6	15.0	10.9	13.4	18.9

Table S22: PEG-600 / HCl / FeCl<sub>3</sub> / H<sub>2</sub>O [Fe(III)] = 40 g/L at 50 °C (*battle ship method*)

HCl (wt% )	PEG-600 (wt% )						
		13.4	19.2	11.0	65.0	15.7	20.0
		11.9	19.0	14.1	55.0	18.8	10.1
		11.0	20.0	17.3	44.8	21.7	10.6
		14.0	10.0	18.8	40.0	18.5	30.7
12.9	25.0	13.0	9.8	20.3	35.0	22.0	29.8
14.1	18.8	9.4	10.0	14.1	35.0	24.8	20.7
15.5	10.6	3.2	89.9	14.0	40.1	28.2	10.0
12.5	30.3	6.3	79.8	15.7	29.7	15.2	30.3
12.4	40.6	9.4	70.0	14.0	29.7	18.6	31.0
13.7	46.2	12.5	59.9	17.6	29.2	14.0	30.0
12.6	44.9	4.7	85.0	17.4	22.1	17.0	20.5
12.4	35.2	7.9	74.9	17.5	12.6	17.2	10.1
10.9	30.0						

Monophasic points: blue

Biphasic points: green

Table S23: [P<sub>44414</sub>] Cl / HNO<sub>3</sub> / H<sub>2</sub>O at 25 °C (*turbidity method*)

HNO <sub>3</sub> (wt% )	[P <sub>44414</sub> ] Cl (wt% )						
		4,0	53,7	0,7	7,6	0,2	2,0
		3,8	51,9	0,4	3,7	0,2	1,9
		2,0	23,3	0,4	3,5	0,2	1,7
		1,1	12,3	0,3	2,8	0,2	1,4

Table S24: [P<sub>44414</sub>] Cl / H<sub>2</sub>SO<sub>4</sub> / H<sub>2</sub>O at 25 °C (turbidity method)

H <sub>2</sub> SO <sub>4</sub> (wt%)	[P <sub>44414</sub> ] Cl (wt%)						
0.0	97.1	4.6	19.3	9.0	14.9	11.7	9.3
1.4	22.7	5.6	18.8	9.7	13.8	12.1	8.8
3.5	21.9	6.3	17.7	9.8	12.7	12.9	8.5
3.9	19.7	6.6	17.0	10.5	12.0	13.4	8.3
		7.5	16.6	10.7	11.1	13.5	7.7
		7.9	16.0	11.1	10.6		
		8.2	15.4	11.6	10.0		

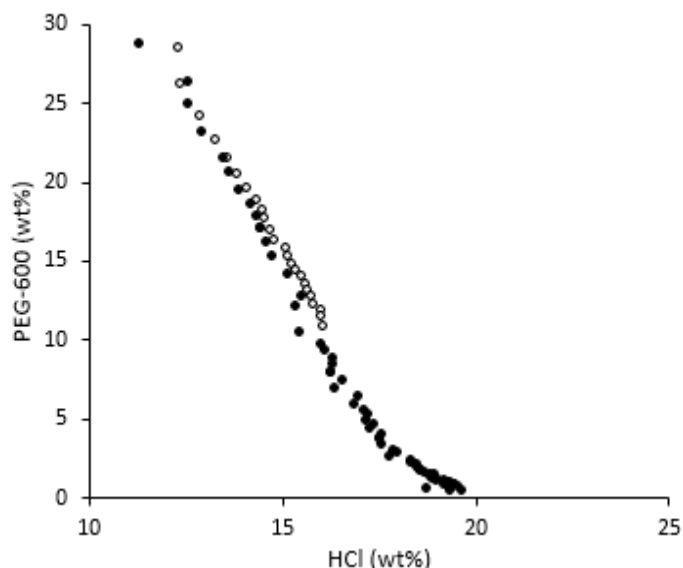


Figure 137. Binodal curves of the system PEG-600/[Fe(III)+HCl 37wt%]/H<sub>2</sub>O [Fe(III)] = 40 g/L at 25 °C obtained using two different HCl providers, Fluka (●) and Sigma Aldrich (○).

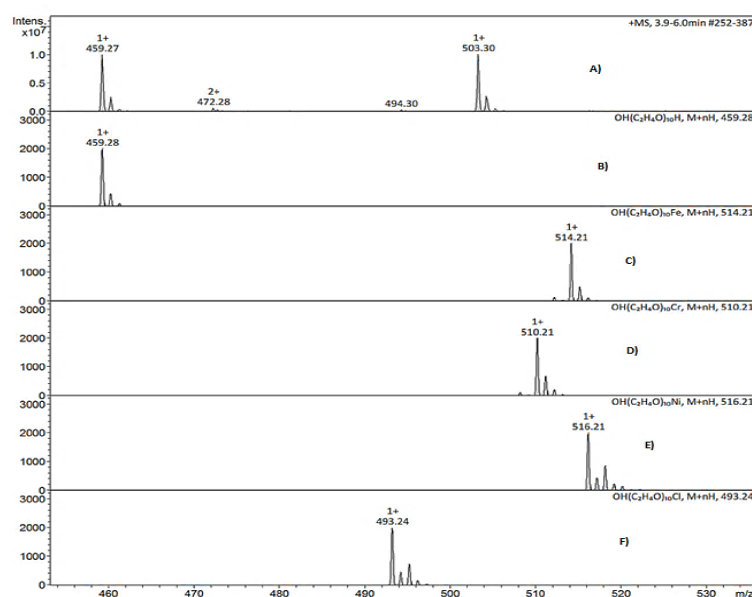


Figure 136. Polymer investigation by ESI-MS. A: polymer phase analyzed after mixing 80wt% of stock solution Fe(III) 35 g/L in 12M HCl and 20 wt% of PEG-600; B: fresh polymer PEG-600; Simulation with the software of the ESI-MS machine to show the form of peaks of PEG-Fe (C), PEG-Cr (D), PEG-Ni (E), PEG-Cl (F).

The Gaussian distribution of the PEG-600 obtained is the one expected (with a maximum peak around 600 Mw, the value showed in figure 22b is equal to 625 m/z because in this case the PEG is charged by 1 Cl<sup>-</sup>, due to the source).

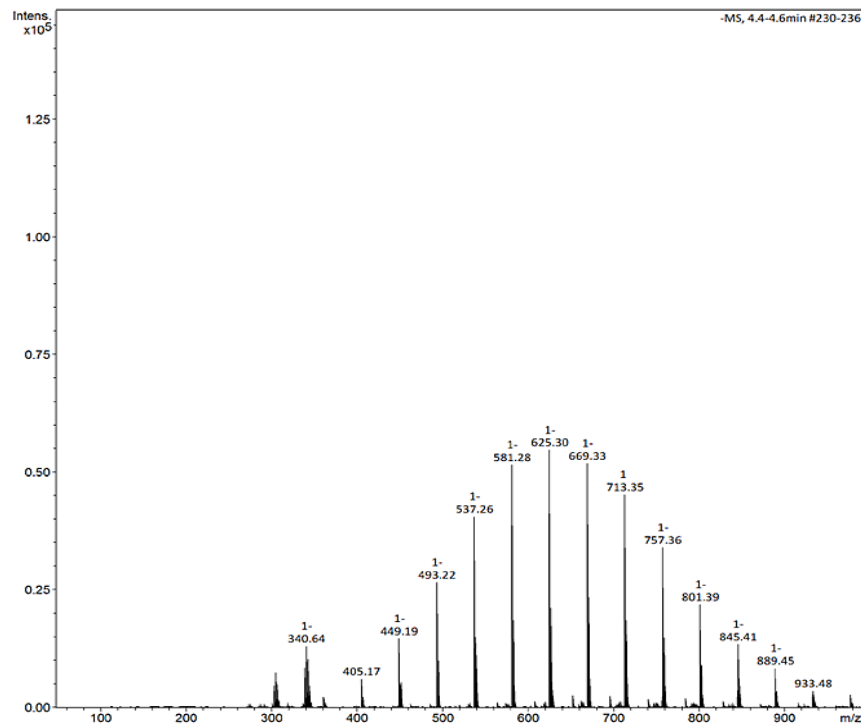


Figure 138. Gaussian's curve of PEG-600 indicates the distribution of the polymer in solution

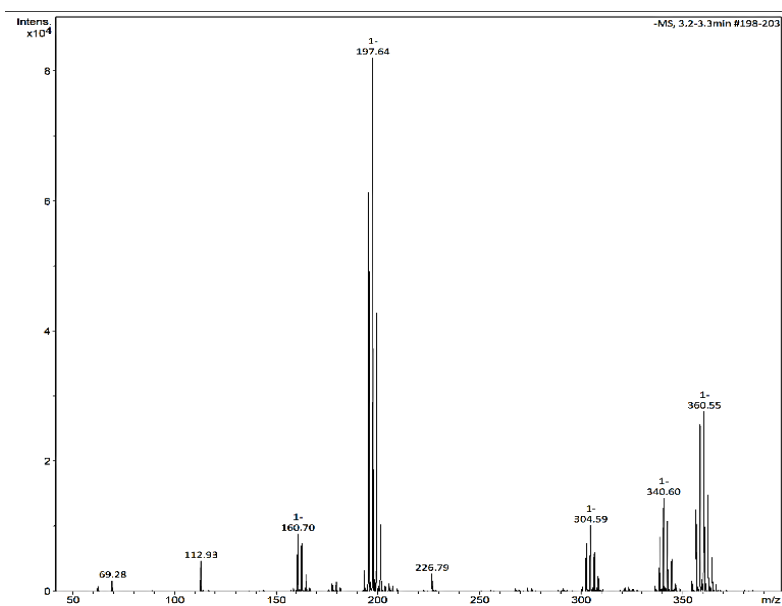


Figure 139. ESI-MS results of the acidic solution Fe(III) + HCl (37 wt% = 12M). Peaks at 197.64 m/z are the characteristic peaks of [Fe(III)Cl<sub>4</sub>]<sup>-</sup> (molecular weight of the species).

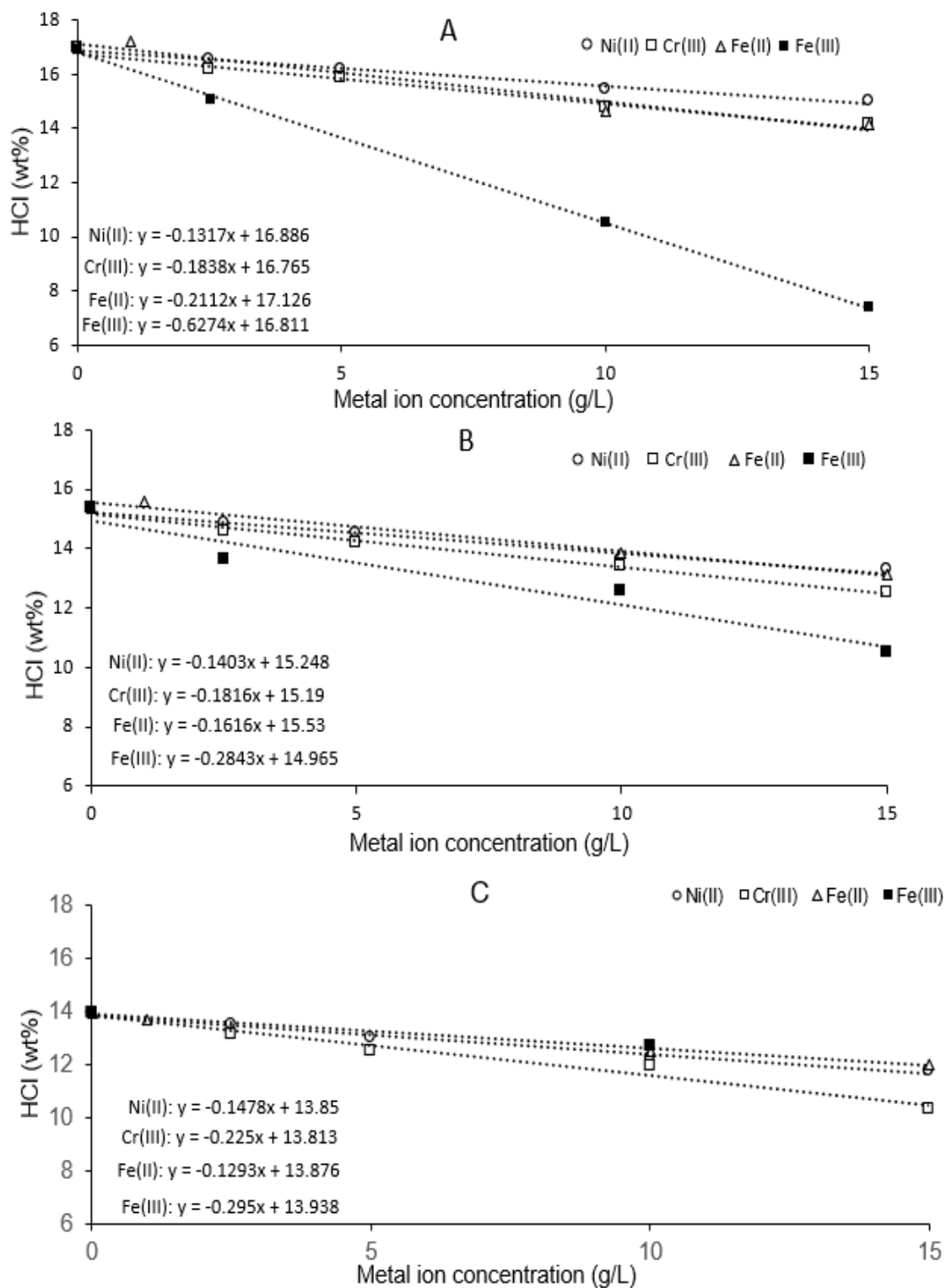


Figure 140. HCl amount (wt%) as a function of metal ion concentration at: A) 20 wt%, B) 30 wt% and C) 40 wt% of IL.

## 2. Na<sub>2</sub>SO<sub>4</sub> media and sulfate bath

### 2.1. Binodal curves for the systems composed of IL (or polymer) / synthetic solution single-metal (or Na<sub>2</sub>SO<sub>4</sub> bath) / water.

Table S26 - PEG-400 / Na<sub>2</sub>SO<sub>4</sub> Bath (turbidity method) at 25°C (1<sup>st</sup> part)

PEG-400 (wt%)	Na <sub>2</sub> SO <sub>4</sub> Bath (wt%)						
14.9	85.08	15.79	80.82	16.92	75.06	17.73	70.13
15.10	84.39	15.87	80.51	16.91	74.66	17.78	69.80
15.18	84.06	15.94	80.02	16.86	74.02	17.84	69.56
15.24	83.73	16.10	79.44	16.94	73.76	17.97	69.25
15.30	83.19	16.12	78.98	17.00	73.51	18.04	68.61
15.35	82.91	16.27	78.43	17.05	73.26	18.15	68.15
15.43	82.55	16.40	77.90	17.12	73.04	18.25	67.67
15.53	82.25	16.44	77.43	17.25	72.51	18.30	67.44
15.57	81.75	16.60	76.93	17.28	72.11	18.48	66.99
15.71	81.43	16.64	76.46	17.39	71.57	18.60	66.58
15.73	81.20	16.69	76.19	17.50	72.11	18.63	66.36
		16.83	75.61	17.56	70.84	18.65	66.10
		16.87	75.32	17.61	70.60	18.62	65.98

Table S27 - PEG-400 / Na<sub>2</sub>SO<sub>4</sub> Bath (turbidity method) at 25°C (2<sup>nd</sup> part)

PEG-400 (wt%)	Na <sub>2</sub> SO <sub>4</sub> Bath (wt%)						
18.03	65.96	21.22	62.45	21.92	59.79	22.63	56.95
20.75	63.77	21.30	62.01	21.99	59.38	22.75	56.73
21.15	63.20	21.40	61.75	22.10	59.01	22.81	56.31
21.09	62.85	21.49	61.33	22.19	58.63	22.87	55.93
		21.57	60.91	22.28	58.32	22.99	55.66
		21.74	60.63	22.68	58.20	23.19	55.08
		21.84	60.21	22.55	57.31		

Table S28 - PEG-400 / Na<sub>2</sub>SO<sub>4</sub> Bath (turbidity method) at 25°C (3<sup>rd</sup> part)

PEG-400 (wt%)	Na <sub>2</sub> SO <sub>4</sub> Bath (wt%)						
22.86	55.16	24.13	51.53	25.36	47.72	26.77	42.14
23.52	54.69	24.22	51.20	25.70	47.19	26.90	41.61
23.42	53.89	24.28	50.90	25.66	46.52	26.98	41.21
23.68	53.44	24.49	50.46	25.83	46.11	27.31	40.50
23.75	53.11	24.56	50.12	25.86	45.82	27.57	39.70
23.84	52.80	24.63	49.83	25.61	45.14	27.81	39.08
23.91	52.45	24.71	49.53	25.84	44.54	28.08	38.49
24.12	51.92	24.76	49.32	25.96	44.09	28.41	37.79
		24.96	48.94	26.07	43.60	28.65	37.07
		25.01	48.62	26.48	43.11	28.84	36.52
		25.23	48.26	26.60	42.45	29.04	36.18

29.44	35.37
29.89	34.55
30.43	33.62

30.85	32.56
31.36	31.30
31.64	30.84

32.12	30.19
32.57	29.39
33.05	28.63

33.36	27.89
-------	-------

Table S29 - PEG-400 / Na<sub>2</sub>SO<sub>4</sub> Bath (turbidity method) at 25°C (4<sup>th</sup> part)

PEG-400 (wt%)	Na <sub>2</sub> SO <sub>4</sub> Bath (wt%)
32.97	27.56
32.97	27.56
34.00	27.14

33.80	26.04
34.21	25.30
34.72	24.80
35.09	24.16
36.24	22.99

37.10	21.76
38.45	20.26
40.90	18.49
40.64	17.73
41.43	17.07

42.21	16.36
42.89	15.76
44.28	14.55
44.69	14.32

Table S30 - PEG-400 / Na<sub>2</sub>SO<sub>4</sub> Bath (battleship method) at 25°C

MONOPHASIC POINTS

PEG-400 (wt%)	Na <sub>2</sub> SO <sub>4</sub> Bath (wt%)
50	10

59.8	5
69.8	2.2
79.8	2
90	2

15.1	84.9
10.6	59.7
20	59.8
10.3	54.8

20.1	54.8
10.1	50.1
20	50
49.8	10.2

BIPHASIC POINTS

PEG-400 (wt%)	Na <sub>2</sub> SO <sub>4</sub> Bath (wt%)
49.6	15.2
60	12.1
10.3	89.7
60	40
69.7	10.3

59.7	20
60	30
64.5	15.2
64.8	25.1
20	80
25.2	74.8
30.3	69.7

34.9	65.1
39.9	60.1
45.1	54.9
50	50
55	45
30	59.8
39.7	60.3

30.1	54.8
54.9	10
54.9	20.1
55.4	29.7
54.9	40
49.8	20.4
49.9	40

Table S30 - PEG-400 / Na<sub>2</sub>SO<sub>4</sub> salt / H<sub>2</sub>O (turbidity method) at 25°C

PEG-400 (wt%)	Na <sub>2</sub> SO <sub>4</sub> salt (wt%)
0.0	13.3
20.5	10.6
20.5	9.7
22.3	9.1
23.5	8.4

24.7	7.8
25.8	7.3
27.0	6.8
29.2	6.2
29.4	5.7
30.1	5.4
31.8	5.0
32.4	4.7

33.5	4.4
34.3	4.1
35.7	3.8
36.6	3.6
37.3	3.4
38.1	3.2
39.0	3.1
40.3	2.8

41.4	2.7
43.5	2.4
44.5	2.2
45.3	2.1
46.4	1.9
47.5	1.8
49.6	1.6

Table S31 - PEG-400 / [Fe(III)+Na<sub>2</sub>SO<sub>4</sub>] / H<sub>2</sub>O (turbidity method) at 25°C

PEG-400 (w%)	only Na <sub>2</sub> SO <sub>4</sub> (wt%)
0.0	11.7
24.4	8.9
24.5	7.8

26.4	7.2
27.1	6.6
28.3	6.2
30.1	5.6
31.4	5.1
33.2	4.6

35.4	4.1
37.5	3.7
39.1	3.3
41.7	2.9
44.0	2.5
47.1	2.0

51.0	1.7
55.2	1.4
51.0	1.3

Table S32 - PEG-400 / [Ni(II)+Na<sub>2</sub>SO<sub>4</sub>] / H<sub>2</sub>O (turbidity method) at 25°C

PEG-400 (w%)	only Na <sub>2</sub> SO <sub>4</sub> (wt%)
0.0	12.3
20.0	9.8

22.8	8.5
27.9	7.0
28.9	5.9
32.0	5.0

33.3	4.2
36.2	3.6
39.6	2.9
42.0	2.4

47.1	1.9
49.2	1.6

Table S33 - PEG-400 / [Cr(III)+Na<sub>2</sub>SO<sub>4</sub>] / H<sub>2</sub>O (turbidity method) at 25°C

PEG-400 (w%)	only Na <sub>2</sub> SO <sub>4</sub> (wt%)
0.0	11.8
28.7	8.4
27.5	6.8

29.1	6.0
30.9	5.3
33.0	4.7
34.7	4.2
35.2	4.0
37.0	3.6

38.1	3.2
39.7	3.0
41.4	2.7
42.7 %	2.4
44.2 %	2.2

45.1 %	2.1
46.1 %	1.9
48.3 %	1.7

Table S34 - PEG-400 / [Cr(VI)+Na<sub>2</sub>SO<sub>4</sub>] / H<sub>2</sub>O (turbidity method) at 25°C ([Cr(VI)]=5 g/L)

PEG-400 (w%)	only Na <sub>2</sub> SO <sub>4</sub> (wt%)
0.0	13.1
22.3	10.2

26.1	8.0
27.8	6.8
29.6	5.9
31.0	5.2
33.9	4.6

35.8	3.8
38.5	3.3
40.2	2.8
42.8	2.4
44.7	2.1

46.7	1.9
49.0	1.6
52.6	1.3

Table S35 - PEG-400 / [Cr(VI)+Na<sub>2</sub>SO<sub>4</sub>] / H<sub>2</sub>O (turbidity method) at 40°C ([Cr(VI)]=5 g/L)

PEG-400 (w%)	only Na <sub>2</sub> SO <sub>4</sub> (wt%)
20.2	10.5
21.7	9.2
23.7	8.4

25.4	7.7
26.6	7.1
28.8	6.5
30.8	5.8
32.1	5.3
32.6	4.9

34.4	4.5
34.8	4.2
37.2	3.8
38.4	3.3
40.3	3.0
41.1	2.8

43.4	2.5
45.0	2.2
47.3	1.9
49.6	1.7
51.6	1.5

Table S36 - PEG-400 / [Cr(VI)+Na<sub>2</sub>SO<sub>4</sub>] / H<sub>2</sub>O (turbidity method) at 25°C ([Cr(VI)]=20 g/L)

PEG-400 (w%)	only Na <sub>2</sub> SO <sub>4</sub> (wt%)
28.5 %	6.8%

29.5 %	6.1%
32.3 %	5.3%

34.3 %	4.7%
35.3 %	4.2%

37.2 %	3.8%
37.5 %	3.6%

<b>39.6</b> %	3.1%
<b>42.2</b> %	2.6%
<b>43.8</b> %	2.4%

<b>47.5</b> %	2.0%
<b>48.2</b> %	1.8%
<b>50.8</b> %	1.5%

<b>53.0</b> %	1.4%
<b>53.8</b> %	1.2%
<b>72.9</b> %	0.7%

Table S37 - PEG-400 / [Mo(VI)+Na<sub>2</sub>SO<sub>4</sub>] / H<sub>2</sub>O (turbidity method) at 25°C

<b>PEG-400 (w%)</b>	<b>only Na<sub>2</sub>SO<sub>4</sub> (wt%)</b>
<b>0.0</b>	13.1
<b>20.8</b>	10.3

<b>24.4</b>	8.5
<b>27.1</b>	7.1
<b>28.8</b>	6.0
<b>32.7</b>	5.1
<b>32.6</b>	4.5

<b>35.5</b>	3.9
<b>38.7</b>	3.2
<b>41.2</b>	2.6
<b>43.5</b>	2.3
<b>45.7</b>	2.0

<b>46.9</b>	1.8
<b>49.0</b>	1.6
<b>51.7</b>	1.3

## List of tables

Table 1. Types of ABS with representative example <sup>39</sup> .....	46
Table 2. Transition metals with corresponding oxidation number extracted by IL-ABS processes <sup>59</sup> .....	48
Table 3. List of ABS, in order of date of publication, used for metal ions extraction. L35 is the tri-block polymer: EO-PO-EO, Mw=1900; L64 is the tri-block polymer PPO-PEO-PPO, Mw=2900. ....	64
Table 4. List of IL-based ABS, in order of date of publication, used for selective metal ions extraction. TBAB is tetrabutylammonium bromide.....	74
Table 5. William Nelson's table. G: good; P: poor; U: unknown.....	78
Table 6. Chemical compounds used during the PhD. ....	84
Table 7. Polymers tested during the PhD. ....	85
Table 8. Binodal curves obtained in different media. The table is divided in ionic liquid systems on the left and polymer systems on the right. M.S. = systems investigated but provided a monophasic behavior.....	86
Table 9. Stock solutions of metal ions used for ESI-MS analysis. ....	98
Table 10. Composition, pH and density of UGCO bath.....	103
Table 11. Composition, pH and density of Na <sub>2</sub> SO <sub>4</sub> bath. ....	103
Table 12. Metal concentration in UGCO bath.....	111
Table 13. IL-based ABS and polymer-based ABS with metal contribution and HCl media....	115
Table 14. List of polymers used to induce a biphasic system with the UGCO bath.....	129
Table 15. Metal concentration in Na <sub>2</sub> SO <sub>4</sub> bath.....	137
Table 16. Ratio of charge, mass and charge density of Mo(VI) under different pH.  z  is the absolute value of ions charge, n is atomic number of ions, M is molar mass of ions.  z /M is the charge density <sup>149</sup> .....	147
Table 17. Stability constant of the species with SO <sub>4</sub> <sup>2-</sup> .....	147
Table 18. Composition, pH, and density of the Na <sub>2</sub> SO <sub>4</sub> bath filtrated.....	161
Table 19. Mass balance step 1 big volume (10 kg). ....	162
Table 20. Working parameters proposed by Lie et al., Sun et al. and this investigation. ....	174
Table 21. Metal concentration in µg/L in water recovered after step 3. ....	186
Table 22. List of "green" DES used for liquid-liquid extraction.....	199

## List of figures

Figure 1. Principales différences entre l'acier et l'acier inoxydable. (site web Aperam).....	12
Figure 2. (A) PEG; (B) PPG, (C) [P <sub>44414</sub> ] Cl. ....	14
Figure 3. Courbes binodales des systèmes : [P <sub>44414</sub> ] Cl/[HCl 37 % en poids]/H <sub>2</sub> O, [Me]= 0 g/L (Δ) ; [P <sub>44414</sub> ] Cl/[Ni(II)+HCl 37 % en poids]/H <sub>2</sub> O à 5 g/L (■) ou 15 g/L (□) de Ni(II) ; [P <sub>44414</sub> ] Cl/[Cr(III)+HCl 37 % en poids]/H <sub>2</sub> O à 5 g/L (●) ou 15 g/L (○) de Cr(III) à 25°C. La flèche indique une augmentation de la concentration en métal. ....	16
Figure 4. Courbes binodales des systèmes: [P <sub>44414</sub> ] Cl/[Fe(III)+HCl 37 wt%]/H <sub>2</sub> O à [Fe(III)] = 0 g/L (Δ), [Fe(III)] = 2.5 g/L (■), [Fe(III)] = 5 g/L (□), [Fe(III)] = 10 g/L (●) et [Fe(III)] = 15 g/L (○) à 25°C.....	16
Figure 5. Diagramme de phase obtenu par la méthode de la bataille navale et de la turbidité pour le système PEG-600/[Fe(III)+HCl 37wt%]/H <sub>2</sub> O - [Fe(III)] = 40 g/L à 50°C. Région monophasique (●), région biphasique (○), courbe binodale obtenue par la méthode de turbidité (Δ). La ligne pointillée (- - -) n'est qu'un guide pour l'œil. ....	17
Figure 6. Ions métalliques extraits dans la phase supérieure du PEG-400 en milieu Na <sub>2</sub> SO <sub>4</sub> à partir de solutions synthétiques mono-métal. ....	19
Figure 7. Courbe binodale pour l'ABS composé de PEG-400 / Na <sub>2</sub> SO <sub>4</sub> / H <sub>2</sub> O et de métaux. ....	19
Figure 8. Instantané du processus (à droite) et schéma de l'étape 1 grand volume (10 kg) (à gauche).....	21
Figure 9. Schéma du brevet pour la récupération du Cr(VI) dans le bain de Na <sub>2</sub> SO <sub>4</sub> . ....	22
Figure 10. Long-term Sustainable Development goals of 6th SOER 2020 <sup>2</sup> .....	27
Figure 11. Aperam residues split in 2019 (from Aperam website). ....	29
Figure 12. Main differences between steel and stainless-steel steel. (Aperam website) .....	30
Figure 13. Rolls of stainless steel produced by Aperam. Site of Isbergues (Fr). ....	30
Figure 14. Schematic representation of 3 baths for pickling process. Each of the baths having a different composition in acids and salts. ....	31
Figure 15. Concentration of metals in the UGCO (left) and Na <sub>2</sub> SO <sub>4</sub> (right) Aperam baths.....	31
Figure 16. Surface finishing steps for stainless steel in Aperam lines. ....	38
Figure 17. Pickling waste generated in the steel streamline <sup>19</sup> .....	40
Figure 18. Polyethylene glycol (PEG). ....	49
Figure 19. Polypropylene glycol (PPG) .....	49
Figure 20. Most common cations and some possible anions in IL <sup>65</sup> .....	50
Figure 21. Tributyl-tetradecyl phosphonium chloride, [P <sub>44414</sub> ] Cl.....	51
Figure 22. Nucleophilic (red) and electrophilic (blue) approaches to quaternary phosphonium salts (Lg: leaving group) <sup>71</sup> .....	51
Figure 23. Phase diagram for the ternary system composed of PEG-600/Na <sub>2</sub> CO <sub>3</sub> /H <sub>2</sub> O at 20°C: (a) ternary representation and (b) orthogonal representation. CP=critical point of the diagram. M=random mixture in the biphasic region of the system. X <sub>T</sub> =composition of top phase and X <sub>B</sub> =composition of bottom phase. The labels 100w H <sub>2</sub> O, 100w Na <sub>2</sub> CO <sub>3</sub> and 100w PEG-600 represent the weight fraction percentages of H <sub>2</sub> O, Na <sub>2</sub> CO <sub>3</sub> and PEG-600 respectively <sup>74</sup> . ....	52
Figure 24. Non-experimental phase diagram, for representative purposes only. The binodal curve is shown in red. Point A located in the monophasic area characterized by a system, point B located in the biphasic area characterized by a two-phase immiscible system. The arrows indicate the initial composition values used to prepare samples A and B. The dotted line indicates the maximum limit of the phase diagram and corresponds to 100 (wt%) of the two components. ....	54

<i>Figure 25. Scheme of an orthogonal ternary phase diagram composed of component 1, component 2, and water (in weight fraction, wt%) and the respective binodal curve (red), tie-lines (grey). Upper phase (component 1-rich phase) is plotted on the y-axis, and lower phase (component 2 rich-phase) is plotted on the x-axis. 1, 2, and 3 (*) represent total compositions of three mixtures. The final composition of the top and bottom phase is represented by the nodes (▪, ▫) U and L, respectively.</i>	55
<i>Figure 26. Phase diagram of PPG 425 + NaCl + water at 25 °C. A) one liquid phase, B) two liquid phases and C) one liquid phase and one solid phase<sup>81</sup>.</i>	58
<i>Figure 27. Phase diagram for Na<sub>2</sub>SO<sub>4</sub> (1) + H<sub>2</sub>O (2) + PEG-4000 (3) at 25°C. S= solid, L=liquid, C=crystal, Ls=liquid saturated<sup>82</sup>.</i>	59
<i>Figure 28. Different binodal curves that illustrated the effect of various parameters on the ability of phase demixing<sup>83,85, 51, 86</sup>.</i>	61
<i>Figure 29. Different binodal curves from bibliography. The arrow in figure c indicates the decrease in temperature in the system.<sup>14,15,87</sup></i>	62
<i>Figure 30. Mechanism proposed by Bulgariu for the extraction of the neutral species (top) and the anionic species (bottom) of Cd(II)-iodide in the PEG phase<sup>8</sup>.</i>	66
<i>Figure 31. Potential process proposed by Muruchi et al.<sup>10</sup></i>	69
<i>Figure 32. Comparison of Cr(VI) reduction in dark control and under solar irradiation with/without addition of PEG.</i>	70
<i>Figure 33. (a) Snapshot of the simulation box at equilibrium state (CrO<sub>4</sub><sup>2-</sup> is represented by the green spheres. HCrO<sub>4</sub><sup>-</sup> is represented by the yellow spheres. The carbon, hydrogen, and oxygen atoms in PEG molecules are represented by the cyan, white, and red spheres, respectively.) (b) The radial distribution of the chromium atoms of HCrO<sub>4</sub><sup>-</sup> or CrO<sub>4</sub><sup>2-</sup> around all of the monomers of PEG molecules in the aggregates.</i>	71
<i>Figure 34. Radius distribution function of water around Na<sup>+</sup>, CrO<sub>4</sub><sup>2-</sup>, SO<sub>4</sub><sup>2-</sup>, HCrO<sub>4</sub><sup>-</sup>, and PEG molecules.</i>	72
<i>Figure 35. Binodal curves for the system [P<sub>44414</sub>][Cl]-HCl-H<sub>2</sub>O at various temperatures and the composition of mixture points A–E studied. Lines are guides to the eye<sup>101</sup>.</i>	75
<i>Figure 36. On the left, phase diagrams of AcABS composed of [P<sub>44414</sub>][Cl], water and the acids HCl (◊), H<sub>2</sub>SO<sub>4</sub> (○) and HNO<sub>3</sub> (Δ). The mixture points E, F and G belong to HNO<sub>3</sub>-based system and H, I and J to H<sub>2</sub>SO<sub>4</sub>-based system. On the right, 2D representation of the binodal curves, starting from the blue and arriving to the purple at :25 °C, 36 °C, 45 °C, 50 °C and 56 °C; illustration of phase behavior for the mixture point of composition A (11.5 wt% acid; 20 wt% IL; 68.5 wt% H<sub>2</sub>O) at 25 and 50 C; metal solutions were used for visual distinction of phases<sup>11</sup>.</i>	76
<i>Figure 37. Procedure for determining an ABS and characterizing it using analytical tools.</i>	83
<i>Figure 38. Apparatus for cloud point titration method at LEPMI laboratory.</i>	87
<i>Figure 39. Binodal curve for system composed by a biphasic inducer, acidic solution, and water. The point A, B, C, D, E, F, G, W, Z, are experimental points found through turbidity method. The black arrows represent the ideal case where the operator immediately recognizes the turbid solution. The red arrows indicate the case where the operator does not recognize the turbid solution. The dotted lines are eye guides indicating the direction that the arrows will follow, and this coincides with the origin of the axes for monophasic samples, while it will coincide with the C1 point for biphasic samples.</i>	89
<i>Figure 40. Samples obtained by the battleship method.</i>	90
<i>Figure 41. Phase diagram of the system PEG-600/HCl (37wt%)/ Metal ions. The black dots and the empty circles are experimental points obtained through the battleship method and indicate the monophasic and the biphasic part of the graph respectively. The triangles</i>	

correspond to the experimental points of the binodal curve obtained by the turbidity method.	91
.....	91
Figure 42. Calibration curve for NMR protocol for PEG determination. ....	98
Figure 43. UGCO bath composition of three different aliquots sent by Aperam. ....	101
Figure 44. Na <sub>2</sub> SO <sub>4</sub> bath composition of three different aliquots sent by Aperam. ....	102
Figure 45. Mo(II) acetate dimer .....	103
Figure 46. From the left to the right: Stock solution Cr(VI) in Na <sub>2</sub> SO <sub>4</sub> /H <sub>2</sub> O; biphasic samples: 20/80, 30/70, 40/60 wt% of PEG-400/stock solution. Stock Solution: 5g/L of Cr(VI), from Na <sub>2</sub> Cr <sub>2</sub> O <sub>7</sub> *2H <sub>2</sub> O salt, 105g/L of SO <sub>4</sub> <sup>2-</sup> , 52.3g/L Na(I), pH=1.80.....	104
Figure 47. From the left to the right: Stock solution Mo(VI) in Na <sub>2</sub> SO <sub>4</sub> /H <sub>2</sub> O; biphasic samples: 20/80, 30/70, 40/60 wt% of PEG-400/stock solution. The stock solution is made by 5g/L of Mo(VI), from Na <sub>2</sub> MoO <sub>4</sub> *2H <sub>2</sub> O salt, 105g/L of SO <sub>4</sub> <sup>2-</sup> , 52.43g/L Na(I), pH=1.87.....	104
Figure 48. From the left to the right: Stock solution Cu(II) in Na <sub>2</sub> SO <sub>4</sub> /H <sub>2</sub> O; biphasic samples: 20/80, 30/70, 40/60 wt% of PEG-400/stock solution. The stock solution is made by 5g/L of Cu(II), from CuSO <sub>4</sub> *5H <sub>2</sub> O salt, 105g/L of SO <sub>4</sub> <sup>2-</sup> , 45g/L Na(I), pH=1.87.....	104
Figure 49. From the left to the right: Stock solution Cr(III) in Na <sub>2</sub> SO <sub>4</sub> /H <sub>2</sub> O; biphasic samples: 20/80, 30/70, 40/60 wt% of PEG-400/stock solution. The stock solution is composed by 0.62 g/L of Cr(III), from Cr <sub>2</sub> (SO <sub>4</sub> ) <sub>3</sub> anhy. salt, 93 g/L of SO <sub>4</sub> <sup>2-</sup> , 43.63 g/L Na(I), pH=1.77.....	104
Figure 50. From the left to the right: Stock solution Ni(II) in Na <sub>2</sub> SO <sub>4</sub> /H <sub>2</sub> O; biphasic samples: 20/80, 30/70, 40/60 wt% of PEG-400/stock solution. The stock solution is composed by 5g/L of Ni(II), from NiSO <sub>4</sub> *6H <sub>2</sub> O salt, 105g/L of SO <sub>4</sub> <sup>2-</sup> , 45g/L Na(I), pH=1.86.....	105
Figure 51. From the left to the right: Stock solution Fe(III) in Na <sub>2</sub> SO <sub>4</sub> /H <sub>2</sub> O; biphasic samples: 20/80, 30/70, 40/60 wt% of PEG-400/stock solution. The stock solution is composed by 5g/L of Fe(III), from Fe <sub>2</sub> (SO <sub>4</sub> ) <sub>3</sub> anhy salt, 105g/L of SO <sub>4</sub> <sup>2-</sup> , 45g/L Na(I), pH=1.84.....	105
Figure 52. From the left to the right: Stock solution Mo(II) in Na <sub>2</sub> SO <sub>4</sub> /H <sub>2</sub> O; biphasic samples: 20/80, 30/70, 40/60 wt% of PEG-400/stock solution. Stock Solution with 0.81 g/L of Mo(II) from C <sub>8</sub> H <sub>12</sub> Mo <sub>2</sub> O <sub>8</sub> – Molibdenum acetate dimer, pH=1.75, 104.1 g/L of SO <sub>4</sub> <sup>2-</sup> , 49.85 g/L of Na(I), 7.2 g/L of H <sub>2</sub> SO <sub>4</sub> .....	105
Figure 53. From the left to the right: Stock solution Mn(VII) in Na <sub>2</sub> SO <sub>4</sub> /H <sub>2</sub> O; biphasic samples: 20/80, 30/70, 40/60, wt% of PEG-400/stock solution. Stock Solution: 5g/L of Mn(VII) from NaMnO <sub>4</sub> *1H <sub>2</sub> O salt, pH=1.83, 105g/L of SO <sub>4</sub> <sup>2-</sup> , 50g/L of Na(I), 4.3 g/L of H <sub>2</sub> SO <sub>4</sub> . ....	105
Figure 54. From the left to the right: Stock solution Mn(II) in Na <sub>2</sub> SO <sub>4</sub> /H <sub>2</sub> O; biphasic samples: 20/80, 30/70, 40/60 wt% of PEG-400/stock solution. S4 is monophasic. Stock Solution with 5g/L of Mn(II) from MnSO <sub>4</sub> *1H <sub>2</sub> O salt, pH=1.85, 105g/L of SO <sub>4</sub> <sup>2-</sup> , 45g/L of Na(I), 4.5 g/L of H <sub>2</sub> SO <sub>4</sub> .....	105
Figure 55. From the left to the right: biphasic samples: 20/80, 30/70, 40/60 wt% of PEG-400/stock solution. Stock Solution with 5g/L of Mo(VI), and 5g/L of Cu(II), from Na <sub>2</sub> MoO <sub>4</sub> *2H <sub>2</sub> O and CuSO <sub>4</sub> *5H <sub>2</sub> O salt respectively, pH=1.85, 105g/L of SO <sub>4</sub> <sup>2-</sup> , 50g/L of Na(I), 9.5 g/L of H <sub>2</sub> SO <sub>4</sub> .....	105
Figure 56. Element repartition (wt%) and volume repartition (vol%) for ABS composed of PEG-600 / UGCO bath (30/70 wt%) at 25°C. ....	112
Figure 57. Element repartition (wt%) and volume repartition (vol%) for ABS composed of [P <sub>44414</sub> ] Cl / UGCO bath (20 / 80 wt%) at 20 °C. ....	113
Figure 58. Binodal curves of the systems: [P <sub>44414</sub> ] Cl/[HCl 37 wt%]/H <sub>2</sub> O (IL = Cytec) (▲)10; [P <sub>44414</sub> ] Cl/[HCl 37 wt%]/H <sub>2</sub> O (IL = Interchim) – this work (Δ);.....	114
Figure 60. Binodal curves of the system: [P <sub>44414</sub> ] Cl / [HCl 37wt%]/H <sub>2</sub> O – [Me(x)] = 0 g/L (Δ); [P <sub>44414</sub> ] Cl/[Ni(II)+HCl 37 wt%]/H <sub>2</sub> O – [Ni(II)] = 2.5 g/L (●); [P <sub>44414</sub> ] Cl/[Ni(II)+HCl 37 wt%]/H <sub>2</sub> O – [Ni(II)] = 5 g/L (○); [P <sub>44414</sub> ] Cl / [Ni(II)+HCl 37 wt%]/H <sub>2</sub> O – [Ni(II)] = 10 g/L (■); [P <sub>44414</sub> ] Cl	

/[Ni(II)+HCl 37 wt%]/H <sub>2</sub> O – [Ni(II)] = 15 g/L (□) at 25°C. The arrow indicates the increase in metal concentration. ....	117
Figure 59. Binodal curves of the systems: [P <sub>44414</sub> ]Cl/[HCl 37 wt%]/H <sub>2</sub> O (IL = Interchim) – this work (Δ); [P <sub>44414</sub> ]Cl/[Cr(III)+HCl 37 wt%]/H <sub>2</sub> O – [Cr(III)] = 2.5 g/L (●); [P <sub>44414</sub> ]Cl/[Cr(III)+HCl 37 wt%]/H <sub>2</sub> O – [Cr(III)] = 5 g/L (○); [P <sub>44414</sub> ]Cl/[Cr(III)+HCl 37 wt%]/H <sub>2</sub> O – [Cr(III)] = 10 g/L (■); [P <sub>44414</sub> ]Cl/[Cr(III)+HCl 37 wt%]/H <sub>2</sub> O – [Cr(III)] = 15 g/L (□) at 25°C. The arrow indicates the increase in metal concentration. ....	117
Figure 61. Binodal curves of the systems: [P <sub>44414</sub> ] Cl/[HCl 37 wt%]/H <sub>2</sub> O, [Me]= 0 gL <sup>-1</sup> (Δ); [P <sub>44414</sub> ] Cl/[Ni(II)+HCl 37 wt%]/H <sub>2</sub> O at 5 g/L (■) or 15 g/L (□) of Ni(II); [P <sub>44414</sub> ] Cl/[Cr(III)+HCl 37 wt%]/H <sub>2</sub> O at 5 g/L (●) or 15 g/L (○) of Cr(III) at 25°C. Arrow indicates increase in metal concentration. The arrow indicates the increase in metal concentration. ....	118
Figure 62. Binodal curves of the system [P <sub>44414</sub> ] Cl/[Fe(II)+HCl 37 wt%]/H <sub>2</sub> O at: [Fe(II)] = 0 g/L (Δ), [Fe(II)] = 1 g/L (■), [Fe(II)] = 10 g/L (□) and [Fe(II)] = 15 g/L (●) at 25°C. Dashed lines (- - -) are only a guide for the eye. ....	119
Figure 63. Binodal curves of the system [P <sub>44414</sub> ] Cl/[Fe(III)+HCl 37 wt%]/H <sub>2</sub> O at [Fe(III)] = 0 g/L (Δ), [Fe(III)] = 2.5 g/L (■), [Fe(III)] = 5 g/L (□), [Fe(III)] = 10 g/L (●) and [Fe(III)] = 15 g/L (○) at 25°C (Point A position explained later in the discussion section).....	119
Figure 64. Phase diagram obtained with the battle ship method for the system [P <sub>44414</sub> ] Cl/[Fe(II)+HCl 37wt%]/H <sub>2</sub> O – [Fe(II)] = 20 g/L. Monophasic samples at both T = 25 °C and 50 °C (■), biphasic samples at both T = 25 °C and T = 50 °C (▲) and samples that become biphasic passing from 25 °C to 50 °C (○). Experimental points B, C, D. The arrow (→) indicates the displacement direction of the point B, C, D increasing the wt% of IL (see text). Dashed lines (- - -) are only a guide for the eye.....	120
Figure 65. Phase diagram obtained by turbidity method for the systems PEG-600/[Fe(III)+HCl 37wt%]/H <sub>2</sub> O – [Fe(III)] = 10 g/L (●) and 40 g/L (○) at 25 °C.....	124
Figure 66. Phase diagram obtained by battle ship and turbidity method for the system PEG-600/[Fe(III)+HCl 37wt%]/H <sub>2</sub> O – [Fe(III)] = 40 g/L at 50°C. Monophasic region (●), biphasic region (○), binodal curve obtained by the turbidity method (Δ). The dashed line (- - -) is only a guide for the eye.....	124
Figure 67. Binodal curves obtained by turbidity method for the system PEG-600/[Fe(III)+HCl 37wt%]/H <sub>2</sub> O – [Fe(III)] = 40 g/L at 50°C (□) and at 25°C (■) and for the systems PEG-600/[Fe(III)+HCl 37wt%]/H <sub>2</sub> O – [Fe(III)] = 10 g/L at 50°C (○) and at 25°C (●). ....	125
Figure 68. Mechanism of PEG extraction of Fe(III). 10-A: inter-chain connection proposed by Bulgariu et al. <sup>43</sup> ; 10-B: Fe(III) connection with the ether group of the polymer; 10-C: octahedral structure of the species (Fe(III)Cl <sub>4</sub> ); 10-D: tetrahedral structure of the species (Fe(III)Cl <sub>4</sub> ); Adapted from ref. Bulgariu et al. <sup>43</sup> .....	128
Figure 69. Metal ions repartition in the biphasic inducer phase for samples: 3EDGE, 4EGDE, PEG-600 and PEG-400. The samples on the left indicate the volume repartition and the position of the biphasic inducers and the aqueous phases after ABS formation.....	131
Figure 70. Metallic ion extraction mixing 30 / 70 wt% of [P <sub>44414</sub> ] Cl / UGCO bath. ....	131
Figure 71. Samples prepared for demonstrating the PPG-425 extraction efficiency on the Na <sub>2</sub> SO <sub>4</sub> bath. Starting from the left to the right: 10/90-20/80-30/70-40/60 wt% of PPG-425/ Na <sub>2</sub> SO <sub>4</sub> bath.....	138
Figure 72. Sample prepared to demonstrate the PEG-400 extraction efficiency on the Na <sub>2</sub> SO <sub>4</sub> bath. Repartition used 50/50 wt% of polymer/bath. ....	139
Figure 73. Binodal curve for ABS composed of PEG-400 / Na <sub>2</sub> SO <sub>4</sub> / H <sub>2</sub> O .....	140
Figure 74. Binodal curve for ABS composed of PEG-400 / Na <sub>2</sub> SO <sub>4</sub> / H <sub>2</sub> O and metals.....	141

Figure 75. Metal ions extracted in the upper PEG-400 phase in Na <sub>2</sub> SO <sub>4</sub> media starting from synthetic solutions mono-element. ....	142
Figure 76. Na(I) repartition (wt%) in the polymer phase for the systems of Fe(III), Ni(II), Cu(II), Cr(VI) and Cr(III). ....	143
Figure 77. Volume distribution for each stock solution mono-element.....	144
Figure 78. Pourbaix diagrams for Fe, Mn, Cr, Ni and Cu at T=25°C. Red lines have been inserted at pH=2 to allow the reader to more easily identify the species present in the solutions investigated in this work.....	145
Figure 79. Chemical structures of chromate (left) and dichromate (right) .....	145
Figure 80. Speciation diagram of Cr(VI) at different pH and concentration (g/L). The red line indicates the concentration considered during my investigation (5g/L).....	146
Figure 81. Reaction that occurs when PEG-400 is mixed with Cr(VI) stock solution.in partition 20/80 wt% of polymer/stock solution Cr(VI) . A) stock solution; B) Biphasic system as soon the polymer encounters the stock solution; C) samples after 24h, left in direct contact with light. ....	146
Figure 82. Extraction mechanism of PEG-400 proposed in this work.....	148
Figure 83. Binodal curves for the systems PEG-400 / [Cr(VI) + Na <sub>2</sub> SO <sub>4</sub> ]/ H <sub>2</sub> O, considering (blue) [Cr(VI) = 5 g/L and T = 25 °C, (yellow) [Cr(VI) = 5 g/L and T = 40 °C, (green) [Cr(VI) = 20 g/L and T = 25 °C. ....	150
Figure 84. (left) Crystal's formation at T=15°C in the upper and lower phase of the samples composed by 20/80 wt% of PEG-400/stock solution of Cr(III) 0.64 g/L.(right) Precipitation effect on the upper and lower phase of sample containing 20/80 wt% of PEG-400/Stock solution of Fe(III) 5 g/L after exposition at 15°C. ....	150
Figure 85. Na <sub>2</sub> SO <sub>4</sub> -H <sub>2</sub> O system. Temperature vs. concentration diagram (M= mirabilite= Na <sub>2</sub> SO <sub>4</sub> *10H <sub>2</sub> O; T = thenardite= Na <sub>2</sub> SO <sub>4</sub> anhydrous; 1 = solubility curve for Na <sub>2</sub> SO <sub>4</sub> *10H <sub>2</sub> O; 2 = solubility curve for Na <sub>2</sub> SO <sub>4</sub> *7H <sub>2</sub> O; 3 = solubility curve for Na <sub>2</sub> SO <sub>4</sub> anhydrous; 4=Na <sub>2</sub> SO <sub>4</sub> /Na <sub>2</sub> SO <sub>4</sub> *10H <sub>2</sub> O boundary system), ....	151
Figure 86. Samples obtained by mixing different wt% of PEG-400 + stock solution Cu(II)+Mo(VI); s <sub>1</sub> = 20/80, s <sub>2</sub> = 30/70, s <sub>3</sub> = 40/60, in wt%, of PEG-400/stock solution. ....	152
Figure 87. PEG-400 extraction efficiency considering Cu(II) and Mo(VI) in the same stock solution (straight line) or separately (dotted line).....	153
Figure 88. Binodal curves for the ABS composed of: (yellow) PEG-400/Na <sub>2</sub> SO <sub>4</sub> bath; (grey) PEG-400/ [Cr(VI) - Na <sub>2</sub> SO <sub>4</sub> salt] / H <sub>2</sub> O; (black) PEG-400/ Na <sub>2</sub> SO <sub>4</sub> salt / H <sub>2</sub> O at 25 °C. ....	154
Figure 89. Element and volume repartition (wt%) for the system composed by 27 wt% of PEG-400 and 73wt% of Na <sub>2</sub> SO <sub>4</sub> bath at two different given temperatures, 25°C and 75 °C.....	158
Figure 90. Extraction efficiency of PEG-400 considering different samples made up respectively of 20%, 30%, and 40% of PEG-400 and the difference in Na <sub>2</sub> SO <sub>4</sub> bath. Values taken from table 23. ....	159
Figure 91. Extraction kinetics of Cr(VI) in the extraction process by using PEG-400.....	160
Figure 92. Snapshot of the process (on the right) and schematic diagram of step 1 big volume (10 kg) (on the left). ....	161
Figure 93. Metal extraction values for step 1 big volume. ....	163
Figure 94. On the left - formation of crystal structures in the Na <sub>2</sub> SO <sub>4</sub> bath with a temperature superior of 50°C.On the right - solid precipitation occurred during the continuous process. ....	164
Figure 95. Snapshot of the extraction column process (on the left) and corresponding schematic diagram (on the right).....	165

Figure 96. Snapshot static mixer process (on the left) and corresponding schematic diagram (on the right). .....	166
Figure 97. Extraction in PEG-400 phase using three different static mixers. ....	166
Figure 98. Step 1 of the process.....	167
Figure 99. Extraction efficiency of Na <sub>2</sub> CO <sub>3</sub> decahydrate in the UPS1. ....	168
Figure 100. Extraction efficiency of Na <sub>2</sub> CO <sub>3</sub> anhydrous in the UPS1. ....	169
Figure 102. (left) Extraction efficiency using Na <sub>2</sub> SO <sub>4</sub> anhydrous on the UPS1. (right) Extraction efficiency using 5wt% of Na <sub>2</sub> SO <sub>4</sub> anhydrous and added water on the UPS1.....	170
Figure 101. Extraction efficiency of Na <sub>2</sub> CO <sub>3</sub> anhydrous plus added water in the UPS1.....	170
Figure 103. Extraction efficiency of NaOH 30% mixed with UPS1 at 80 °C. ....	171
Figure 104. Triphasic systems when considering Na <sub>2</sub> CO <sub>3</sub> (left) and NaOH 30% (right) to separate the chromium from the polymer in big volume. ....	172
Figure 105. (left) Samples prepared for chromium precipitation through NaHSO <sub>3</sub> . A) 25 wt%, B) 30 wt% and C) 35 wt% of sodium bisulfate used. (right) Second test for chromium precipitation.....	173
Figure 106. UPS1 exposed to the sunlight. Starting from the left to the right: UPS1 as soon as was separated from the lower phase in the step 1, UPS1 exposed to the sunlight for 12 hours, UPS1 exposed to the sunlight for 24 hours. ....	173
Figure 107. Conversion of Cr(VI) (left) to Cr(III)(right) by UV-visible spectrophotometer. Monophasic solution containing 85 mg/L Cr(VI), 560 g/L PEG-400, pH=2 obtained by the addition of H <sub>2</sub> SO <sub>4</sub> , working temperature 65 °C. ....	174
Figure 108. Light box used as UV source for step 2. ....	175
Figure 109. Characteristics of the various apparatus used for the investigation. ....	175
Figure 110. Cr(g/L) precipitation in function of the time at 2 different exposures of the light and at the darkness.....	176
Figure 111. Cr(VI) precipitation in function of the time for three different light source: pure UV, UV-visible and pure visible light. ....	177
Figure 112. Cr precipitation in function of pH. ....	177
Figure 113. Graphical explanation of the mechanism of reaction of step 2. ....	179
Figure 114. Filter press used for large volumes (left). Schematic working mechanism of the filter press (right) .....	180
Figure 115. Pressure of the fluid in function of time of experiments for three different membranes used in the filter press. ....	180
Figure 116. Four different types of precipitates obtained during the investigation. ....	181
Figure 117. Wide scan or survey spectrum at the top and the high-resolution spectrum at the bottom of XPS analysis of the solid precipitation at the end of the step 2. Starting from the first band on the left to the third on the right there are Cr(OH) <sub>3</sub> , CrO <sub>3</sub> and Cr <sub>2</sub> O <sub>3</sub> . ....	182
Figure 118. XRD and SEM for solid sample C in Figure 116. ....	183
Figure 119. EDX spectrum for solid sample C in Figure 116. The main peaks in the spectra are characterized by the Cr, O, Na, C, Si and S. The blue arrow and the corresponding circle of the same color indicate the position of the sulfate. ....	183
Figure 120. Step 2 of the process. ....	184
Figure 121. Step 3 - Distillation process proposed in this work (700g of polymer treated)..	185
Figure 122. TGA analysis on the liquid phase from step 2.....	186
Figure 123. Steric exclusion chromatography spectrum for demonstrating PEG-degradation. Pure PEG in red and PEG after distillation step 3 in blue .....	187
Figure 124. Step 3 of the process. ....	187

Figure 125. Species concentration (wt%) and volume repartition (vol %) in the upper polymer phase of ABS obtained by using 40 wt% of PEG-400 fresh (yellow) and recycled (orange) at 80 °C.....	188
Figure 126. Schema of the patent for Cr(VI) recovery from Na <sub>2</sub> SO <sub>4</sub> bath.....	189
Figure 127. Cl <sup>-</sup> free determination through Ion Chromatography for the UGCO bath investigation. The value is given in mg/L.....	197
Figure 128. Metal repartitions and volume repartition for different systems composed of PPG-425 / UGCO bath.....	198
Figure 129. Metallic ions extraction with “green” DES from Table 9. ....	199
Figure 130. Cyanex 923 <sup>®</sup> , mixture of trihexyl phosphine oxide (a), trioctyl phosphine oxide (b), dioctylhexyl phosphine oxide (c) and dihexyloctyl phosphine oxide (HBA). ....	200
Figure 131. Trihexyl tetradecyl phosphonium chloride+ Decanoic acid.....	200
Figure 132. Metallic ions extraction for phosphorus-based DES.....	200
Figure 133. Extraction efficiency for ammonium chloride-based DES composed of Tetra-heptyl ammonium chloride with: (blue) Lauric acid (2:1), (red) Decanoic acid (2:1), (green) Oleic acid (2:1).....	201
Figure 134. Extraction efficiency for ammonium chloride-based DES composed of Decanoic acid with: (blue) Tetra-heptyl ammonium chloride (2:1) and (red) Tetra-hexyl ammonium chloride (2:1).....	201
Figure 135. Extraction efficiency for ammonium chloride-based DES composed of Decanoic acid with: (blue) Tetra-heptyl ammonium chloride (2:1) and (red) Dimethyl dioctadecyl ammonium chloride (2:1). ....	202
Figure 137. Polymer investigation by ESI-MS. A: polymer phase analyzed after mixing 80wt% of stock solution Fe(III) 35 g/L in 12M HCl and 20 wt% of PEG-600, B: fresh polymer PEG-600; Simulation with the software of the ESI-MS machine to show the form of peaks of PEG-Fe (C), PEG-Cr (D), PEG-Ni (E), PEG-Cl (F). ....	209
<i>Figure 136. Binodal curves of the system PEG-600/[Fe(III)+HCl 37wt%]/H<sub>2</sub>O [Fe(III)] = 40 g/L at 25 °C obtained using two different HCl providers, Fluka (●) and Sigma Aldrich (○). ....</i>	209
Figure 138. Gaussian’s curve of PEG-600 indicates the distribution of the polymer in solution .....	210
Figure 139. ESI-MS results of the acidic solution Fe(III) + HCl (37 wt% = 12M). Peaks at 197.64 m/z are the characteristic peaks of [Fe(III)Cl <sub>4</sub> ] <sup>-</sup> (molecular weight of the species). ....	210
Figure 140. HCl amount (wt%) as a function of metal ion concentration at: A) 20 wt%, B) 30 wt% and C) 40 wt% of IL. ....	211

## Bibliography

- 1 E. Sinoimeri, V. Maia-Fernandes, J. Cognard, J. Pereira, L. Svecova, I. Guillotte and I. Billard, *Phys. Chem. Chem. Phys.*, DOI:10.1039/d0cp03689g.
- 2 P. István, *The European environment-state and outlook 2020. Knowledge for transition to a sustainable Europe*, 2020, vol. 60.
- 3 H. M. Cobb, *The history of stainless steel*, 2011, vol. 48.
- 4 Outokumpu, *Handbook of Stainless Steel*, 2013.
- 5 L. A. Fernando and D. R. Zaremski, *Metall. Trans. A, Phys. Metall. Mater. Sci.*, 1988, **19 A**, 1083–1100.
- 6 R. D. Rogers, A. H. Bond, C. B. Bauer, J. Zhang and S. T. Griffin, *J. Chromatogr. B Biomed. Appl.*, 1996, **680**, 221–229.
- 7 H. F. Koch, J. Shen and D. M. Roundhill, *Sep. Sci. Technol.*, 2000, **35**, 623–629.
- 8 L. Bulgariu, D. Bulgariu, I. Sârghie and T. Măluțan, *Cent. Eur. J. Chem.*, 2007, **5**, 291–302.
- 9 P. Wang, F. Zhang, P. Li, T. Sun, Y. Pan and Y. Zhang, *J. Mol. Liq.*, 2018, **260**, 180–185.
- 10 L. Muruchi, N. Schaeffer, H. Passos, C. M. N. Mendonça, J. A. P. Coutinho and Y. P. Jimenez, *ACS Sustain. Chem. Eng.*, 2019, **7**, 1778–1785.
- 11 V. Mogilireddy, M. Gras, N. Schaeffer, H. Passos, L. Svecova, N. Papaiconomou, J. A. P. Coutinho and I. Billard, *Phys. Chem. Chem. Phys.*, 2018, **20**, 16477–16484.
- 12 N. Schaeffer, H. Passos, M. Gras, V. Mogilireddy, J. P. Leal, G. Pérez-Sánchez, J. R. B. Gomes, I. Billard, N. Papaiconomou and J. A. P. Coutinho, *Phys. Chem. Chem. Phys.*, 2018, **20**, 9838–9846.
- 13 N. Schaeffer, M. Gras, H. Passos, V. Mogilireddy, C. M. N. Mendonça, E. Pereira, E. Chainet, I. Billard, J. A. P. Coutinho and N. Papaiconomou, *ACS Sustain. Chem. Eng.*, 2019, **7**, 1769–1777.
- 14 C. M. S. S. Neves, S. P. M. Ventura, M. G. Freire, I. M. Marrucho and J. A. P. Coutinho, *J. Phys. Chem. B*, 2009, **113**, 5194–5199.
- 15 L. I. N. Tomé, J. F. B. Pereira, R. D. Rogers, M. G. Freire, J. R. B. Gomes and J. A. P. Coutinho, *Phys. Chem. Chem. Phys.*, 2014, **16**, 2271–2274.
- 16 P. Sun, K. Huang, J. Lin and H. Liu, *Ind. Eng. Chem. Res.*, 2018, **57**, 11390–11398.
- 17 Aperam, *Made for Life*, 2019.
- 18 Woodard & Curran, Inc., *Ind. Waste Treat. Handb.*, 2006, 409–496.
- 19 F. Rögener, M. Sartor, A. Bán, D. Buchloh and T. Reichardt, *Resour. Conserv. Recycl.*, 2012, **60**, 72–77.
- 20 Life Dime, Spent Pickling Liquor Treatment, <https://lifedime.eu/en/spent-pickling-liquor-treatment/>, (accessed 27 January 2021).
- 21 and C. J. L. Richard, Hoak D., *Ind. Eng. Chem. Res.*, 1948, **40**, 2062–2067.
- 22 T. Özdemir, C. Öztin and N. S. Kincal, *Chem. Eng. Commun.*, 2006, **193**, 548–563.
- 23 W. Kladnig, *J. Iron Steel Res. Int.*, 2008, **15**, 1–6.
- 24 1924, 1,515,799.
- 25 GB483821, 1938.
- 26 2,005,120, 1935, 3–5.
- 27 2003021103, 2003, 1.
- 28 J. Saji, T. Prasada Rao, C. S. P. Iyer and M. L. P. Reddy, *Hydrometallurgy*, 1998, **49**, 289–296.
- 29 A. Agrawal, S. Kumari and K. K. Sahu, *J. Environ. Manage.*, 2011, **92**, 3105–3111.
- 30 M. D. Lanagan and D. C. Ibana, *Miner. Eng.*, 2003, **16**, 237–245.
- 31 J. Konczyk, C. Kozłowski and W. Walkowiak, *Desalination*, 2010, **263**, 211–216.
- 32 G. Csicsovszki, T. Kékesi and T. I. Török, *Hydrometallurgy*, 2005, **77**, 19–28.

- 33 M. W. Beijerinck, *Zeitschrift für Chemie und Ind. der Kolloide*, 1910, **7**, 16–20.
- 34 P. A. Albertsson, *Nature*, 1956, **177**, 771–774.
- 35 and U. W. S. Jesse N. Baskir, T. Alan Hatton, *Protein Partitioning in Two-Phase Aqueous Polymer Systems*, 1988, vol. 34.
- 36 H. O. Johansson, T. Matos, J. S. Luz, E. Feitosa, C. C. Oliveira, A. Pessoa, L. Bülow and F. Tjerneld, *J. Chromatogr. A*, 2012, **1233**, 30–35.
- 37 Y. Xu, M. A. Souza, M. Z. R. Pontes, M. Vitolo and A. Pessoa, *Brazilian Arch. Biol. Technol.*, 2003, **46**, 741–750.
- 38 P. Albertsson, *Adv. Protein Chem.*, 1970, **24**, 309–341.
- 39 M. Iqbal, Y. Tao, S. Xie, Y. Zhu, D. Chen, X. Wang, L. Huang, D. Peng, A. Sattar, M. A. B. Shabbir, H. I. Hussain, S. Ahmed and Z. Yuan, *Biol. Proced. Online*, 2016, **18**, 1–18.
- 40 J. P. Chen and M. S. Lee, *Enzyme Microb. Technol.*, 1995, **17**, 1021–1027.
- 41 M. R. Helfrich, M. El-Kouedi, M. R. Etherton and C. D. Keating, *Langmuir*, 2005, **21**, 8478–8486.
- 42 J. Benavides and M. Rito-Palomares, *J. Chromatogr. B Anal. Technol. Biomed. Life Sci.*, 2006, **844**, 39–44.
- 43 A. S. Schmidt, A. M. Ventom and J. A. Asenjo, *Enzym. Microb. Technol.*, 1994, **16**, 131–142.
- 44 T. I. Zvarova, V. M. Shkinev, G. A. Vorob'eva, B. Y. Spivakov and Y. A. Zolotov, *Mikrochim. Acta*, 1984, **84**, 449–458.
- 45 K. Ghosh, M. Maiti, S. Lahiri and V. Afzal Hussain, *J. Radioanal. Nucl. Chem.*, 2014, **302**, 925–930.
- 46 R. Karmakar and K. Sen, *J. Mol. Liq.*, 2019, **273**, 231–247.
- 47 H. Li Chum, V. R. Koch, L. L. Miller and R. A. Osteryoung, *J. Am. Chem. Soc.*, 1975, **97**, 3264–3265.
- 48 J. S. Wilkes, J. A. Levisky, R. A. Wilson and C. L. Hussey, *Inorg. Chem.*, 1982, **21**, 1263–1264.
- 49 Y. Akama, M. Ito and S. Tanaka, *Talanta*, 2000, **53**, 645–650.
- 50 Y. Akama and A. Sali, *Talanta*, 2002, **57**, 681–686.
- 51 T. E. Sintra, R. Cruz, S. P. M. Ventura and J. A. P. Coutinho, *J. Chem. Thermodyn.*, 2014, **77**, 206–213.
- 52 Y. Li, X. Lu, J. Hao and C. Chen, *J. Chem.*, , DOI:10.1155/2013/857272.
- 53 Y. Chen, Y. Meng, S. Zhang, Y. Zhang, X. Liu and J. Yang, *J. Chem. Eng. Data*, 2010, **55**, 3612–3616.
- 54 R. Schurhammer and G. Wipff, *J. Phys. Chem. B*, 2018, **122**, 10143–10157.
- 55 K. E. Gutowski, G. A. Broker, H. D. Willauer, J. G. Huddleston, R. P. Swatloski, J. D. Holbrey and R. D. Rogers, *J. Am. Chem. Soc.*, 2003, **125**, 6632–6633.
- 56 Z. Du, Y. L. Yu and J. H. Wang, *Chem. - A Eur. J.*, 2007, **13**, 2130–2137.
- 57 A. Valadares, C. F. Valadares, L. R. de Lemos, A. B. Mageste and G. D. Rodrigues, *Hydrometallurgy*, 2018, **181**, 180–188.
- 58 D. Depuydt, W. Dehaen and K. Binnemans, *Ind. Eng. Chem. Res.*, 2015, **54**, 8988–8996.
- 59 I. Billard and M. G. Freire, *Extraction of metals with ABS To cite this version : HAL Id : hal-02272199 Extraction of metals with ABS*, 2019.
- 60 L. W. McKeen, *The Effect of Long Term Thermal Exposure on Plastics and Elastomers*, 2013.
- 61 Treccani - Italia, Polimero in Vocabolario -Treccani, <https://www.treccani.it/vocabolario/polimero/>, (accessed 23 February 2021).
- 62 A. G. Cemile Ozdemir Dinc, Gunay Kibarer, *J. Appl. Polym. Sci.*, 2010, **116**, 2658–2667.
- 63 C. Özdemir and A. Güner, *Eur. Polym. J.*, 2007, **43**, 3068–3093.
- 64 N. V. Plechkova and K. R. Seddon, *Chem. Soc. Rev.*, 2008, **37**, 123–150.

- 65 C. J. Bradaric, A. Downard, C. Kennedy, A. J. Robertson and Y. Zhou, *Green Chem.*, 2003, **5**, 143–152.
- 66 S. V. Dzyuba and R. A. Bartsch, *Tetrahedron Lett.*, 2002, **43**, 4657–4659.
- 67 D. R. MacFarlane, A. L. Chong, M. Forsyth, M. Kar, R. Vijayaraghavan, A. Somers and J. M. Pringle, *Faraday Discuss.*, 2018, **206**, 9–28.
- 68 J. Zhou, H. Sui, Z. Jia, Z. Yang, L. He and X. Li, *RSC Adv.*, 2018, **8**, 32832–32864.
- 69 P. R. Ro. Chang Samuel Hsu, *Springer Handbook of Petroleum Technology*, Springer., 2017.
- 70 T. J. Geldbach, D. Zhao, N. C. Castillo, G. Laurency, B. Weyershausen and P. J. Dyson, *J. Am. Chem. Soc.*, 2006, **128**, 9773–9780.
- 71 A. C. Vetter, K. Nikitin and D. G. Gilheany, *Chem. Commun.*, 2018, **54**, 5843–5846.
- 72 J. F. Knifton, *J. Mol. Catal.*, 1987, **43**, 65–77.
- 73 J. F. B. Pereira and J. A. P. Coutinho, in *Liquid-Phase Extraction*, 2019, pp. 157–182.
- 74 E. V Capela, J. H. P. M. Santos, I. Boal-Palheiros, J. A. P. Coutinho, S. P. M. Ventura and M. G. Freire, *Chem. Eng. Educ.*, 2019, **53**, 112–120.
- 75 J. C. Merchuk, B. A. Andrews and J. A. Asenjo, 1998, **711**, 285–293.
- 76 B. G. Alvarenga, L. S. Virtuoso, N. H. T. Lemes and P. O. Luccas, *J. Chem. Thermodyn.*, 2013, **61**, 45–50.
- 77 J. C. Phys, P. J. Carvalho, R. D. Rogers, J. A. P. Coutinho, D. C. V Belchior, E. Sintra, P. J. Carvalho and R. C. Soromenho, , DOI:10.1063/1.5012020.
- 78 N. Ni and S. H. Yalkowsky, *Int. J. Pharm.*, 2003, **254**, 167–172.
- 79 K. P. Ananthapadmanabhan and E. D. Goddard, *Langmuir*, 1987, **3**, 25–31.
- 80 B. Y. Zaslavsky, N. D. Gulaeva, S. Djafarov, E. A. Masimov and L. M. Miheeva, *J. Colloid Interface Sci.*, 1990, **137**, 147–156.
- 81 E. L. Cheluget, S. Gelinias, J. H. Vera and M. E. Weber, *J. Chem. Eng. Data*, 1994, **39**, 127–130.
- 82 M. E. Taboada, O. A. Rocha and A. Graber, 2001, **46**, 308–311.
- 83 N. Schaeffer, H. Passos, M. Gras, V. Mogilireddy, J. P. Leal, G. Pérez-Sánchez, J. R. B. Gomes, I. Billard, N. Papaiconomou and J. A. P. Coutinho, *Phys. Chem. Chem. Phys.*, 2018, **20**, 9838–9846.
- 84 A. M. Hyde, S. L. Zultanski, J. H. Waldman, Y. L. Zhong, M. Shevlin and F. Peng, *Org. Process Res. Dev.*, 2017, **21**, 1355–1370.
- 85 L. Das, S. P. Paik and K. Sen, *J. Chem. Eng. Data*, 2019, **64**, 51–59.
- 86 S. P. M. Ventura, S. G. Sousa, L. S. Serafim, Á. S. Lima, M. G. Freire and J. A. P. Coutinho, *J. Chem. Eng. Data*, 2012, **57**, 507–512.
- 87 R. Sadeghi and F. Jahani, *J. Phys. Chem. B*, 2012, **116**, 5234–5241.
- 88 V. G. Lacerda, A. B. Mageste, I. J. B. Santos, L. H. M. da Silva and M. do C. H. da Silva, *J. Power Sources*, 2009, **193**, 908–913.
- 89 P. da R. Patrício, M. C. Mesquita, L. H. M. da Silva and M. C. H. Da Silva, *J. Hazard. Mater.*, 2011, **193**, 311–318.
- 90 L. Bulgariu and D. Bulgariu, *Sep. Purif. Technol.*, 2013, **118**, 209–216.
- 91 P. R. Patrício, R. C. Cunha, S. J. Rodriguez Vargas, Y. L. Coelho, L. H. Mendes Da Silva and M. C. Hespanhol Da Silva, *Sep. Purif. Technol.*, 2016, **158**, 144–154.
- 92 J. Liu, K. Huang, K. Xie, Y. Yang and H. Liu, *Water Res.*, 2016, **93**, 187–194.
- 93 A. Hamta and M. R. Dehghani, *J. Mol. Liq.*, 2017, **231**, 20–24.
- 94 W. C. M. de Oliveira, G. D. Rodrigues, A. B. Mageste and L. R. de Lemos, *Chem. Eng. J.*, 2017, **322**, 346–352.
- 95 L. Das, S. P. Paik and K. Sen, *J. Chem. Eng. Data*, 2019, **64**, 51–59.
- 96 G. Yin, S. Li, Q. Zhai, Y. Jiang and M. Hu, *Thermochim. Acta*, 2013, **566**, 149–154.
- 97 D. Depuydt, W. Dehaen and K. Binnemans, *Ind. Eng. Chem. Res.*, 2015, **54**, 8988–8996.

- 98 B. Onghena, T. Opsomer and K. Binnemans, *Chem. Commun.*, 2015, **51**, 15932–15935.
- 99 N. Schaeffer, H. Passos, M. Gras, S. J. Rodriguez Vargas, M. C. Neves, L. Svecova, N. Papaiconomou and J. A. P. Coutinho, *ACS Sustain. Chem. Eng.*, 2020, **8**, 12260–12269.
- 100 N. Schaeffer, M. Gras, H. Passos, V. Mogilireddy, C. M. N. Mendonça, E. Pereira, E. Chainet, I. Billard, J. A. P. Coutinho and N. Papaiconomou, *ACS Sustain. Chem. Eng.*, 2019, **7**, 1769–1777.
- 101 A. F. M. Cláudio, A. M. Ferreira, S. Shahriari, M. G. Freire and J. A. P. Coutinho, *J. Phys. Chem. B*, 2011, **115**, 11145–11153.
- 102 J. C. W. Paul T. Anastas, *Green Chemistry: Theory and Practice*, Oxford Uni., 1998.
- 103 R. D. Rogers and K. R. Seddon, *Ionic liquids: industrial applications for green chemistry*, 2002.
- 104 H. F. SMYTH, C. P. CARPENTER and C. S. WEIL, *J. Am. Pharm. Assoc. Am. Pharm. Assoc. (Baltim.)*, 1950, **39**, 349–354.
- 105 M. Petkovic, D. O. Hartmann, G. Adamová, K. R. Seddon, L. P. N. Rebelo and C. S. Pereira, *New J. Chem.*, 2012, **36**, 56–63.
- 106 B. Onghena, J. Jacobs, L. Van Meervelt and K. Binnemans, *Dalt. Trans.*, 2014, **43**, 11566–11578.
- 107 C. M. S. S. Neves, S. Shahriari, J. Lemus, J. F. B. Pereira, M. G. Freire and J. A. P. Coutinho, *Phys. Chem. Chem. Phys.*, 2016, **18**, 20571–20582.
- 108 Y. Deng, J. Chen and D. Zhang, *J. Chem. Eng. Data*, 2007, **52**, 1332–1335.
- 109 S. P. M. Ventura, C. M. S. S. Neves, M. G. Freire, I. M. Marrucho, J. Oliveira and J. A. P. Coutinho, *J. Phys. Chem. B*, 2009, **113**, 9304–9310.
- 110 C. Prevenzione, P. Reparto and A. Interne, *DETERMINAZIONE DEL CARBONIO ORGANICO TOTALE*, 2001.
- 111 PH meter | instrument | Britannica, <https://www.britannica.com/technology/pH-meter>, (accessed 1 February 2021).
- 112 D. M. Finkelstein, R. E. Schumacker and R. G. Lomax, *Technometrics*, 2015, **47**, 522–522.
- 113 Measuring Principle of Karl Fischer Moisture Titrators, <https://www.gpsil.co.uk/our-products/karl-fischer-titrators/measuring-principle#>, (accessed 1 February 2021).
- 114 E. M. A. Hussein, *Radiation Mechanics: Principles and Practice*, [https://books.google.fr/books?hl=it&lr=&id=3XQ2jplbsegC&oi=fnd&pg=PP1&dq=MECHANISMS++Esam+M.A.+Hussein,+in+Radiation+Mechanics,+2007+Photoabsorption&ots=0rOEqHcJAJ&sig=S8Abf7\\_GjP0tJxRFR2CxxmBUz4E#v=onepage&q&f=false](https://books.google.fr/books?hl=it&lr=&id=3XQ2jplbsegC&oi=fnd&pg=PP1&dq=MECHANISMS++Esam+M.A.+Hussein,+in+Radiation+Mechanics,+2007+Photoabsorption&ots=0rOEqHcJAJ&sig=S8Abf7_GjP0tJxRFR2CxxmBUz4E#v=onepage&q&f=false), (accessed 25 January 2021).
- 115 W. G. Schrenk and W. G. Schrenk, in *Analytical Atomic Spectroscopy*, Springer US, 1975, pp. 211–242.
- 116 MERCK, .
- 117 H. L. T. C.S. Ho, C.W.K. Lam, M.H.M. Chan, R.C.K. Cheung, L.K. Law, K.F. Ng, M.W.M. Suem, *Pancreat. Cancer, Cyst. Neoplasms Endocr. Tumors Diagnosis Manag.*, 2003, **24**, 3–12.
- 118 L. Konermann, E. Ahadi, A. D. Rodriguez and S. Vahidi, *Anal. Chem.*, 2013, **85**, 2–9.
- 119 V. Mogilireddy, M. Gras, N. Schaeffer, H. Passos, L. Svecova, N. Papaiconomou, J. A. P. Coutinho and I. Billard, *Phys. Chem. Chem. Phys.*, 2018, **20**, 16477–16484.
- 120 C. Deferm, A. Van Den Bossche, J. Luyten, H. Oosterhof, J. Fransaer and K. Binnemans, *Phys. Chem. Chem. Phys.*, 2018, **20**, 2444–2456.
- 121 S. A. Rim, D. M. Amine, B. Nasr-Eddine and J. P. Canselier, *J. Hazard. Mater.*, 2009, **167**, 896–903.
- 122 D. P. Fagnant, G. S. Goff, B. L. Scott, W. Runde and J. F. Brennecke, *Inorg. Chem.*, 2013, **52**, 549–551.
- 123 M. G. Freire, A. F. M. Cláudio, J. M. M. Araújo, J. A. P. Coutinho, I. M. Marrucho, J. N.

- C. Lopes and L. P. N. Rebelo, *Chem. Soc. Rev.*, 2012, **41**, 4966–4995.
- 124 C. M. S. S. Neves, M. G. Freire and J. A. P. Coutinho, *RSC Adv.*, 2012, **2**, 10882–10890.
- 125 Y. H. Choi, Y. S. Song and D. H. Kim, *J. Chromatogr. A*, 2010, **1217**, 3723–3728.
- 126 B. Onghena, T. Opsomer and K. Binnemans, *Chem. Commun.*, 2015, **51**, 15932–15935.
- 127 M. Gras, N. Papaiconomou, N. Schaeffer, E. Chainet, F. Tedjar, J. A. P. Coutinho and I. Billard, *Angew. Chemie - Int. Ed.*, 2018, **57**, 1563–1566.
- 128 C. M. S. S. Neves, S. P. M. Ventura, M. G. Freire, I. M. Marrucho and J. A. P. Coutinho, *J. Phys. Chem. B*, 2009, **113**, 5194–5199.
- 129 D. C. V. Belchior, T. E. Sintra, P. J. Carvalho, M. R. C. Soromenho, J. M. S. S. Esperança, S. P. M. Ventura, R. D. Rogers, J. A. P. Coutinho and M. G. Freire, *J. Chem. Phys.*, 2018, **148**, 193842.
- 130 N. Schaeffer, G. Perez-Sanchez, H. Passos, J. R. B. Gomes, N. Papaiconomou and J. A. P. Coutinho, *Phys. Chem. Chem. Phys.*, 2019, 7462–7473.
- 131 Y. Marcus and A. Loewenschuss, *Annu. Rep. Prog. Chem., Sect. C Phys. Chem.*, 1985, **81**, 81–135.
- 132 Y. Marcus, *J. Chem. Soc., Faraday Trans.*, 1991, **87**, 2995–2999.
- 133 N. J. Bridges, K. E. Gutowski and R. D. Rogers, *Green Chem.*, 2007, **9**, 177–183.
- 134 L. G. Sillén and A. E. Martell, *Stability constants of metal-ion constants*, Chemical Society, 1964.
- 135 Z. L. Xie and A. Taubert, *ChemPhysChem*, 2011, **12**, 364–368.
- 136 C. M. S. S. Neves, R. de Cássia S. Sousa, M. M. Pereira, M. G. Freire and J. A. P. Coutinho, *Biochem. Eng. J.*, 2019, **141**, 239–246.
- 137 X. Tang, J. Han, Y. Hu, Y. Wang, Y. Lu, T. Chen and L. Ni, *Fluid Phase Equilib.*, 2014, **383**, 100–107.
- 138 J. G. Huddleston, H. D. Willauer, S. T. Griffin and R. D. Rogers, *Ind. Eng. Chem. Res.*, 1999, **38**, 2523–2539.
- 139 K. P. Ananthapadmanabhan and E. D. Goddard, *Langmuir*, 1987, **3**, 25–31.
- 140 L. I. N. Tomé, J. F. B. Pereira, R. D. Rogers, M. G. Freire, J. R. B. Gomes and J. A. P. Coutinho, *J. Phys. Chem. B*, 2014, **118**, 4615–4629.
- 141 J. F. B. Pereira, K. A. Kurnia, M. G. Freire, J. A. P. Coutinho and R. D. Rogers, *ChemPhysChem*, 2015, **16**, 2219–2225.
- 142 G. Rayner-Canham and T. Overton, *Descriptive inorganic chemistry: Fifth edition*, W. H. Freeman and Company, New York, 5th editio., 2009.
- 143 R. Sartori, L. Sepulveda, F. Quina, E. Lissi and E. Abuin, *Macromolecules*, 1990, **23**, 3878–3881.
- 144 L. Bulgariu and D. Bulgariu, *J. Chromatogr. A*, 2008, **1196–1197**, 117–124.
- 145 G. W. Brady, M. B. Robin and J. Varimbi, *Inorg. Chem.*, 1964, **3**, 1168–1173.
- 146 T. A. Graber, M. E. Taboada, J. A. Asenjo and B. A. Andrews, *J. Chem. Eng. Data*, 2001, **46**, 765–768.
- 147 L. A. Ferreira, J. A. Teixeira, L. M. Mikheeva, A. Chait and B. Y. Zaslavsky, *J. Chromatogr. A*, 2011, **1218**, 5031–5039.
- 148 N. R. da Silva, L. A. Ferreira, L. M. Mikheeva, J. A. Teixeira and B. Y. Zaslavsky, *J. Chromatogr. A*, 2014, **1337**, 3–8.
- 149 Y. Zhang, T. Sun, Q. Hou, Q. Guo, T. Lu, Y. Guo and C. Yan, *Sep. Purif. Technol.*, 2016, **169**, 151–157.
- 150 R. D. Rogers and C. B. Bauer, *J. Chromatogr. B Biomed. Appl.*, 1996, **680**, 237–241.
- 151 R. D. Rogers, A. H. Bond and C. B. Bauer, *Pure Appl. Chem.*, 1993, **65**, 567–572.
- 152 C. Rodriguez-Navarro, E. Doehne and E. Sebastian, *Cem. Concr. Res.*, 2000, **30**, 1527–1534.
- 153 D. Banerjee and H. W. Nesbitt, *Geochim. Cosmochim. Acta*, 1999, **63**, 1671–1687.
- 154 R. Chapaneri, G. Critchlow and I. Sutherland, .

155 M. C. Biesinger, B. P. Payne, A. P. Grosvenor, L. W. M. Lau, A. R. Gerson and R. S. C. Smart, *Appl. Surf. Sci.*, 2011, **257**, 2717–2730.

